DESIGN, SYNTHESIS, AND OPTIMIZATION OF RECOVERABLE AND RECYCLABLE SILICA-IMMOBILIZED ATOM TRANSFER RADICAL POLYMERIZATION CATALYSTS

A Thesis
Presented to
The Academic Faculty

by

Joseph V. Nguyen

In Partial Fulfillment
of the Requirements for the Degree
Doctor of Philosophy in the
School of Chemical and Biomolecular Engineering

Georgia Institute of Technology
February 2005

DESIGN, SYNTHESIS, AND OPTIMIZATION OF RECOVERABLE AND RECYCLABLE SILICA-IMMOBILIZED ATOM TRANSFER RADICAL POLYMERIZATION CATALYSTS

Approved by:

Dr. Christopher W. Jones
School of Chemical and Biomolecular Engineering
Georgia Institute of Technology

Dr. Marcus Weck
School of Chemistry and Biochemistry
Georgia Institute of Technology

Dr. Charles A. Eckert
School of Chemical and Biomolecular Engineering
Georgia Institute of Technology

Dr. Z. John Zhang
School of Chemistry and Biochemistry
Georgia Institute of Technology

Dr. F. Joseph Schork
School of Chemical and Biomolecular Engineering
Georgia Institute of Technology

Date Approved: February 28, 2005

ACKNOWLEDGEMENTS

This Thesis is by far the most significant scientific accomplishment in my life and it would be impossible without people who supported me and believed in me.

The first person I would like to thank is my advisor Chris Jones. During these years I have learned from your enthusiasm and integral view on research and mission for providing only high-quality work and not less. You have afforded me a great deal of flexibility and independence to perform my research, which allowed me to keep my drive and sanity. Besides being an excellent advisor, you have been a good friend, for that I thank you.

Secondly, I would like to thank my loving parents and family for their support. They have taught me many lessons that cannot be derived from science and engineering. I am this person today because of them.

A journey is easier when you travel together. I would like to thank my fiancée Elaine Chan for her comfort and understanding, but above all else, your love for me. I will truly enjoy our journey through life together. Instead of thanking you, I will tell you how much I love you.

Lastly, I would like to thank God for giving me the strength and faith to accomplish my goals. I am also grateful to those that were not mentioned here.

TABLE OF CONTENTS

TABLE OF CONTENTS (continued)

TABLE OF CONTENTS (continued)

LIST OF TABLES

LIST OF TABLES (continued)

LIST OF FIGURES

LIST OF FIGURES (continued)

LIST OF FIGURES (continued)

LIST OF FIGURES (continued)

LIST OF FIGURES (continued)

LIST OF ABBREVIATIONS

AIBN	2,2[-Azobis(2-methylpropionitrile)
APTMS	3-aminopropyltrimethoxysilane
ATRA	Atom Transfer Radical Addition
ATRP	Atom Transfer Radical Polymerization
BPN	2-Bromopropionitrile
Bpy	bipyridine
CHN	Carbon, Hydrogen, and Nitrogen microanalyses
CLRP	Controlled/"Living" Radical Polymerization
CP	Cross Polarization
CPG	control pore glass
CRP	Controlled Radical Polymerization
DPS	dipropylsulfide
DSC	differential scanning calorimetry
EA	elemental analysis
EO-PO-EO	poly(ethylene glycol)-block-poly(propylene glycol)-block-poly-(ethylene glycol)
HMDS	hexamethyldisilazane
HMTETA	CuBr/hexamethyltriethylenetetramine
ICP-AES	Inductive coupling plasma - atom emission spectroscopy
k_{act}	activation rate constant
k_{deact}	deactivation rate constant

LIST OF ABBREVIATIONS (continued)

MADIX	MAcromolecular Design via the Interchange of Xanthates
MAS	magic angle spinning
Me_6TREN	Tris(2-(dimethylamino)ethyl)amine
MMA	methyl methacrylate
M_n	number average molecular weight
$M_{n,Exp}$	experimental number average molecular weight
$M_{n,Th}$	theoretical number average molecular weight
MPTMS	(3-Mercaptopropyl)trimethoxysilane
M_t^n	metal with n oxidation state
M_t^{n+1}	metal with n+1 oxidation state
M_w	weight average molecular weight
$[M_o]$	initial monomer concentration
$[M_t]$	monomer concentration at time t
PCA	2-pyridinecarboxaldehyde
PDI	polydispersity
PMI	pyridylmethanimine
PMITMS	[3-(Trimethoxysilanyl)-propyl]-2-pyridylmethanimine
PMMA	poly(methyl methacrylate)
ppm	concentration in parts per million
PPMI	N-(n-Propyl)-2-pyridylmethanimine
pSdMBpy	4-Methyl-4'-(4-propylsulfanylbutyl)-2,2'-bipyridinyl

LIST OF ABBREVIATIONS (continued)

RAFT	Reversible Addition Fragmentation chain Transfer
R_{Cu}	residual copper content
SdMBpyTMS	4'-{4-[3-(Trimethoxysilanyl)propylsulfanyl]butyl}-4-methyl-2,2'-bipyridinyl
TEOS	tetraethyl orthosilicate
TGA	thermogravimetric analysis
TMB	1,3,5-trimethylbenzene
XRD	x-ray diffraction

SUMMARY

Despite the growing interest in heterogeneous polymerization catalysis, the majority of the polymerization catalysts used industrially are single-use entities that are left in the polymer product. Recoverable and recyclable polymerization catalysts have not reached the industrial utility of single-use catalysts because the catalyst and product separation have not become economical. The successful development of recyclable transition metal polymerization catalysts must take a rational design approach, hence academic and industrial researchers need to further expand the fundamental science and engineering of recyclable polymerization catalysis to gain an understanding of critical parameters that allow for the design of economically viable, recoverable solid polymerization catalysts.

Unfortunately, the rapid development of Atom Transfer Radical Polymerization over the past 10 years has not resulted in its wide spread industrial practice. Numerous reports regarding the immobilization of transition metal ATRP catalysts, in attempts to increase its applicability, have extended the fundamentals of recyclable polymerization catalysis. However, for industrial viability, more research is required in the area of how immobilization methodology and support structure affect the catalyst polymerization performance, regeneration, and recyclability. A comprehensive rational catalyst design approach was undertaken to answer these questions.

CHAPTER 1

EVOLUTION TOWARDS RECOVERABLE HETEROGENEOUS POLYMERIZATION CATALYSIS

Background

Heterogeneous catalysis

A *catalyst* was first defined by J. J. Berzelius in 1835 as a compound which increases the rate of a chemical reaction but which is not consumed by the reaction. A more specific description defines catalysis as the "modification (usually acceleration) of a chemical reaction rate by addition of a catalyst, which combines with the reactants but is ultimately regenerated so that its amount remains unchanged and the chemical equilibrium of the conditions of the reaction is not altered [1]." As one can see, ideas of what constitutes catalysis and the mechanism of catalytic activity have undergone continuous refinement. Understanding of catalysis from both a theoretical and practical point of view is essential to chemists and chemical engineers.

The chemical catalysis field can be broadly divided into two categories, homogeneous and heterogeneous catalysis. By traditional definitions, homogeneous catalysis implies that the chemical reaction occurs in a single phase, of which the reactant, products, and catalyst are in the same phase, usually liquid (**Figure 1.1**). In contrast, a heterogeneous catalysis involves different phases; usually a solid catalyst is used in liquid or gas phase reaction [2-4][1].

[1] Here we use the traditional definitions of homogeneous (soluble) and heterogeneous (insoluble) catalysts. The alternative definitions introduced by Schwartz [2] and refined by Finke and co-workers [3, 4] are not used (homogeneous, single site; and heterogeneous, multisite).

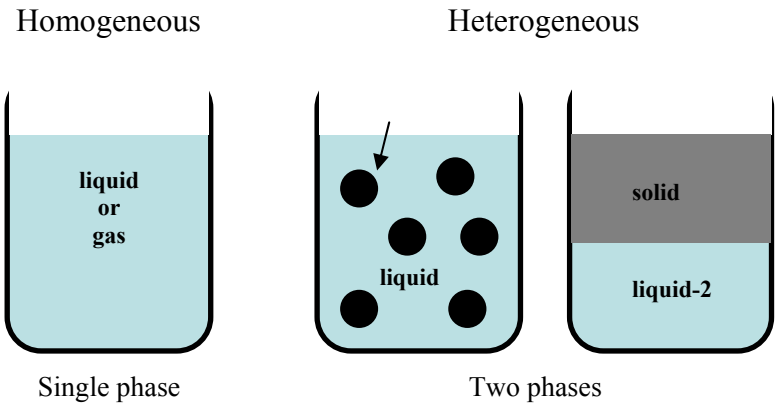

Figure 1.1 Representation of homogeneous and heterogeneous system.

Homogeneous catalysis has become an invaluable tool for organic chemists, allowing them to perform many new chemical reactions [5]. The strengths of homogeneous catalysts in general are their often higher activity and selectivity towards the desired product, and better reproducibility compared to heterogeneous catalysts. However, in general they are more vulnerable to poisoning, have shorter lifetimes, and are less thermally stable compared to heterogeneous catalysts [6-8]. There are far fewer homogeneous catalysts, compared to heterogeneous catalysts, used in large scale industrial processes today. Homogeneous catalysts in large part are difficult to separate from the reaction medium and can cause reactor fouling. This is a great disadvantage if one considers that many expensive precious metal complexes are used as homogeneous catalysts. On the other hand, heterogeneous catalysts allow for easier recovery, absence of corrosion, and higher stability. Since these catalysts can be easily recovered, the catalyst can potentially be recycled or utilized in continuous processes. Lastly, one of the main disadvantages of heterogeneous catalysts is they tend to be multi-sited. Hence in most cases, the catalyst is not as active or selective as homogeneous systems.

The application of heterogeneous catalysis is more convenient for technological development, and not surprisingly, heterogeneous catalysts are used in upwards of 90% of the chemical reactions performed industrially on a large scale (e.g., bulk chemical and petroleum industries) [6-8]. However, when some homogeneous systems are replaced with traditional heterogeneous catalysts (e.g., precious metals, mixed metal oxides), the catalyst performs insufficiently compared to homogeneous standards (i.e. lower selectivity and activity). This shortcoming was addressed via the concept of hybrid catalysts. The concept reflected the idea and search for an "ideal" catalyst, where the hybrid catalyst was heterogeneous with respect to the reaction medium, thereby allowing for easy separation, while its application could ensure all the advantages of the homogeneous catalytic system (all active centers are uniform and show ideally 100% selectivity towards the desired reaction). The concept of an "ideal" catalyst reflects the traditional definition of heterogeneous catalysis[1].

The quest for an "ideal" catalyst has opened up a new field within heterogeneous catalysis called *heterogenized homogeneous catalysis*, where research has been conducted on the preparation of immobilized homogeneous molecular catalysts [7]. It is now commonly accepted that there is no significant difference in the mechanisms of substrate adsorption and product desorption for both homogeneous and heterogeneous catalysis, thus the transfer of active centers from solution to the surface of a solid is a fairly natural process [7] (**Figure 1.2)**.

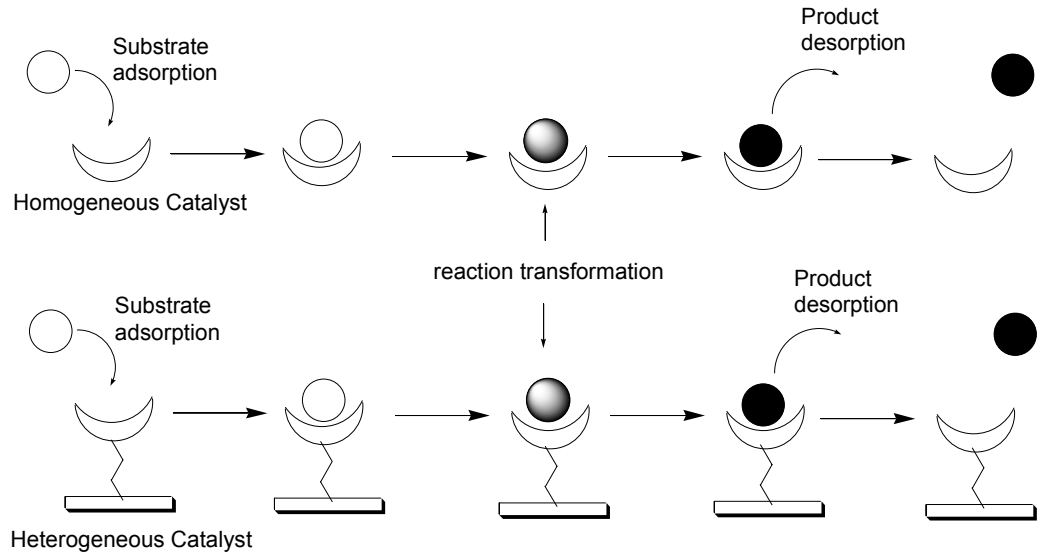

Figure 1.2 Homogeneous and heterogeneous mechanism for general catalytic reaction.

Figure 1.3 shows an example of the transformation of homogeneous Jacobsen's Mn-Salen catalyst [9] to an immobilized heterogeneous analogue [10, 11]. Great care is used to preserve the active molecular character of the catalyst during the immobilization; therefore the catalytic performances should remain identical, but the heterogenized homogeneous catalyst can be recovered and recycled.

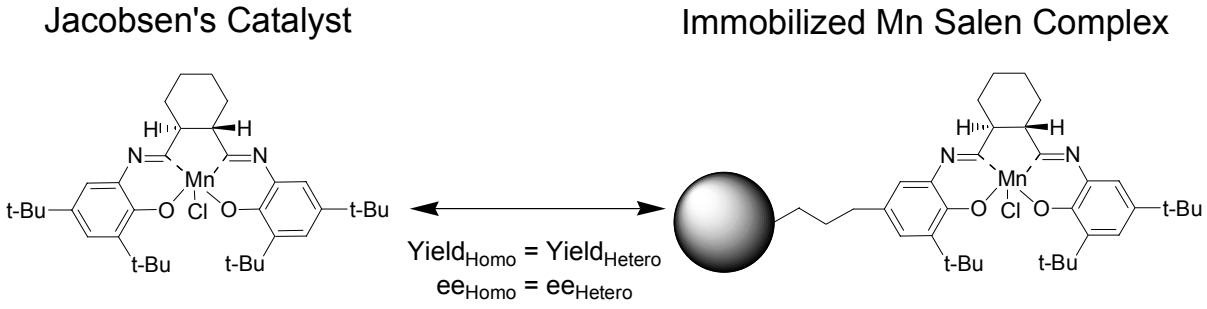

Figure 1.3 The ideal immobilization of homogeneous Jacobsen's Mn-Salen catalyst [10, 11].

Heterogeneous polymerization catalysis

Polymerization catalysts are perhaps the only class of catalysts that are not routinely recovered and recycled on a large scale. Because catalyst recovery and separation from the product polymer is difficult, most polymerization catalysts are single-use entities and in many cases, such as with Ziegler Natta catalysts for olefin polymerization, the catalyst is so highly active it can economically be left in the final polymer product [12-14]. Despite the widespread application of single-use heterogeneous catalysts for olefin polymerization, there are many unique polymers that can be made with less active transition metal-based catalysts, but catalyst disposal with the product is not cost-effective. In other cases, there are reasons why removal of any catalyst residues from the final polymer product can be critically important – for example in polymers for biomedical [15-17] and electronic applications [18-21].

In general there are two types of transition metal polymerization catalysts: (1) catalysts that proceed via coordination-insertion mechanism, where monomer is added between a metal carbon bond, such as metallocene and Ziegler Natta catalysts [12-14], and (2) catalysts that initiate or mediate the polymerization, but are never chemically bonded to the polymer product. There are examples of both types of catalysts that can be potentially recycled (**Figure 1.4**).

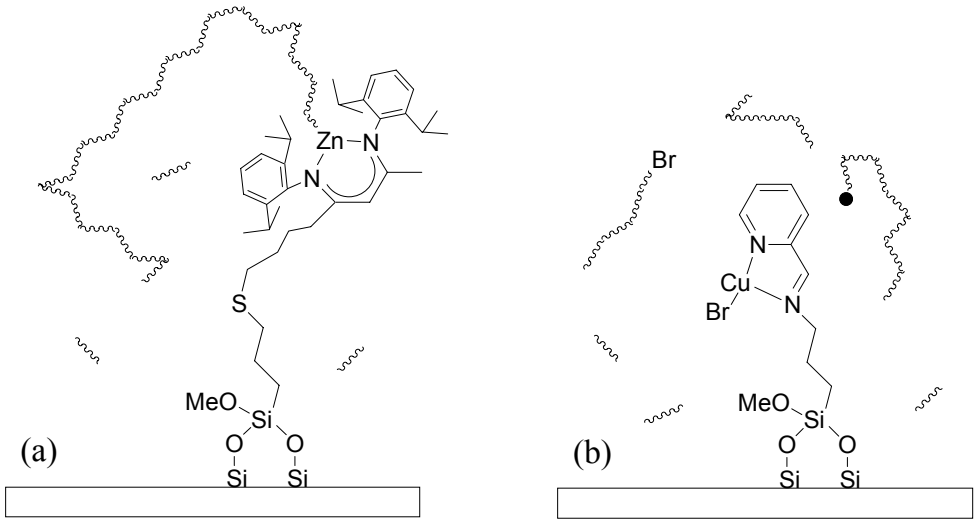

Figure 1.4 Example of two immobilized polymerization systems. Monomer addition via cis insertion mechanism for silica-immobilized Zn-BDI complex [22, 23] (a) and transition metal mediated ATRP of immobilized Cu/PMI complex [24] (b).

For example, Yu and Jones recently immobilized a Zn-β-diiminate (BDI) complex [25] that is active for lactide polymerization and epoxide/CO_2 copolymerizations on various silica supports (**Figure 1.4a**) [22, 23]. Like Ziegler Natta polymerization catalysts, propagation proceeds via a monomer coordination-insertion mechanism, thereby forming a new metal-polymer covalent bond after each addition. However, the recovered catalysts were only moderately effective in recycle experiments and significant amounts of polymer remained associated with the solid catalysts after use [26]. A final reaction quench to cleave the bond between the polymer and metal resulted in decomposition of the metal center, highlighting a difficulty with attempted recycle with metal complex catalysts that operate by a coordination-insertion mechanism. Theoretically this catalyst could be recycled, but in practice, the right quenching and catalyst regeneration process has not been elucidated.

In contrast, effective recovery of polymerization catalysts that never contain a covalent bond between the catalyst and the growing polymer chains is much easier, as no problematic quenching step is necessary. Indeed such a system exists in controlled radical polymerizations mediated by transition metal complexes, or Atom Transfer Radical Polymerization (ATRP) (**Figure 1.4b**). In this polymerization, the transition metal complex regulates the halogen transfer process, thereby keeping the radical concentration low and allowing for concise macromolecular control and growth of the polymer chains. The following chapter will give an overview of ATRP.

Preparation of heterogeneous catalyst

The preparation and investigation of immobilized metal complexes has been studied for many years now. The results of these studies have yielded many different synthetic strategies for immobilizing metal complexes. In general there are two types of methodologies for immobilizing metal complexes; the first involves inclusion of the metal complex in the volume of the matrix and the second involves immobilization of the complex on the matrix surface [6-8, 27]. Further classification of the catalyst type can be distinguished by the type matrix (solid support), nature of catalyst attachment to the solid support, and nuclearity of the attached active center. These factors must be considered collectively when designing the "ideal" catalyst for the desired catalytic reaction system.

The simplest method for preparing a solid immobilized catalyst is the inclusion of metal complexes in the volume of the matrix. The supports are often organic polymers or inorganic solids that contain a tortuous or an ordered pore structure. Impregnation [28, 29], sol-gel [30, 31], and ship-in-the-bottle [32, 33] syntheses are a few examples of

techniques that have been devised to physically absorb (physisorption), chemically bond, or entrap metal complexes in these supports (**Figure 1.5**). The common theme is to dissolve the metal complex or precursors in a solvent and then disperse the solution in with the support. Then the metal complex incorporates inside the pore or precursors assemble a metal complex inside the pore of the solid. The solvent or any undesired material is subsequently evaporated, extracted, or burned away to form the final catalyst particle. The metal complex is then effectively immobilized by physisorption, a chemical bond, or encapsulation with the support framework.

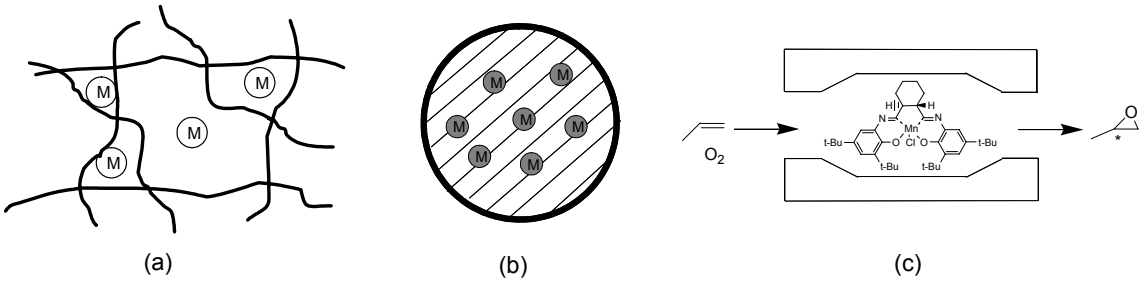

Figure 1.5 Examples of entrapped transition metal complexes: in a porous organic polymer (a), in a porous inorganic solid (b), and reaction scheme for epoxidation reaction using entrapped Jacobsen's catalyst synthesized via ship-in-a-bottle technique [34] (c).

The catalyst immobilization and support structure together allow for reactants and products to diffuse in and out of the catalyst particle and prevents the metal complexes from diffusing out of porous polymer, sol-gel, and zeolite structures because of the metal complex interaction with the support or the smaller dimension of the pore opening. **Figure 1.5c** shows how an entrapped Jacobsen's Mn-Salen catalyst prepared via ship-in-a-bottle technique can be used for the asymmetric olefin epoxidation reaction [34]. In addition, for the support to allow for effective mass transport and metal complex accessibility, the stability of the metal complex inside the support under reaction conditions and the mechanical strength of the support play an important role, as they dictate whether the complex will decompose or diffuse/leach into the reaction medium. Leaching metal complexes into the liquid phase will prevent the full recovery of all catalytic species and potentially contaminate products that need to be metal-free.

These immobilization methods have mainly been used for small molecule catalysis because the size restriction of the pore openings will only allow for relatively small substrates and products to diffuse in and out. There is limited application of these catalysts for olefin polymerization for the production of high molecular weight polymers, with those that do exist mostly single-use entities such as supported metallocene and Ziegler Natta catalysts [12-14]. Generally, these polymerizations are performed in the gas phase, with the catalyst fracturing and allowing for rapid polymer growth under reaction conditions. In these cases, the concentration of the metal in the final polymer is extremely low due to the high activity of the catalysts and therefore it is not necessary to recover the catalyst.

The second methodology for supporting metal complexes is immobilization of the complexes on the support surface, which now includes supports that are nonporous in addition to porous. **Figure 1.6** shows examples of catalysts synthesized by these methods. The metal complex can be immobilized on the solid support surface via physisorption, ion-exchange, a covalent bond (metal-support bond), or covalent ligand tethering (ligand-support bond). Covalent ligand tethering (anchoring) is the most versatile method because of its applicability towards a broad range of suitable catalysts, reaction types, and solvents (**Figure 1.6b**) [7, 35-37].

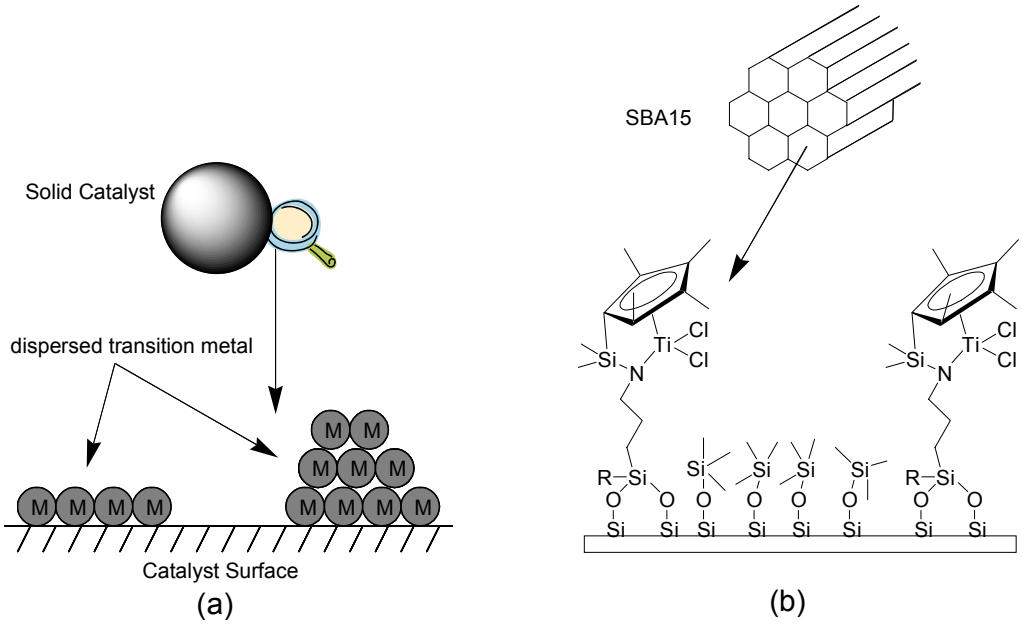

Figure 1.6 Examples of transition metal complexes supported on solid surface: dispersed metal (a) and a site-isolated SBA15 immobilized Ti-CGC synthesized by patterning methodology [38, 39] (b).

Immobilized homogeneous catalysts with well-defined, homogeneously dispersed active sites are the most difficult to synthesize, hence immobilized molecular catalysts tend to be multi-site solids. To claim the preparation of a single-site catalyst, extensive characterization is required to prove complete uniformity of all immobilized species, and as such, there are no proven examples in the open literature of a purely single-site catalyst[2]. In addition, primarily only academic researchers are interested in preparing single-site catalysts, whereas industrial researchers are more concerned with optimizing catalytic properties, such as rates, selectivity, yields, and most importantly, economics. Nevertheless, catalysts synthesized by these methods have been used in a wide range of catalytic applications ranging from small molecule conversions to polymerizations, and are utilized by a diverse group of end-users including organic chemists, academic researchers and by a number of industries including the fine chemical, pharmaceutical, and petrochemical industries.

Table 1.1 summarizes the applicability and drawbacks of the above mentioned immobilization strategies. Not only is it important to select the correct strategy to immobilize the metal complexes to ensure catalytic activity and selectivity is maintained, proper selection of the catalyst support is also crucial to the immobilization and reaction process.

[2] However, there are many literature reports that claim "single-site" heterogenized homogeneous catalyst preparation.

Table 1.1 Summary of common immobilization strategies for metal complexes

Immobilization Method	Physisorption	Entrapped, Ship-in-a-bottle	Ion pair	Covalent ligand tethering
Applicability	Broad	Restricted	Restricted	Restricted
Drawback	Competition with solvents	Substrate size and diffusion	Competition with polar or ionic substrates	Difficulty of preparation

Catalyst support

In practice, the key criteria and properties for an effective catalyst support are (1) inertness to undesired reactions, (2) mechanical stability, (3) stability under reaction and regeneration conditions, (4) high surface area solids (usually), and (5) low cost [6-8]. For transition metal complexes, an essential requirement of these solids is chemical inertness between the solid support and the organometallic active metal center, because the active center may deactivate via interactions with the support. Several examples of supports are shown in **Figure 1.7**. A variety of cross-linked polymers are used as catalyst supports. These supports are designed to be more soluble or swellable in solvent at reaction temperature, and catalyst recovery is achieved upon catalyst precipitation below reaction temperature (**Figure 1.7a**). However, organic polymer supports can be expensive, therefore silica is commonly used as a support because it is relatively inert to most chemical reagents and inexpensive **(Figure 1.7b)**. Silica supports are also more mechanically and thermally stable then organic supports. However when immobilizing

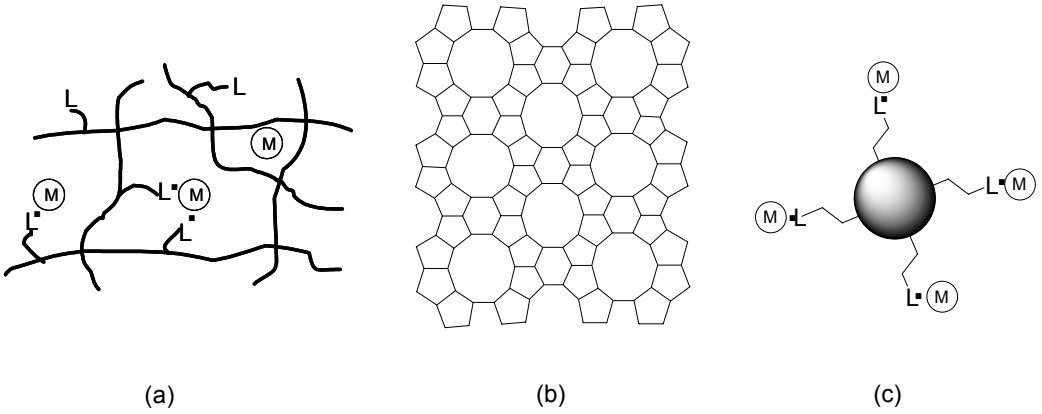

(a) (b) (c)

Figure 1.7 Examples of supports for the immobilization of transition metal complexes: polymer (a), ZSM-5 zeolite (b), and inorganic solid (c). M = metal and L = ligand.

metal complexes, silanols on silica can interact strongly with the complex and change the chemical nature of the metal center. For this reason, great care must be taken when designing silica-supported metal complexes.

When designing a heterogeneous catalyst, one routinely uses porous supports because porous solids have higher surfaces that allow for higher site density per unit volume of catalyst. However, the use of porous supports for polymerization catalysts when catalyst recovery is important can be troublesome. In addition to mass transport limitations caused by polymer in the pores, the product polymer can become entangled in the pores, preventing easy separation of the catalyst from the product polymer. Polymerizations are not reactions where product desorption is straightforward. To avoid this problem, non-porous solids can be used when catalyst recovery is desired (**Figure 1.7c**). The lack of internal porosity eliminates polymer entanglement. However, diameters of most supports are typically on the micron scale. Particles larger than 1μm can be recovered in batch reactors by filtration, sedimentation, or centrifugation. However, these solids have low external surface areas that limit active site density,

yielding low reaction rates. To circumvent the aforementioned shortcomings of both porous and large non-porous supports, one must go to nanosize nonporous supports. These supports (50-100 nm diameter) have a very large SA/V ratio.

Summary

The design of heterogenized homogeneous catalysts is not trivial, for this reason researchers must take a rational approach to catalyst design that encompasses many key aspects including: (1) choice of immobilization method, (2) selection of the support, (3) optimization of reaction conditions and, (4) maximizing catalyst recovery and (5) recyclability. Furthermore, to be industrially attractive, the catalyst needs to possess similar or better catalytic performance than the state-of-the-art process, possess high mechanical and thermal stability, and be economically viable. Despite the growing interest in heterogeneous polymerization catalysis, the majority of the polymerization catalysts used industrially are single-use entities that are left in the polymer product. Recoverable and recyclable polymerization catalysts have not reached the industrial utility of single-use catalysts because the catalyst and product separation have not become economical. Therefore academic and industrial researchers need to further expand the fundamental science and engineering of recyclable polymerization catalysis to gain an understanding of critical parameters that allow for the design of economically viable, recoverable solid polymerization catalysts.

References

[1] Encylcopaedia Britannica Online, Encylcopaedia Britannica, Inc. http://www.britannica.com, 2005.

[2] J. Schwartz, Accounts of Chemical Research 18 (1985) 302.

[3] Y. Lin and R. G. Finke, Inorganic Chemistry 33 (1994) 4891.

[4] J. D. Aiken, III, Y. Lin, and R. G. Finke, Journal of Molecular Catalysis A: Chemical 114 (1996) 29.

[5] A. Nakamura and M. Tsutsui, Principles and Use of Homogeneous Catalysis, 1983.

[6] C. N. Satterfield, Heterogeneous Catalysis in Industrial Practice. 2nd Ed, McGraw-Hill, Inc., New York, NY, 1991.

[7] Y. I. Yermakov, B. N. Kuznetsov, and V. A. Zakharov, Studies in Surface Science and Catalysis, Vol. 8: Catalysis by Supported Complexes, Elsevier Scientific Publishing Company, New York, NY, 1981.

[8] J. M. Thomas, J. W. Thomas, and Editors, Principles and Practice of Heterogeneous Catalysis, 1996.

[9] E. N. Jacobsen, W. Zhang, A. R. Muci, J. R. Ecker, and L. Deng, Journal of the American Chemical Society 113 (1991) 7063.

[10] D.-W. Park, S.-D. Choi, S.-J. Choi, C.-Y. Lee, and G.-J. Kim, Catalysis Letters 78 (2002) 145.

[11] L. Canali, E. Cowan, C. L. Gibson, D. C. Sherrington, and H. Deleuze, Chemical Communications (Cambridge) (1998) 2561.

[12] G. G. Hlatky, Chemical Reviews (Washington, D. C.) 100 (2000) 1347.

[13] H. C. L. Abbenhuis, Angewandte Chemie, International Edition 38 (1999) 1058.

[14] F. Ciardelli, A. Altomare, and M. Michelotti, Catalysis Today 41 (1998) 149.

[15] B. J. O'Keefe, S. M. Monnier, M. A. Hillmyer, and W. B. Tolman, Journal of the American Chemical Society 123 (2001) 339.

[16] M. H. Chisholm, J. Gallucci, and K. Phomphrai, Chemical Communications (Cambridge, United Kingdom) (2003) 48.

[17] P. Dobrzynski, J. Kasperczyk, H. Janeczek, and M. Bero, Macromolecules 34 (2001) 5090.

[18] K. Matyjaszewski, Controlled Radical Polymerization, American Chemical Society, Washington, DC, 1998.

[19] K. Matyjaszewski, Controlled/Living Radical Polymerization: Progress in ATRP, NMP, and RAFT, Oxford University Press, Washington, DC, 2000.

[20] K. Matyjaszewski, Advances in Controlled/Living Radical Polymerization, Oxford University Press, Washington, DC, 2003.

[21] K. Matyjaszewski and J. Xia, Chemical Reviews 101 (2001) 2921.

[22] K. Yu and C. W. Jones, Organometallics 22 (2003) 2571.

[23] K. Yu and C. W. Jones, Journal of Catalysis 222 (2004) 558.

[24] D. M. Haddleton, D. Kukulj, and A. P. Radigue, Chemical Communications (1999) 99.

[25] M. Cheng, E. B. Lobkovsky, and G. W. Coates, Journal of the American Chemical Society 120 (1998) 11018.

[26] C. W. Jones, M. W. McKittrick, J. V. Nguyen, and K. Yu, Topics in Catalysis (2004) In press.

[27] J. A. Schwarz, C. Contescu, and A. Contescu, Chemical Reviews (Washington, D. C.) 95 (1995) 477.

[28] A. J. Van Dillen, R. J. A. M. Terorde, D. J. Lensveld, J. W. Geus, and K. P. De Jong, Journal of Catalysis 216 (2003) 257.

[29] J. R. Regalbuto, M. Schrier, X. Hao, W. A. Spieker, J. G. Kim, J. T. Miller, and A. J. Kropf, Studies in Surface Science and Catalysis 143 (2002) 45.

[30] F. Gelman, J. Blum, and D. Avnir, New Journal of Chemistry 27 (2003) 205.

[31] F. Gelman, J. Blum, and D. Avnir, Journal of the American Chemical Society 124 (2002) 14460.

[32] C. Schuster and W. F. Holderich, Catalysis Today 60 (2000) 193.

[33] R. A. Sheldon, I. W. C. E. Arends, and H. E. B. Lempers, Catalysis Today 41 (1998) 387.

[34] G. Gbery, A. Zsigmond, and K. J. Balkus, Jr., Catalysis Letters 74 (2001) 77.

[35] F. Ciardelli, G. Braca, C. Carlini, G. Sbrana, and G. Valentini, Journal of Molecular Catalysis 14 (1982) 1.

[36] D. C. Bailey and S. H. Langer, Chemical Reviews (Washington, DC, United States) 81 (1981) 109.

[37] L. L. Murrell, Adv. Mater. Catal. (1977) 235.

[38] M. W. McKittrick and C. W. Jones, Journal of Catalysis 227 (2004) 186.

[39] M. W. McKittrick and C. W. Jones, Journal of the American Chemical Society 126 (2004) 3052.

CHAPTER 2

INTRODUCTION TO ATOM TRANSFER RADICAL POLYMERIZATION: HOMOGENEOUS AND HETEROGENEOUS SYSTEMS

Background

Controlled radical polymerization

The synthesis of new polymeric materials with well-defined compositions, architectures, and functionalities has long been a goal of polymer chemistry. As early as 1936, Ziegler proposed that anionic polymerization of styrene and butadiene by addition of monomer to an alkyl lithium initiator proceeds without chain transfer or termination [1]. During this polymerization, the number of polymer molecules remains constant. Szwarc later coined the term "living" polymerization for the method because the chain ends remain active until killed [2]. Since there is no termination, the active chain ends remain after all the monomer has been polymerized, and when fresh monomer is added, polymerization resumes.

The general characteristics of a "living" polymerization are: (1) all chain ends grow at the same rate, (2) the molecular weight is determined by the ratio of concentrations of the monomer and initiator, (3) very narrow molecular weight distribution characterized by the polydispersity (M_w/M_n) near one (M_w is weight average molecular weight and M_n is number average molecular weight), and (4) linear evolution of molecular weights with conversion [3]. This unique method of polymerization can efficiently produce polymers and block copolymers of predetermined molecular weights with distinctive architectural structures and physical properties.

Before 1991 much of the academic and industrial research on living polymerization was focused on anionic [4], cationic [5], coordination [6], and ring-opening polymerizations [7]. The realization of living free radical polymerizations has not yet occurred, even though conventional radical polymerization processes accounted for approximately 50% of all commercially produced polymers and was responsible for >3% of GNP in the United States [8]. Conventional free radical polymerization is a more attractive method than those mentioned above because of its ability to polymerize a variety of monomers over a wide range of conditions and produce high molecular weight polymers. Furthermore, the radical process is more tolerant of functional groups, water, and impurities [9]. However, the development of a "true" living free radical polymerization has not overcome the main deficiency of radical polymerizations -- a *complete absence* of chain termination events due to bimolecular radical recombination and disproportionation – therefore there are no living free radical polymerizations.

In the past 10 years, an exponential growth in the development and understanding of new controlled radical polymerization (CRP) methods has occurred. CRP methods can produce polymers with polydispersities lower than 1.5 and reaction times on the scale of hours, compared to PDI > 2 and reactions times of seconds for conventional free radical polymerizations[4]. Currently there are three CRP systems which seem to be most successful (1) CRP mediated by nitroxides [10] (e.g., TEMPO), (2) CRP mediated degenerative transfer by dithioesters [11] and xanthates [12, 13] (RAFT and MADIX process, reversible addition fragmentation chain transfer and macromolecular design via the interchange of xanthates, respectively), and (3) CRP mediated by transition metal complex catalyzed Atom Transfer Radical Polymerization (ATRP) [14-16]. **Figure 2.1**

shows typical molecular species that regulate the radical concentration in the above mentioned polymerization methods.

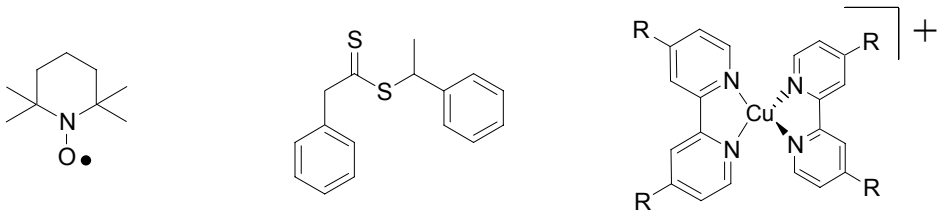

(a) (b) (c)

Figure 2.1 Molecular species that regulate radical concentration in CLRP methods. Nitroxide mediated TEMPO (a), RAFT degenerative transfer mediated by dithioester PEPDTA (b), and transition metal mediated ATRP CuBr/bipyridine complex (c).

Collectively, these methods are based on establishing a dynamic equilibrium between growing free radicals and various types of dormant species. Although these new methods possess the majority of the characteristics of "living" polymerization, a small amount of chain termination, chain transfer, and side reactions does occur (<10%) [8, 17, 18]. Consequently, it does not meet the strict definition of "living" polymerization, and the methods are more properly termed controlled/"living" radical polymerizations (CLRP). In addition to the characteristics of "living" polymerizations, CLRP methods are characterized by [8, 17, 18][3]:

[3] It is understood that controlled radical polymerization methods do not meet the current definition of "living" polymerizations (absense of termination). However for consistency with the literature nomenclature, we will continue to use controlled/"living" radical polymerizations to describe these systems. For more on this debate please refer to J. Polym. Sci. Polym. Chem. A 38 (2000) 1706.

Characteristics of CLRP method

1) Fast exchange between dormant species and growing radicals.

2) A small portion of chains involved in chain breaking reactions.

3) Fast and quantitative initiation.

4) Linear kinetic plots in semi-logarithmic coordinates ($\ln[M_o]$ /$[M_t]$ vs. time), if the reaction is first order in monomer concentration. Deviation from linearity may suggest termination or slow initiation.

5) Linear evolution of molecular weights with conversion. Lower molecular weights are indicative of chain transfer while higher molecular weights suggest inefficient initiation or coupling.

6) Polydispersities should decrease with conversion. PDI tend to increase at higher conversions because of poor transport and termination.

7) End functionalities are not affected by slow initiation or slow exchange process, but are only reduced by chain breaking.

Figure 2.2 shows kinetic plots of prototypical well-controlled radical polymerizations and outlines deviations from ideality [8, 17, 18].

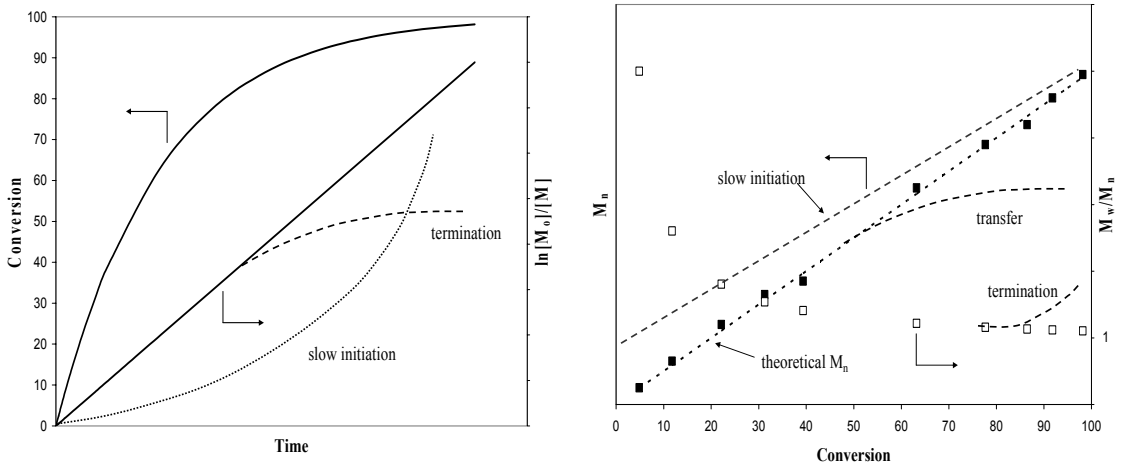

Figure 2.2 Prototypical kinetic plots for controlled radical polymerization. Conversion and $\ln[M_o]/[M_t]$ vs. time (left) and evolution of M_n and M_w/M_n vs. conversion (right).

Among the most versatile of these methods is ATRP because of its tolerance to water and other protic species, and ability to polymerize a wide range of monomers in various solvents under a variety of reaction conditions. It is clearly advantageous over anionic and cationic polymerizations that can be very sensitive to protic reagents and require stringent reaction conditions [4, 5]. Unfortunately, soluble ATRP homogeneous polymerization catalysts cannot be used in most industrial continuous and batch processes because catalytic efficiency is low, thereby requiring long reaction times and a large amount of catalyst relative to monomer. In some cases, post-treatment methods to remove residual catalysts increase the cost, but also waste the catalyst. Since ATRP is catalyzed by transition metal complexes, it is amenable to metal complex immobilization on solid supports. In addition, the polymerization proceeds via an atom transfer mechanism; at no point during the polymerization are the metal complexes covalently bonded to growing polymer chains. Thus, the potential to recover and recycle the transition metal ATRP catalyst exists.

Atom transfer radical polymerization

Homogeneous ATRP

Controlled/"living" radical polymerizations mediated by metal halide complexes or ATRP was first reported in 1995 independently by Matyjaszewski [14, 15, 19] and Sawamoto [16] utilizing Cu(I)X/bipyridines (X = Cl, Br) and $RuCl_2(PPH_3)_3$, respectively. ATRP finds its roots in atom transfer radical addition (ATRA) [20]. ATRA is an efficient method for carbon-carbon bond formation in organic synthesis. In these reactions, a transition metal catalyst acts as a carrier of the halogen atom in a reversible redox process. By analogy, ATRP is a sequence of ATRA reactions forming long polymer chains (**Figure 2.3**).

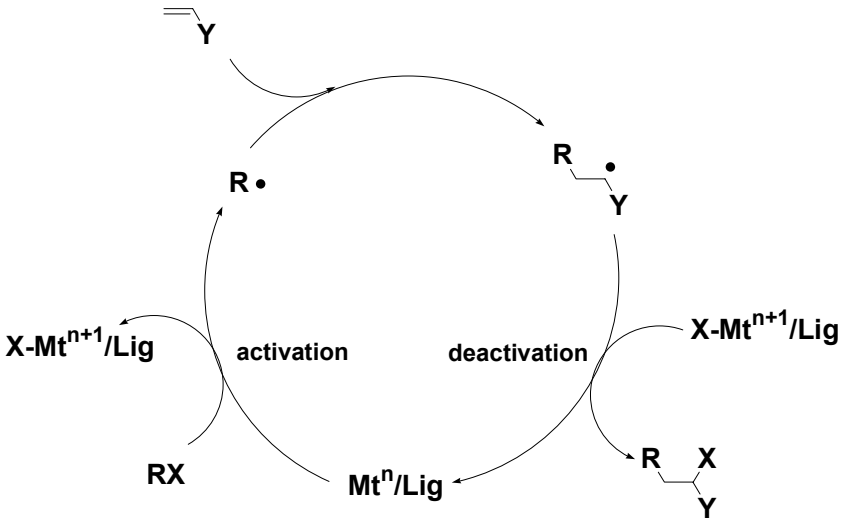

Figure 2.3 Mechanism for transition metal catalyzed ATRA [20].

In an ATRP polymerization, a monomeric or polymeric alkyl halide (R-X or P_n-X) transfers its halogen atom reversibly to a transition metal complex (M_t^n-X/Ligand), forming an organic radical ($P_n^\bullet$) and a higher oxidation state transition metal complex (X-M_t^{n+1}-X/Ligand) (**Figure 2.4**) [8, 9, 17, 18]. The equilibrium between the M_t^n-X/Ligand and X-M_t^{n+1}-X/Ligand species is strongly shifted towards lower oxidation M_t^n-X/Ligand complex ($k_{deact} >> k_{act}$); therefore the radical concentration is kept low, allowing for controlled monomer addition with reduced termination (propagation is first order in radical concentration, termination is second order). However, unlike living polymerization techniques, chain transfer and termination do occur, but no more than ~10% of the total growing chain terminates during the initial stages of polymerization.

A successful ATRP will not only have a very small contribution of chain termination, but also have uniform growth of all other polymer chains, which is accomplished through fast initiation and rapid reversible deactivation. The catalyst is the most important component of ATRP because it determines the position of the atom transfer equilibrium and the dynamics of exchange between the dormant and active species. The requirements for efficient ATRP catalyst are: (1) the metal center must have two readily accessible oxidation states separated by one electron, (2) the metal must have a reasonable affinity toward a halogen, (3) the coordination sphere around the metal should be expandable upon oxidation to accommodate a halogen, and (4) the ligand must complex to the metal rather strongly [9]. **Figure 2.5** shows some examples of different materials/polymers that can be synthesized by ATRP in terms of composition, topology, and functionality [9].

Overall reaction

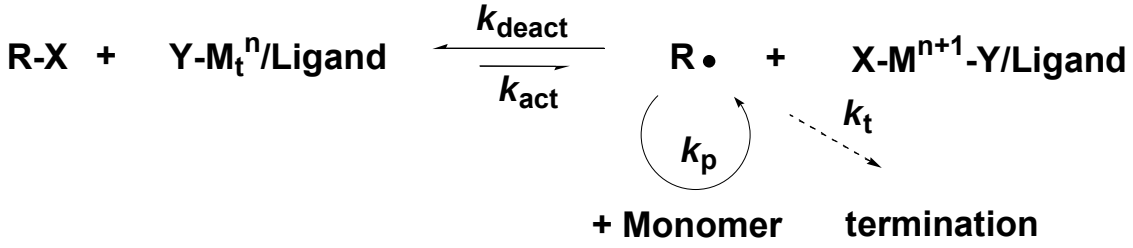

X = Cl, Br, or I

M_t^n = Cu^I, Ru^{II}, Fe^{II}, Ni^{II}, etc.

Initiation

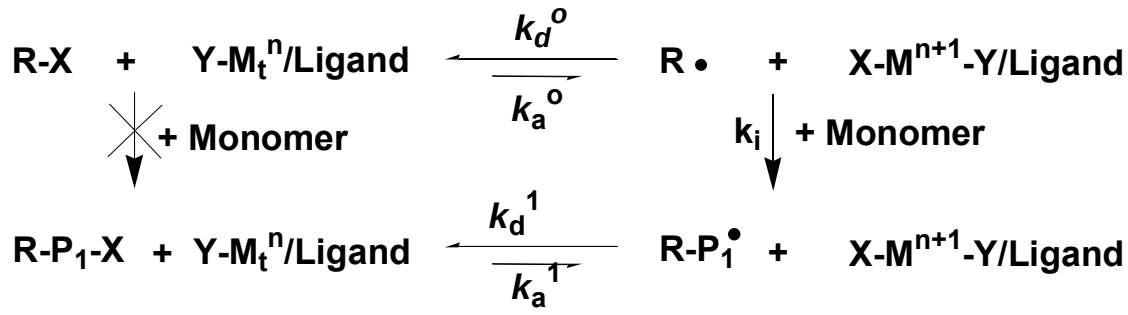

Propagation

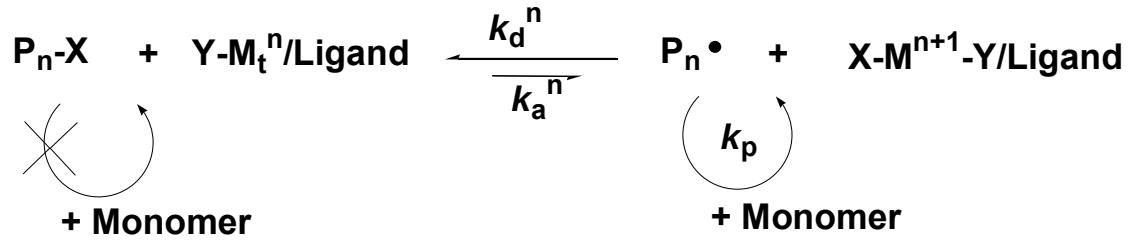

Termination

Figure 2.4 Mechanism for transition metal catalyzed ATRP.

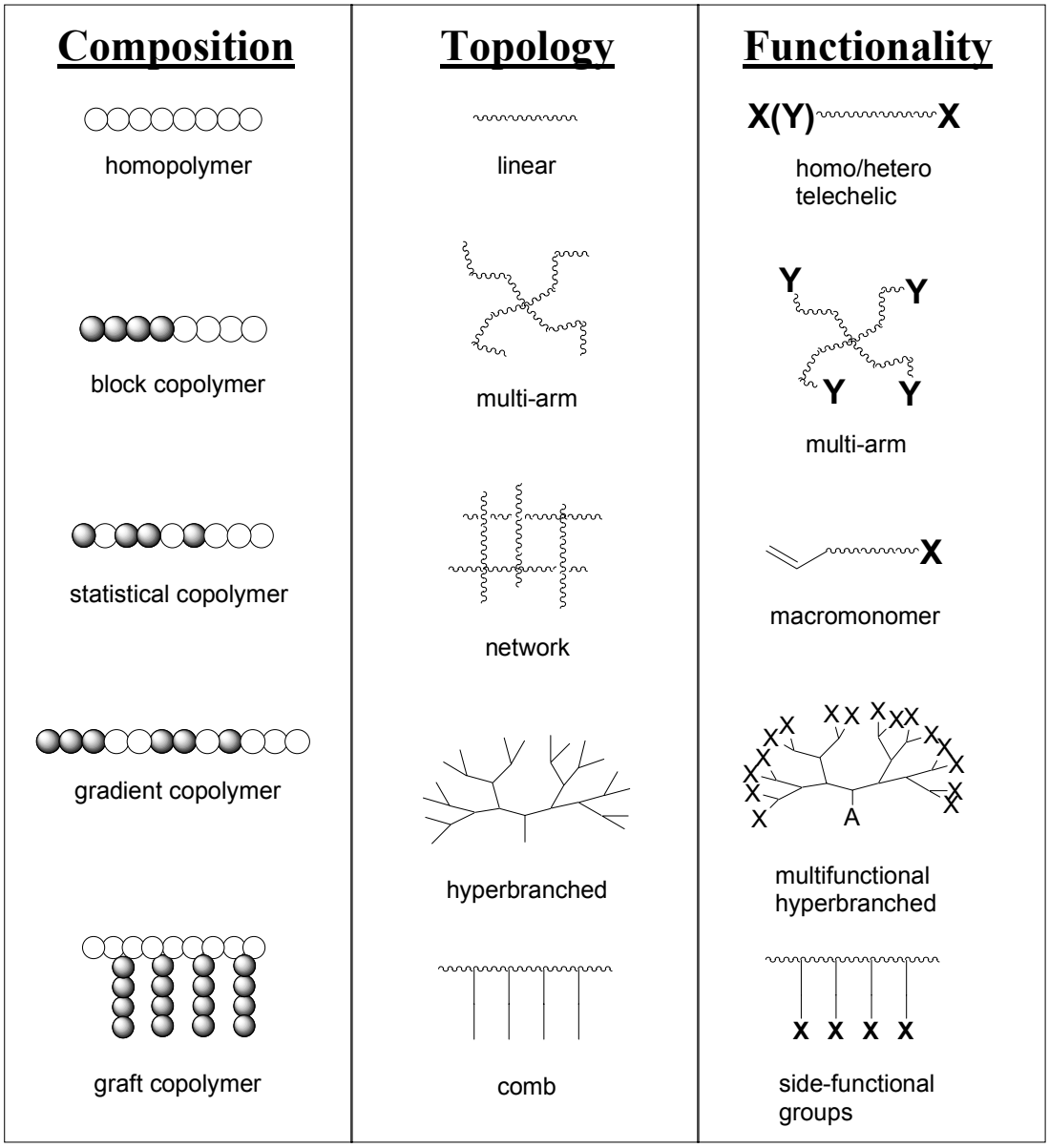

Figure 2.5 Materials made by ATRP adapted from [9].

A typical ATRP system consists of the monomer, an initiator with a transferable halogen, a transition metal catalyst with a suitable ligand, and sometimes an additive. What makes ATRP so versatile is the wide range of conditions and combination of components that can be used. Various systems based on Cu [14, 15, 21], Ru [16, 22, 23], Fe [24, 25], Ni [26, 27], and Re [28] have been developed for ATRP of styrene, (meth)acrylates, (meth)acrylamides, and acrylonitrile to produce well-defined polymers [9]. The polymerization may be carried out in the bulk, in solution, or in aqueous heterogeneous systems (i.e., emulsions, suspensions [9]). The reaction temperatures are rather mild (room temperature to 150 ºC). Lastly, the end functionality can be easily displaced. The copper-based catalysts are among the most efficient from the point of view of rates, selectivities, and cost.

One of the major challenges in ATRP is the removal and recycling of the catalyst, as large amounts of catalyst residue in the polymer may prevent its exploitation industrially [9, 29]. In a typical ATRP recipe, the initiator-to-catalyst ratio is usually 1:1 (typically 0.1-1.0% w/w), which is one catalyst molecule mediating one polymer chain, although in some catalyst systems, catalyst concentrations can be as low as 10 mol% to initiator [30-32].[4] Even so, this accounts for a large amount of metal needed to mediate a controlled polymerization. Generally, the Cu(I) species is a dark reddish color and the Cu(II) species is green; consequently, the residual catalyst in the polymer mixture deeply colors the product. Additional purification is required to remove the catalyst. Passing the

[4] At first glance, ATRP "catalysts" may not seem to meet the strict definition of a catalyst. ATRP is a transition metal mediated polymerization that is stoichiometric in metal for most polymerization recipes (i.e., one catalyst complex mediating the growth of one polymer chain). In this regard, it can be best viewed as a chain transfer agent. However, since in the absence of the catalyst the polymerization does not get initiated and since each complex mediates multiple activation and deactivation steps (turnovers), the complexes are commonly referred to as catalysts.

polymer solution through silica or alumina gel, or precipitation of the polymer from solution is commonly done on the laboratory scale. The disadvantages of these types of post-treatment are cost (due to catalyst waste), time, difficulties in scaling up, loss of polymer, and difficulties in separating the catalyst from functional polymers that interact with the copper catalyst. There are several approaches that have been evaluated for catalyst removal, including treatment with ion-exchange resin [33], use of fluorous biphasic systems [34], use of ionic liquids [35-37], and use of precipitons [38]. These methods require post-treatment of polymerization solution. Another method that provides a convenient way to recover the catalyst is catalyst immobilization. Immobilization of the ATRP transition metal complexes on organic or inorganic support materials is the most attractive method for recovery, because the catalyst can be recovered easily and potentially recycled. Further fundamental understanding of theoretical and practical ATRP methodologies leading to industrial utility will be important because it is projected that CLRP may affect a market of $20 billion/year in such areas as adhesives, dispersants, coatings, surfactants, thermoplastic elastomers, lubricants, and gel additives, as well as in many electronic and biomedical applications [8, 9, 17, 18, 29].

Heterogeneous ATRP

There are several reports in the literature describing methods to immobilize ATRP catalysts on various supports [29]. Three types of catalyst immobilization methods have been generally employed (**Figure 2.6**): (**I**) catalyst physically adsorbed (physisorbed) on silica [39-42], (**II**) catalyst covalently immobilized (tethered) on silica [43-54] and polymers [46, 55-59], and (**III**) a dual immobilized catalyst/soluble deactivator system [44, 60-64]. In general copper catalyzed systems have been the most successful while utilizing aminoimines, bipyridine, and multidentate aliphatic amines as ligands.

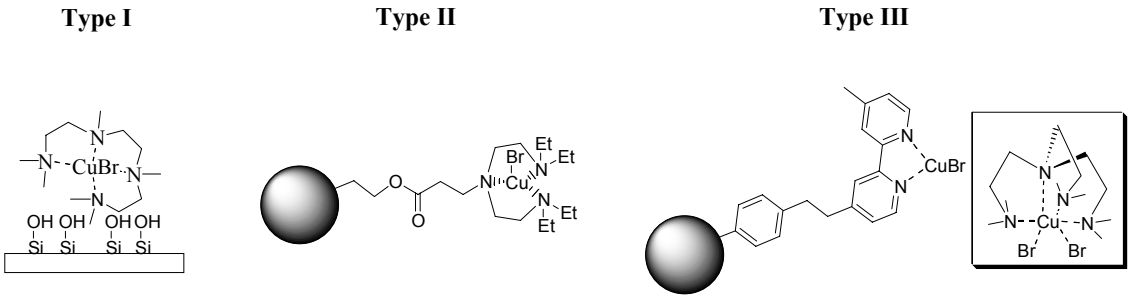

SiO_2/HMTETA/CuBr SiO_2-TEDETA/CuBr PS8-dMBpy/CuBr:Me_6TREN/$CuBr_2$

Figure 2.6 Three different types of immobilized ATRP catalyst. Physisorption (Type I), covalently immobilized (Type II), and dual immobilized catalyst/soluble deactivator system (Type III).

Catalysts of type I are easily prepared, but catalyst leaching often occurs because the catalyst complex is not firmly bonded to the support surface. Tethered catalysts of type II are generally harder to prepare but allow for facile catalyst recovery and recycle. The downside to these systems is that the surface-tethered complexes can be less accessible to the growing polymer chains than leached or homogeneous complexes. In this system, transport limitations manifest themselves as increased polymerization rates (due to decreased deactivation events), higher molecular weights, and broad polymer polydispersities. To circumvent these problems, catalysts of type III were developed. Type III catalyst systems have shown some of the best polymerizations results. A soluble deactivating catalyst is introduced in very small quantities to help improve the deactivation process, thus acting as a molecular shuttle between the growing polymer chains and the surface-tethered complexes (**Figure 2.7**). Without the deactivator, many monomer units are added to the growing polymer chain before the growing radical is deactivated by reaction with a deactivator complex (**Figure 2.7 b-d**). In contrast, with the deactivator, only a small number of monomer units are added before the soluble deactivator caps the growing polymer chains (**Figure 2.7 g-i**). Although this method works well, there are several drawbacks to this system. Due to the presence of some homogeneous species, there will always be metal contaminants in the product polymer that will need to be removed. Furthermore, these immobilized/soluble hybrid systems have only been successful for polymer supports [44, 60-64], which can be more expensive than silica supports.

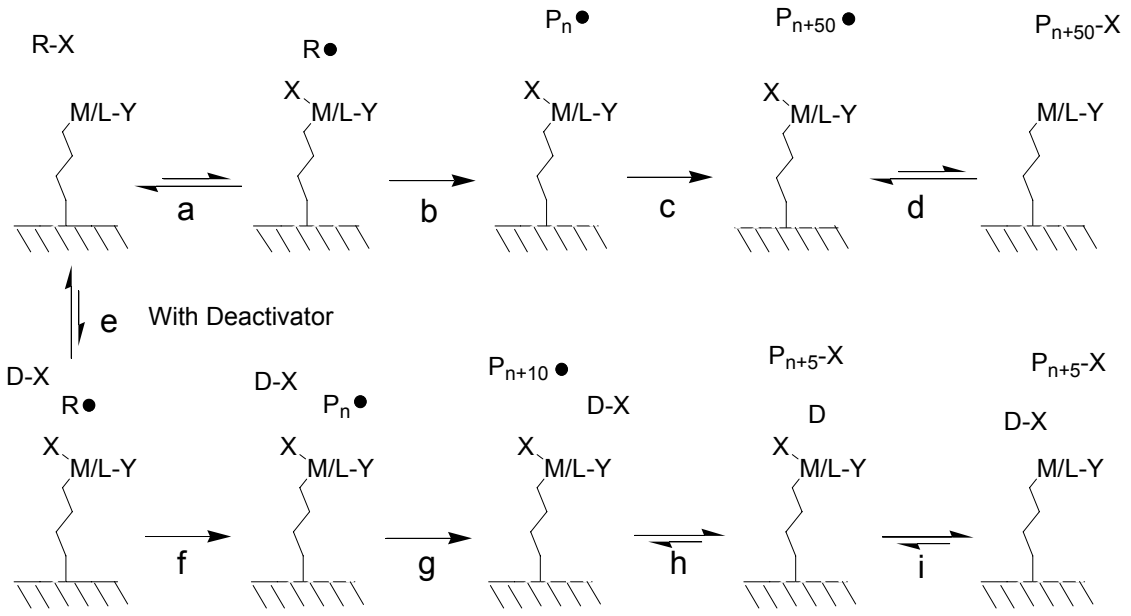

Figure 2.7 Mechanism for dual immobilized catalyst/soluble deactivator system.

A final catalyst immobilization method that does not fit into the above categories is the reversibly hydrogen-bonded catalyst recently reported by Shen and coworkers. **Figure 2.8** shows how they utilized a multi-point hydrogen bonding interaction to immobilize a CuBr/ligand complex to its complementary hydrogen bonding pair that was covalently immobilized on silica [65] or a polymer resin [66]. When the polymerization reaches reaction temperature, the hydrogen bonds dissociate and release the catalysts from the solid support, and the polymerization proceeds in the liquid phase. After the polymerization is complete, the temperature is lowered and the catalysts reattach to the support via hydrogen bonds. Some catalyst is eventually lost due to entanglement in the polymer (up to 2%).

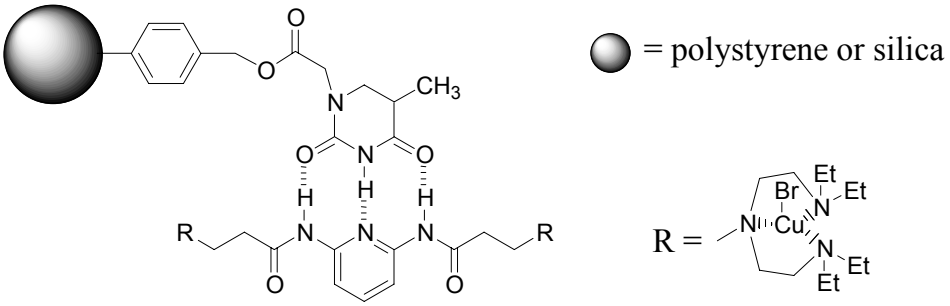

Figure 2.8 Shen's immobilized reversible hydrogen-bonded ATRP catalyst [65, 66].

From the many ATRP catalyst systems described above, immobilizing an effective ATRP polymerization catalyst is not trivial because not all systems resulted in a recoverable and recyclable catalysts. Of the many immobilization methods described, covalently tethered ATRP catalysts appeared to show the most promise in terms of control, stability, and recyclability. Now that the area of covalently tethered ATRP catalyst has matured resulting in some well-behaved and recoverable systems, a new direction must be taken to drive ATRP towards eventual industrial practice. In addition to immobilizing new ATRP complexes, optimization of reported tethered systems should continue. Can these systems be improved upon? What are the limitations of these catalysts? These are some of the questions that still need to be addressed. The motivation and goals of this thesis are outlined in the following chapter.

References

[1] K. Ziegler, Angewandte Chemie 49 (1936) 499.

[2] M. Szwarc, M. Levy, and R. Milkovich, Journal of the American Chemical Society 78 (1956) 2656.

[3] O. W. Webster, Science 251 (1991) 887.

[4] J. Smid, Journal of Polymer Science, Part A: Polymer Chemistry 40 (2002) 2101.

[5] J. P. Kennedy, Journal of Polymer Science, Part A: Polymer Chemistry 37 (1999) 2285.

[6] V. C. Gibson and E. L. Marshall, Comprehensive Coordination Chemistry II 9 (2004) 1.

[7] R. R. Schrock, Accounts of Chemical Research 23 (1990) 158.

[8] K. Matyjaszewski, Advances in Controlled/Living Radical Polymerization, Oxford University Press, Washington, DC, 2003.

[9] K. Matyjaszewski and J. Xia, Chemical Reviews 101 (2001) 2921.

[10] M. K. Georges, R. P. N. Veregin, P. M. Kazmaier, and G. K. Hamer, Macromolecules 26 (1993) 2987.

[11] J. Chiefari, Y. K. Chong, F. Ercole, J. Krstina, J. Jeffery, T. P. T. Le, R. T. A. Mayadunne, G. F. Meijs, C. L. Moad, G. Moad, E. Rizzardo, and S. H. Thang, Macromolecules 31 (1998) 5559.

[12] P. Corpart, D. Charmot, T. Biadatti, S. Zard, and D. Michelet, (Rhodia Chimie, Fr.). Application: WO 98-FR1316, 1998, p. 70 pp.

[13] D. Charmot, P. Corpart, H. Adam, S. Z. Zard, T. Biadatti, and G. Bouhadir, Macromolecular Symposia 150 (2000) 23.

[14] J.-S. Wang and K. Matyjaszewski, Journal of the American Chemical Society 117 (1995) 5614.

[15] J.-S. Wang and K. Matyjaszewski, Macromolecules 28 (1995) 7572.

[16] M. Kato, M. Kamigaito, M. Sawamoto, and T. Higashimura, Macromolecules 28 (1995) 1721.

[17] K. Matyjaszewski, Controlled Radical Polymerization, American Chemical Society, Washington, DC, 1998.

[18] K. Matyjaszewski, Controlled/Living Radical Polymerization: Progress in ATRP, NMP, and RAFT, Oxford University Press, Washington, DC, 2000.

[19] J.-S. Wang and K. Matyjaszewski, Macromolecules 28 (1995) 7901.

[20] K. Matyjaszewski, Current Organic Chemistry 6 (2002) 67.

[21] D. M. Haddleton, C. B. Jasieczek, M. J. Hannon, and A. J. Shooter, Macromolecules 30 (1997) 2190.

[22] R. M. Johnson, P. S. Corbin, C. Ng, and C. L. Fraser, Macromolecules 33 (2000) 7404.

[23] C. Ng and C. L. Fraser, Polymeric Materials Science and Engineering 80 (1999) 84.

[24] B. Gobelt and K. Matyjaszewski, Macromolecular Chemistry and Physics 201 (2000) 1619.

[25] K. Matyjaszewski, S. Coca, S. G. Gaynor, M. Wei, and B. E. Woodworth, Macromolecules 30 (1997) 7348.

[26] J. P. Youngblood and T. J. McCarthy, Polymer Preprints (American Chemical Society, Division of Polymer Chemistry) 41 (2000) 1554.

[27] C. Moineau, M. Minet, P. Teyssie, and R. Jerome, Macromolecules 32 (1999) 8277.

[28] S. H. Chan, L. S. M. Lam, C. W. Tse, K. Y. K. Man, W. T. Wong, A. B. Djurisic, and W. K. Chan, Macromolecules 36 (2003) 5482.

[29] Y. Shen, H. Tang, and S. Ding, Progress in Polymer Science 29 (2004) 1053.

[30] Y. Inoue and K. Matyjaszewski, Macromolecules 37 (2004) 4014.

[31] J. Gromada, J. Spanswick, and K. Matyjaszewski, Macromolecular Chemistry and Physics 205 (2004) 551.

[32] J. Queffelec, S. G. Gaynor, and K. Matyjaszewski, Macromolecules 33 (2000) 8629.

[33] K. Matyjaszewski, T. Pintauer, and S. Gaynor, Macromolecules 33 (2000) 1476.

[34] D. M. Haddleton, S. G. Jackson, and S. A. F. Bon, Journal of the American Chemical Society 122 (2000) 1542.

[35] T. Sarbu and K. Matyjaszewski, Macromolecular Chemistry and Physics 202 (2001) 3379.

[36] T. Biedron and P. Kubisa, Macromolecular Rapid Communications 22 (2001) 1237.

[37] A. J. Carmichael, D. M. Haddleton, S. A. F. Bon, and K. R. Seddon, Chemical Communications (2000) 1237.

[38] M. E. Honigfort, W. J. Brittain, T. Bosanac, and C. S. Wilcox, Macromolecules 35 (2002) 4849.

[39] Y. Shen, S. Zhu, and R. Pelton, Macromolecular Rapid Communications 21 (2000) 956.

[40] Y. Shen, S. Zhu, F. Zeng, and R. Pelton, Macromolecular Chemistry and Physics 201 (2000) 1387.

[41] Y. Shen, S. Zhu, F. Zeng, and R. H. Pelton, Macromolecules 33 (2000) 5427.

[42] Y. Shen and S. Zhu, AIChE Journal 48 (2002) 2609.

[43] G. Kickelbick, H.-j. Paik, and K. Matyjaszewski, Macromolecules 32 (1999) 2941.

[44] S. C. Hong and K. Matyjaszewski, Macromolecules 35 (2002) 7592.

[45] D. M. Haddleton, D. J. Duncalf, D. Kukulj, and A. P. Radigue, Macromolecules 32 (1999) 4769.

[46] D. M. Haddleton, D. Kukulj, and A. P. Radigue, Chemical Communications (1999) 99.

[47] Y. Shen, S. Zhu, and R. Pelton, Macromolecules 34 (2001) 5812.

[48] Y. Shen, S. Zhu, F. Zeng, and R. Pelton, Journal of Polymer Science, Part A: Polymer Chemistry 39 (2001) 1051.

[49] T. Opstal, K. Melis, and F. Verpoort, Catalysis Letters 74 (2001) 155.

[50] B. De Clercq, F. Lefebvre, and F. Verpoort, Applied Catalysis, A: General 247 (2003) 345.

[51] J. V. Nguyen and C. W. Jones, Journal of Polymer Science, Part A: Polymer Chemistry 42 (2004) 1367.

[52] J. V. Nguyen and C. W. Jones, Journal of Polymer Science, Part A: Polymer Chemistry 42 (2004) 1384.

[53] J. V. Nguyen and C. W. Jones, Macromolecules 37 (2004) 1190.

[54] R. Kroll, C. Eschbaumer, U. S. Schubert, M. R. Buchmeiser, and K. Wurst, Macromolecular Chemistry and Physics 202 (2001) 645.

[55] Y. Shen, S. Zhu, and R. Pelton, Macromolecules 34 (2001) 3182.

[56] S. Liou, J. T. Rademacher, D. Malaba, M. E. Pallack, and W. J. Brittain, Macromolecules 33 (2000) 4295.

[57] M. E. Honigfort and W. J. Brittain, Macromolecules 36 (2003) 3111.

[58] K. R. Kumar, J. N. Kizhakkedathu, and D. E. Brooks, Macromolecular Chemistry and Physics 205 (2004) 567.

[59] T. Kotre, O. Nuyken, and R. Weberskirch, Macromolecular Chemistry and Physics 205 (2004) 1187.

[60] S. C. Hong, H.-J. Paik, and K. Matyjaszewski, Macromolecules 34 (2001) 5099.

[61] Y. Inoue, S. C. Hong, J.-F. Lutz, D. Neugebauer, C. Stissel, and K. Matyjaszewski, Polymer Preprints 43 (2002) 193.

[62] S. C. Hong, J.-F. Lutz, Y. Inoue, C. Strissel, O. Nuyken, and K. Matyjaszewski, Macromolecules 36 (2003) 1075.

[63] S. C. Hong, D. Neugebauer, Y. Inoue, J.-F. Lutz, and K. Matyjaszewski, Macromolecules 36 (2003) 27.

[64] E. Duquesne, P. Degee, J. Habimana, and P. Dubois, Chemical Communications (2004) 640.

[65] S. Ding, J. Yang, M. Radosz, and Y. Shen, Journal of Polymer Science, Part A: Polymer Chemistry 42 (2003) 22.

[66] J. Yang, S. Ding, M. Radosz, and Y. Shen, Macromolecules 37 (2004) 1728.

CHAPTER 3

RESEARCH PROJECT MOTIVATION AND GOALS

Motivation

There is a great deal of interest in immobilizing homogeneous organometallic or transition metal polymerization catalysts on solid supports for the purpose of recovery and reuse. Catalyst recovery and reuse are important when metal residue is not desired in the final product. In addition, wasted catalyst increases the cost of the final product. Large-scale industrial heterogeneous polymerization catalysts are currently limited to one-time use catalysts such as supported metallocenes and Ziegler Natta catalysts [1-3]. These catalysts are highly active and can produce very high molecular weight polymers ($MW > 10^6$); therefore it is more economical to leave the residual metal in the polymer. However, less active transition metal polymerization catalysts that tend to produce much lower molecular weight polymers cannot be left in the product because of toxicity, product discoloration, and expense. Despite the driving force to develop recyclable polymerization catalysts, few effective recoverable, recyclable solid supported polymerization catalysts exist.

Studies concerning Atom Transfer Radical Polymerization (ATRP) have skyrocketed during the past decade because ATRP can synthesize polymeric materials with well-defined composition, architecture, and functionality in a controlled/"living" manner [4-8]. However, the application of ATRP in industrial processes has not yet been realized due to costly and time-demanding post-polymerization methods to remove residual metal from the polymerization solution. Catalyst immobilization is a common

solution to this problem, but early studies led to poor catalysts that produced polymers with higher target molecular weights and broad polydispersities [9-13].

Although there are many isolated studies focusing on immobilizing ATRP metal complexes that produce well-defined polymers and allow for efficient catalyst recovery, there are no in depth studies of catalyst design and investigation of how catalyst structure affect performance. This is not surprising because the sole advantage of ATRP is to produce well-defined polymers with specific architecture and composition. The synthetic strategies for immobilizing ATRP catalysts have matured over the past five years resulting in recoverable catalysts possessing good polymerization behavior (i.e., high conversions and low PDIs). Now that some well-behaved immobilized ATRP catalyst systems have been reported, a shift in focus towards improving and optimizing current systems, and developing protocols for catalyst recycling should take precedence, hopefully leading to eventual widespread industrial practice. There have been some reports addressing the optimization of synthetic/immobilization strategy (e.g., immobilization methodologies and support type variation), reaction conditions, and catalyst recycling, a truly comprehensive study encompassing the catalyst design process has not been reported. A comprehensive study of the immobilized ATRP catalyst design process should include:

ATRP catalyst design process

1. Selection of ATRP transition metal complex catalyst systems.

2. Catalyst synthesis leading to a thorough characterization of the immobilized transition metal complexes.

3. Investigation of immobilization methodology and its influences on ATRP catalyst performance.

4. Investigation of the silica supports (porosity, pore size, and pore structure) and targeted polymer molecular weight (reaction conditions) influences on ATRP polymerization behavior.

5. Catalyst recovery, regeneration, and recycling, which will cover catalyst separation and regeneration methodologies, and catalyst stability.

6. Provide a fundamental understanding for silica-immobilized ATRP catalysts concerning catalyst structure and property, catalyst preparation, and reaction, recovery, regeneration, and recycling protocols.

ATRP catalyst selection

As mentioned previously, the majority of the reported literature has reported on immobilized copper/ligand ATRP catalysts [8, 10, 14-35]. Of these, aminoimine, bipyridine, and multidentate aliphatic amine ligands are the most promising in terms of polymerization rates and macromolecular control [14, 18, 20, 21, 27, 31, 33-36]. In addition, towards potential future industrial application, bidentate aminoimine and bipyridine copper catalysts are advantageous in terms of catalyst synthesis, mild reaction conditions, stability, and recyclability. I have chosen to immobilize Haddleton's CuBr/pyridylmethanimine complex [36-38] and Matyjaszewski's CuBr/bipyridine complex [39-41] onto various silica supports, and study their behavior for the controlled radical polymerization of methyl methacrylate (MMA) (**Figure 3.1**).

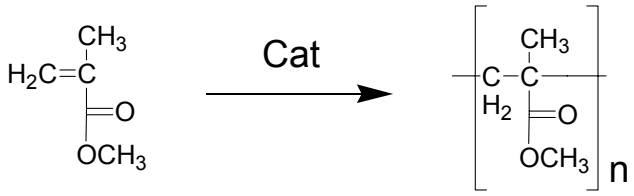

Figure 3.1 Polymerization of methyl methacrylate to poly(methyl methacrylate).

Haddleton and coworkers first reported that aminoimine such as alkyl pyridylmethanimine (PMI) ligands can be used for ATRP for a number of monomers [36-38]. They found that increasing the alkyl length improved the solubility of metal/ligand complex as well as the control. Furthermore, these ligands were easy to synthesize because imine-forming condensation reactions are very versatile and can be driven to near quantitative yields. Haddleton and coworkers later extended their metal/ligand systems onto immobilized solids (**Figure 3.2**) [16]. I have chosen to immobilize Haddleton's CuBr/pyridylmethanimine complex onto various silicas because of the above reasons, but also because variations in the immobilization methodology have not been previously addressed. Studies that I have performed concerning immobilized CuBr/PMI complexes are detailed here in Chapters 2 and 3.

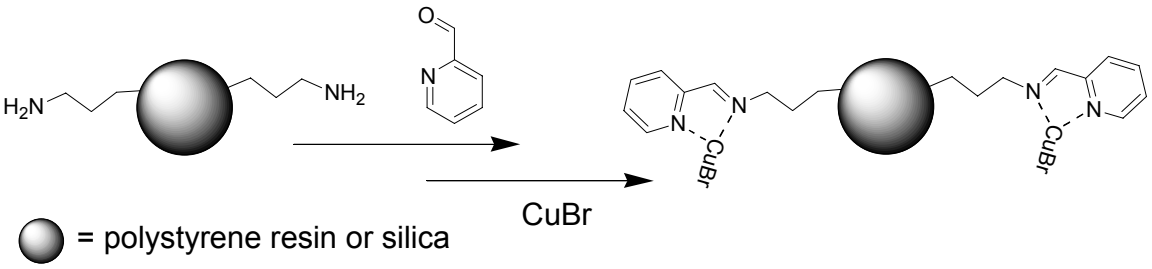

Figure 3.2 Haddleton's immobilization scheme for CuBr/PMI complexes [16].

Secondly, I have chosen to work on Matyjaszewski's CuBr/bipyridine (Bpy) ATRP system. Matyjaszewski and coworkers have elegantly pioneered the concept of ATRP using the bipyridine system [39-41]. Since then, numerous studies have been performed on this system to elucidate the reaction mechanism and catalyst structure during the polymerization, and it can be considered as the benchmark for all newly reported ATRP catalyst systems.

Perhaps realizing the disadvantages of ATRP early on, Matyjaszewski and coworkers reported the first immobilized ATRP catalyst system on silica using commercially available aliphatic amine organosilanes as ligands [10]. Unfortunately, work in this study did not result in a well-behaved ATRP catalyst because of mass transport problems and catalyst complex interactions with the silica support. Future work led to immobilization of CuBr/bipyridine complexes immobilized on polymer resins, however slow mass transport and the slow deactivation process contributed to the poor polymerization results (low conversions and broad PDIs). These results lead to the development of the dual immobilized catalyst/soluble deactivator system [18, 20]. The dual immobilized catalyst/soluble deactivator system is still considered one of the best immobilized ATRP systems reported (**Figure 3.3**). Surprisingly, there were no reports of silica-immobilized CuBr/bipyridine catalysts for ATRP prior to this work. Even more so, considering the vast amount of literature on bipyridines reported, there are only a hand full of publications concerning silica-immobilized bipyridines [42-45]. To this end, I chose to develop new synthetic strategies to immobilize well-defined CuBr/bipyridine complexes on silica for their utility in ATRP. Studies that I have performed concerning immobilized CuBr/bipyridine complexes are detailed here in Chapters 4 and 5.

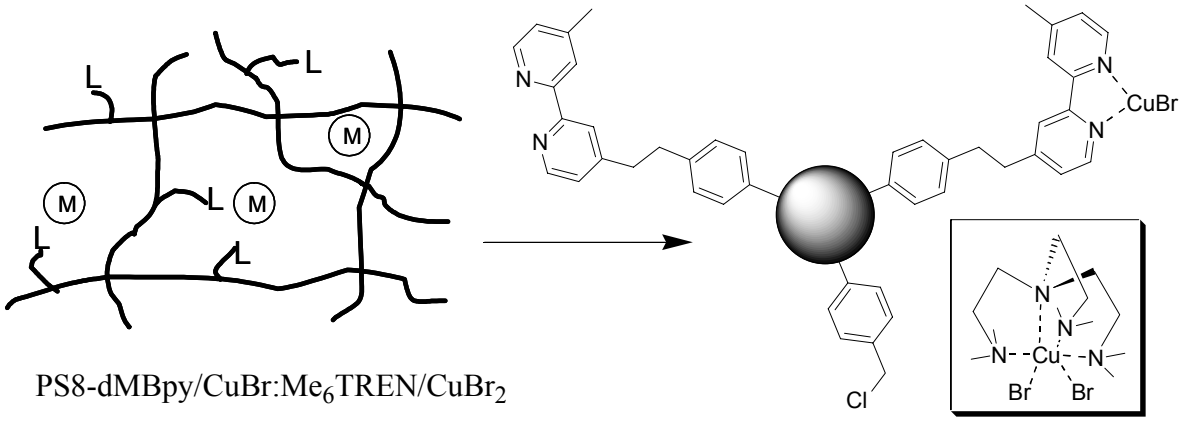

Figure 3.3 Matyjaszewski's dual immobilized catalyst/soluble deactivator system [18, 20].

Role of the immobilization methodology

I investigated different methodologies for immobilize covalently tethered ATRP metal complexes. In general, I hypothesized that the smallest number of synthetic grafting steps for immobilizing the catalyst should result in a more well-defined, less heterogeneous, active center. Therefore, one of the main goals of my work was to develop catalyst immobilization techniques involving a minimum number of synthetic grafting steps. This characteristic trait would reduce the catalyst cost, making the technology industrially more attractive.

Role of the support

In addition to investigating different immobilization methodologies, I also want to probe the role of the silica support on polymerization performance. Specifically, I seek to understand how the support's structure (i.e., porosity, pore size, and order) affect the controlled polymerization performance of different molecular weight targets. I have chosen to evaluate several different silicas ranging from different pore sizes, degree of ordering of the pores, interconnectivity of the pores, and extent of porosity of the supports. The first support is mesoporous SBA15 [46, 47]. SBA15 is synthesized using tetraethyl orthosilicate (TEOS) and triblock copolymer ethylene oxide-propylene oxide-ethylene oxide ($EO_{20}PO_{70}EO_{20}$) under acidic aqueous conditions (**Figure 3.4**). The triblock copolymer directs the formation of straight hexagonal pores. By varying the synthesis conditions, the surface area and pore diameter can be tailored. The next support is controlled pore glass (CPG), which has a larger average pore diameter and a random interconnecting pore network. Transport through the pore network is facilitated by the larger interconnecting pores, but the surface area is considerably lower, thus providing reduced catalyst loading. Lastly, I will use nonporous, nanosized, fume silica Cabosil-EH5. Transport of monomer and growing polymer to the catalyst surface is less of an issue with Cabosil-EH5, but the size of the catalyst particles make them harder to recover.

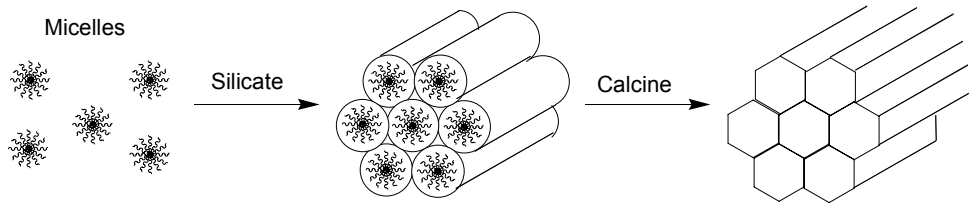

Figure 3.4 Synthesis of mesoporous SBA15 material.

Catalyst recovery, regeneration, and recycling

Lastly, these catalysts need to be fully recoverable and recyclable. The catalyst stability was probed by testing for recyclability and extent of copper leaching found in the polymer or polymerization solution. Furthermore, reported methodologies to regenerate the catalyst when required have been haphazard at best, therefore the catalyst regeneration process was studied in more detail.

Summary

As mentioned previously, a truly comprehensive study of the immobilized ATRP catalyst design process has not been reported. A more comprehensive study will provide a better grasp on how ATRP can be implemented into commercial practice, as well as contribute new ideas and methodologies to the scientific community. The goal of this thesis was to perform a comprehensive study of the immobilized ATRP catalyst design process that addresses the following fundamental science and engineering questions of interests to academic and industrial researchers have:

1. Currently, what are the best catalyst systems to use for supported ATRP?
2. How should the ATRP complexes be immobilized?
3. How is the immobilization going to affect the catalyst performance?
4. What support should be used and how is it going to affect polymerization performance?
5. What are the protocols to use, recover, regenerate, and recycle the catalyst?
6. What are the limitations of immobilized ATRP catalysts?

References

[1] G. G. Hlatky, Chemical Reviews (Washington, D. C.) 100 (2000) 1347.

[2] H. C. L. Abbenhuis, Angewandte Chemie, International Edition 38 (1999) 1058.

[3] F. Ciardelli, A. Altomare, and M. Michelotti, Catalysis Today 41 (1998) 149.

[4] K. Matyjaszewski, Controlled Radical Polymerization, American Chemical Society, Washington, DC, 1998.

[5] K. Matyjaszewski, Controlled/Living Radical Polymerization: Progress in ATRP, NMP, and RAFT, Oxford University Press, Washington, DC, 2000.

[6] K. Matyjaszewski, Advances in Controlled/Living Radical Polymerization, Oxford University Press, Washington, DC, 2003.

[7] K. Matyjaszewski and J. Xia, Chemical Reviews 101 (2001) 2921.

[8] Y. Shen, H. Tang, and S. Ding, Progress in Polymer Science 29 (2004) 1053.

[9] D. M. Haddleton, D. J. Duncalf, D. Kukulj, and A. P. Radigue, Macromolecules 32 (1999) 4769.

[10] G. Kickelbick, H.-j. Paik, and K. Matyjaszewski, Macromolecules 32 (1999) 2941.

[11] T. Opstal, K. Melis, and F. Verpoort, Catalysis Letters 74 (2001) 155.

[12] U. S. Schubert, C. H. Weidl, C. Eschbaumer, R. Kroell, and M. R. Buchmeiser, Polymeric Materials Science and Engineering 84 (2001) 514.

[13] B. De Clercq, F. Lefebvre, and F. Verpoort, Applied Catalysis, A: General 247 (2003) 345.

[14] S. Ding, J. Yang, M. Radosz, and Y. Shen, Journal of Polymer Science, Part A: Polymer Chemistry 42 (2003) 22.

[15] S. Faucher and S. Zhu, Macromolecular Rapid Communications 25 (2004) 991.

[16] D. M. Haddleton, D. Kukulj, and A. P. Radigue, Chemical Communications (1999) 99.

[17] S. C. Hong, J.-F. Lutz, Y. Inoue, C. Strissel, O. Nuyken, and K. Matyjaszewski, Macromolecules 36 (2003) 1075.

[18] S. C. Hong and K. Matyjaszewski, Macromolecules 35 (2002) 7592.

[19] S. C. Hong, D. Neugebauer, Y. Inoue, J.-F. Lutz, and K. Matyjaszewski, Macromolecules 36 (2003) 27.

[20] S. C. Hong, H.-J. Paik, and K. Matyjaszewski, Macromolecules 34 (2001) 5099.

[21] M. E. Honigfort and W. J. Brittain, Macromolecules 36 (2003) 3111.

[22] Y. Inoue, S. C. Hong, J.-F. Lutz, D. Neugebauer, C. Stissel, and K. Matyjaszewski, Polymer Preprints 43 (2002) 193.

[23] T. Kotre, O. Nuyken, and R. Weberskirch, Macromolecular Chemistry and Physics 205 (2004) 1187.

[24] R. Kroll, C. Eschbaumer, U. S. Schubert, M. R. Buchmeiser, and K. Wurst, Macromolecular Chemistry and Physics 202 (2001) 645.

[25] K. R. Kumar, J. N. Kizhakkedathu, and D. E. Brooks, Macromolecular Chemistry and Physics 205 (2004) 567.

[26] S. Liou, J. T. Rademacher, D. Malaba, M. E. Pallack, and W. J. Brittain, Macromolecules 33 (2000) 4295.

[27] Y. Shen and S. Zhu, Macromolecules 34 (2001) 8603.

[28] Y. Shen and S. Zhu, AIChE Journal 48 (2002) 2609.

[29] Y. Shen, S. Zhu, and R. Pelton, Macromolecular Rapid Communications 21 (2000) 956.

[30] Y. Shen, S. Zhu, and R. Pelton, Macromolecules 34 (2001) 3182.

[31] Y. Shen, S. Zhu, and R. Pelton, Macromolecules 34 (2001) 5812.

[32] Y. Shen, S. Zhu, F. Zeng, and R. Pelton, Macromolecular Chemistry and Physics 201 (2000) 1387.

[33] Y. Shen, S. Zhu, F. Zeng, and R. Pelton, Journal of Polymer Science, Part A: Polymer Chemistry 39 (2001) 1051.

[34] Y. Shen, S. Zhu, F. Zeng, and R. H. Pelton, Macromolecules 33 (2000) 5427.

[35] J. Yang, S. Ding, M. Radosz, and Y. Shen, Macromolecules 37 (2004) 1728.

[36] D. M. Haddleton, C. B. Jasieczek, M. J. Hannon, and A. J. Shooter, Macromolecules 30 (1997) 2190.

[37] D. M. Haddleton, M. C. Crossman, B. H. Dana, D. J. Duncalf, A. M. Heming, D. Kukulj, and A. J. Shooter, Macromolecules 32 (1999) 2110.

[38] D. M. Haddleton, D. J. Duncalf, D. Kukulj, M. C. Crossman, S. G. Jackson, S. A. F. Bon, A. J. Clark, and A. J. Shooter, European Journal of Inorganic Chemistry (1998) 1799.

[39] J.-S. Wang and K. Matyjaszewski, Journal of the American Chemical Society 117 (1995) 5614.

[40] J.-S. Wang and K. Matyjaszewski, Macromolecules 28 (1995) 7572.

[41] J.-S. Wang and K. Matyjaszewski, Macromolecules 28 (1995) 7901.

[42] N. W. Barnett, R. Bos, H. Brand, P. Jones, K. F. Lim, S. D. Purcell, and R. A. Russell, Analyst (Cambridge, United Kingdom) 127 (2002) 455.

[43] P. Ghosh and T. G. Spiro, Journal of the American Chemical Society 102 (1980) 5543.

[44] J. V. Nguyen and C. W. Jones, in Journal of Catalysis, 2005.

[45] C. D. Nunes, M. Pillinger, A. A. Valente, I. S. Goncalves, J. Rocha, P. Ferreira, and F. E. Kuhn, European Journal of Inorganic Chemistry (2002) 1100.

[46] D. Zhao, J. Feng, Q. Huo, N. Melosh, G. H. Frederickson, B. F. Chmelka, and G. D. Stucky, Science (Washington, D. C.) 279 (1998) 548.

[47] D. Zhao, Q. Huo, J. Feng, B. F. Chmelka, and G. D. Stucky, Journal of the American Chemical Society 120 (1998) 6024.

Thesis Research Prelude

The remaining body of this thesis highlights the accomplishments of the research work. Although most of this work has been done in parallel, the chapters are specifically ordered to demonstrate a direct evolution and path towards a potentially viable industrial ATRP catalyst that is fully recoverable and recyclable. Each chapter is preceded by an abstract summarizing the accomplished work and a brief introduction. The final chapters will collectively summarize project accomplishments and address the potential impact of the work on the academic and industrial sectors. Additionally, future directions in the area of immobilized ATRP catalysts are discussed, specifically concerning improvements of the existing system discussed here and potentially new immobilized copper/Bpy system. Finally, new areas of investigation are proposed.

CHAPTER 4

PROBING THE ROLE OF SYNTHETIC METHOD AND SUPPORT POROSITY ON THE STRUCTURE AND PERFORMANCE OF SILICA-SUPPORTED CUBR/PYRIDYLMETHANIMINE ATOM TRANSFER RADICAL POLYMERIZATION CATALYSTS: I. CATALYST PREPARATION AND CHARACTERIZATION.

Abstract

Silica-supported CuBr/ pyridylmethanimine (PMI) complexes that facilitate the atom transfer radical polymerization (ATRP) of methyl methacrylate are prepared and characterized. Four different synthetic routes including multi-step grafting (M1), two-step grafting (M2), one-pot (M3) and pre-assembled complex (M4) methods are evaluated on three different silica supports (mesoporous SBA-15 with 50 and 100 Å pores and non-porous Cab-O-Sil EH5). The resulting solids are characterized by a battery of techniques including thermogravimetric analysis / differential scanning calorimetry (TGA/DSC), FT-Raman spectroscopy, ^{13}C and ^{29}Si magic angle spinning (MAS) and cross-polarization magic angle spinning (CP-MAS) spectroscopy, low temperature nitrogen physisorption and elemental analysis. The combination of elemental analysis and spectroscopic results indicate that a variety of different surface species likely exist for most catalysts, including copper species that are both mono and bis-coordinated by PMI ligands as well as PMI-free copper bromide species interacting with the silica surface. M4 appears to give a material with the smallest amount of uncomplexed ligand (by FT-Raman spectroscopy) and hence the most homogeneous material. Following M4, the metallation efficiency decreases M2 ≥ M3 > M1, with M1 giving a material with a highly heterogeneous surface composition.

Introduction

Two general synthetic schemes have been used to immobilize covalently tethered copper-based ATRP catalysts on inorganic or organic supports. In the first method, the complex is built stepwise on the solid using a grafting approach [1-6]. This can lead to a highly heterogeneous surface with many types of copper sites formed with varying reactivity. As an alternative, the complex can be pre-assembled homogeneously and this homogeneous complex can be immobilized on the solid. Although this approach has not been routinely employed in ATRP catalyst design, supported copper complexes have been prepared using this methodology for other purposes [7-9]. Both of these methodologies as well as hybrids of the two approaches are systematically explored here.

In addition to designing the molecular active site, one also has to carefully control the properties of the support. Primarily, organic polymers [1-6, 10-12] and silica [2, 3, 12-20] have been used as supports due to their low cost and ease of handling. In the case of porous inorganic polymers such as silica, the exact nature of the porosity can have a strong impact on catalytic properties, especially when transport plays an important role. Because the accessibility of the growing chains to the deactivating surface-bound metal complexes can be critical in ATRP [2, 13], understanding the role of porosity is extremely important. Here I report a systematic study of the role of synthetic methodology and support structure in the ATRP of methyl methacrylate (MMA) using silica-supported CuBr/PMI catalysts. In the first part of this work, I investigate four different synthetic protocols for the immobilization of CuBr/PMI complexes on various silica supports and characterize the resulting solids [21] (**Figure 4.1**).

Results and Discussion

Synthetic immobilization methodology

Four different methods of immobilizing CuBr/PMI complexes on silica have been employed. Each subsequent method is designed to potentially reduce the heterogeneity of the surface sites in the solid. The first method (M1), shown in **Figure 4.1a**, is the multi-step approach outlined previously by Haddleton [3] and Brittain [4, 5]. The last three methods incorporate the use of the [3-(trimethoxy-silanyl)-propyl]-2-pyridylmethanimine (PMITMS) immobilizable ligand. Like M1, the metallation step for method 2 (M2), the two-step approach, occurs after the ligand has been covalently grafted to the silica surface (**Figure 4.1b**). In method 3 (M3) and method 4 (M4), the CuBr/PMI complex is formed *in situ*; these methods are referred to here as the one-pot (**Figure 4.1c**) and pre-assembled complex (**Figure 4.1d**) approaches, respectively. Each synthetic approach was applied to mesoporous SBA-15 with 50 and 100 Å pores and the nonporous, fumed silica Cabosil-EH5.

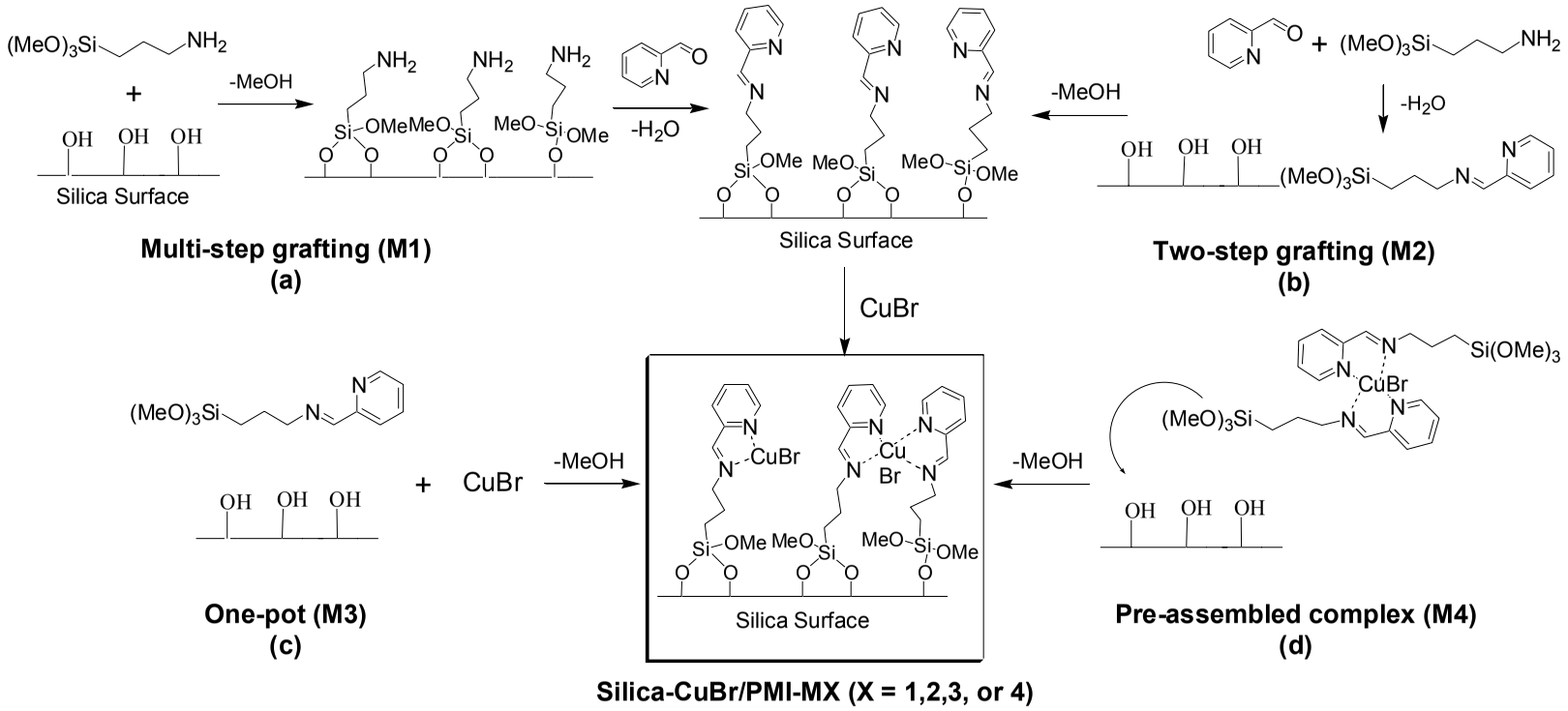

Figure 4.1 Four different synthetic routes to immobilized silica CuBr/PMI complexes

Synthesis and spectroscopic studies of PMITMS

The immobilizable PMI ligand [3-(Trimethoxy-silanyl)-propyl]-2-pyridylmethanimine (PMITMS) was synthesized homogeneously using methods similar to the approach used for homogeneous and supported PMI ligand [3-5, 22, 23]. Care was taken to insure that the PMI ligand was pure as it was straightforward to purify the ligand before addition to the support, unlike in some previous studies of supported Cu ATRP catalysts [17]. An excess of 2-pyridine carboxaldehyde (PCA) was added to 3-aminopropyl trimethoxysilane (APTMS), with the excess PCA removed via careful vacuum distillation after reaction. The disappearance of the aldehyde proton and amine protons, as well as the appearance of the imine proton was monitored by ^{1}H NMR. Quantitative conversion of the aldehyde group to the imine was achieved and the immobilizable ligand was recovered free of any residual starting materials which could lead to unselective binding sites on the surface (^{1}H NMR shown in **Figure 4.2**).

The synthesis and the immobilization of PMITMS were followed by FT-Raman spectroscopy (**Figure 4.3**) and the characteristic Raman shifts are summarized in **Table 4.1** [24]. In **Figure 4.3a**, the ν(N-H) and ν(aliphatic C-H) vibrations for APTMS appear at 3313 and 2800-2900 cm^{-1}, respectively. Unfortunately the vibration due to the ν(Si-OMe) in the range 1190-1100 and 850-800 cm^{-1} were not strong enough to be detected conclusively. **Figure 4.3b** shows FT-Raman of PCA, the ν(aromatic C-H), ν(C=O), ν(pyridyl ring), and ν(in-plane CH) vibrations appear at 3056, 1708, 1585, and 993 cm^{-1}, respectively. The FT-Raman spectrum of PMITMS resulting from the reaction of APTMS and PCA is shown in **Figure 4.3c**. The two spectra (4.3a + 4.3b) can be

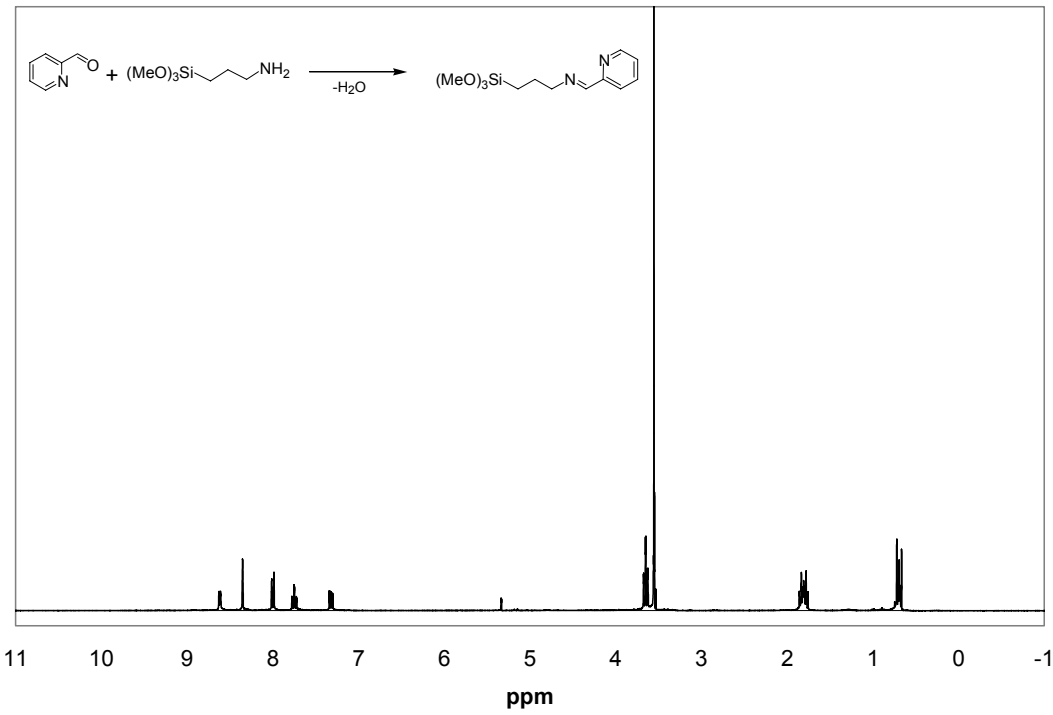

Figure 4.2 ^{1}H NMR spectrum of PMITMS in CD_2Cl_2.

superimposed and the disappearance of the ν(N-H) and ν(C=O), along with the appearance of the ν(C=N) at 1650 cm^{-1} are noted. The metal complex was subsequently formed when 2 equivalents of PMITMS and 1 equivalent of CuBr were added in THF. The ν(C=N), ν(pyridyl ring), and ν(in-plane CH) vibrations shift slightly to 1625, 1560, and 1007 cm^{-1}, respectively. This observation was attributed to the change in the chemical environment around the chelating nitrogen atoms due to CuBr coordination. These results are consistent with FT-Raman spectra of metal coordination complexes with bidentate chelating nitrogen ligands reported in the literature [25]. However, the mono and bis copper coordinated PMI species could not be distinguished by FT-Raman. There also remain visible shoulders at 1650, 1585, and 993 cm^{-1} that could be assigned to uncoordinated PMITMS ligand.

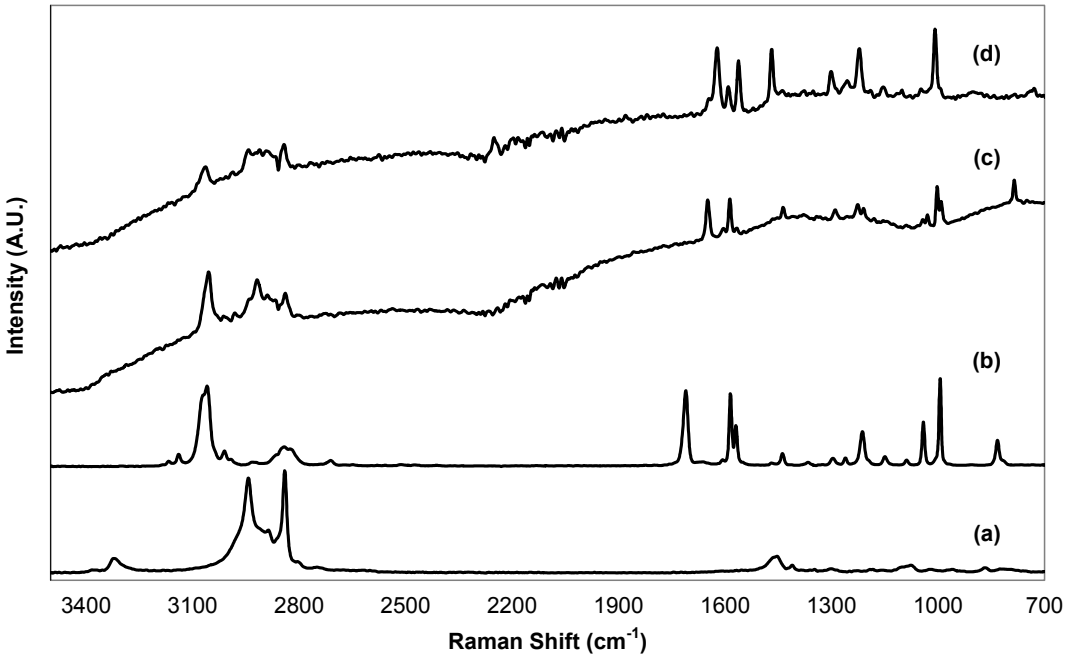

Figure 4.3 FT-Raman spectroscopy study of CuBr/PMITMS syntheses: (a) APS (b) PCA (c) PMITMS (d) CuBr/PMITMS.

Table 4.1 FT-Raman results for spectroscopic studies of PMITMS.

Entry	Compound	ν(N-H)	ν(C=O)	ν(pyridyl)	ν(inplane CH)	ν(C=N)
1	APS	3313	----	----	----	----
2	PCA	----	1708	1585	993	----
3	PMITMS	----	----	1585	993	1650
4	CuBr/PMITMS	----	----	1560	1007	1625

Silica supports

The SBA-15 materials were prepared according the procedure previously described by Stucky et al. [26, 27]. For the 100 Å pore material, TMB was used as a swelling agent to increase the pore size. The mesoporous silicates were characterized by nitrogen physisorption to determine the surface area and pore size of the pristine silica supports (**Table 4.2**). Thermogravimetric analysis approximated the total silanol concentration to be 2.0 mmol-OH g-solid^{-1} for 50 and 100 Å materials. X-ray powder diffraction was used to determine the order of the porosity and the overall structure of the SBA-15. The XRD patterns (not shown) were consistent with a hexagonal pore structure [26-28]. Cab-O-Sil EH5 is a commercially available fumed, nonporous silica from Cabot. Multiparticle aggregates have a length of 0.2-0.3 micron (individual particles have nanosized features), a surface area of 335 m^2/g, and 2.7 mmol-OH g-solid^{-1} by nitrogen physisorption and TGA, respectively (consistent with product data sheet [29]).

Table 4.2 Nitrogen physisorption results of silica supports.

Entry	Material	Pore Diameter[1] (Å)	BET SA m^2/g	Silanol Conc.[2] (mmol OH/g solid)
1	SBA15(50)	50	701	~2.0
2	SBA15(100)	100	896	~2.0
3	Cab-O-Sil EH5	----	335	~2.7

1. Based on BJH analysis of the adsorption branch of the isotherm.
2. Total silanol content as estimated by TGA.

Synthesis and characterization of immobilized CuBr/PMI complex on silica

In method 1 (M1), APTMS was covalently grafted on pristine SBA-15 (50 Å pores) to give a white powder containing about 1.36 mmol amine g-solid^{-1} by TGA, designated SBA15(50)-NH_2-M1. From FT-Raman spectroscopy, the amine functionalized SBA-15 displayed a band at 3296 cm^{-1} due to the primary amine (**Figure 4.4a**). Subsequently, PCA was added to the immobilized primary amine binding site, yielding the corresponding immobilized PMI ligand, to give a yellowish white powder containing about 1.13 mmol ligand g-solid^{-1} by TGA, designated SBA15(50)-PMI-M1.

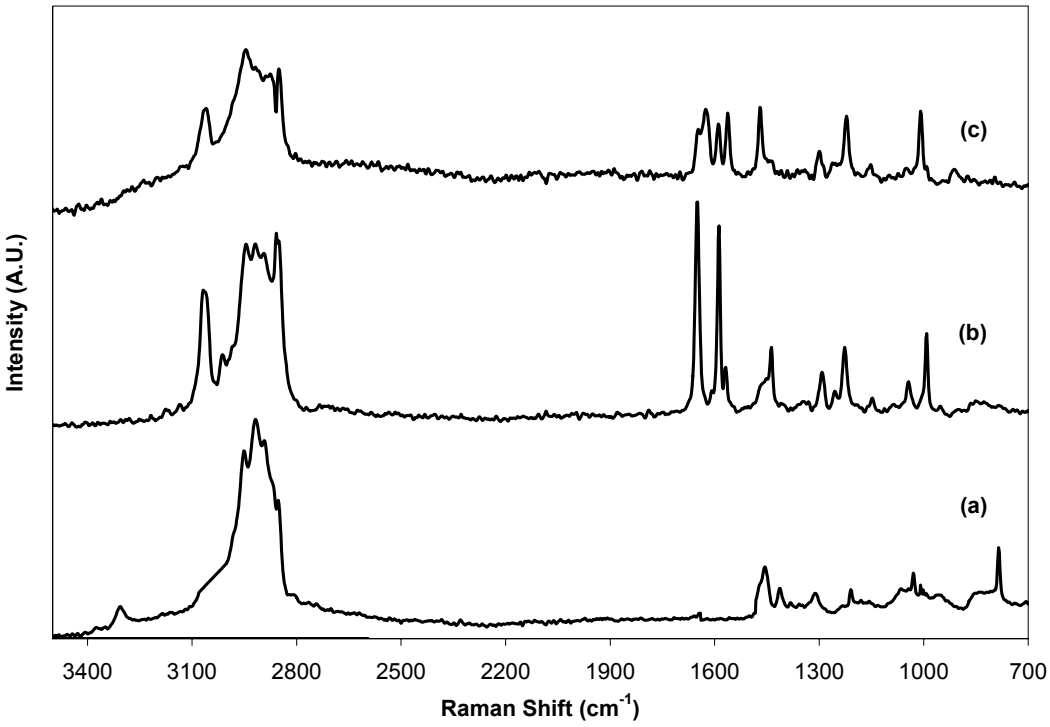

Figure 4.4 FT-Raman spectroscopy study of multi-step grafting approach on SBA15(50): (a) SBA15(50)-NH_2-M1 (b) SBA15(50)-PMI-M1 (c) SBA15(50)-CuBr/PMI-M1.

Approximately 92% of the amines were converted to the imines by TGA. **Figure 4.4b** shows FT-Raman spectra of SBA15(50)-PMI-M1 material. It shows the complete disappearance of the amine band (3296 cm^{-1}) and the appearance of bands at 3058, 1650, 1587, and 991 cm^{-1}, corresponding to ν(aromatic C-H), ν(C=N), ν(pyridyl ring), and ν(in-plane CH), respectively. The FT-Raman spectrum was similar to the homogeneous PMITMS ligand (**Figure 4.1c**), verifying the formation of the intended ligand structure. The coordination of the CuBr to the immobilized ligand was carried out by treating the SBA15(50)-PMI-M1 (2.00 g) with slurry of CuBr (0.16 g, ligand/metal mole ratio = 2) in toluene at 110 °C. A dark reddish brown solid was recovered and washed with copious amounts of dry toluene, hexanes, and dichloromethane. The solvent wash aided the removal of much of the uncoordinated CuBr and physisorbed chemical species from the pores and support surface. This material is designated SBA15(50)-CuBr/PMI-M1. CHN and Cu analysis determined a surface loading of 1.07 mmol ligand g-catalyst^{-1} and 0.48 mmol Cu g-catalyst^{-1}, respectively. This corresponded to 89% of the PMI ligands complexed with CuBr. The % PMI ligands complexed were calculated according to the following equation:

$$\% \text{ PMI Complexed} = [(\text{mmol Cu g-catalyst}^{-1})/[(\text{mmol PMI ligand g-catalyst}^{-1})/2]] \times 100$$

A value of 100% PMI coordinated signifies that the number of Cu atoms is consistent with coordination to two immobilized PMI ligands. Deviations from a 100 % means that uncoordinated PMI ligands must exist (<100%), mono Cu coordinated PMI ligands likely exist (100 > X > 200%), or Cu adsorbed to the silica surface with no organic ligand likely

exists (>200%). This quantity is an only a measure of the metallation efficiency and should not be used as the only indication of what surface species exist on the silica surface. FT-Raman showed vibrational shifts, after metallation, of the ν(imine), ν(pyridyl ring) and ν(in-plane C-H) signals to 1625 and 1562 cm^{-1} and 1007 cm^{-1}, respectively (**Figure 4.4c**). This was consistent with FT-Raman spectrum of the CuBr/PMITMS in **Figure 4.1d**, verifying Cu coordination by the ligand. However, there remains a visible shoulder at 1650 cm^{-1}, which was attributed to uncoordinated ligand. Again, the distinction between mono and bis copper coordinated PMI ligands could not be assigned, for reasons already mentioned.

The use of an immobilizable PMITMS ligand, in M2, M3, and M4 eliminated the inherent uncertainty in M1 of how much ligand was loaded on the silica surface. Use of PMITMS can also reduce the number of different organic functionalities that can exist on the surface to complete PMI ligands (no adsorbed aldehyde or free amine if the pre-formed ligand remains intact), but it does not eliminate the many different ways the PMI ligand can interact with the surface and the metal. **Figure 4.5** shows some of the numerous possible surface functionalities on silica, when the multi-step grafting approach is used.

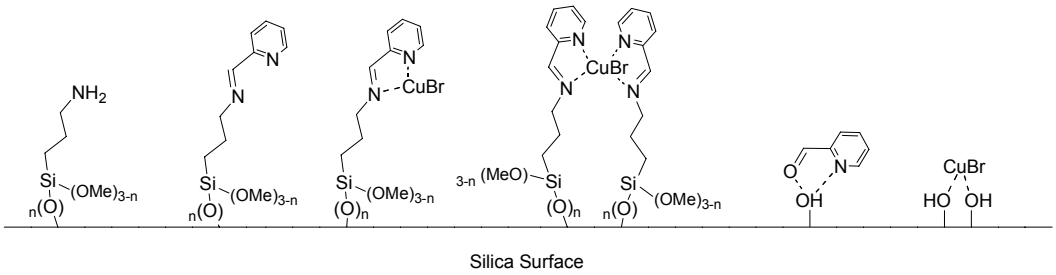

Figure 4.5 Potential immobilized species from multi-step grafting approach.

Method 2, the 2-step approach, first involved covalently grafting the PMITMS ligand on SBA-15 similar to APTMS, yielding a yellowish white powder containing about 1.13 mmol ligand g-solid^{-1}, designated SBA15(50)-PMI-M2. The FT-Raman spectra for this material showed identical signals as seen in SBA15(50)-PMI-M1. **Figure 4.6** shows the solid state ^{13}C CP-MAS NMR result for the direct immobilization of PMITMS ligand. The lower spectrum is the solution ^{13}C NMR spectra of PMITMS (**Figure 4.6a**). The ^{13}C CP-MAS NMR spectra of SBA15(50)-PMI-M2 (**Figure 4.6b**) possesses the same signals as the homogeneous form, but much broader because the PMI ligands are now immobilized. The signal at 8.7 ppm corresponds to the -CH_2Si- carbon, indicating the PMI ligands were covalently anchored to the silica surface. The weak band in the region between 192-190 ppm was determined to be the spinning sideband of the 122.8 and 120.2 ppm signals.

Metallation of SBA15(50)-PMI-M2 was done in a similar manner to method 1, yielding a dark reddish brown powder consisting of about 1.09 mmol ligand g-catalyst^{-1}, 0.51 mmol Cu g-catalyst^{-1}, and 95% PMI complexed, designated SBA15(50)-CuBr/PMI-M2. The FT-Raman of SBA15(50)-CuBr/PMI-M2 was again comparable to SBA15(50)-CuBr/PMI-M1, but the shoulder at 1650 cm^{-1} was not as pronounced. By using the PMITMS ligand, incomplete conversion of the amine species and the reaction of the PCA ligand precursor with the silica surface may be completely avoided. However, the method does not eliminate the CuBr from adsorbing to the surface silanols.

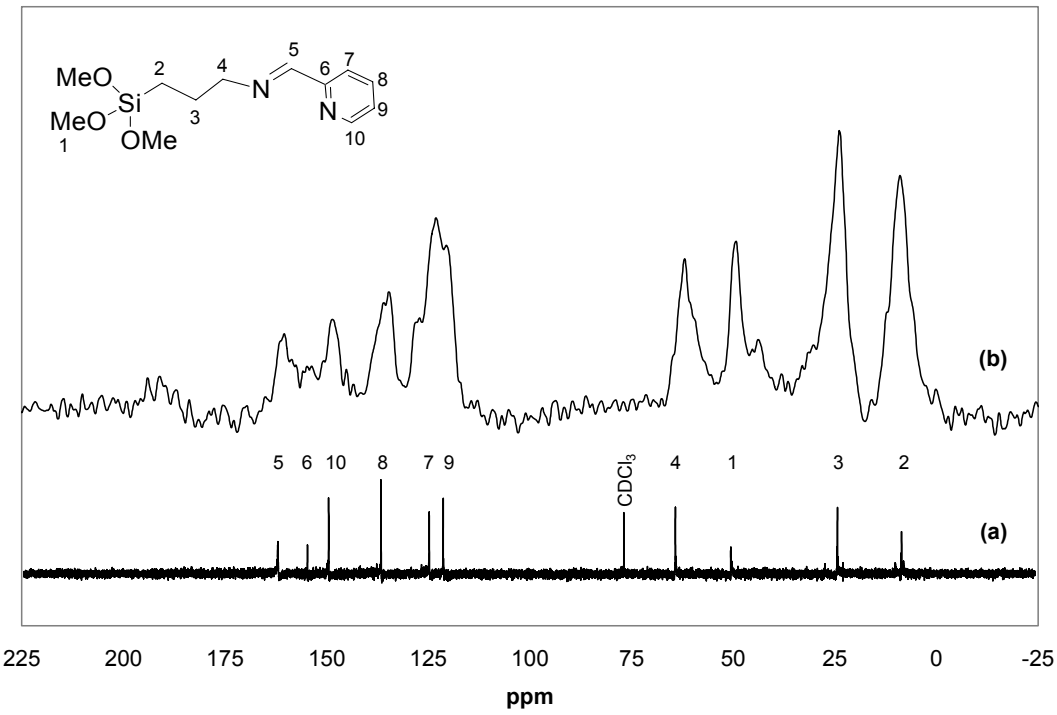

Figure 4.6 ^{13}C Solution and Solid State CP-MAS (TOSS) NMR spectra of PMI species. PMITMS in $CDCl_3$ (a) and SBA15(50)-PMI-M2 (b), respectively; * indicates spinning sideband for signal centered between 122-120 ppm.

The one-pot and pre-assembled complex approaches (M3 and M4, respectively) were devised to improve the metallation step of the supported catalyst. It was envisioned that the immobilizable ligand will self-assemble with the metal, ideally with a ligand/metal ratio of 2, and then covalently attach to the silica surface. M3 involved adding all the reagents and support in one-pot, while M4 involved pre-assembling the metal/ligand complex *in situ* and then adding the support. Both methods yielded dark reddish brown powders that were washed extensively with solvents to remove free PMITMS ligand, CuBr/PMITMS complex and CuBr that remained in the pores and on the surface. Solids prepared in this way were designated SBA15(50)-CuBr/PMI-M3 and

-M4, respectively. CHN and Cu analysis of the solids indicated loadings of 1.02 mmol ligand g-catalyst^{-1}, 0.42 mmol Cu g-catalyst^{-1}, and 83% PMI complexed (M3), and 1.07 mmol ligand g-catalyst^{-1}, 0.48 mmol Cu g-catalyst^{-1}, and 89% ligands complexed (M4). FT-Raman spectra of both catalysts were similar to the metallated spectra for M1 and M2, with a shoulder still seen in M3 and little or no shoulder in M4. A comparison of the FT-Raman spectra of CuBr/PMI complexes immobilized on SBA15(50), M1 thru M4, are shown in **Figure 4.7**.

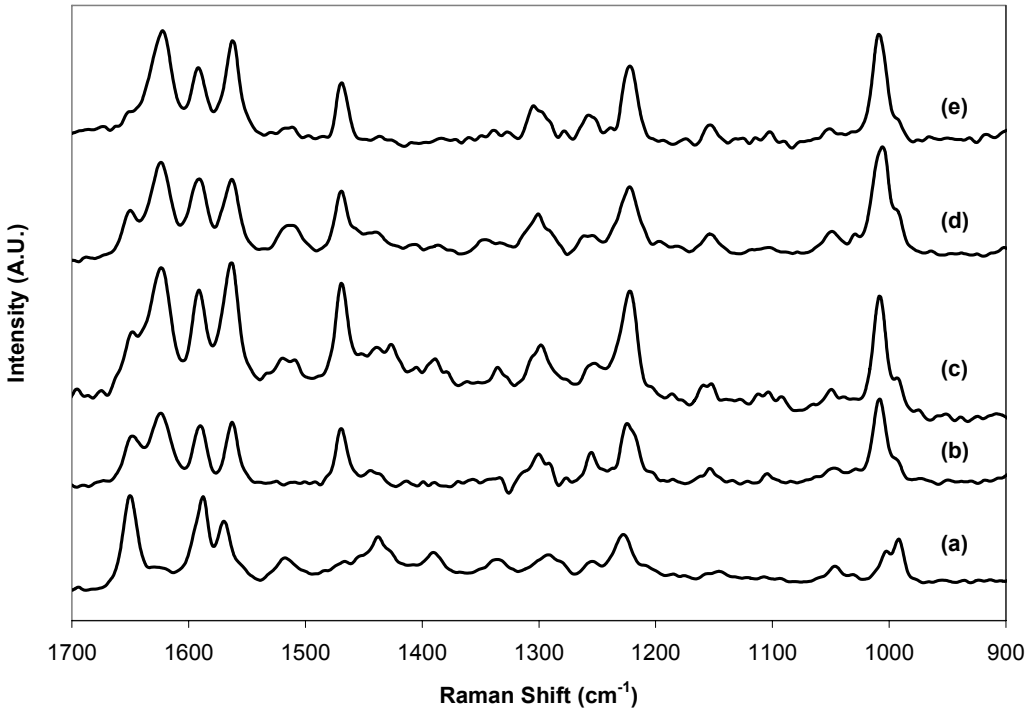

Figure 4.7 FT-Raman spectra of different synthetic methods immobilized CuBr/PMI on SBA15(50): (a) SBA15(50)-PMI-M2 (b) SBA15(50)-CuBr/PMI-M1 (c) SBA15(50)-CuBr/PMI-M2 (d) SBA15(50)-CuBr/PMI-M3 (e) SBA15(50)-CuBr/PMI-M4.

The syntheses of CuBr/PMI complex immobilized on SBA-15 (100 Å pores) and Cab-O-Sil EH5 for each method were prepared in a similar manner as described above. **Table 4.3** summarizes the complete thermogravimetric and elemental analysis results. These catalysts were synthesized on various silica supports to investigate how the silica support structure changes the polymerization performance.

Table 4.3 Thermogravimetric and elemental analysis of immobilized silica CuBr/PMI complexes.

Entry	Materials	TGA PMI Loading[1] (mmol/g cat)	EA PMI Loading[2] (mmol/g cat)	EA Cu Loading[3] (mmol/g cat)	% Loaded[4] (TGA, EA)	Ligand Density (PMI/nm^2)
1	SBA(50)-CuBr/PMI-M1	0.99	1.07	0.48	97, 89	1.23
2	SBA(50)-CuBr/PMI-M2	1.13	1.09	0.51	91, 95	1.23
3	SBA(50)-CuBr/PMI-M3	1.13	1.02	0.42	75, 83	1.14
4	SBA(50)-CuBr/PMI-M4	1.03	1.07	0.48	93, 89	1.22
5	SBA(100)-CuBr/PMI-M1	1.30	1.18	0.62	96, 106	1.16
6	SBA(100)-CuBr/PMI-M2	1.08	1.19	0.48	90, 81	1.08
7	SBA(100)-CuBr/PMI-M3	1.20	1.30	0.56	93, 86	1.23
8	SBA(100)-CuBr/PMI-M4	1.35	1.21	0.49	72, 81	1.12
9	Cab-O-Sil-CuBr/PMI-M1	0.94	0.88	0.43	91, 98	1.98
10	Cab-O-Sil-CuBr/PMI-M2	0.87	0.98	0.37	84, 75	2.24
11	Cab-O-Sil-CuBr/PMI-M3	1.14	1.27	0.71	125, 112	3.30
12	Cab-O-Sil-CuBr/PMI-M4	1.12	1.19	0.50	89, 84	2.88

1. Ligand loading based on thermogravimetric analysis of % organic mass loss between 200 and 500 ºC.
2. Ligand loading based on elemental analysis % carbon content.
3. Copper loading based on elemental analysis % copper content.
4. % PMI ligand complexed based on ligand/metal ratio equal to 2.

Surface structure and composition

Table 4.3 summarizes the results from thermogravimetric (TGA) and elemental analysis (EA). The ligand loadings were calculated based on two –OMe units reacting to the silica surface. This was confirmed by solid state ^{29}Si MAS and CP-MAS NMR results (CP-MAS spectrum shown in **Figure 4.8**). From the ^{29}Si spectrum, three signals at -50.2, -57.6, and -64.4 ppm were identified as T^1, T^2, and T^3 sites, respectively [30]. The signals correspond to one, two, and three –OMe units reacting to the silica surface. The T^2 signal was the predominant signal in both the MAS and CP-MAS spectra suggesting most of the PMI ligands were anchored by two -Si-O- bonds to the surface, but a distribution of one, two, and three surface anchored PMI ligands exist. The TGA ligand loadings were determined by the organic loss between 200 and 500 °C**.** The EA ligand loadings were calculated based on the total carbon content by CHN analysis. The TGA and EA ligand loadings agree well, and the differences were within reasonable experimental error between the two techniques. The ligand loadings were approximately 1.0 mmol PMI g-catalyst^{-1} for all the materials.

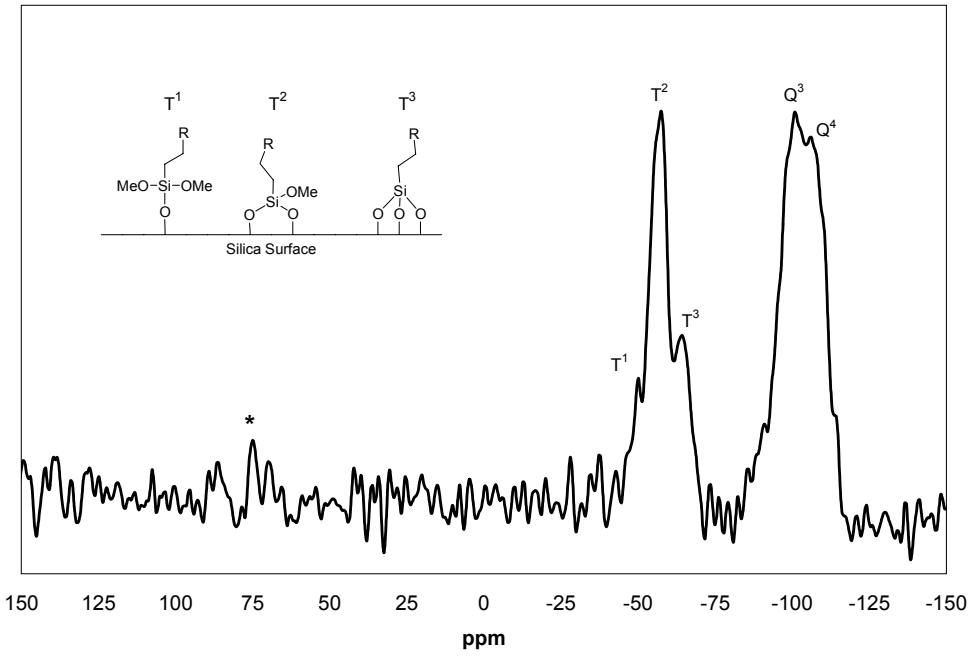

Figure 4.8 ^{29}Si Solid State CP-MAS NMR of SBA15(50)-PMI-M2; * indicates spinning sideband for signal centered at -57 ppm.

Based on the BET surface area of the silica supports and the ligand loadings determined by EA, on average the number of PMI ligands per square nanometer for SBA15(50), SBA15(100), and Cab-O-Sil EH5 were 1.20, 1.15, and 2.60 PMI-ligands nm^{-2}, respectively. This quantity would be an average measure of how far apart the ligands are spaced on the surface. These values are important, as the proximity of ligands from each other will influence the bis coordination ability of the immobilized complexes. Statistically, PMI ligands supported on Cab-O-Sil EH5 have a greater opportunity to have two PMI ligands coordinated to one CuBr because they are closer in proximity to one another on average. This advantage could be less important in catalysts prepared using M4, as a pre-formed bis complex is formed before immobilization in this case.

Spectroscopic studies of CuBr coordination

Each subsequent method was designed to improve the metallation of the catalyst and to investigate the catalyst performance. **Figure 4.7** shows a comparison of the FT-Raman spectra for M1 thru M4 on 50 Å SBA-15 in the range of 900 – 1700 cm^{-1}. **Figure 4.7a** shows SBA15(50)-PMI-M2, an uncoordinated covalently bound PMI ligand. The signals of interest are the ν(C=N), ν(pyridyl ring), and ν(in-plane ring) at 1650, 1585, and 991 cm^{-1}, respectively. When the CuBr was coordinated to the immobilized PMI ligand, the ν(C=N), ν(pyridyl ring), and ν(in-plane ring) signals shift to 1625, 1560, and 1007 cm^{-1}, respectively. The efficiency of the metallation can be qualitatively interpreted from the shoulder remaining at 1650 cm^{-1}. The increasing metallation efficiency for CuBr/PMI complexes immobilized on SBA15(50) can be described as follows: M1 < M3 ≤ M2 < M4, interpreted from **Figure 4.7**. This observation could not be distinguished by TGA and EA because these techniques only give the total elemental or organic loading. If the metallation efficiency was based on EA alone, it would be described as follows: M3 < M2 < M4 < M1. This ranking of the efficiency of coordination in the immobilized CuBr/PMI complexes would be inaccurate, as indicated by the FT-Raman spectra. Although the % PMI complexed suggested >80% of the PMI ligands were coordinated for SBA15(50) materials, the intensity of the shoulder at 1650 cm^{-1} for M1, M2, and M3 indicates the percentage of uncoordinated ligand could be higher than 20%. To rationalize the differences in coordination inferred from the elemental analysis and FT-Raman data, one can speculate that free CuBr may be adsorbed to the silica surface via a Si-OH-CuBr interaction, resulting in inflated % PMI complexed values, especially for methods 1-3. In a control experiment, it was found that

after CuBr was mixed in a solution of toluene and bare silica, the EA of the recovered silica powder revealed a large concentration of Cu (3.6 mmol Cu g-SiO_2^{-1}), even after extensive washing with toluene, hexane, dichloromethane and THF. Hence, organic ligand-free sections of the silica supports can effectively adsorb free CuBr if the uncomplexed metal salt is contacted with the supports.

On a molecular level, there are five competing processes involving the immobilization of CuBr/PMI complex: (1) rate CuBr coordinates to surface immobilized PMI ligand; (2) rate bare CuBr adsorbs to silica; (3) rate PMITMS reacts to surface; (4) rate mono CuBr/PMITMS reacts to surface; and (5) rate bis CuBr/PMITMS reacts to surface. M1 and M2 involved the first two processes, since M1 possess the lesser-defined immobilized PMI ligand, the metallation was worse. M3 potentially involves all five processes. In M4; the CuBr molecules were coordinated to the free PMITMS ligand prior to the addition of the silica source and hence rates (4) and (5) are expected to be of primary importance. Because the metallation occurs in homogeneous solution in M4, it is more likely to produce surface structures that are akin to what is believed to be the homogeneous catalyst than in M1-M3.

Summary

A number of methodologies for immobilization of CuBr/PMI ATRP complexes on silica supports were evaluated. Four different methods were employed on three structurally different silica supports. The catalysts were characterized by thermogravimetric and elemental analysis, and FT-Raman spectroscopy. Solid state ^{13}C and ^{29}Si CP-MAS NMR results indicated that the intended PMI ligands were immobilized on the silica surface and predominantly consisted of intact PMI ligands anchored by two -Si-O- bonds. The PMI ligand loadings agreed well within experimental error between TGA and EA. The results suggested that >80% of the ligands were coordinated to CuBr for all synthetic methods. This suggested that some uncoordinated PMI ligands exist on the silica surface. However, the intensity of the shoulder at 1650 cm^{-1}, attributed to uncomplexed ligand, in the FT-Raman spectrum, indicates that potentially fewer PMI ligands were coordinated for M1, M2, and M3. This suggests that perhaps CuBr adsorbed to the silica surface in samples made via these methods. The metallation efficiency increases as follows: M1 < M3 ≤ M2 < M4 (qualitatively determined by FT-Raman by residual shoulder at 1650 cm^{-1}). This differs from the overall metal loading of the solids determined by EA: M3 < M2 < M4 < M1. This ranking determined by EA includes physisorbed, organic ligand-free CuBr species that appear to be present in catalysts made by M1-M3. Method 4, the approach using a pre-assembled complex appears to result in a more structurally homogeneous immobilized ATRP complex. The polymerization performances of these catalysts will be compared against each synthetic approach and as a function of silica support structure in Chapter 5.

Experimental Section

Characterization

Thermogravimetric analysis (TGA) was carried out using a Netzsch simultaneous thermal analyzer STA 409 PC *Luxx* (TGA/DSC) by heating to 1000 °C at 20 K/min. Silica pore diameters and surface areas were determined using nitrogen physisorption data obtained with a Micromeritics ASAP 2000 system. The samples were pretreated at 90 °C for 1 h and 150 °C overnight under vacuum. The surface areas were analyzed by the BET method and the pore size distribution was determined using the BJH method applied to the adsorption branch of the isotherm [28]. X-ray powder diffraction patterns were recorded using CuK_α radiation on a Scintag X1 powder diffractometer. FT-Raman spectroscopy was performed using a Bruker IFS 66v/S equipped with dual FT-IR and FT-Raman benches and a CaF_2 beamsplitter. ^1H and ^{13}C solution NMR measurements were performed using a Mercury Vx 300 MHz with CD_2Cl_2 or $CDCl_3$ used as solvent. Solid state ^{13}C and ^{29}Si cross-polarization magic angle spinning (CP-MAS) NMR spectra were collected on a Bruker DSX 300 and 400 MHz instruments, respectively. Typical ^{13}C CP-MAS parameters were 10000 scans, a 90º pulse length of 4 μs, and a delay of 4 s between scans. Typical ^{29}Si CP-MAS parameters were 2000 scans, a 90º pulse length of 5 μs, and a delay of 10 s between scans. Copper and silicon elemental analyses were performed by Galbraith Laboratories, Inc, Knoxville, TN or Chemisar Laboratories, Guelph, Canada, using ICP-AES. Carbon, hydrogen, and nitrogen contents were determined via CHN analysis by Galbraith Laboratories, Inc, Knoxville, TN or Chemisar Laboratories, Guelph, Canada.

Chemicals

Methylenechloride-d_2 (CD_2Cl_2; Cambridge Isotope Laboratories, Inc.; 99.8%), chloroform-d ($CDCl_3$; Cambridge Isotope Laboratories, Inc.; 99.8%), and propylamine (Acros; 99+%) were dried over 4 Å molecular sieves and stored under nitrogen. Copper (I) bromide (CuBr; Acros; 98%) was purified by stirring in glacial acetic acid for 5 hrs, washed with absolute ethanol and anhydrous diethyl ether, dried under vacuum for 12 hrs at room temperature, and stored under nitrogen. Anhydrous methanol (MeOH, Alfa Aesar, >99%), 3-Aminopropyltrimethoxysilane (APTMS; Aldrich; 97%) and 2-pyridinecarboxaldehyde (PCA; Aldrich; 99%) were used as received and stored under nitrogen. Cab-O-Sil EH5 (Cabot) was dried under vacuum for 12 hrs at room temperature and stored under nitrogen. Poly(ethylene glycol)-block-poly(propylene glycol)-block-poly(ethylene glycol) (EO-PO-EO; Aldrich), hydrochloric acid (HCl; JT-Baker; A.C.S. Reagent), tetraethyl orthosilicate (TEOS; Acros; 98%), and 1,3,5 trimethylbenzene (TMB; Aldrich; 97%) were used as received. Hexanes (Aldrich; >99%) and methylene chloride (CH_2Cl_2; Aldrich; >99%) were dried and deoxygenated using a purification system and stored under nitrogen in a glovebox [31].

Syntheses

[3-(Trimethoxy-silanyl)-propyl]-2-pyridylmethanimine (PMITMS)

To a 100 mL round-bottom flask were added 5.54 g of APTMS (0.031 mol), 3.64 g of PCA (.034 mol), and 30 mL of anhydrous MeOH. The reaction solution was stirred at 75 °C for 24 hrs under argon. The product was isolated by removal of the light volatiles (MeOH and PCA) by vacuum distillation and stored under dry nitrogen in a glovebox to yield a dark brown viscous oil: $C_{12}H_{20}N_2O_3Si$ (yield: 90 %, purity: 99 %). ^{1}H-NMR (CD_2Cl_2): δ = 0.69 (t, 2H, -SiC$\underline{H}_2$-), 1.81 (m, 2H, -SiCH$_2$C$\underline{H}_2$-), 3.55 (s, 9H, (-Si-OC$\underline{H}_3$)$_3$), 3.65 (t, 2H, -SiCH$_2$CH$_2$C$\underline{H}_2$-), 7.32 (t, 1H, -CCHC$\underline{H}$CHCHN-), 7.75 (t, 1H, -CCHCHC$\underline{H}$CHN-), 8.00 (d, 1H, -CC$\underline{H}$CHCHCHN-), 8.35 (s, 1H, -CH$_2$NC$\underline{H}$-), 8.61 (d, 1H, -CCHCHCHC$\underline{H}$N-). ^{13}C-NMR (CDCl3): δ = 8.67 (-Si$\underline{C}$H$_2$-), δ = 24.47 (-SiCH$_2$$\underline{C}H_2$-), δ = 50.55 (-SiCH$_2CH_2$$\underline{C}H_2$N-), δ = 64.22 (-Si-(O$\underline{C}H_3$)$_3$), δ = 121.33 (-CCHCH$\underline{C}$HCHN-), δ = 124.76 (-C$\underline{C}$HCHCHCHN-), δ = 136.62 (-CCH$\underline{C}$HCHCHN-), δ = 149.50 (-CCHCHCH$\underline{C}$HN-), δ = 154.71 (-$\underline{C}$CHCHCHCHN-), δ = 162.04 (-CH$_2$$\underline{C}H_2$N=$\underline{C}$H-).

SBA-15 (50 Å pores)

Mesoporous silica SBA-15 was synthesized utilizing the triblock poly(ethylene oxide)-poly(propylene oxide)-poly(ethylene oxide) (EO-PO-EO) nonionic surfactant as the structure-directing agent [26, 27]. In a typical preparation, 12.43 g of EO-PO-EO, 273.92 g of DI H_2O, and 86.60 g 38% aqueous HCl were stirred at room temperature until the triblock copolymer completely dissolved. Then 27.05 g of TEOS was added to the solution and stirred for 5 minutes. The mixture was distributed into ten PARR

Teflon-line autoclaves and agitated at 50 °C for 20 hrs. The solid product was recovered by filtration, washed with DI H_2O extensively, and air-dried at 50 °C overnight. Calcination was carried out by slowly increasing temperature from room temperature to 200 °C at 1.2 K/min under nitrogen enriched atmosphere. The temperature was held at 200 °C for 1 hr and then slowly increased to 500 °C at 2 K/min under oxygen enriched atmosphere. The temperature was held at 500 °C for 6 hrs. The solid product was dried under vacuum for 12 hrs and stored under dry nitrogen in a glovebox, yielding approximately 8 g of solid.

SBA-15 (100 Å pores)

Large pore SBA-15 was synthesized similar to the 50 Å material except 1,3,5-trimethylbenzene (TMB) was used as a swelling co-solvent. In a typical preparation, 12.00 g of EO-PO-EO, 317.77 g of DI H_2O, 1.50 g of TMB, and 86.60 g 38% aqueous HCl were stirred at room temperature until the triblock copolymer completely dissolved. Then 25.63 g of TEOS was added to the solution and stirred for 5 min. The mixture was distributed into ten PARR Teflon-line autoclaves and agitated at 35 °C for 20 hrs and then aged at 100 °C without stirring for 24 hrs. The solid product was recovered by filtration, washed with DI H_2O extensively, and air-dried at 50 °C overnight. Calcination was carried out under the same conditions described for the 50 Å pore material. The solid product was dried under vacuum for 12 hrs and stored under dry nitrogen in a glovebox, yielding approximately 8 g of solid.

Syntheses of CuBr/propyl-2-pyridylmethanimine (CuBr/PMI) immobilized catalysts

All catalyst syntheses described below were prepared, recovered, and washed under dry nitrogen in a glovebox. Schlenk techniques were used for manipulating reaction mixtures outside the nitrogen glovebox. All solvents used in the synthesis of these materials were anhydrous and deoxygenated.

Preparation of SBA-15(50Å)-CuBr/Propyl-2-pyridylmethanimine immobilized catalyst. Method 1: Multi-step Grafting Approach – SBA15(50)-CuBr/PMI-M1.

(A) Preparation of amine functionalized silica surface – SBA15(50)-NH_2-M1. To a 250 mL round-bottom flask, 2.00 g of APTMS was added to a slurry of 3.00 g of SBA15 (50 Å pores) in 100 mL of toluene. The reaction mixture was stirred at 110 °C for 48 hrs under argon. The solid product was recovered and washed, once with 100 mL of toluene, once with 100 mL of hexane, and once with 100 mL of dichloromethane. The solid product was dried under vacuum at room temperature for 12 h and stored under dry nitrogen in a glovebox, yielding a white powder containing 1.36 mmol $–NH_2$ g-solid^{-1} by TGA.

(B) Preparation of SBA-15(50Å)-3-propyl-2-pyridylmethanimine functionalized surface – SBA15(50)-PMI-M1. To a 250 mL round-bottom flask, 1.09 g of PCA (10.2 mmol) was added to a slurry of 2.50 g of SBA15(50)-NH_2-M1 (3.4 mmol of amine) in 100 mL MeOH. The reaction mixture was stirred at 75 °C for 24 hrs under argon. The solid product was recovered and washed, once with 100 mL of toluene, once with 100 mL of hexane, and once with 100 mL of dichloromethane. The solid product was dried under vacuum at room temperature for 12 hrs and stored under dry nitrogen in

a glovebox, yielding a yellowish white powder containing 1.13 mmol PMI g-solid^{-1} by TGA.

(C) Metallation of SBA-15(50Å)-3-propyl-2-pyridylmethanimine with CuBr – SBA15(50)-CuBr/PMI-M1. To a 100 mL round-bottom flask, 0.16 g of CuBr (1.13 mmol) was added to a slurry of 2.00 g of SBA15(50)-PMI-M1 (2.26 mmol of ligand) in 50 mL of toluene. The reaction mixture was stirred at 110 °C for 24 hrs under argon. The solid product was recovered and washed, once with 100 mL of toluene, once with 100 mL of hexane, and once with 100 mL of dichloromethane. The dark reddish brown powder was dried under vacuum at room temperature for 12 hrs and stored under dry nitrogen in a glovebox. CHN, Si, and Cu analyses showed 1.07 mmol PMI g-catalyst^{-1} and 0.48 mmol Cu g-catalyst^{-1}, respectively.

Preparation of SBA-15(50Å)-CuBr/3-propyl-2-pyridylmethanimine immobilized catalyst. Method 2: 2-Step Approach – SBA15(50)-CuBr/PMI-M2.

(A) Preparation of SBA-15(50Å)-3-propyl-2-pyridylmethanimine functionalized surface – SBA15(50)-PMI-M2. To a 250 mL round-bottom flask, 1.50 g of PMITMS was added to a slurry of 3.00 g of SBA15 (50 Å pores) in 100 mL of toluene. The reaction mixture was stirred at 110 °C for 48 hrs under argon. The solid product was recovered and washed, once with 100 mL of toluene, once with 100 mL of hexane, and once with 100 mL dichloromethane. The solid product was dried under vacuum at room temperature for 12 hrs and stored under dry nitrogen in a glovebox, yielding a yellow powder containing 1.04 mmol PMI g-solid^{-1} by TGA.

(B) Metallation of SBA-15(50Å)-3-propyl-2-pyridylmethanimine with CuBr – SBA15(50)-CuBr/PMI-M2. To a 100 mL round-bottom flask, 0.15 g of CuBr (1.04 mmol) was added to a slurry of 2.00 g of SBA15(50)-PMI-M2 (2.08 mmol of ligand) in 50 mL of toluene. The reaction mixture was stirred at 110 °C for 24 hrs under argon. The solid product was recovered and washed, once with 100 mL toluene, once with 100 mL of hexane, and once with 100 mL of dichloromethane. The dark reddish brown powder was dried under vacuum at room temperature for 12 hrs and stored under dry nitrogen in a glovebox. CHN, Si, and Cu analyses showed 1.09 mmol PMI g-catalyst^{-1} and 0.51 mmol Cu g-catalyst^{-1}, respectively.

Preparation of SBA-15(50Å)-CuBr/3-propyl-2-pyridylmethanimine immobilized catalyst. Method 3: One-pot Approach – SBA15(50)-CuBr/PMI-M3.

To a 250 mL round-bottom flask**,** 1.00 g of PMITMS (3.73 mmol) was added to a slurry of 0.27 g of CuBr (1.86 mmol) and 2.00 g of SBA15 (50 Å pores) in 100 mL of toluene. The reaction mixture was stirred at 110 °C for 48 hrs under argon. The solid product was recovered and washed, once with 100 mL of toluene, once with 100 mL of hexane, and once with 100 mL of dichloromethane. The dark reddish brown powder was dried under vacuum at room temperature for 12 hrs and stored under dry nitrogen in a glovebox. CHN, Si, and Cu analyses showed 1.02 mmol PMI g-catalyst^{-1} and 0.42 mmol Cu g-catalyst^{-1}, respectively.

Preparation of SBA-15(50Å)-CuBr/3-propyl-2-pyridylmethanimine immobilized catalyst. Method 4: Pre-assembled Complex Approach–SBA15(50)-CuBr/PMI-M4.

To a 250 mL two-neck round-bottom flask, a solution 1.00 g of PMITMS (3.73 mmol) and 5 mL of toluene was slowly added to a stirring mixture of 0.27 g of CuBr (1.86 mmol) in 100 mL of toluene. The resulting light brown mixture was then stirred at 70 °C for 30 minutes under argon or until the reaction mixture appears to be a dark reddish brown homogeneous solution. Under positive argon pressure, 2.00 g of SBA-15 (50 Å pores) was added to the reaction mixture through the flask's second neck. Then the reaction mixture was stirred at 110 °C for 48 hrs. The solid product was recovered and washed, once with 100 mL of toluene, once with 100 mL of hexane, and once with 100 mL of dichloromethane. The dark reddish brown powder was dried under vacuum at room temperature for 12 hrs and stored under dry nitrogen in a glovebox. CHN, Si, and Cu analyses showed 1.07 mmol PMI g-catalyst^{-1} and 0.48 mmol Cu g-catalyst^{-1}, respectively.

Preparation of SBA-15(100Å) and Cab-O-Sil EH5 – CuBr/PMI immobilized catalyst. Methods 1 thru 4:

In a similar manner to the methods described above for SBA-15 (50 Å pores), a supported CuBr/PMI complex was immobilized on a larger pore SBA-15 (100 Å pores) and nonporous Cab-O-Sil EH5 silica supports for all methods (M1 thru M4). All the immobilized catalysts were recovered, washed, and stored under the same conditions. CHN, Si, and Cu analyses are summarized in **Table 4.4**.

Table 4.4 CHN, Si, and Cu elemental analyses for immobilized silica CuBr/PMI catalysts.

Entry	Materials	% C	% H	% N	% Si	% Cu
1	SBA(50)-CuBr/PMI-M1	10.84	1.86	2.40	34.63	1.80
2	SBA(50)-CuBr/PMI-M2	14.26	2.06	2.72	32.79	2.59
3	SBA(50)-CuBr/PMI-M3	15.22	2.06	2.65	32.55	2.80
4	SBA(50)-CuBr/PMI-M4	15.10	1.89	2.75	31.63	2.05
5	SBA(100)-CuBr/PMI-M1	15.30	2.47	3.00	28.87	3.59
6	SBA(100)-CuBr/PMI-M2	12.31	1.74	2.91	29.70	2.66
7	SBA(100)-CuBr/PMI-M3	13.72	1.64	3.23	29.17	3.13
8	SBA(100)-CuBr/PMI-M4	15.67	2.76	3.48	36.60	3.34
9	Cab-O-Sil-CuBr/PMI-M1	10.38	1.13	2.47	36.71	2.69
10	Cab-O-Sil-CuBr/PMI-M2	10.77	2.04	2.44	33.60	2.14
11	Cab-O-Sil-CuBr/PMI-M3	13.14	1.41	3.18	27.90	3.89
12	Cab-O-Sil-CuBr/PMI-M4	13.83	1.34	3.30	33.56	3.06

References

[1] S. C. Hong, H.-J. Paik, and K. Matyjaszewski, Macromolecules 34 (2001) 5099.

[2] S. C. Hong and K. Matyjaszewski, Macromolecules 35 (2002) 7592.

[3] D. M. Haddleton, D. Kukulj, and A. P. Radigue, Chemical Communications (1999) 99.

[4] S. Liou, J. T. Rademacher, D. Malaba, M. E. Pallack, and W. J. Brittain, Macromolecules 33 (2000) 4295.

[5] M. E. Honigfort and W. J. Brittain, Macromolecules 36 (2003) 3111.

[6] Y. Shen, S. Zhu, and R. Pelton, Macromolecules 34 (2001) 3182.

[7] Z. Zhang, S. Dai, R. D. Hunt, Y. Wei, and S. Qiu, Advanced Materials (Weinheim, Germany) 13 (2001) 493.

[8] S. Dai, M. C. Burleigh, Y. H. Ju, H. J. Gao, J. S. Lin, S. J. Pennycook, C. E. Barnes, and Z. L. Xue, Journal of the American Chemical Society 122 (2000) 992.

[9] S. Dai, M. C. Burleigh, Y. Shin, C. C. Morrow, C. E. Barnes, and Z. Xue, Angewandte Chemie, International Edition 38 (1999) 1235.

[10] S. C. Hong, D. Neugebauer, Y. Inoue, J.-F. Lutz, and K. Matyjaszewski, Macromolecules 36 (2003) 27.

[11] S. C. Hong, J.-F. Lutz, Y. Inoue, C. Strissel, O. Nuyken, and K. Matyjaszewski, Macromolecules 36 (2003) 1075.

[12] Y. Shen, S. Zhu, and R. Pelton, Macromolecular Rapid Communications 21 (2000) 956.

[13] G. Kickelbick, H.-j. Paik, and K. Matyjaszewski, Macromolecules 32 (1999) 2941.

[14] D. M. Haddleton, D. J. Duncalf, D. Kukulj, and A. P. Radigue, Macromolecules 32 (1999) 4769.

[15] Y. Shen, S. Zhu, F. Zeng, and R. Pelton, Macromolecular Chemistry and Physics 201 (2000) 1387.

[16] Y. Shen, S. Zhu, F. Zeng, and R. H. Pelton, Macromolecules 33 (2000) 5427.

[17] Y. Shen, S. Zhu, F. Zeng, and R. Pelton, Journal of Polymer Science, Part A: Polymer Chemistry 39 (2001) 1051.

[18] Y. Shen, S. Zhu, and R. Pelton, Macromolecules 34 (2001) 5812.

[19] Y. Shen and S. Zhu, Macromolecules 34 (2001) 8603.

[20] T. Opstal, K. Melis, and F. Verpoort, Catalysis Letters 74 (2001) 155.

[21] J. V. Nguyen and C. W. Jones, Journal of Polymer Science, Part A: Polymer Chemistry 42 (2004) 1367.

[22] D. M. Haddleton, C. B. Jasieczek, M. J. Hannon, and A. J. Shooter, Macromolecules 30 (1997) 2190.

[23] D. M. Haddleton, D. J. Duncalf, D. Kukulj, M. C. Crossman, S. G. Jackson, S. A. F. Bon, A. J. Clark, and A. J. Shooter, European Journal of Inorganic Chemistry (1998) 1799.

[24] H. Baranska, A. Labudzinska, and J. Terpinski, Laser Raman Spectrometry, Wiley, New York, 1987.

[25] C. D. Nunes, M. Pillinger, A. A. Valente, I. S. Goncalves, J. Rocha, P. Ferreira, and F. E. Kuhn, European Journal of Inorganic Chemistry (2002) 1100.

[26] D. Zhao, Q. Huo, J. Feng, B. F. Chmelka, and G. D. Stucky, Journal of the American Chemical Society 120 (1998) 6024.

[27] D. Zhao, J. Feng, Q. Huo, N. Melosh, G. H. Frederickson, B. F. Chmelka, and G. D. Stucky, Science (Washington, D. C.) 279 (1998) 548.

[28] M. Kruk, M. Jaroniec, C. H. Ko, and R. Ryoo, Chemistry of Materials 12 (2000) 1961.

[29] C. Corp., Product Data Sheet for Untreated Fumed Silica Cab-O-Sil EH5 http://www.cabot-corp.com (2002)

[30] D. W. Sindorf and G. E. Maciel, Journal of the American Chemical Society 105 (1983) 3767.

[31] A. B. Pangborn, M. A. Giardello, R. H. Grubbs, R. K. Rosen, and F. J. Timmers, Organometallics 15 (1996) 1518.

CHAPTER 5

PROBING THE ROLE OF SYNTHETIC METHOD AND SUPPORT POROSITY ON THE STRUCTURE AND PERFORMANCE OF SILICA-SUPPORTED CUBR/PYRIDYLMETHANIMINE ATOM TRANSFER RADICAL POLYMERIZATION CATALYSTS: II. POLYMERIZATION OF METHYL METHACRYLATE

Abstract

A systematic study of the effect of synthesis method and catalyst structure on the Atom Transfer Radical Polymerization (ATRP) performance of CuBr/ pyridylmethanimine (PMI) complexes supported on silica is described. Four different synthetic routes including multi-step grafting (M1), two-step grafting (M2), one-pot (M3) and pre-assembled complex (M4) methods are evaluated on three different silica supports (mesoporous SBA-15 with 50 and 100 Å pores and non-porous Cab-O-Sil EH5). The resulting solids are utilized for ATRP of methyl methacrylate (MMA). The catalysts allowed for moderate to poor control of the polymerization, with polydispersity indices (PDIs) ranging from 1.46 to above 2. The materials made using the pre-assembled complex (M4) and one-pot (M3) approaches were generally more effective than those prepared using a grafting method (M1, M2) on porous silica, whereas all methods gave similar performing catalysts on the nonporous support. Nonporous Cab-O-Sil EH5 was the most effective support due to its small particle size, lack of porosity and its relative compatibility in reaction media. All catalysts leached copper into solution in small amounts. In addition, the catalysts could be effectively recycled, with improved "controlled" character in recycle runs (PDIs ~ 1.2).

Introduction

There are many examples in the literature involving the immobilization of an ATRP metal/ligand complex on various supports [1-27], but few systematic studies of multiple methods of immobilizing a single type of catalyst. In Chapter 4 of this work, four different synthetic schemes were used to immobilize CuBr/pyridylmethanimine (PMI) ATRP catalysts on various silica supports and the resulting solids were characterized in detail [28]. Extensive characterization revealed that method 4 (M4), the pre-assembled complex methodology, resulted in a more structurally homogeneous immobilized ATRP complex. However, catalyst characterization does not reveal how effective the catalyst will perform. Here the new materials synthesized in Chapter 4 are evaluated as catalysts for the ATRP of methyl methacrylate (**Figure 5.1**). The polymerization performances are compared to a homogeneous analog and as a function of synthetic methodology (M1-M4) and support structure.

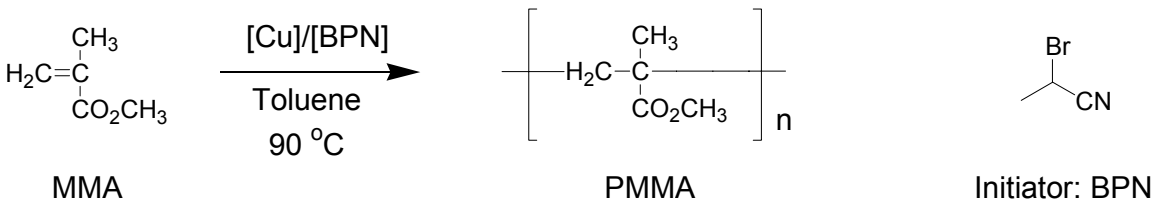

Figure 5.1 Reaction scheme for ATRP of methyl methacrylate.

Results

Homogeneous PPMI/CuBr polymerizations

N-(n-propyl)-2-pyridylmethanimine (PPMI) ligand was synthesized as a homogeneous analogue for comparison with immobilized CuBr/PMI catalysts on silica [29]. **Figure 5.2** shows the kinetic results for the homogeneous polymerization. The polymerization had an initial rate of 0.78 mol L^{-1} hr^{-1} and reached 73 % conversion of monomer after 12 hours. The first-order kinetic plot was linear for low conversions, but the plot deviates at higher conversion likely due to increased chain termination at higher conversion levels. The M_n increases linearly with conversion and is slightly higher than the predicted. The PDI decreases with conversion, leveling out at approximately 1.13. The linear kinetics and narrow PDI was evidence that the polymerization was controlled. These results are consistent with those reported by Haddleton [30].

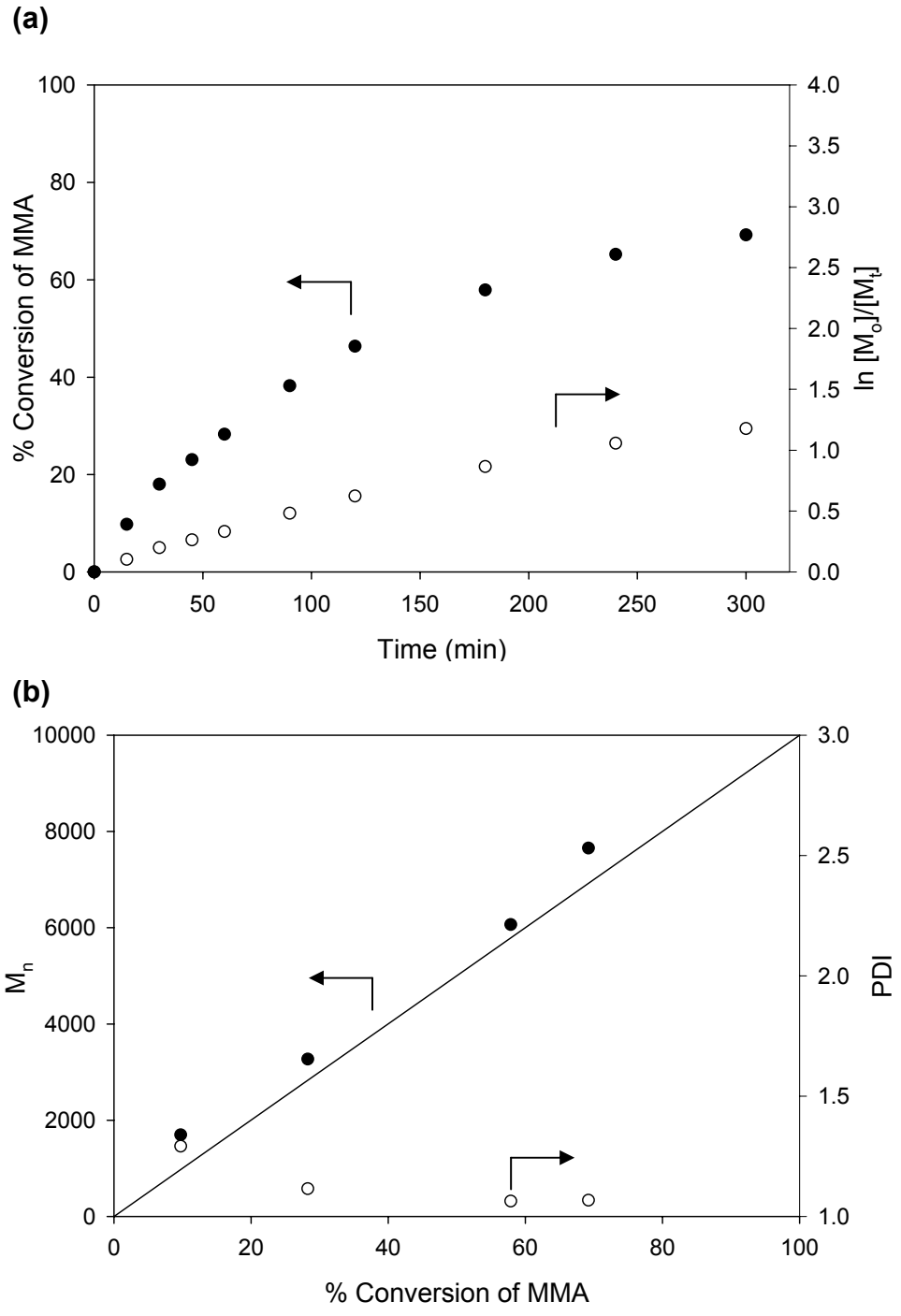

Figure 5.2 Kinetic plots for homogeneous polymerization with CuBr/PPMI catalyst. Evolution of conversion and $\ln[M_o]/[M_t]$ with time (a) and evolution of M_n and PDI with monomer conversion (b) See experimental section for polymerization conditions.

Heterogeneous silica immobilized CuBr/PMI polymerizations

Table 5.1 and **Table 5.2** summarizes the polymerization results using all the various fresh catalysts. In all experiments, no observable catalyst settling occurred when the polymerization solution was stirred. For CuBr/PMI catalysts immobilized by M1 thru M4 on SBA-15 with 50 Å pores, the initial rate ranged from 0.31 to 0.65 mol L^{-1} hr^{-1}. The final conversions were measured after 24 hours. The polymerization proceeded slower than the homogeneous polymerization after the first hour (homogeneous, 73% after 12 hrs; heterogeneous 67-82% after 24 hrs). The kinetic plots showed evidence of a large degree of termination based on the nonlinear nature of the first-order kinetic plot and evolution of M_n with conversion, **Figure 5.3 and 5.4**. Most of the polymerizations were uncontrolled, with PDIs above or approaching 2.0. Polymerization with M3 showed the most control with a PDI of 1.58. Interestingly, M4, an *in-situ* metallation method similar to M3, exhibited poor polymerization behavior similar to M1 and M2. To verify this observation, new batches of catalyst for SBA15(50)-CuBr/PMI-M3 and SBA15(50)-CuBr/PMI-M4 were prepared and evaluated, with consistent polymerization results observed. In all cases, the polymers were of higher molecular weight than predicted and showed only a limited increase in molecular weight with conversion.

Table 5.1 Polymerizations of MMA results of immobilized silica CuBr/PMI catalysts: Kinetic results and polymer characterization.

Entry	Materials	Initial Rate (mol/L hr)	t (hrs)	% Conv	$M_{n,Th}$	$M_{n,Exp}$	PDI
1	CuBr/PPMI	0.78	12	73	7300	7800	1.13
2	SBA(48)-CuBr/PMI-M1	0.31	24	82	8200	15400	1.97
3	SBA(48)-CuBr/PMI-M2	0.54	24	70	7000	13600	1.96
4	SBA(48)-CuBr/PMI-M3	0.62	24	67	6700	8700	1.58
5	SBA(48)-CuBr/PMI-M4	0.65	24	82	8200	10300	2.27
6	SBA(100)-CuBr/PMI-M1	0.04	7	64	6400	11000	2.05
7	SBA(100)-CuBr/PMI-M2	1.05	7	83	8300	13900	1.90
8	SBA(100)-CuBr/PMI-M3	1.17	7	84	8400	14200	1.52
9	SBA(100)-CuBr/PMI-M4	1.26	7	78	7800	12100	1.60
10	Cab-O-Sil-CuBr/PMI-M1	1.39	7	83	8300	11200	1.46
11	Cab-O-Sil-CuBr/PMI-M2	2.05	6	85	8500	12200	1.64
12	Cab-O-Sil-CuBr/PMI-M3	1.87	8	81	8100	13600	1.66
13	Cab-O-Sil-CuBr/PMI-M4	1.68	8	80	8000	12500	1.57

[MMA]/[Cu]/[BPN] = 100/1/1 in 25% by v/v MMA in toluene at 90 ºC.

Table 5.2 Polymerizations of MMA results of immobilized silica CuBr/PMI catalysts: Leached copper analysis.

Entry	Materials	Theoretical[1] R_{Cu} (ppm)	Actual[2] R_{Cu} (ppm)	% Leached
1	CuBr/PPMI	8460	----	----
2	SBA(48)-CuBr/PMI-M1	7480	42	0.56
3	SBA(48)-CuBr/PMI-M2	8720	47	0.54
4	SBA(48)-CuBr/PMI-M3	9090	10	0.11
5	SBA(48)-CuBr/PMI-M4	7480	34	0.45
6	SBA(100)-CuBr/PMI-M1	9500	169	1.78
7	SBA(100)-CuBr/PMI-M2	7400	80	1.08
8	SBA(100)-CuBr/PMI-M3	7310	191	2.61
9	SBA(100)-CuBr/PMI-M4	7860	10	0.13
10	Cab-O-Sil-CuBr/PMI-M1	7400	186	2.51
11	Cab-O-Sil-CuBr/PMI-M2	7230	317	4.39
12	Cab-O-Sil-CuBr/PMI-M3	7570	23	0.30
13	Cab-O-Sil-CuBr/PMI-M4	7670	56	0.73

1. Assumption all copper on catalysts leaches into the polymer.
2. Residual copper content determined by elemental analyses (detection limit was 10 ppm).

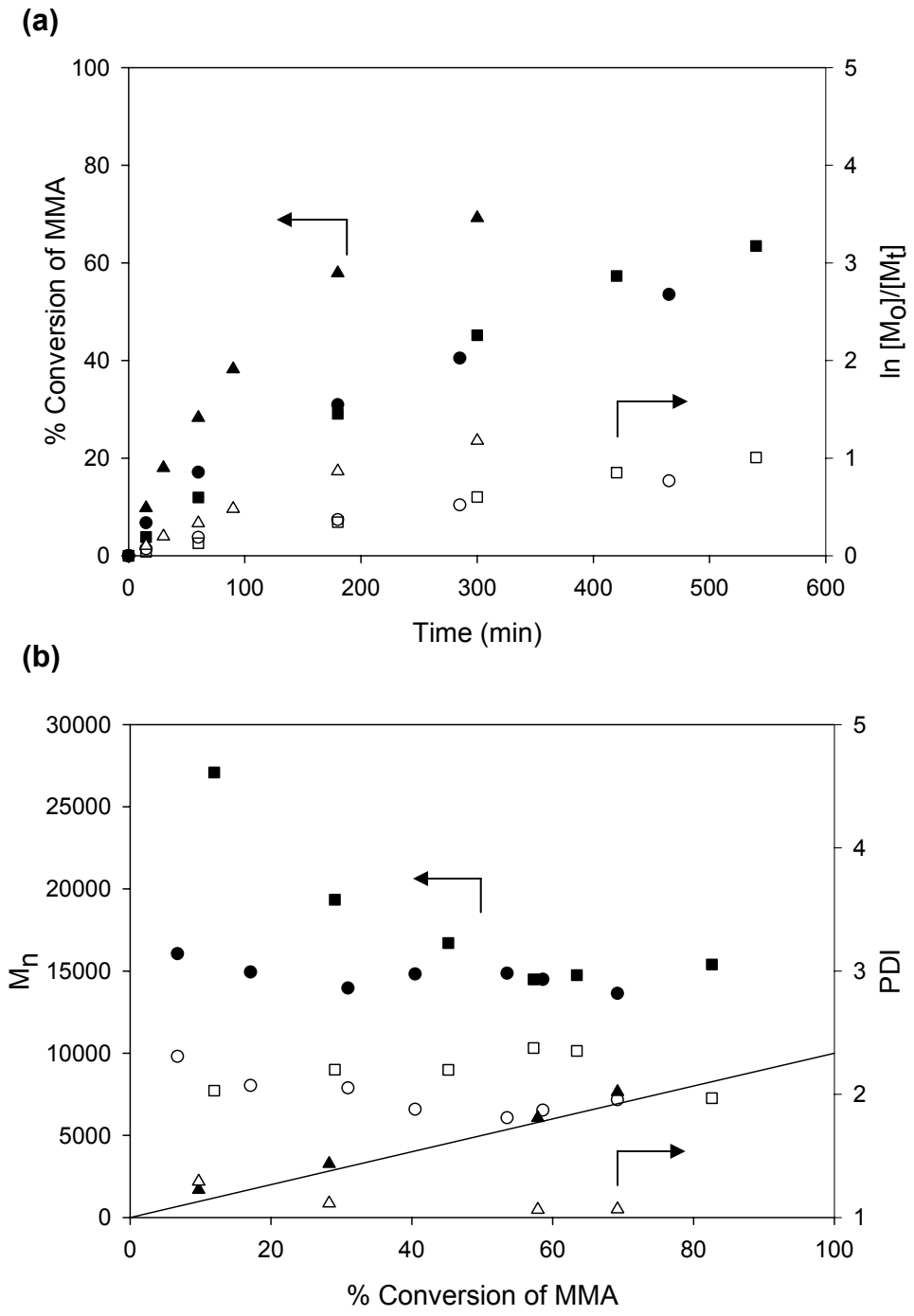

Figure 5.3 Kinetic plots for heterogeneous polymerizations with SBA15(50)-CuBr/PMI–M1 and M2 catalysts. Evolution of conversion and $\ln[M_o]/[M_t]$ with time (a) and evolution of M_n and PDI with monomer conversion. SBA15(50)-CuBr/PMI–M1 (■, □), SBA15(50)-CuBr/PMI–M2 (●, ○), and homogeneous CuBr/PPMI catalyst (▲, △). Theoretical M_n line (-). See experimental section for polymerization conditions.

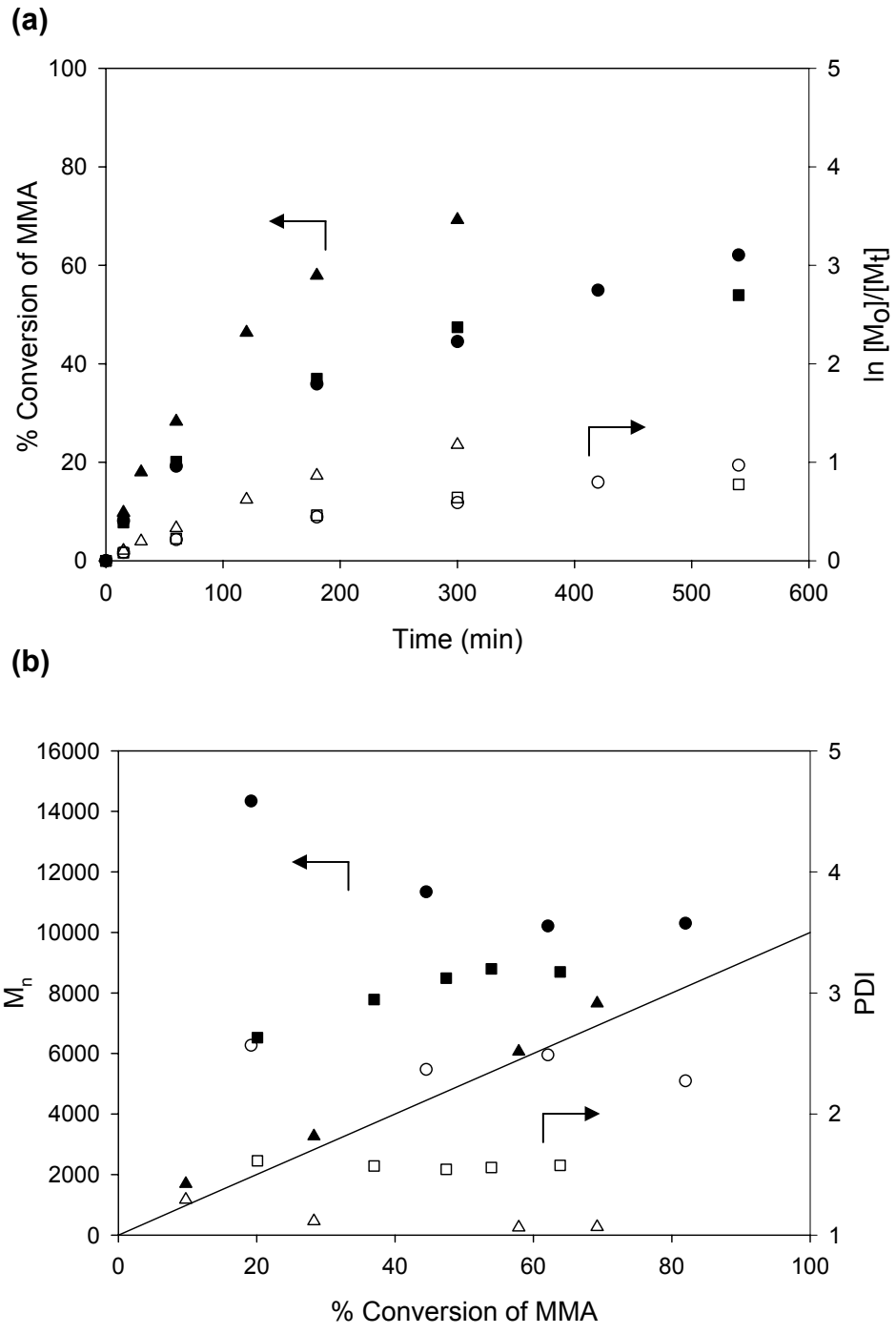

Figure 5.4 Kinetic plots for heterogeneous polymerizations with SBA15(50)-CuBr/PMI–M3 and M4 catalysts. Evolution of conversion and $\ln[M_o]/[M_t]$ with time (a) and evolution of M_n and PDI with monomer conversion. SBA15(50)-CuBr/PMI–M3 (■, □), SBA15(50)-CuBr/PMI–M4 (●, ○), and homogeneous CuBr/PPMI catalyst (▲, △). Theoretical M_n line (-). See experimental section for polymerization conditions.

For the catalysts supported on SBA-15 with 100 Å pores, polymerization results for M3 and M4 were comparable to CuBr/PMI immobilized systems reported by Haddleton [7] and Brittain [1, 9]. The initial rate ranged from 0.04 to 1.26 mol L^{-1} hr^{-1}. The final conversions were measured after 7 hours. The rate of the polymerization proceeded faster than the homogeneous polymerizations for M2, M3, and M4. **Figure 5.5 and 5.6** shows the kinetic plots for the polymerization with CuBr/PMI complexes immobilized on SBA15(100) by M1 thru M4. The first order kinetic plots show evidence of chain termination (**Figure 5.5a and 5.6a**). The MWs were higher than the predicted in all cases (**Figure 5.5b and 5.6b**). M1 and M2 catalysts showed poor polymerization control, which is evident by to the broad molecular weight distributions. The M4 catalyst followed the theoretical MW line more closely than catalyst M3. From **Figure 5.6b**, the evolution of PDI with conversion shows that M4 reaches its minimum PDI earlier in the polymerization than the other methods. At earlier stages in the polymerization the PDI was 1.52 for M4 and remained around 1.60, while for M3, the PDI was 2.17 and decreased with conversion, a more classic profile for a controlled or quasi-controlled system [31, 32].

For CuBr/PMI catalysts supported on nonporous Cab-O-Sil, the initial rate ranged from 1.39 to 2.05 mol L^{-1} hr^{-1} and were generally higher than CuBr/PMI catalysts immobilized on SBA15(50 and 100). The final conversions were >80% after 8 hours. **Figure 5.7 and 5.8** shows the kinetic plots for polymerizations with CuBr/PMI complexes immobilized on Cab-O-Sil by M1 thru M4. The first order kinetic plot shows evidence of some chain termination (**Figure 5.7a and 5.8a**), especially at higher conversions. The plots of molecular weight with conversion were linear (**Figure 5.7b**

and 5.8b) and relatively parallel with the theoretical line, although molecular weights were always higher than predicted. This observation is common to supported ATRP catalysts, and can result from poor deactivation of the growing chain at the outset of the polymerization [1-4, 7-23]. All the catalysts exhibit some degree of control over the polymerizations with PDIs ranging from 1.46 to 1.66 for the final polymer. The M1 catalyst and M2 catalyst behaved similarly kinetically. Likewise, catalyst M3 and catalyst M4 behaved alike, with both exhibiting fair to moderate control throughout the polymerization.

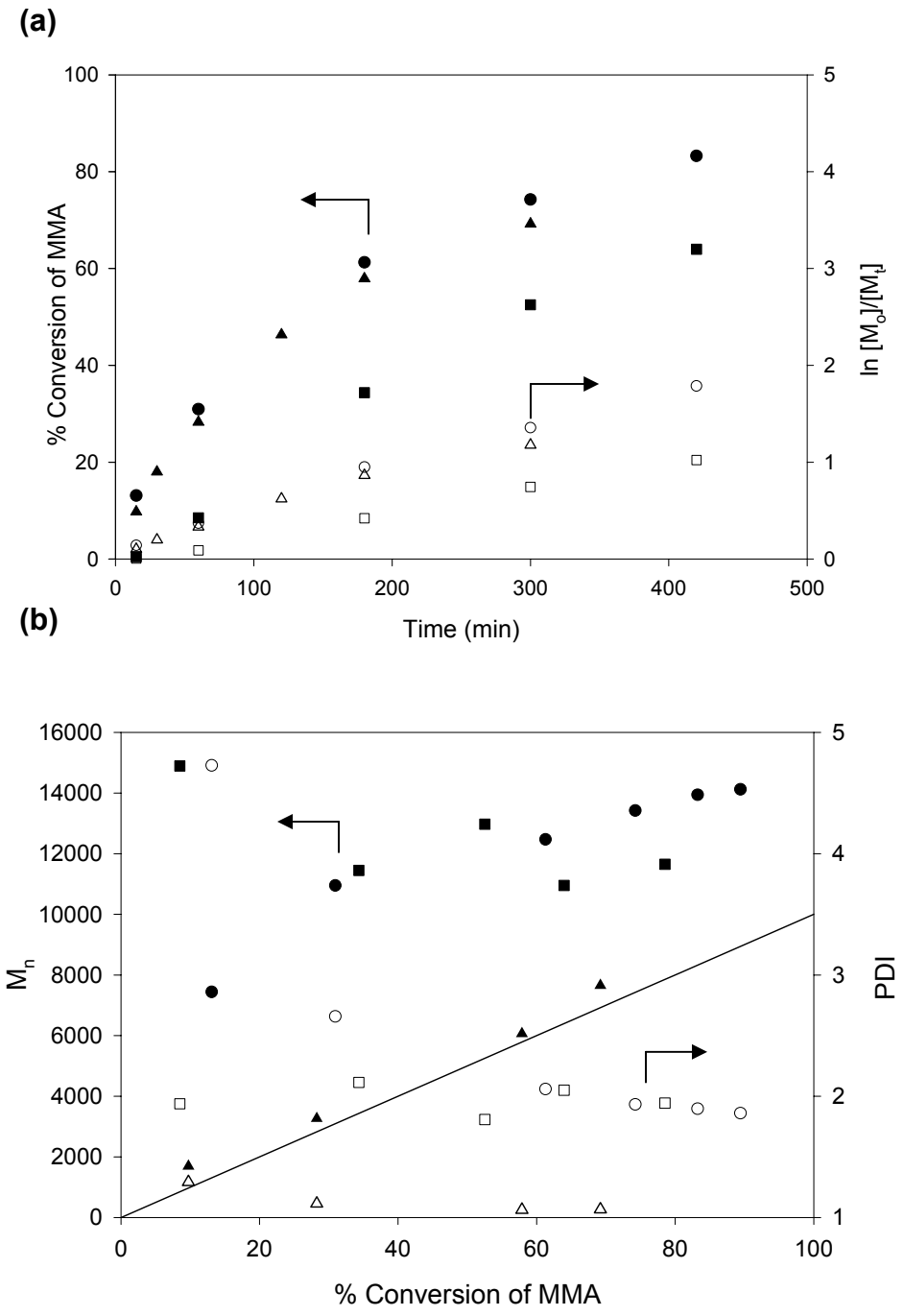

Figure 5.5 Kinetic plots for heterogeneous polymerizations with SBA15(100)-CuBr/PMI–M1 and M2 catalysts. Evolution of conversion and $\ln[M_o]/[M_t]$ with time (a) and evolution of M_n and PDI with monomer conversion. SBA15(100)-CuBr/PMI–M1 (■, □), SBA15(100)-CuBr/PMI–M2 (●, ○), and homogeneous CuBr/PPMI catalyst (▲, △). Theoretical M_n line (-). See experimental section for polymerization conditions.

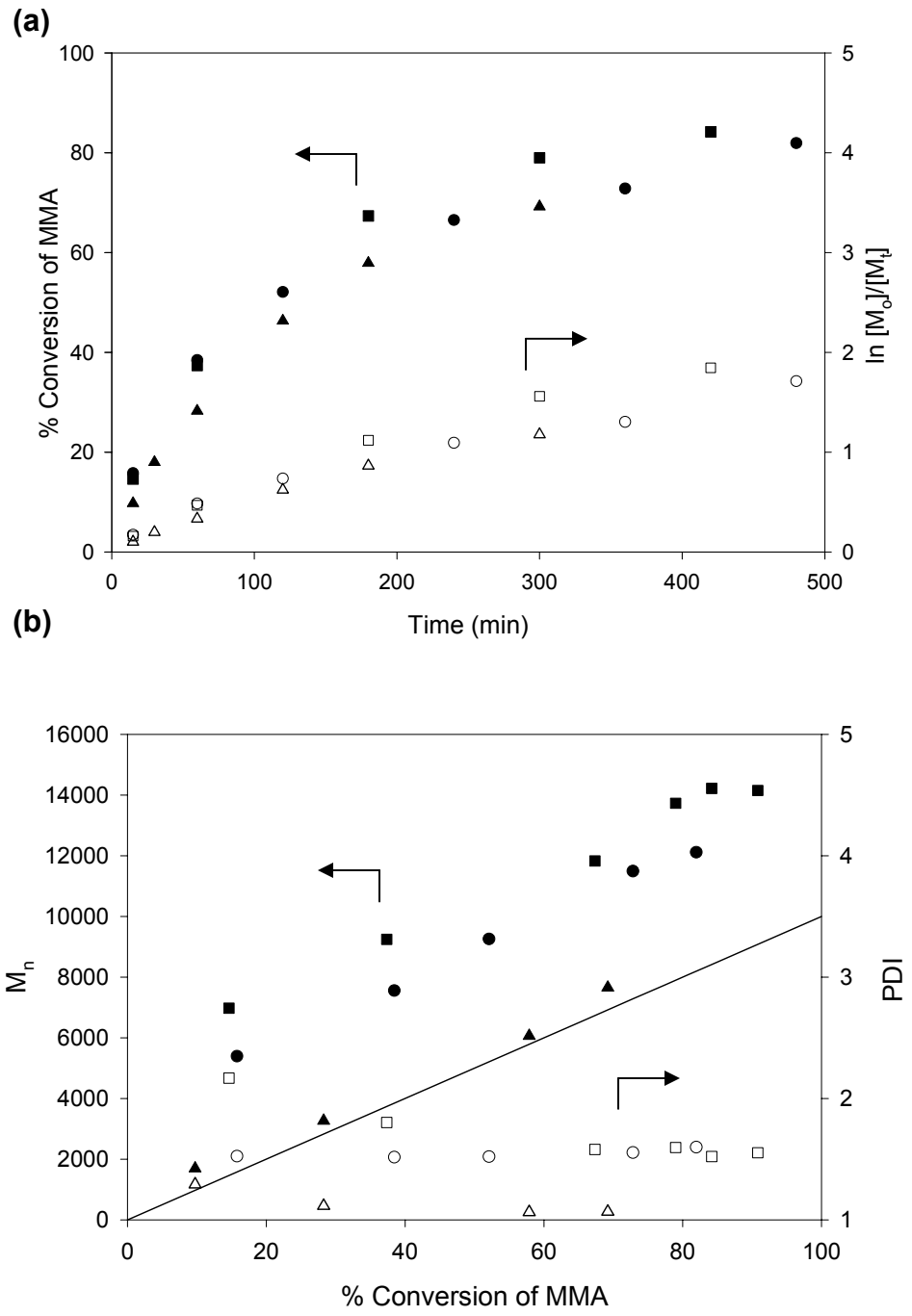

Figure 5.6 Kinetic plots for heterogeneous polymerizations with SBA15(100)-CuBr/PMI–M3 and M4 catalysts. Evolution of conversion and $\ln[M_o]/[M_t]$ with time (a) and evolution of M_n and PDI with monomer conversion. SBA15(100)-CuBr/PMI–M3 (■, □), SBA15(100)-CuBr/PMI–M4 (●, ○), and homogeneous CuBr/PPMI catalyst (▲, △). Theoretical M_n line (-). See experimental section for polymerization conditions.

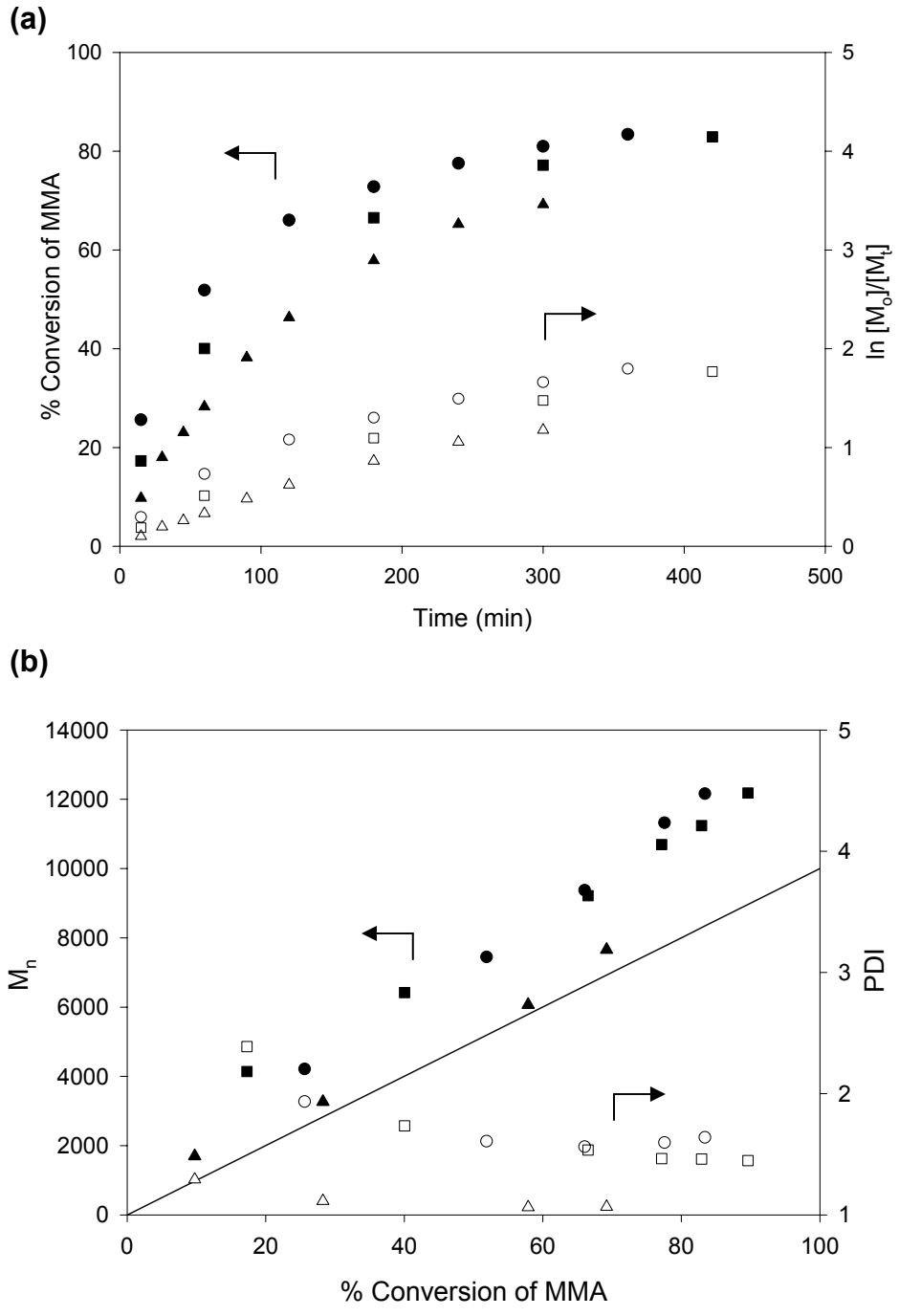

Figure 5.7 Kinetic plots for heterogeneous polymerizations with Cab-O-Sil-CuBr/PMI–M1 and M2 catalysts. Evolution of conversion and $\ln[M_o]/[M_t]$ with time (a) and evolution of M_n and PDI with monomer conversion. Cab-O-Sil-CuBr/PMI–M1 (■, □), Cab-O-Sil-CuBr/PMI–M2 (●, ○), and homogeneous CuBr/PPMI catalyst (▲, △). Theoretical M_n line (-). See experimental section for polymerization conditions.

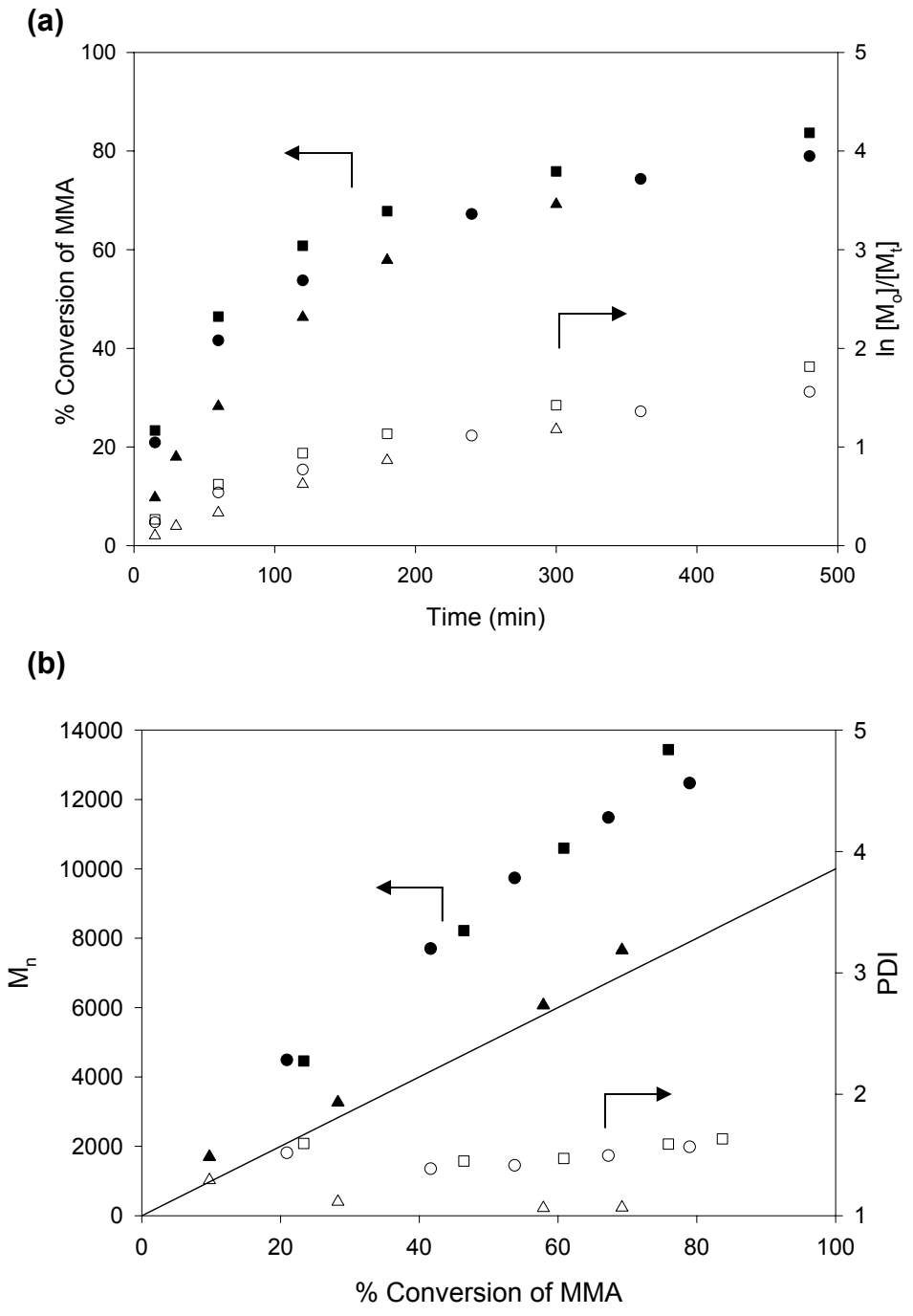

Figure 5.8 Kinetic plots for heterogeneous polymerizations with Cab-O-Sil-CuBr/PMI–M3 and M4 catalysts. Evolution of conversion and $\ln[M_o]/[M_t]$ with time (a) and evolution of M_n and PDI with monomer conversion. Cab-O-Sil-CuBr/PMI–M3 (■, □), Cab-O-Sil-CuBr/PMI–M4 (●, ○), and homogeneous CuBr/PPMI catalyst (▲, △). Theoretical M_n line (-). See experimental section for polymerization conditions.

Discussion

Effect of immobilization method

Based on the polymerization results described above, the synthetic method employed has a pronounced influence on catalyst structure and performance. For the porous SBA-15 supports, catalysts prepared by M1 and M2 were clearly ineffective. The observed kinetics displayed signs of significant chain termination and the PDIs of the polymers produced by these catalysts were very broad, approaching 2 on both porous supports. In contrast, catalysts prepared using M3 displayed better performance, giving polymers with relatively narrow molecular weight distributions near 1.5. Interestingly, catalysts prepared using M4 showed stark differences depending on the pore size of the support. On the narrow pore, 50 Å SBA-15, extremely poor polymerization control was observed, with highly nonlinear kinetics and a very broad PDI of 2.27. In contrast, on the more open 100 Å SBA-15, M4 yielded a catalyst that produced polymers with moderate control, giving a PDI of 1.6. Potential causes for this difference are discussed below.

A slightly different trend was observed for catalysts supported on the nonporous Cab-O-Sil silica. For this support, all the synthetic methods performed similarly, with the catalyst made via M1 appearing to give slightly more control over the polymerization. It is noteworthy that catalysts prepared using M1 and M2 were ineffective at controlling the polymerization on SBA-15 supports, but reasonably effective at promoting controlled polymerizations on Cab-O-Sil. For both of these methods, the metallations were done after the ligand immobilization; thus, if there were any bare, unfunctionalized silanols on the silica surface, some of the CuBr could be adsorbed to these PMI-free sites on the

silica surface. In a control experiment, CuBr adsorbed onto silica showed no activity towards the polymerization of MMA. If this adsorption on bare silica occurs, not all the Cu sites would be active for controlling ATRP and there would be an imbalance in the metal to initiator ratio - all the initiators could not be activated at the same time. This could lead to uncontrolled polymerization and broad molecular weight distributions as observed in catalysts prepared by M1 and M2 on SBA-15. FT-Raman spectra [28] indicate that there likely exists some uncoordinated PMI ligand on the surface in SBA-15 catalysts prepared by M1 and M2, which supports the above hypothesis.

In contrast, as mentioned above, the M1 and M2 derived Cab-O-Sil catalysts give good control over the polymerization. This may be due to a lower percentage of unligated copper species on these materials. The support surface area for Cab-O-Sil is approximately 2-3-folds less than the SBA-15 supports. Since the ligand loadings were comparable for all catalysts synthesized (~1.0 mmol PMI g-catalysts^{-1}), the available surface area for CuBr to adsorb on the bare silica surface was substantially less for Cab-O-Sil. The CuBr may have coordinated with the immobilized ligand to a greater extent on the functionalized Cab-O-Sil supports than on the SBA-15 supports. The higher ligand density on Cab-O-Sil (2.60 PMI-ligands nm^{-2}) [28] should improve the coordination in general and make bis coordination more likely than when these methods are used on SBA-15 (1.20 and 1.15 PMI-ligands nm^{-2} for 50 and 100 Å, respectively [28]). Thus, with Cab-O-Sil supports with a dense loading of ligands, there may be a greater propensity to form PMI-ligated species, leading to effective catalysts.

As noted before, all the heterogeneous polymerizations behaved kinetically similarly to several previously reported immobilized copper ATRP systems [2, 14, 16,

17], with the best control reported here akin to moderate levels of control achievable with other copper complex/support combinations. There was initially a period of uncontrolled polymerization that occurred before the equilibrium between Cu(I) and Cu(II) was established. From **Figure 5.3b and 5.4b**, the observed MWs were several times higher than the predicted MWs initially for catalysts immobilized on SBA15(50). The same observation can be made for M1, M2, and M3 catalysts immobilized on SBA15(100), (**Figure 5.5b and 5.6b**). These observations may be attributable to inefficient initiation. Only the SBA15(100)-M4 and Cab-O-Sil catalysts gave reasonably controlled polymerizations.

Haddleton [8] and Brittain [1, 9] immobilized their PMI ligands via a method most akin to M1. A stepwise procedure was utilized to graft the PMI ligand on the various supports (as in M1 here), but the metallation of the solids was not analogous to this study. Whereas the catalysts prepared here were recovered and purified after metallation, in the previous studies, the metallation was carried out *in-situ* in the presence of the monomer and initiator. Despite this difference, there doesn't seem to be a significant effect on the polymerization performance between the two different metallation and polymerization procedures, as the Cab-O-Sil-CuBr/PMI-M1 catalyst reported here performs similarly to immobilized PMI (M1) ligand on nonporous silica and cross-linked poly(styrene) resin supports [8]. However, there does seem to be a difference in the polymerization behavior when comparing the support's structure and properties. Haddleton and Brittain investigated PMI ligands supported on organic polymers that are more solvent swellable/compatible at reaction temperatures than silica. The compatibility of the support with the solvent appears to have a positive impact on the

control of the polymerization. Haddleton obtains molecular weight distribution of 1.56 for poly(styrene)-PMI-M1 and Brittain obtains 1.45 for poly(ethylene)-PMI-M1 and 1.29 for JandaJel-PMI-M1 supported systems. As mentioned previously, it was postulated that better control was exhibited in when using JandaJel as a support because it has a more flexible cross-linker compared to the poly(styrene) resin [9]. The increased swellability of these supports and lack of adsorption sites for ligand precursors (Si-OH groups) overcome the inherent limitations of the ligand immobilization method (M1) that are apparent on the porous silica supports described here. The importance of the catalysts accessibility will be discussed further below.

Effect of silica support structure

Of the three silica supports evaluated, Cab-O-Sil EH5 was by far the most effective. This material is a commercially available fumed silica with a very small primary particle size, making it moderately miscible in hot toluene. Furthermore, it has no measurable porosity, meaning that all of its surface area is external. In contrast, SBA-15 is a mesoporous silica material with straight mesopores in a hexagonal array. Although the mesopores are connected by small micropores [33], these micropores can be considered unimportant for the diffusion of relatively large species like polymer chains. Hence, in these polymerizations, each pore in the SBA-15 is essentially an isolated reaction environment with only a single entrance point and exit point at each end. These very different porosities of the supports would be expected to play a role in the effectiveness of the polymerizations. Indeed porosity does play a key role because the

accessibility of the catalyst complex can be limited by the size of the pore and growing polymer.

Transport limitations within porous solid catalysts when small molecule reactions are being promoted are usually thought to decrease reaction rates and lead to slower overall kinetics. For ATRP, internal transport limitations can have a number of potential effects. The fact that Cab-O-Sil supported catalysts give the best control over the polymerization regardless of the synthetic method (M1-M4) points to the paramount importance of access of the growing polymer chain to the metal complexes. In this case, when there is no porosity and the catalyst particle size allows partial miscibility in the reaction media, the growing polymer chain can access the $CuBr_2$/PMI complexes relatively easily and return to their dormant state. The ease of this deactivation process is critical to having a controlled polymerization. When considering the porous SBA-15 catalysts, I observe that the polymerizations are generally less controlled, with the restricted mobility of the growing chains within the pores affecting the polymerization process. In addition, the presence of porosity directly affects the rates of polymerization. The average initial rates for each support were 0.53, 0.88, 1.74 mol L^{-1} hr^{-1} for SBA15(50), SBA15(100), and Cab-O-Sil, respectively. The initial rate for polymerization with homogeneous CuBr/PPMI complex was 0.78 mol L^{-1} hr^{-1}. The conversion after 1 hour increases as follows: SBA15(50) < SBA15(100) < Cab-O-Sil. Interestingly, the support that gave the slowest rate resulted in the worst control over the polymerization. This is opposite the trend that might be expected with homogeneous catalysts. For homogeneous systems, the greater the equilibrium towards the deactivated complex, the slower the propagation rate and the better degree of control expected in the

process. The combination of slow polymerization rates and concomitant poor control in SBA15(50) supported materials may be attributed to inefficient deactivation caused by the narrow, non-interconnected pores that create isolated reaction environments. Increasing the pore size by using SBA15(100) increases the overall rate and results in slightly better control of the polymerization. These observations are consistent with entrapment of some growing polymer chains within the mesopores of the support. When the nonporous Cab-O-Sil support is used, it is observed that the overall polymerization rate is higher than in the homogeneous system but the polymerization is less controlled than the solid-free system. This is consistent with inefficient deactivation causing both increased reaction rates and increased polydispersity among the polymer chains.

As noted above, the catalyst SBA15(50)-CuBr/PMI-M4 displayed unique behavior in the polymerization of MMA. Although FT-Raman spectra indicated that nearly all the PMI ligands were coordinated to copper and elemental analysis data implied comparable copper loadings to other catalysts, this catalyst was observed to give the poorest control over the polymerization. In addition, the catalyst prepared using M3 on the same support gave relatively good control over the polymerization, as did catalysts derived from M3 and M4 over SBA15(100).

These observations might be rationalized by considering the size of the pores relative to the bis-coordinated CuBr/PMI complex. In M4, a preformed, bis-coordinated complex is added to the support material. If the immobilizable PMI ligand is fully extended, the ligand would extend roughly 12 Å from the silica surface. With a 50 Å pore diameter, it is easy to visualize how one or more bis-coordinated CuBr/PMI complexes could effectively block all access to the channels, preventing access to any

complexes that are immobilized inside the pores. This could lead to inefficient transport of species from inside the pores to the bulk solution and ineffective initiation and utilization of the sites within the mesopores. In contrast, using M3 for catalyst immobilization, a preformed complex is not used and a substantially higher concentration of smaller, mono-coordinated PMI ligands is expected to occur on the surface. This could lead to less pore blockage and could facilitate transport between the pore space and the bulk solution, giving a more effective catalyst. In addition, on a support with 100 Å pores, pore blockage is expected to be less problematic and therefore catalysts prepared via M3 and M4 are expected to have similar internal transport rates. Indeed, these catalysts behave similarly.

The results in Chapter 4 of this work indicate that relatively well-defined copper complexes akin to those used in homogeneous experiments are most likely to occur when specific immobilization methods are used. In particular, it was determined that the metallation efficiency was M4 > M2 ≥ M3 > M1. Here I observe that the various synthetic protocols had the largest impact when mesoporous silica supports were used, with the ability of each catalyst to mediate a controlled polymerization roughly following the above trend. In all cases on SBA-15 supports, polymerizations were only moderately controlled at best. In contrast, on non-porous semi-soluble supports, the synthetic method was found to have little impact on performance and all catalysts gave a moderate degree of control over the polymerization. These results imply that complex accessibility and support/solvent compatibility are paramount and the exact structure of the copper sites (mono-coordinated, bis-coordinated, etc.) is of substantially less importance on supported catalysts. These observations are in-line with results of other investigations

that show that soluble or flexible supports and long support-surface linkages lead to systems with better control [9, 10, 13, 14].

Catalyst leaching

All the catalysts exhibited loss of copper during the polymerization. The polymerization solutions were a light yellowish color after the reaction was complete. The color could be a result of free ligand or complex because PMITMS and PPMI ligand in toluene give a yellow solution. The copper coordinated ligand is reddish brown for Cu(I) and dark green for Cu(II). This observation suggests the yellow color was mainly due to free PMITMS ligand. There possibly were some free ligands or complex physisorbed to the silica surface despite the use of the dichloromethane wash that was shown to remove a large fraction of the adsorbed species, as Zhu showed that nitrogen-containing ATRP ligand/CuBr complexes adsorb strongly to silica [12, 15, 17]. This free ligand could effectively stabilize homogeneous species, removing copper from surface sites. There could also be coordinated PMITMS ligand not covalently immobilized to the surface as shown in **Figure 5.9**. A further possible cause of leaching could be structural rearrangements of the surface copper species during reaction, with the structural changes required upon copper oxidation leading to creation of unstable species that lead to leaching.

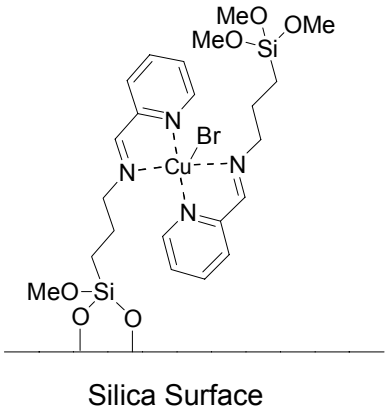

Figure 5.9 Potential immobilized CuBr/PMI species.

Elemental analyses on the recovered polymers for ppm levels of copper were performed and the results are summarized in **Table 5.2** The theoretical residual copper content, R_{Cu}, was calculated assuming all the immobilized copper leached into the polymerization solution (the monomer conversion and mass of initiator was accounted for in the calculation). If 100 % conversion of monomer was achieved and all the copper remained in the polymer, the R_{Cu} would be 6173 ppm. The maximum copper concentration increases when the degree of polymerization is lower. In all polymerizations performed, copper leached into the polymerization solution, but no higher than 317 ppm or no more than 0.0317 % w/w Cu in the polymer. The percent leached shows that in most cases the percentage of leached copper was less than 1 % of the theoretical R_{Cu}, however some cases leached 2 % or higher. Catalysts immobilized by M4 (pre-assembled complexes) consistently leached less copper compared to the other methods. The amount of leaching that is observed is similar to other systems reported in the literature (not all publications quantify leaching). Brittain reported 5-7% of the

original copper used in the ATRP reaction remained in the unpurified polymer in their supported CuBr/PMI systems [9]. Zhu reports no more than 33.4 ppm residual copper in the polymers or no more than 2-3% loss of initial catalysts used when grafted CuBr/tetraethyldiethylenetriamine systems are used [10, 13, 16]. Matyjaszewski reports no more than 107 ppm residual copper in the polymers using a mixed soluble/heterogeneous systems based on CuBr/ bipyridine [3, 4]. In my work with immobilized CuBr/bipyridine (Bpy) complexes, it appears the Bpy ligand coordinates more strongly to Cu compared to PMI and observed Cu leaching is lower [34].

Catalyst recycling

Several of the catalysts were tested for recyclability and the results are summarized in **Table 5.3**. Whereas Matyjaszewski and coworkers [4] and Zhu and coworkers [16] sometimes regenerate the catalyst by reducing all the Cu(II) back to the Cu(I) state, in this work, the catalysts were recycled without any regeneration [10, 13-15, 17]. The first use of each catalyst behaved similarly to the results described above. Interestingly, the second use resulted in polymers with narrower molecular weight distributions, but the observed polymerization rates were lower. After the fourth reuse of SBA15(100) catalysts, the activity was greatly reduced (28% conversion in 12 hrs). This could be due to catalyst structural changes or due to a build-up of polymer that could not be washed away remaining entangled in the pores, blocking accessible immobilized CuBr/PMI complexes. Upon recycling the Cab-O-Sil supported catalysts, it was observed that the polymerization rates were not significantly reduced until after the fourth reuse. In addition, it was found that the polymerizations were still well-controlled after

the sixth catalyst reuse (high conversion and relatively low PDI). Using the procedure described here, these catalysts can be recycled without catalyst regeneration. Potential reasons why catalyst reuse results in improved control are discussed below.

The residual copper content in the polymer was determined by elemental analysis. From **Table 5.3**, no more than 187 ppm copper was in the final polymer. After each subsequent reuse of the catalysts more copper leached into solution and this loss of copper may have affected the control of the polymerization. Several control experiments were performed to potentially shed some insight on the observations from catalysts reuse. The various experiments and results are described and summarized in **Table 5.4**.

Table 5.3 Catalysts recycling results for immobilized silica CuBr/PMI catalysts.

Entry	Materials	Time (hrs)	% Conv	$M_{n,Th}$	$M_{n,Exp}$	PDI	R_{Cu}[1]
1	SBA(100)-CuBr/PMI-M4-1	5	82	8200	15800	1.73	70
2	SBA(100)-CuBr/PMI-M4-2	7	75	7500	12600	1.52	32
3	SBA(100)-CuBr/PMI-M4-3	9	69	6900	12100	1.53	64
4	SBA(100)-CuBr/PMI-M4-4	12	28	2800	9900	1.59	104
5	Cab-O-Sil-CuBr/PMI-M4-1	7	83	8300	17000	1.57	49
6	Cab-O-Sil-CuBr/PMI-M4-2	7	70	7000	10800	1.24	10
7	Cab-O-Sil-CuBr/PMI-M4-3	12	84	8400	12100	1.24	99
8	Cab-O-Sil-CuBr/PMI-M4-4	12	76	7600	10900	1.21	187
9	Cab-O-Sil-CuBr/PMI-M4-5	19	70	7000	9800	1.24	85
10	Cab-O-Sil-CuBr/PMI-M4-6	48	83	8300	11800	1.35	151
11	Cab-O-Sil-CuBr/PMI-M3-1	17	89	8900	17300	1.74	94
12	Cab-O-Sil-CuBr/PMI-M3-2	14	85	8500	12100	1.28	134

[MMA]/[Cu]/[BPN] = 100/1/1 in 25% by v/v MMA in toluene at 90 ºC.

1. Residual copper content determined by elemental analyses (detection limit was 10 ppm).

There are two key attributes that the used catalysts have that the fresh catalysts do

not: (a) Cu(II), and (b) leached copper species. One potential reason why lower PDIs and better control is observed after the first use is that the catalyst complex leached off the support and could not be washed away during the centrifuging process. After recovering the catalyst from the first polymerization, the recovered polymerization solution was notably a light yellowish color, attributed to leached ligand and/or complex, as noted above. To test whether the leached ligand and/or complex could effectively control the polymerization, an experiment with the addition of 5 mol% of soluble CuBr/PPMI catalyst to a polymerization reaction with fresh immobilized CuBr (Cab-O-Sil-CuBr/PMI-M4) was undertaken (**Table 5.4**, entry 3). The polymer produced had a slightly broader molecular weight distribution, but with $M_{n,Exp}$ closer to the $M_{n,Th}$. This experiment shows that the addition of a small amount of soluble CuBr catalyst cannot produce polymers with good control and low PDI. In contrast, addition of the same amount of soluble $CuBr_2$/PPMI complex results in a well-controlled polymerization (**Table 5.4**, entry 4). This observation is consistent with previous studies of homogeneous ATRP systems where addition of $CuBr_2$ complex at the beginning of the polymerization would help control the polymerization initially [31, 32, 35]. The $CuBr_2$ complex was observed to decrease the rate of polymerization, decrease the amount of uncontrolled propagation, and therefore give a narrower PDI.

Table 5.4 Control experiments for immobilized silica CuBr/PMI catalysts.

Entry	Experiment	Time (hrs)	% Conv	$M_{n,Th}$	$M_{n,Exp}$	PDI
1	Cab-O-Sil-CuBr/PMI-1	7	83	8300	17000	1.57
2	Cab-O-Sil-CuBr/PMI-2	7	70	7000	10800	1.24
3	Control 2 – 5 mol% CuBr/PPMI[1]	24	83	8300	13900	1.71
4	Control 3 – 5 mol% $CuBr_2$/PPMI[2]	24	21	2100	3800	1.25
5	Control 4 – 0.3 Deactivator[3]	24	89	8900	16000	1.77
6	Control 5 – Sequence[4]	24	91	9100	20700	1.62
7	Control 6 – Initiator pretreatment[5]	24	92	9200	11800	1.38
8	Control 7 – Hot toluene wash[6]	24	93	9300	14300	1.85
9	Control 8 – Cab-O-Sil- 50/50[7]	24	93	9300	18500	1.63

[MMA]/[Cu]/[BPN] = 100/1/1 in 25% by v/v MMA in toluene at 90 ºC.

1. Added 5 mol% CuBr/PPMI to immobilized CuBr for polymerization with Cab-O-Sil-CuBr/PMI-M4.
2. Added 5 mol% $CuBr_2$/PPMI to immobilized CuBr for polymerization with Cab-O-Sil-CuBr/PMI-M4.
3. Added 0.3 mol% $CuBr_2$/Me_6TREN to immobilized CuBr for polymerization with Cab-O-Sil-CuBr/PMI-M4.
4. Added MMA after Cab-O-Sil-CuBr/PMI/Initiator/Toluene had been brought to temperature (2hrs).
5. Pretreated Cab-O-Sil-CuBr/PMI-M4 with initiator at 90 ºC for 2 hrs, recovered, and washed catalysts with toluene.
6. Stirred Cab-O-Sil-CuBr/PMI-M4 in toluene at 90 ºC for 2 hrs, recovered, and washed catalysts with toluene.
7. 50/50 Cu(I)/Cu(II) metal ratio was incorporated into the synthesis of Cab-O-Sil-CuBr/$CuBr_2$/PMI-M4 catalyst.

Matyjaszewski uses this approach to give a mixed soluble/heterogeneous catalyst system that exhibits good polymerization control [3, 4]. A soluble deactivator complex, $CuBr_2$/Me_6TREN, is employed in tandem with polymer-immobilized CuBr/dMBpy complexes to control of the polymerization, with that particular homogeneous complex chosen because it has a strong reducing power and prefers to be in the Cu(II) state. When the deactivator is in the Cu(I) state it readily reduces the immobilized $CuBr_2$/ligand complex and is itself oxidized to the Cu(II). It has been shown that a soluble complex with a stronger reducing power than the tethered complex is desired in a mixed

soluble/heterogeneous catalyst system [3, 4]. It was observed that soluble $CuBr_2$/dMBpy deactivator complex cannot control polymerization like $CuBr_2$/Me_6TREN when used with its immobilized CuBr/dMBpy counterpart. Hence, it was expected that free $CuBr_2$/PMITMS complex should be a poor reducing complex because it would be similar electronically to the immobilized catalyst. Interestingly, here I observe that addition of 5 mol% the homogeneous analogue of similar structure to the tethered species ($CuBr_2$/PPMI) appears to control the polymerization well, although conversions were lower.

The preferred deactivator complex developed by Matyjaszewski was evaluated with my catalyst system. The experiment was carried out under conditions similar to those that yielded the best published results (0.3 mol% $CuBr_2$ Me_6TREN to immobilized CuBr/dMBpy), except the immobilized catalyst was Cab-O-Sil-CuBr/PMI-M4. The results indicate that this amount of added deactivator could not control the polymerization with the CuBr/PMI/SiO_2 system. Although the soluble deactivator effectively functions with Matyjaszewski's polymer supported CuBr/dMBpy systems, the deactivator fails to polymerize controllably with these silica immobilized catalysts in my hands. It is possible that this small amount of the deactivator complex is strongly adsorbed to the silica surface, potentially preventing the complex from freely moving in solution and deactivating the growing polymer chain. Zhu showed that the aliphatic amine complex, CuBr/HMTETA, strongly adsorbs to silica [12, 15, 17] and I verified this with $CuBr_2$/Me_6TREN [34]. Experiments with a larger amount of $CuBr_2$/Me_6TREN (5 mol%) resulted in less than satisfactory results (94% conversion; $M_{n,Exp}$ = 14800; PDI = 1.81) as

well. In contrast, addition of the soluble $CuBr_2$/PPMI complex (entry 4) performed quite well. This may be due to weaker adsorption on bare silica for this bulkier complex.

After the first use of the catalysts, an established concentration of $CuBr_2$ exists as a result of bimolecular terminations in the first polymerization. Upon catalyst reuse, this Cu(II) is believed to contribute to the improved control compared to the first use of the catalyst. This Cu(II) would efficiently deactivate the polymer chains at early stages of the polymerization, allowing for increased control of the reaction process. This would be analogous to previous homogenous studies where a percentage of Cu(II) was added to the polymerization so that the need for self regulation and radical termination processes become unimportant [35]. To try and develop a system that exhibited controlled polymerization, several additional experiments were undertaken. In control 5, it was attempted to generate the $CuBr_2$ *in situ* by adding the monomer after the Cab-O-Sil-CuBr/PMI-M4, initiator, and toluene mixture were heated for 2 hours at 90 ºC. The premise of this experiment was the initiator can function with the immobilized complex to pre-establish a finite Cu(II) concentration before the polymerization begins. The experiment proved to be unsuccessful because an improved PDI was not achieved and the $M_{n,Exp}$ was considerably higher than previous experiments ($M_{n,Exp}$ = 20700; entry 6 of **Table 5.4**). The high molecular weight may be attributed to bimolecular coupling of the initiator radicals to effectively terminate two radicals before monomer was added. To circumvent this problem, another experiment was undertaken (**Table 5.4**, entry 7) where the Cab-O-Sil-CuBr/PMI-M4 catalyst was pretreated with one equivalent of initiator BPN in toluene at 90 ºC for 2 hours in pressure tube reactor. After which, the mixture was returned to the glovebox where the catalyst was recovered and washed with copious

amounts of fresh toluene, removing any initiator or initiator derived organic species. The recovered catalyst was returned to the pressure tube reactor and the appropriate amounts of fresh MMA, toluene, and an additional 1 equivalent of initiator were added. This time the polymerization proceeded at the level of control closer to the second reuse of Cab-O-Sil-CuBr/PMI-M4 catalyst (**Table 5.4**, entries 2 and 7). To eliminate the unlikely possibility that the increased control was due to additional wash of free ligand with hot toluene, control 7 was performed similarly to control 6 except without the initiator pretreatment. The catalysts was stirred in toluene at 90 ºC for 2 hours, recovered, and washed with copious amount of fresh toluene. The polymerization with this recovered catalyst was ineffective compared to previous control experiment (**Table 5.4**, entry 8). This was strong evidence that the low PDI for control 6 was directly caused by the pretreatment with the initiator and not because of the additional solvent wash. Surprisingly, upon immobilizing a 50/50 mixture of Cu(I) and Cu(II), improved control over the polymerization is not observed (**Table 5.4** entry 9; $M_{n,Exp}$ = 18500 and PDI = 1.63). This result implies that the presence of Cu(II) in solution may be what causes good polymerization control and that Cu(II) on the solid support at the outset of the polymerization is not in itself enough to give good control. Furthermore, it indicates that substantial leaching may primarily occur after exposure to initiator, possibly because of a structural change that occurs after the complex is oxidized to the Cu(II) state [36, 37]. These results are consistent with studies on a related Bpy system concurrently studied. For silica-immobilized Bpy complexes, little or no leaching is observed and the catalyst can not be effectively recycled in the absence of added homogeneous species [34]. This result is also consistent with the good behavior of Matyjaszewski's polymer immobilized

dMBpy/CuBr – soluble $Me_6TREN/CuBr_2$ polymerization system, which is made effective by addition of small amounts of Cu(II). Interestingly, there are no reports in the open literature of supported ATRP catalysts that give good control over the polymerization yet have been conclusively shown to result in no leaching of copper species. A small amount of leaching may be a pre-requisite for achieving good control.

Chain extension of PMMA-Br macroinitiator

Chain extension experiments were performed to determine whether the polymerizations proceeded in a pseudo-living manner. In addition, these preliminary experiments could show if block copolymers could be synthesized. A seed or macroinitiator polymer was synthesized using pretreated Cab-O-Sil-CuBr/PMI-M4 catalyst to ensure the polymer's molecular weight distribution was narrow initially. The polymerization conditions were [MMA]/[Cu]/[BPN] = 100/1/1 in 25% v/v MMA in toluene at 90 ºC and the reaction was stopped after 3 hours to reduce the amount of chain termination that occurs at higher conversion. The polymerization reached 63% conversion and the macroinitiator polymer recovered had a $M_{n,Exp}$ = 6800 and PDI = 1.30, designated PMMA-Br. The subsequent polymerization for the chain extension utilized a higher [Monomer]/[Initiator] concentration in order to observe a significant separation between the macroinitiator polymer and extended polymer in the GPC traces ([Monomer]/[Cu]/[PMMA-Br] = 300/1/1 in 25% v/v monomer in toluene for 24 hours at 90 ºC using fresh pretreated Cab-O-Sil-CuBr/PMI-M4). The extension of the macroinitiator polymer chain was performed with MMA to make an extended homopolymer because the required polymerization conditions were well established. The

polymerization for the PMMA-PMMA homopolymer proceeded to 78% conversion, $M_{n,Th}$ = 30200, $M_{n,Exp}$ = 26900, and PDI = 1.63. The $M_{n,Exp}$ was lower than the $M_{n,Th}$ because some dead chains likely existed at the beginning of the polymerizations. These dead chains would lower the M_n, as well as broaden the molecular weight distribution of the polymer. A clear shift of the GPC traces between the macroinitiator and extended homopolymer was observed. In addition to synthesizing a chain extended homopolymer, styrene (Sty) was also used to extend the macroinitiator polymer to prepare block-PMMA-block-PSty copolymer. The polymerization for the block copolymer proceeded to 46% conversion, $M_{n,Th}$ = 21300, $M_{n,Exp}$ = 28700, and PDI = 1.89. Although the molecular weight distribution was broader in this chain extension case, the incorporation of a poly(styrene) block was accomplished. A UV-vis/GPC trace and ^{1}H NMR confirmed the incorporation of a poly(styrene) block that was not previously present in the macroinitiator (PMMA-Br). Further experimentation is needed to optimize the copolymer polymerization conditions to obtain narrower molecular weight distributions. Nevertheless, polymers synthesized with silica immobilized CuBr/PMI catalyst could be extended to make homopolymers and block copolymers, demonstrating that at least a fraction of the polymer chains have reactive halocarbon end groups.

Summary

Four different synthesis methodologies for immobilization of CuBr/PMI ATRP complexes on three different silica supports were evaluated in the polymerization of methyl methacrylate. CuBr/PMI complexes immobilized on porous SBA-15 supports were ineffective catalysts when prepared via M1 and M2. M3 was a relatively effective immobilization method for all supports. M4 was only effective for the larger pore support SBA15(100) and nonporous Cab-O-Sil EH5. Cab-O-Sil EH5 was an effective support for all immobilization methodologies due to its small particles size, nonporous nature and relative miscibility in the polymerization solution. Overall, the polymerization results indicated that the silica-supported catalysts described here were less efficient at controlling the polymerization than Haddleton's and Brittain's immobilized PMI catalysts that were immobilized on polymers [1, 8, 9].

All catalysts leached ligand and/or complex into solution based on the yellowish color of the solution after the polymerization and the elemental analysis results. The catalyst particles were effectively recovered by filtration and centrifugation techniques. Trace analysis of copper in the polymer revealed a small amount of copper remaining in the polymer (no more than 0.032 % Cu by w/w in polymer in all samples tested or no more than 5 mol% Cu leached off the catalyst). Although, use of a dichloromethane wash during synthesis was able to remove a majority of the physisorbed species, some leachable species clearly remained or leaching was induced by structural changes in the surface copper species during polymerization.

Several catalysts were tested for recyclability. It was demonstrated that these catalysts could be recycled without regeneration back to the Cu(I) oxidation state. Catalysts immobilized by M4 on SBA15(100) and Cab-O-Sil were used up to 4 and 6 times, respectively. The polymerization rate was significantly reduced after each reuse for SBA15(100), possibly due to polymer entanglement in the pores. Polymerizations with Cab-O-Sil immobilized catalysts did not exhibit these features and the activity does not significantly decrease until the fourth reuse (still with good control up to sixth reuse). Control experiments showed that the recyclability of the catalysts was most likely due to the presence of small amounts of homogeneous Cu(II) species present with this catalyst system.

Overall, of the four catalyst design methods, M4, the pre-assembled complex approach, appears to be the most effective method to immobilizing structurally homogeneous complexes on silica supports that effectively polymerize MMA. However, CuBr/PMI complexes can be immobilized by other methods and still exhibit good polymerization behavior if a nonporous support with a small particle size such as Cab-O-Sil EH5 is used. It was shown that the slight leaching that occurs with these catalysts can actually lead to enhanced polymerization behavior and improved control.

Experimental Section

Characterization

^{1}H-NMR measurement was performed using a Mercury Vx 300 MHz. Cu elemental analysis by inductive coupled plasma (ICP-AES) was analyzed by Chemisar Laboratories, Guelph, Ontario, Canada. Conversion of the monomer was determined using a Shimadzu GC 14-A gas chromatograph equipped with a FID detector using a HP-5 column (30 M length, 0.25 mm inner diameter, and 0.25 μm film thickness). The temperature program was: heating from 50 °C to 140 °C at 30 K/min and from 140 to 300 °C at 40 K/min under constant pressure with inlet and detector temperatures set constant at 330 °C. The molecular weight and molecular weight distributions were determined by gel permeation chromatography (GPC) using American Polymer Standards columns (10^5, 10^3, 10^2 Å) equipped with Waters 510 pump and a Waters 410 differential refractometer. THF was used as an eluent at the flow rate of 1 mL/min. Nine linear PMMA standards (700 – 2100K) were used for calibration of methyl methacrylate polymers.

Chemicals

Methyl methacrylate (MMA; Aldrich; 99%) and styrene (Sty; Aldrich; 99%) were passed three times through an inhibitor removal column (Aldrich-311332), distilled once under reduced pressure, degassed by three freeze/thaw cycles and stored under nitrogen at -22 °C. Toluene for polymerization (Acros; 99.8%) was distilled under reduced pressure over sodium/benzophenone, degassed by three freeze/thaw cycles, and stored under nitrogen. 2-Bromopropionitrile (BPN; Aldrich; 97%), chloroform-d ($CDCl_3$; Cambridge Isotope Laboratories, Inc.; 99.8%), methylene chloride-d_2 (CD_2Cl_2; Cambridge Isotope Laboratories, Inc.; 99.8%), and propylamine (Acros; 99+%) were dried with 4 Å molecular sieves and stored under nitrogen. 2-Bromopropionitrile was stored in a 0.47 M stock solution in dry toluene under nitrogen. Copper (I) bromide (CuBr; Acros; 98%) was stirred in glacial acetic acid for 5 h, washed with absolute ethanol and anhydrous diethyl ether, dried under vacuum for 12 h at room temperature, and stored under nitrogen. Anhydrous methanol (MeOH, Alfa Aesar, >99%), Copper (II) bromide ($CuBr_2$, Aldrich; 99%), and 2-pyridinecarboxaldehyde (PCA; Aldrich; 99%) were used as received and stored under nitrogen. THF (Aldrich, HPLC grade inhibitor-free, >99%) was used as received for the eluent in GPC analysis. Tris(2-(dimethylamino)ethyl)amine (Me_6TREN) was synthesized according to literature procedures[21], dried with $MgSO_4$, and stored under nitrogen in a glovebox.

Synthesis

N-(n-propyl)-2-pyridylmethanimine, PPMI

To a 100 mL round-bottom flask were added 2.28 g of propylamine (0.038 mol), 4.54 g of PCA (.042 mol), and 30 mL of anhydrous MeOH. The reaction solution was stirred at 75 °C for 24 h under argon. The product was isolated by vacuum distillation of the light volatiles (MeOH and PCA) and stored under dry nitrogen in a glovebox to yield an orange oil: $C_9H_{12}N_2$, **2** (yield: 95+ %, 99% purity). ^{1}H-NMR ($CDCl_3$): δ = 0.92 (t, 3H, -CH_3), 1.70 (m, 2H, -$CH_2C\underline{H}_2CH_3$), 3.60 (t, 2H, -$C\underline{H}_2CH_2CH_3$), 7.26 (t, 1H, -CCHC<u>H</u>CHCHN-), 7.69 (t, 1H, -CCHCHC<u>H</u>CHN-), 7.94 (d, 1H, -CC<u>H</u>CHCHCHN-), 8.33 (s, 1H, -$CH_2NC\underline{H}$-), 8.60 (d, 1H, -CCHCHCHC<u>H</u>N-).

Experimental methods

Polymerization

For polymerization with the homogeneous CuBr/PPMI catalyst, the following recipe was typical: [MMA]/[PPMI]/[Cu]/[BPN] = 100/2/1/1 in 25% v/v MMA in toluene. For example, to a 50 mL round-bottom flask with a sidearm valve, 4.00 g of MMA (0.04 mol, 4.24 mL), 0.12 g of PPMI (0.80 mmol), 0.06 g of CuBr (0.40 mmol), and 0.06 g of BPN (0.40 mmol, 855 μL of initiator stock solution) were added in 11.03 g of toluene (12.73 mL) under argon. The polymerization vessel was immersed in an oil bath preset to 90 °C. At set time intervals, 0.1 mL aliquots of polymerization solution were removed via syringe and placed in a vial. The vials were immediately quenched in a dry ice/acetone bath. Subsequently, 25 μl of sample was added to 1.5 mL THF for GC analysis. The remaining sample was dried, re-dissolved in HPLC grade THF to 8.0

mg/mL, and filtered through a Gelman Acrodisc PTFE filter (0.2 μm) for GPC analysis. The conversion of MMA was followed by GC and molecular weights and molecular weight distributions were determined by GPC.

For polymerization using an immobilized CuBr/PMI catalyst, the following recipe was typical: [MMA]/[Cu]/[BPN] = 100/1/1 in 25% v/v MMA in toluene. For instance, to a 10 mL Schlenk tube with a sidearm valve, 0.20 g of SBA15(50)-CuBr/PMI-M4 (9.60×10^{-2} mmol of Cu, 0.48 mmol Cu/g-catalyst), 0.96 g of MMA (9.60 mmol), and 205 μL of initiator stock solution BPN (9.60×10^{-2} mmol) were added to 2.65 g of toluene under argon. The polymerization vessel was immersed in an oil bath preset to 90 °C. Samples were taken at preset times and quenched using the procedure described above. Kinetic analysis and polymer characterization were carried out in a similar manner described for the homogeneous polymerization. After the polymerization, the catalysts were recovered from the remaining polymerization solution by sedimentation (SBA15(50 and 100)) or centrifugation (Cab-O-Sil EH5). The polymers were then precipitated in 50 mL of hexane and the polymers were recovered and dried as a white powder. The dried polymers were analyzed for trace amounts of copper.

Catalyst recycling

For polymerization with the immobilized CuBr/PMI catalyst when catalyst recycling was planned, the following recipe was typical: [MMA]/[Cu]/[BPN] = 100/1/1 in 25% v/v MMA in toluene. For example, to a 15 mL pressure tube reactor 0.25 g of SBA15(100)-CuBr/PMI-M4 (9.76×10^{-2} mmol of Cu, 0.48 mmol Cu/g-catalyst), 0.976 g of MMA (9.76 mmol), and 209 μL of initiator stock solution BPN (9.76×10^{-2} mmol)

were added to 2.70 g of toluene under argon or nitrogen. A 25 μL sample was taken immediately after mixing and prior to start of the polymerization to establish the reference conversion point at time zero. The polymerization vessel was immersed in an oil bath preset to 90 °C for a set time. The polymerization vessel was cooled by immersing in a dry ice/acetone bath and retransferred into a glovebox. A 25 μL sample was taken after the polymerization to determine the final conversion by GC. The polymerization solution was transferred into a 20 mL scintillation vial and filled with toluene (under nitrogen) for catalyst recovery. The vial was then centrifuged for 20 minutes at 3000 rpm. After centrifugation, the vial containing a lower solid catalysts layer and an upper liquid polymerization solution layer was transferred back into the glovebox and the supernatent toluene/polymerization solution was decanted. Fresh toluene was again added to the used catalyst for the first wash. The vial was shaken vigorously to disperse the catalysts from the bottom of the vial. The wash and centrifugation procedure was repeated twice. After the second wash, the toluene was decanted and the catalyst was returned to the 15 mL pressure tube in the glovebox and the appropriate amounts of fresh MMA, toluene, and BPN were added (approximately the same concentrations for first catalyst use). The polymerization vessel was re-immersed in an oil bath preset at 90 °C for a set time. The final conversion was determined as previously described. The polymers (first use, second use, etc.) were precipitated from the supernatant toluene/polymer solution described above by addition to 50 mL of hexane. The polymer was recovered and dried. The polymer's molecular weight and molecular weight distribution were determined by GPC. The dried polymers were analyzed for trace amounts of copper.

Chain extension

For polymerization with the immobilized CuBr/PMI catalyst when polymer chain extension was planned, the following procedure was followed. The catalyst used in these experiments was pretreated with initiator to avoid uncontrolled propagation observed when using fresh catalyst. In a 15 mL pressure tube reactor, 0.5 g of Cab-O-Sil-CuBr/PMI-M4 was pretreated with 515 μL of BPN stock solution in 5 g of toluene at 90 ºC for 2 hours. After which, the sealed pressure tube reactor was transferred back into the glovebox and the catalyst was recovered by filtration, washed with copious amounts of toluene, and dried on the vacuum line overnight. The seed or macroinitiator (PMMA-Br) was synthesized using the following polymerization conditions: [MMA]/[Cu]/[BPN] = 100/1/1 in 25% v/v MMA in toluene for 3 hours at 90 ºC. For instance, to a 15 mL pressure tube, 0.30 g of pretreated Cab-O-Sil-CuBr/PMI-M4 (14.46×10^{-2} mmol of Cu, 0.48 mmol Cu/g-catalyst), 1.45 g of MMA (14.47 mmol), and 309 μL of initiator stock solution BPN (14.46×10^{-2} mmol) were added to 4.00 g of toluene under nitrogen in the glovebox. The polymerization vessel was sealed and immersed in an oil bath preset to 90 °C. The Cab-O-Sil-CuBr/PMI-M4 catalyst was removed from the polymerization solution by centrifugation. The recovered polymerization solution was passed through a pipette silica gel column to remove any leached species. The polymer was then precipitated in 50 mL dry hexanes, recovered by filtration, washed with copious amounts of hexanes, and dried on the vacuum line overnight. The conversion and other attributes of the macroinitiator polymer were characterized as described in polymerization section above. Chain extension were performed with addition of fresh MMA (homopolymer) or

fresh Styrene (Sty) (block copolymer) under the following polymerization condition using fresh pretreated Cab-O-Sil-CuBr/PMI-M4: [Monomer]/[Cu]/[PMMA-Br] = 300/1/1 in 25% v/v monomer in toluene for 24 hours at 90 ºC. For instance for MMA, to a 15 mL pressure tube, 0.06 g of pretreated Cab-O-Sil-CuBr/PMI-M4 (2.95×10^{-2} mmol of Cu, 0.48 mmol Cu/g-catalyst), 0.88 g of MMA (8.8 mmol), and 0.2 g of PMMA-Br macroinitiator (M_n = 6800; 2.95×10^{-2} mmol of Br assuming all chains were living) were added to 3.25 g of toluene under nitrogen in the glovebox. The polymerization vessel was sealed and immersed in an oil bath preset to 90 °C. Catalyst was recovered by centrifugation. The polymers were then precipitated in 50 mL of hexane and the polymers were recovered and dried as a white powder. The conversion and characterization of the chain extended polymer were characterized as described in polymerization section above.

References

[1] S. Liou, J. T. Rademacher, D. Malaba, M. E. Pallack, and W. J. Brittain, Macromolecules 33 (2000) 4295.

[2] G. Kickelbick, H.-j. Paik, and K. Matyjaszewski, Macromolecules 32 (1999) 2941.

[3] S. C. Hong, H.-J. Paik, and K. Matyjaszewski, Macromolecules 34 (2001) 5099.

[4] S. C. Hong and K. Matyjaszewski, Macromolecules 35 (2002) 7592.

[5] S. C. Hong, D. Neugebauer, Y. Inoue, J.-F. Lutz, and K. Matyjaszewski, Macromolecules 36 (2003) 27.

[6] S. C. Hong, J.-F. Lutz, Y. Inoue, C. Strissel, O. Nuyken, and K. Matyjaszewski, Macromolecules 36 (2003) 1075.

[7] D. M. Haddleton, D. J. Duncalf, D. Kukulj, and A. P. Radigue, Macromolecules 32 (1999) 4769.

[8] D. M. Haddleton, D. Kukulj, and A. P. Radigue, Chemical Communications (1999) 99.

[9] M. E. Honigfort and W. J. Brittain, Macromolecules 36 (2003) 3111.

[10] Y. Shen and S. Zhu, Macromolecules 34 (2001) 8603.

[11] Y. Shen and S. Zhu, AIChE Journal 48 (2002) 2609.

[12] Y. Shen, S. Zhu, and R. Pelton, Macromolecular Rapid Communications 21 (2000) 956.

[13] Y. Shen, S. Zhu, and R. Pelton, Macromolecules 34 (2001) 3182.

[14] Y. Shen, S. Zhu, and R. Pelton, Macromolecules 34 (2001) 5812.

[15] Y. Shen, S. Zhu, F. Zeng, and R. Pelton, Macromolecular Chemistry and Physics 201 (2000) 1387.

[16] Y. Shen, S. Zhu, F. Zeng, and R. Pelton, Journal of Polymer Science, Part A: Polymer Chemistry 39 (2001) 1051.

[17] Y. Shen, S. Zhu, F. Zeng, and R. H. Pelton, Macromolecules 33 (2000) 5427.

[18] J. Yang, S. Ding, M. Radosz, and Y. Shen, Macromolecules 37 (2004) 1728.

[19] S. Ding, J. Yang, M. Radosz, and Y. Shen, Journal of Polymer Science, Part A: Polymer Chemistry 42 (2003) 22.

[20] U. S. Schubert, C. H. Weidl, C. Eschbaumer, R. Kroell, and M. R. Buchmeiser, Polymeric Materials Science and Engineering 84 (2001) 514.

[21] T. Opstal, K. Melis, and F. Verpoort, Catalysis Letters 74 (2001) 155.

[22] S. Faucher and S. Zhu, Macromolecular Rapid Communications 25 (2004) 991.

[23] E. Duquesne, P. Degee, J. Habimana, and P. Dubois, Chemical Communications (2004) 640.

[24] Y. Inoue, S. C. Hong, J.-F. Lutz, D. Neugebauer, C. Stissel, and K. Matyjaszewski, Polymer Preprints 43 (2002) 193.

[25] T. Kotre, O. Nuyken, and R. Weberskirch, Macromolecular Chemistry and Physics 205 (2004) 1187.

[26] R. Kroll, C. Eschbaumer, U. S. Schubert, M. R. Buchmeiser, and K. Wurst, Macromolecular Chemistry and Physics 202 (2001) 645.

[27] K. R. Kumar, J. N. Kizhakkedathu, and D. E. Brooks, Macromolecular Chemistry and Physics 205 (2004) 567.

[28] J. V. Nguyen and C. W. Jones, Journal of Polymer Science, Part A: Polymer Chemistry 42 (2004) 1367.

[29] D. M. Haddleton, C. B. Jasieczek, M. J. Hannon, and A. J. Shooter, Macromolecules 30 (1997) 2190.

[30] D. M. Haddleton, M. C. Crossman, B. H. Dana, D. J. Duncalf, A. M. Heming, D. Kukulj, and A. J. Shooter, Macromolecules 32 (1999) 2110.

[31] J.-L. Wang, T. Grimaud, and K. Matyjaszewski, Macromolecules 30 (1997) 6507.

[32] A. Snijder, B. Klumperman, and R. van der Linde, Macromolecules 35 (2002) 4785.

[33] M. Imperor-Clerc, P. Davidson, and A. Davidson, Journal of the American Chemical Society 48 (2000) 11925.

[34] J. V. Nguyen and C. W. Jones, Macromolecules 37 (2004) 1190.

[35] H. Zhang, B. Klumperman, W. Ming, H. Fischer, and R. van der Linde, Macromolecules 34 (2001) 6169.

[36] T. Pintauer, J. Qiu, G. Kickelbick, and K. Matyjaszewski, Inorganic Chemistry 40 (2001) 2818.

[37] G. Kickelbick, T. Pintauer, and K. Matyjaszewski, New Journal of Chemistry 26 (2002) 462.

CHAPTER 6

DESIGN, BEHAVIOR, AND RECYCLING OF SILICA-SUPPORTED CUBR-BIPYRIDINE ATOM TRANSFER RADICAL POLYMERIZATION CATALYSTS

Abstract

A new strategy for immobilizing CuBr/bipyridine (bpy) complexes on silica surfaces is described. An immobilizable, organosilane-containing bpy ligand (SdMBpyTMS) is synthesized and complexed with CuBr followed by addition to four different silica supports, mesoporous SBA-15 with 50 and 100 Å pores, controlled pore glass (CPG) with 240 Å pores, and non-porous Cab-O-Sil EH5. The resulting solids are characterized by a battery of techniques. Characterization of these solids revealed that a mixture of covalently immobilized mono- and bis-copper coordinated complexes, uncoordinated ligand, and in some cases physisorbed copper exists on the silica surface.

The resulting solids are utilized for ATRP of methyl methacrylate (MMA). Whereas catalysts supported on mesoporous SBA-15 are ineffective at controlling the polymerization, CuBr/SdMBpy complexes immobilized on CPG(240) and Cab-O-Sil are effective at mediating the controlled polymerization of methyl methacrylate. Polymerizations with these catalysts achieved >70% conversion, narrow molecular weight distributions ($1.29 < PDI < 1.52$), and low (undetectable) residual copper content in the final polymer. A new methodology for catalyst regeneration is described utilizing a simple treatment of the used catalyst with AIBN. The AIBN regenerated catalysts can be recycled with moderate conversions and narrow molecular weight distributions comparable to the first catalyst use.

Introduction

In Chapters 4 and 5, silica immobilized CuBr/PMI complexes were immobilized on various silica materials via four distinct synthetic methodologies [1]. The catalysts prepared by the pre-assembled complex (M4) resulted in a more structurally homogeneous immobilized CuBr/PMI complex and effectively polymerized MMA [2]. However, slight copper leaching was observed for all catalysts, hence, it was not definitive if the enhanced polymerization behavior and control were due to leached species. Lastly, the catalyst leaching did not affect the ability for the catalyst to be recycled up to six times. Although silica immobilized CuBr/PMI complexes were effectively used as ATRP catalysts, improvement in terms of catalyst stability could be made by changing the ligand. Matyjaszewski's benchmark CuBr/bipyridine complex [3, 4] could provide additional catalyst stability because the bipyridine ligand does not possess a hydrolysable aminoimine linkage as in the case of PMI [5, 6].

Matyjaszewski and coworkers reported the first immobilized CuBr/bipyridine complexes immobilized on polymer resin, however mass transport limitations affected the deactivation process, contributing to the poor polymerization results. These results lead to the development of the dual immobilized catalyst/soluble deactivator system [7, 8]. The dual immobilized catalyst/soluble deactivator system is still considered one of the best immobilized ATRP systems reported. In my opinion, improvements in the synthetic immobilization methodology and support selection could eliminate the need for addition of soluble deactivators.

Here, I report the synthesis of a well-defined, immobilizable bpy ligand, 4-{4-[3-(trimethyoxy - silanyl) – propylsulfanyl] - butyl}-4'-methyl-[2,2'] bipyridyl or SdMBpyTMS, followed by the direct immobilization of CuBr/SdMBpyTMS ATRP complexes on various silica supports of different structure and porosity (**Figure 6.1**). The new catalysts are evaluated in the ATRP of methyl methacrylate (MMA) with a focus on polymerization control, catalyst recovery, recyclability, and stability.

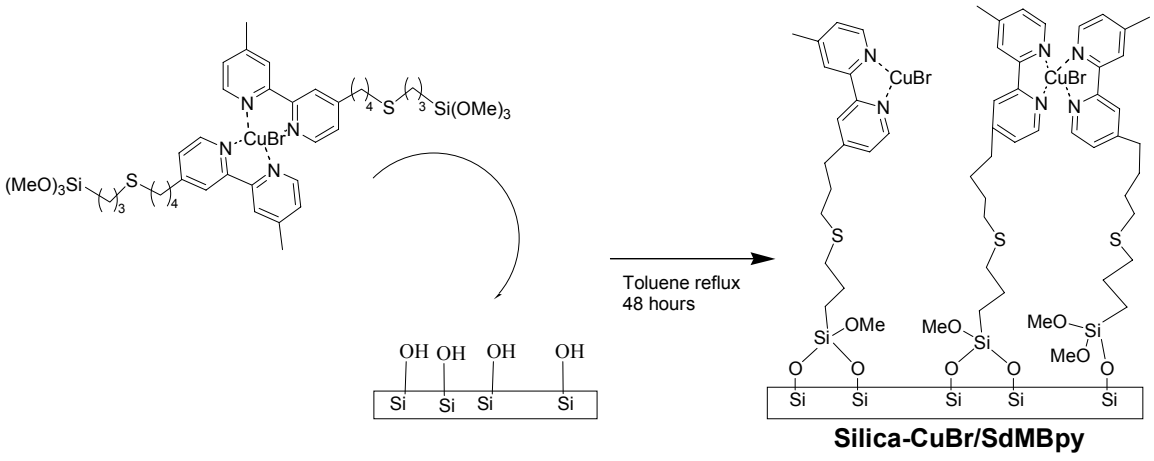

Figure 6.1 Direct immobilization of CuBr/SdMBpyTMS complex on silica via pre-assembled complex approach.

Results and Discussion

Synthesis of immobilizable bipyridine ligand

Matyjaszewski [7, 8], Zhu [9-12], Brittain [13, 14], and Haddleton [15] have all reported useful methods for covalent immobilization of ATRP complexes on polymeric or silica supports. In many cases, excellent control of the polymerization can be obtained [7-9, 11-14]. However, in all cases, a multi-step grafting procedure was used and this synthetic methodology can lead to heterogeneous materials with a variety of different types of surface species [1, 2]. For bpy ligands/complexes covalently tethered on supports, only a multi-step grafting method has been reported [7, 16-21]. Additional methods of incorporating bpy complexes into substrates include physical adsorption [22], ion exchange [23], encapsulation [24], and others techniques [25-30]. These ill-defined approaches can also produce materials with many different surface species possessing different activities. Preparation of an immobilizable, preformed CuBr/Bpy complex may allow for the preparation of more well-defined solid materials for supported ATRP. To this end, an immobilizable bpy ligand was synthesized homogeneously using a modified procedure similar to the approach used for supported 4,4'-dimethyl-2,2' bipyridine (dMBpy) ligands [7, 16-18, 25] (**Figure 6.2**). A dMBpy precursor was functionalized with an allyl group on one of the molecule's two methyl groups [31]. The terminal double bond gives a versatile handle to synthesize a variety of immobilizable dMBpy ligands. Initial attempts to hydrosilylate the allyl dMBpy with trimethoxysilane in the presence of Pt catalysts failed to produce the desired immobilizable dMBpy ligand, possibly due to coordination of the Pt catalyst by the bpy ligands. To circumvent this

problem, a simple thiol coupling reaction was utilized to make a thioether linkage [32]. Five equivalents of (3-mercaptopropyl) trimethoxysilane (MPTMS) were added to an equivalent of allyl dMBpy in the presence of a catalytic amount of AIBN to produce 4'-{4-[3- (Trimethoxy - silanyl) - propylsulfanyl] - butyl}-4-methyl-[2,2'] bipyridinyl or SdMBpyTMS (**Figure 6.2**). The coupling reaction proceeded quantitatively and by ^{1}H NMR, the concomitant absence of the double bond and thiol protons and the appearance of methylene protons adjacent to the thioether linkage were noted. The SdMBpyTMS compound possesses several important features that make it a good immobilizable ATRP ligand – a reactive, immobilizable unit, flexible linker, and metal binding sites. It is noted that there are reported syntheses of asymmetric immobilizable bpy organosilanes in the literature; however these materials were never isolated as pure compounds [18, 25]. For this work, a homogeneous analog to SdMBpyTMS was synthesized in a similar manner except without the immobilizable unit (pSdMBpy). This homogeneous analog will be used to study the effects the sulfur linkage modification may have on the polymerization (**Figure 6.5** page 152).

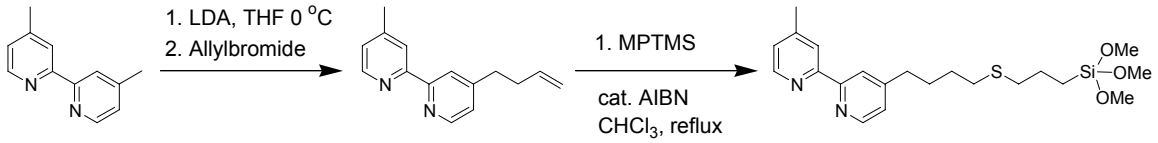

Figure 6.2 Synthesis of immobilizable SdMBpyTMS ligand.

Silica supports

The SBA-15 materials were prepared according the procedure previously described by Stucky et al. [33, 34]. For the 100 Å pore material, TMB was used as a swelling agent to increase the pore size. The mesoporous silicates were characterized by nitrogen physisorption to determine the surface area and pore size of the pristine silica supports. The surface areas were 795 and 895 m^2/g for SBA-15(50) and SBA-15(100), respectively. Thermogravimetric analysis approximated the total silanol concentration to be 2.0 mmol-OH g-solid^{-1} for 50 and 100 Å materials. X-ray powder diffraction was used to determine the order of the porosity and the overall structure of the SBA-15. The XRD patterns (not shown) were consistent with a hexagonal pore structure [33-35]. CPG(240) and Cab-O-Sil EH5 are commercially available silica from CPG, Inc. and Cabot, respectively. The CPG(240) has a particle size of 74-125 μm, a mean pore diameter of 242 Å, a surface area of 88 m^2/g, and 1.05 mmol-OH g-solid^{-1}. Cab-O-Sil is a fumed, nonporous silica with multiparticle aggregates having a length of 0.2-0.3 micron (individual particles have nanosized features), a surface area of 335 m^2/g, and 2.7 mmol-OH g-solid^{-1}. These silica supports provide a wide range of pore sizes and surface structures to probe how the silica support structure affects the polymerization performance.

Immobilization of CuBr/SdMBpyTMS complex on various silica supports

The covalent immobilization of CuBr/SdMBpyTMS complex was performed similarly to the "pre-assembled complex approach" reported previously for immobilized CuBr/PMITMS catalysts (**Figure 6.1**, Method 4 [1]). This approach appeared to result in a more structurally homogeneous immobilized ATRP complex that can allow for polymerization with relatively good control and high conversion using immobilized silica-CuBr/PMI (pyridylmethanimine) catalysts [1, 2]. In a nitrogen glovebox, the complex was pre-assembled (1:2 CuBr/SdMBpyTMS molar ratio, target bis-coordination) in dry toluene at 70 ºC before the bare, pristine silica support was added. The reaction mixture was allowed to reflux for 2 days under argon before the immobilized complex was recovered by filtration or centrifugation in the nitrogen glovebox. An extensive wash with dry dichloromethane was performed to remove excess unreacted ligand or complex and uncoordinated CuBr [1, 2].

The CuBr/SdMBpyTMS complex was covalently immobilized on the following silica supports: SBA-15 (50 and 100 Å pores), CPG (240 Å pores), and nonporous fume silica Cab-O-Sil EH5 (designated as: silica support-CuBr/SdMBpy). The compositions of the immobilized catalysts were determined by elemental and thermogravimetric analyses (**Tables 6.1**). The SdMBpy ligand loadings were calculated based on average 1-2 –OMe units reacting with the surface silanols, as determined by ^{29}Si MAS and CP-MAS NMR (spectra not shown). The calculated loadings from TGA and elemental analysis were in good agreement. The ligand and copper loadings were substantially lower than those reported by Matyjaszewski on polymeric supports [7, 8] (CuBr/PS8-

dMBpy; 2.40 mmol ligand/g Cat and 1.58 mmol Cu/g Cat, respectively). The copper loadings are tabulated using "% loaded" values as previously described [1, 2].

% SdMBpy Complexed = [(mmol Cu g-catalyst^{-1})/[(mmol SdMBpy ligand g-catalyst^{-1})/2]] × 100

A value of 100 % SdMBpy coordinated signifies that the number of Cu atoms is consistent with coordination to two immobilized SdMBpy ligands. Deviations from a 100 % mean that uncoordinated SdMBpy ligands must exist (<100 %), mono Cu coordinated SdMBpy ligands likely exist (100 > X > 200 %), or Cu adsorbed to the silica surface with no organic ligand likely exists (>200 %). This quantity is an only a measure of the metallation efficiency and should not be used as the only indication of what surface species exist on the silica surface.

Table 6.1 Thermogravimetric and elemental analysis for immobilized silica CuBr/SdMBpy catalysts.

Entry	Catalysts	L Loading[1] (mmol/g Cat)	L Loading[2] (mmol/g Cat)	Cu Loading[3] (mmol/g Cat)	% Loaded[4] (TGA, EA)
1	SBA15(50)-CuBr/SdMBpy	0.64	0.66	0.45	141, 137
2	SBA15(100)-CuBr/SdMBpy	0.73	0.73	0.66	182, 182
3	CPG(240)-CuBr/SdMBpy	0.31	0.36	0.44	284, 246
4	Cab-O-Sil-CuBr/SdMBpy	0.58	0.62	0.38	131, 123

1. Based on thermogravimetric analysis.
2. Based on total carbon content by CHN elemental analysis.
3. Based on total copper content by ICP-AES elemental analysis.
4. Calculated assuming a ligand/metal mole ratio of 2.

The % loaded results suggest that mono- and bis-copper coordinated centers exist on the surface for SBA-15(50 and 100 Å) and Cab-O-Sil supports because the % loaded [1, 2] values were above 100% (**Table 6.1**). The copper loading for the CPG(240) immobilized catalyst suggests that the surface is dominated by copper centers coordinated with one SdMBpy ligand and a small fraction of the copper centers are physisorbed to the silica surface (% loaded > 200 %). Experimental evidence to support these suppositions is given below.

The immobilization of the SdMBpyTMS ligand and complex were characterized by ^{13}C CP-MAS NMR and FT-Raman spectroscopy. The uncoordinated SdMBpyTMS ligand was directly immobilized on to SBA15(100) and probed by ^{13}C CP-MAS NMR spectroscopy (**Figure 6.3**). The bottom spectra is the solution ^{13}C NMR of the SdMBpyTMS ligand in chloroform-d (**Figure 6.3a**). The solid state ^{13}C CP-MAS NMR spectra of SBA15(100)-SdMBpy (**Figure 6.3b**) possesses the same signals as the homogeneous form, but much broader because the SdMBpy ligands are now covalently immobilized and cannot rotate freely. The signal at 7.4 ppm corresponds to the -CH_2Si-carbon, indicating the SdMBpy ligands were covalently anchored to the silica surface(verified by ^{29}Si MAS NMR). The weak bands centered at 192 and 105 ppm were determined to be the spinning sidebands of the 122 and 34 ppm signals, respectively.

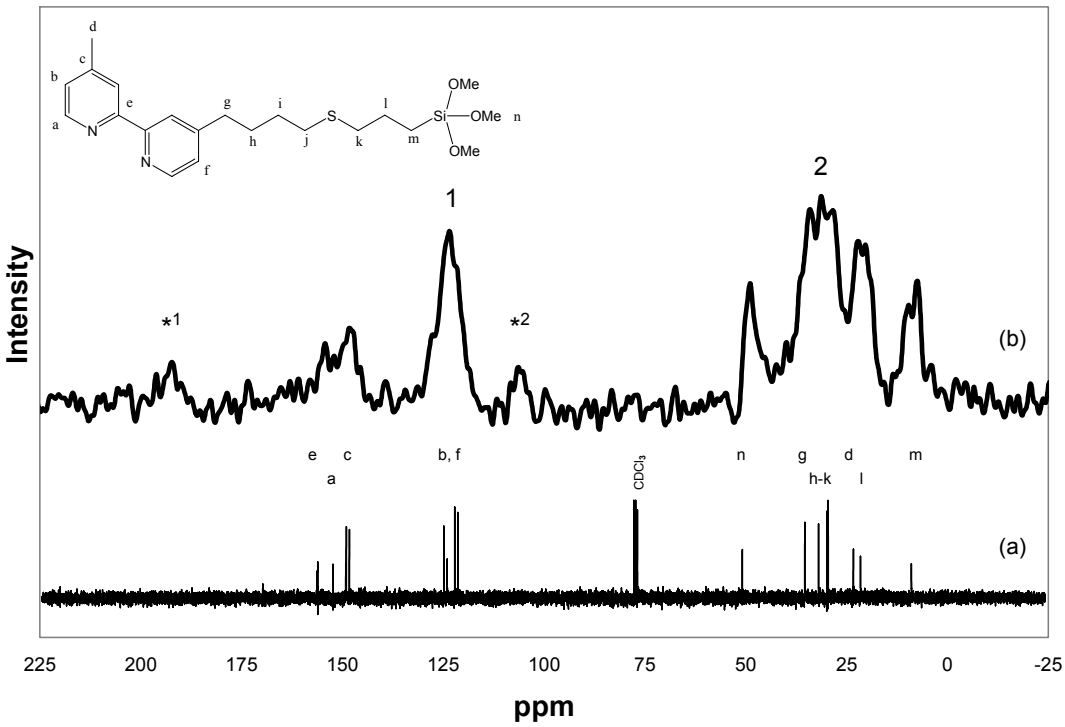

Figure 6.3 ^{13}C Solution and Solid State NMR Spectra of immobilized Bpy species: (a) SdMBpyTMS and (b) SBA15(100)-SdMBpy by CP-MAS.

The immobilization of the CuBr/SdMBpyTMS complex onto silica was characterized by FT-Raman spectroscopy (**Figure 6.4**). **Figure 6.4a** shows FT-Raman spectra of SdMBpyTMS ligand. **Table 6.2** summarizes the signals of interest for the SdMBpyTMS ligand [36]. **Figure 6.4b and c** are the spectra for the immobilization on SBA-15(50) and SBA-15(100), respectively. The signals for the pyridyl rings and in-plane CH stretch were shifted to 1610 and 1554, and 1013 cm^{-1} (from 1607, 1560, and 996 cm^{-1}, respectively) which can be attributed to coordination of CuBr to the immobilized ligand. These signal shifts were consistent with those reported in the literature [1, 16, 17]. The slight peak shoulders remaining at 1607 cm^{-1} and more noticeably at 996 cm^{-1} may be attributed to uncoordinated ligands. Hence, it has been

shown by ^{13}C CP-MAS NMR and FT-Raman that CuBr/SdMBpy complexes were covalently immobilized, but more importantly that traces of uncoordinated ligands likely exist on the surface in addition to the immobilized mono and bis-coordinated complexes.

Table 6.2 FT-Raman spectroscopy of immobilized silica CuBr/SdMBpy catalysts.

Entry	Material	ν(pyridyl ring)	ν(inplane CH)	ν(CSC)
1	SdMBpyTMS	1607 & 1560	996	731
2	Silica-CuBr/SdMBpy	1610 & 1554	1013	731

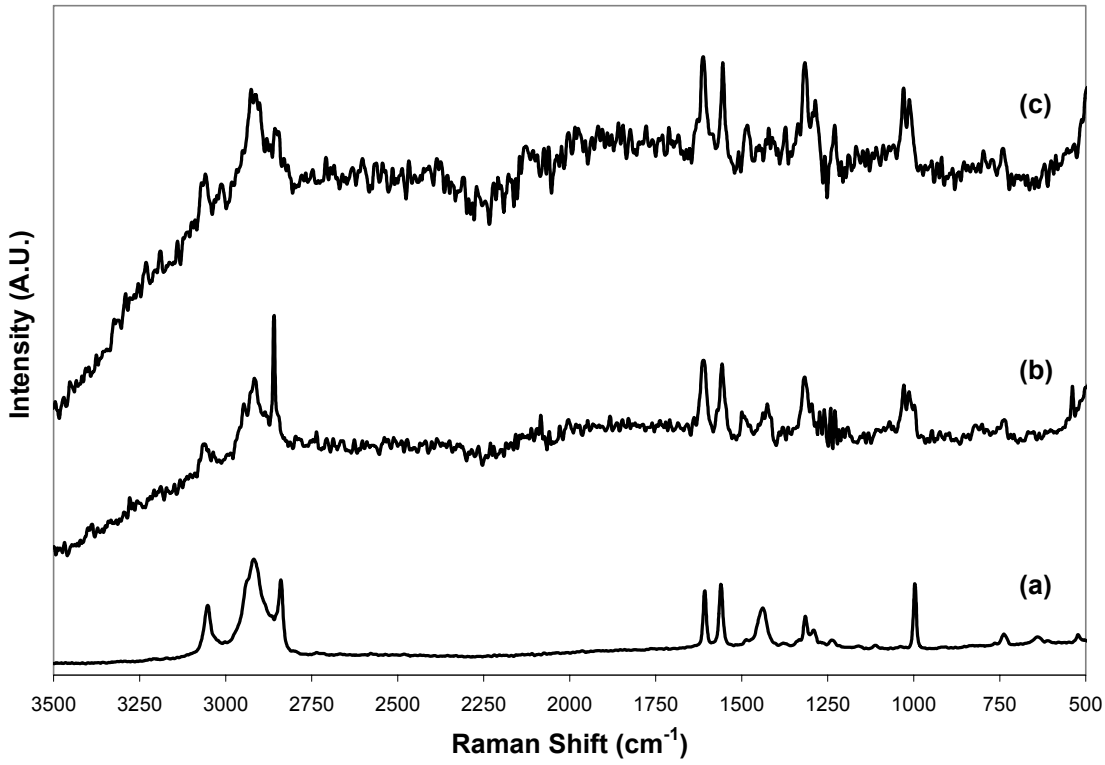

Figure 6.4 FT-Raman spectra of Bpy species: (a) SdMBpyTMS, (b) SBA15(50)-CuBr/SdMBpy, and (c) SBA15(100)-CuBr/SdMBpy.

Comparison of immobilization methods in the literature

Covalent immobilization of tethered bpy ligands or complexes has been reported on polymer backbones [7, 8, 37] and inorganic supports [16-18, 25] in the literature (note that incorporation of bpy complexes using methods other than formation of covalent linkages will not be discussed here because these methods will likely result in significant leaching of the complex from the solid) [38]. Barnett [18], Goncalves [16, 17], and Matyjaszewski [7, 8] have utilized a multi-step grafting approach to covalently immobilize (tether) bpy ligands to the surface. Although Barnett proposed the synthesis of an immobilizable bpy ligand to be covalently tethered to silica particles, the immobilizable ligand was never isolated prior to the addition of the solid support [18].

To illustrate the difficulty associated with a multi-step grafting approach, consider the work of Goncalves. Goncalves immobilized an oxomolybdenum/bpy complex on silica for the epoxidation of cyclooctene [16, 17]. To tether or graft a bpy ligand to the surface, the dMBpy ligand was modified by first unsymmetrically deprotonating dMBpy with an LDA solution, followed by reacting the latter with 3-chloropropyl functionalities tethered to the surface. In the reported procedure, the silica surface was derivatized with 3-chloropropyltrimethoxysilane, resulting in 1.68 mmol Cl/g-solid. After contacting the Li-dMBpy with the solid, the Cl composition decreased to 1.07 mmol Cl/g-Solid, corresponding to *ca.* 21% elimination of the Cl and addition of 0.29 mmol Bpy/g-Solid. Then the ligand was heterogeneously metallated with excess $MoO_2Cl_2(THF)_2$ to give the supported oxomolybdenum/bpy complex. By Mo microanalysis, an excess of Mo complex was incorporated into the solid (0.87 mmol Mo/g-Solid vs. theoretical 0.29 mmol Mo/g-Solid) suggesting that in addition to coordinating to the bpy, the Mo complex

reacted with the bare silica surface. This ill-defined method for bpy complex immobilization poses several problems for ATRP applications. The unreacted Cl is undesired because halogen groups are potential initiating groups in ATRP (see reports of surface initiated ATRP in the literature [39-41]). In addition, the use of strong bases such as alkyl-lithium reagents is known to degrade silica materials; hence, the Li-Bpy can react with Si-O-Si and Si-OH bonds on the silica surface as well as with the intended chloropropyl groups [42]. Lastly, metal complexes bonded to the bare surface may possess drastically different reactivity than the tethered metal/ligand complexes. In a system where rapid initiation and good transport is essential, these problems are not amenable for well controlled ATRP. My attempts to immobilize CuBr/dMBpy complex on silica by this method resulted in a low ligand loading that was likely too limited for useful ATRP application.

Matyjaszewski reports bpy ligand/complexes immobilized on only polymer supports [7, 8], not silica. Like the Goncalves procedure, an asymmetrically deprotonated dMBpy ligand is reacted with a tethered Cl group (benzyl chloride) on the polymer bead support (PS8-dMBpy). The elimination of the Cl was reported to be quantitative (initially 1.14 mmol Cl/g-resin; reacted 1.15 mmol ligand/g-resin), indicating that the multi-step grafting method is more useful for polymeric supports as there are limited side reactions [7, 8]. However, it is later surmised that residual benzyl chloride sites can act as initiating sites that lead to polymerization off the support, coating the catalyst particle [8]. In addition, there are several other examples in the literature of tethering bpy ligands onto polymer backbones and a recent review summarizes these [37].

In this work, the immobilization of the ATRP complex was performed using the "pre-assembled complex approach" [1]. The procedure involved constructing the CuBr/SdMBpyTMS (1:2 ratio to target bis-coordination) complex in solution prior to addition of the support (**Figure 6.1**). The advantage of the method is it reduces the potential interactions of bare CuBr with the surface. This is important because it was found that the surface silanols can act as a chemical ligand for the CuBr and the physisorbed CuBr cannot be removed readily, although a thorough wash with dichloromethane has been demonstrated to effectively remove free ligand and metal complex that might be present in the materials [1, 2]. The physisorbed, ligand-free CuBr was found to possess no activity for ATRP [2]. Using this technique, more well-defined immobilized complexes may be prepared, although the presence of small amounts of bare CuBr resulting from traces of pre-assembled complex decomposition upon immobilization can not be ruled out, as non-aqueous solvent washes will not remove these species and the spectroscopic techniques utilized could not detect them.

Homogeneous control polymerizations of MMA with CuBr/pSdMBpy.

pSdMBpy was synthesized as a homogeneous analog to the SdMBpyTMS immobilizable complex to determine whether the sulfur linkage affects the polymerization performance. **Figure 6.5** shows the different catalyst systems that were employed in control polymerizations. The results of these control experiments are summarized in **Table 6.3**. **Figure 6.6** shows the first order kinetic plots and the evolution of M_n and PDI with conversion for the homogeneous control experiments. Polymerization with the typical CuBr/dMBpy catalyst in toluene solvent proceeded in

well-controlled manner, reaching 80% conversion, with $M_{n,Exp}$ agreeing well with $M_{n,Th}$, and with the resulting polymer having a narrow molecular weight distribution (PDI = 1.30, entry 1, **Table 6.3**). When using the homogeneous analog of the immobilizable complex, CuBr/pSdMBpy (**Figure 6.5b**), the conversion only reached 58%, but was better controlled (PDI = 1.18, entry 2, **Table 6.3**). The lower conversion and improved PDI are likely due to better solubility due to the long flexible linker causing more efficient chain deactivation [4, 43, 44]. When the solvent was switched from toluene to diphenyl ether, the polymerization with CuBr/pSdMBpy was much improved owing to the increased solubility of the complex in diphenyl ether [4, 43-45]. The conversion reached 94%, the $M_{n,Exp}$ agreed well with $M_{n,Th}$, and the molecular weight distribution was narrow (PDI = 1.22, entry 3, **Table 6.3**). The last control experiment involved using dipropyl sulfide (DPS) as an additive to see how the thioether affects the polymerization with CuBr/dMBpy (**Figure 6.5c**). This polymerization proceeded similarly to CuBr/pSdMBpy polymerization in toluene (entry 4, **Table 6.3**), suggesting that the thioether does not inhibit the polymerization or affect the ability of the metal complexes to mediate the polymerization.

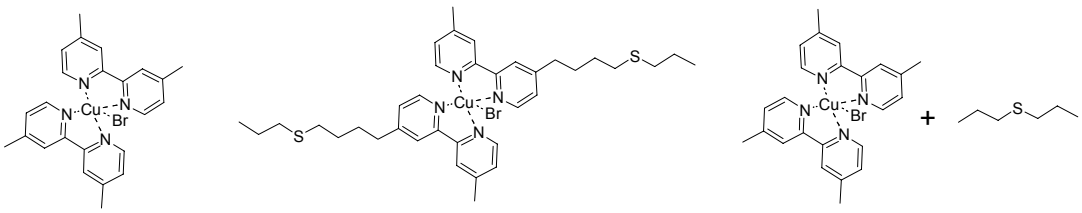

Scheme 6.5 Various CuBr/Bpy systems for homogeneous control experiments.

Table 6.3 Polymerizations with homogeneous, control CuBr/Bpy catalysts.

Entry	Catalyst	Time (hrs)	% Conv	$M_{n,Th}$	$M_{n,Exp}$	PDI
1	CuBr/SdMBpy	16	80	23900	24900	1.30
2	CuBr/p-SdMBpy	7	58	17400	18300	1.18
3	CuBr/p-SdMBpy[1]	6	94	28200	30200	1.22
4	CuBr/dMBpy/DPS	7	62	18900	20100	1.32

Polymerization conditions: [MMA]/[Ligand]/[Cu]/[BPN] = 300/2/1/1 in 50% by v/v MMA in toluene or diphenyl ether at 90 ºC. 1. Diphenyl ether was the solvent.

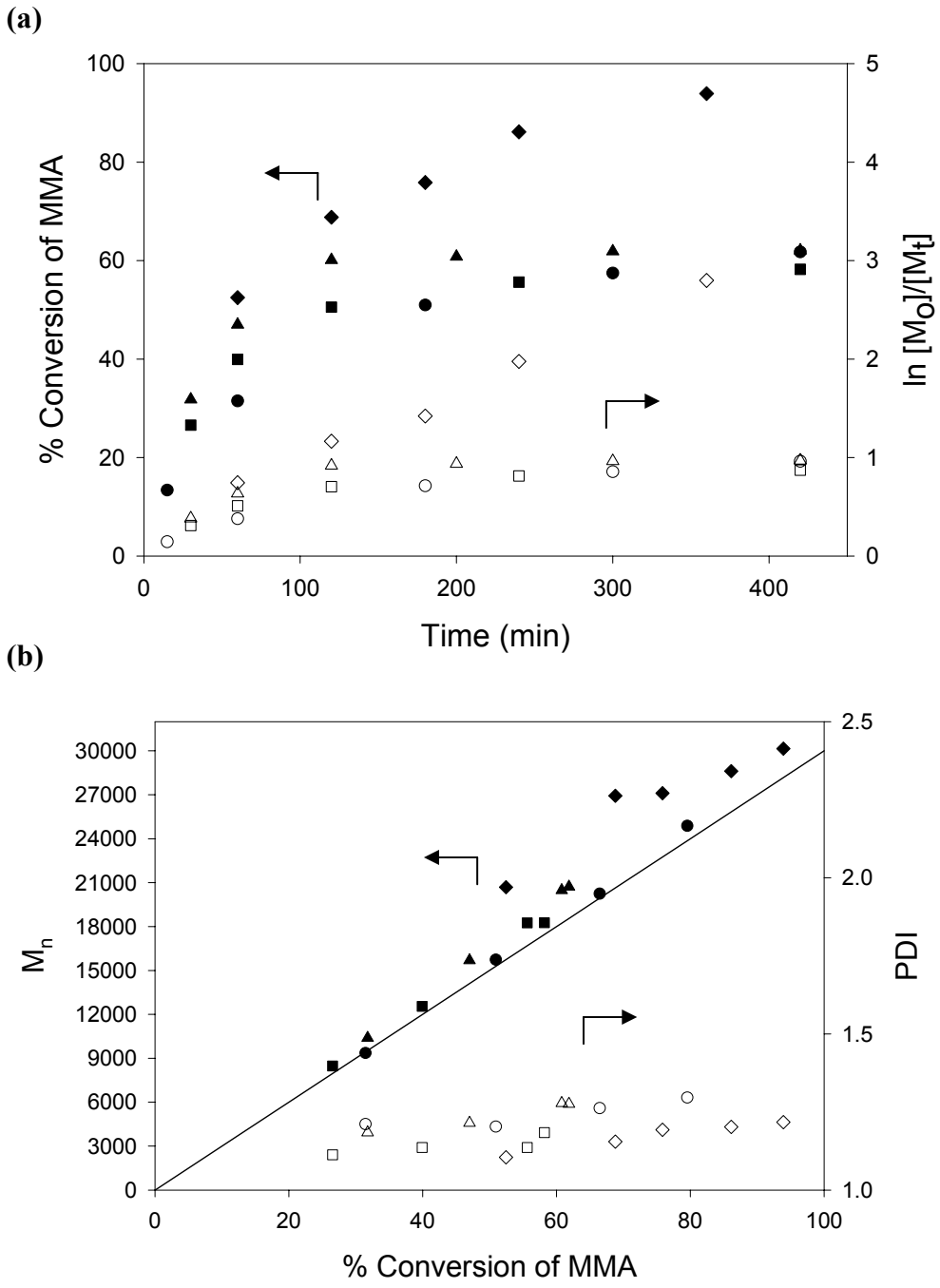

Figure 6.6 Kinetic plots for control experiments for homogeneous polymerizations with CuBr/Bpy catalyst. Evolution of conversion and $\ln[M_o]/[M_t]$ with time (a) and evolution of M_n and PDI with monomer conversion (b). CuBr/dMBpy in toluene (●,○), CuBr/dMBpy/DPS in toluene (▲,△), CuBr/pSdMBpy in toluene (■,□), and CuBr/pSdMBpy in diphenyl ether (◆,◇). Theoretical M_n curve (-). [MMA]/[Cu]/[BPN] = 300/1/1 in 50% by v/v MMA in toluene or diphenyl ether at 90 °C.

Results for polymerization of MMA for silica immobilized CuBr/SdMBpy catalysts

The silica immobilized CuBr/SdMBpy catalysts were tested for the polymerization of MMA at [MMA]/[Cu]/[BPN] = X/1/1 in Y% by v/v MMA in toluene at 90 ºC (X = 300, Y = 50 or X = 100, Y = 25). Two different monomer/initiator ratios were chosen to determine how the target molecular weight affects the control of the polymerization. In addition, the role of silica support porosity was probed by utilizing four silica supports with substantially different pore structures. **Figure 6.7** shows the first order kinetic plots and the evolution of M_n and PDI with conversion for polymerizations with [MMA]/[BPN] = 100. **Table 6.4** summarizes the results of the polymerizations. Copper complexes supported on the SBA-15 supports were ineffective for controlling the polymerization. SBA15(50)-CuBr/SdMBpy polymerized with low conversion (44%) and very broad molecular weight distribution (PDI = 4.74). The larger pore size SBA15(100)-CuBr/SdMBpy allowed for higher conversion (77%) and better control (2.11), but still uncontrolled when compared to well-behaved homogeneous ATRP catalysts (PDI ~ 1.3 or better). However, CuBr/SdMBpy immobilized on CPG(240) and Cab-O-Sil were effective ATRP polymerization catalysts polymerizing with moderately high conversion (>70%) and good control (PDI < 1.35 or lower).

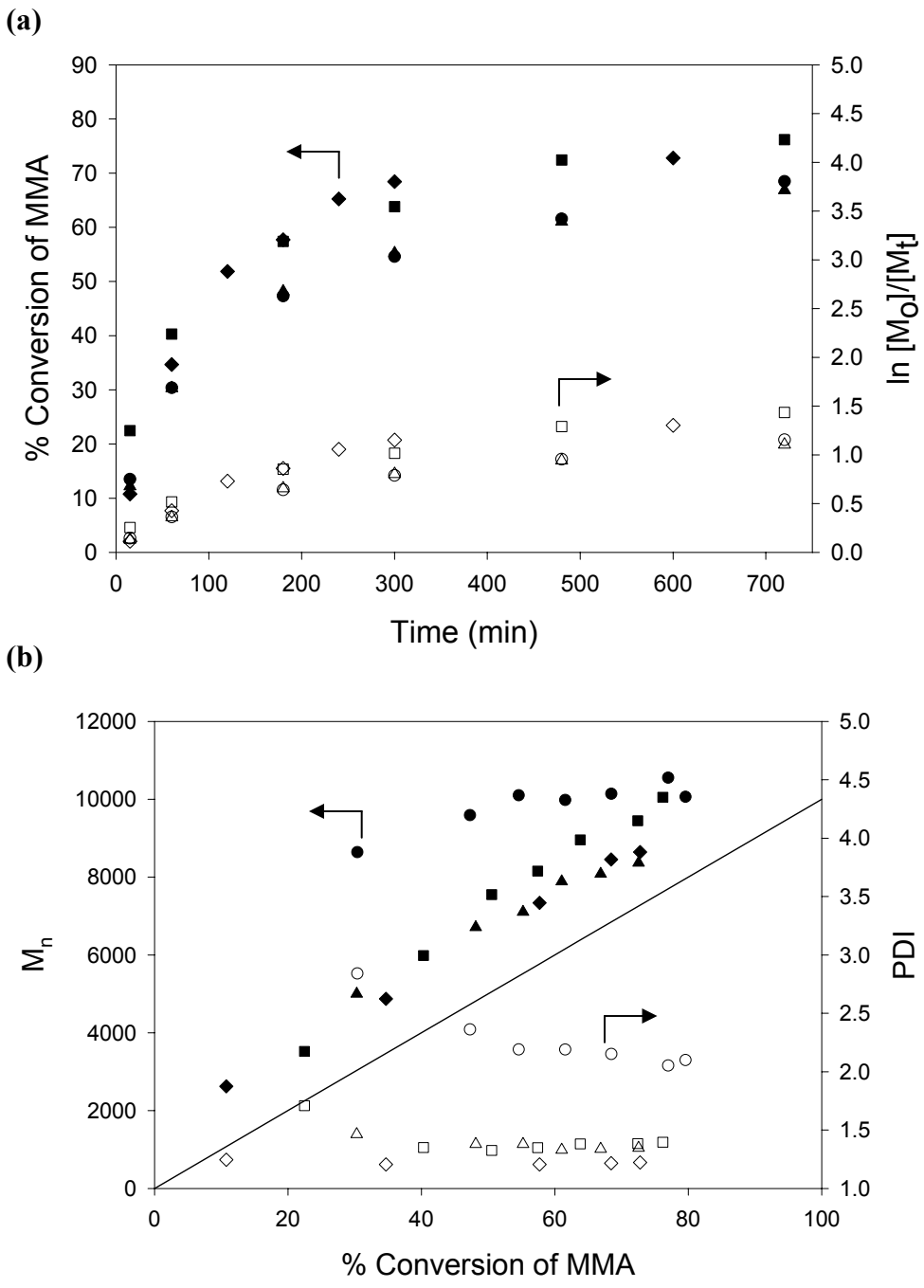

Figure 6.7 Kinetic plots for control experiments for silica-CuBr/SdMBpy polymerization catalysts, [MMA]/[BPN] = 100. Evolution of conversion and $\ln[M_o]/[M_t]$ with time (a) and evolution of M_n and PDI with monomer conversion (b). SBA15(100)-CuBr/SdMBpy (●,○), CPG(240)-CuBr/SdMBpy (▲,△), Cab-O-Sil-CuBr/SdMBpy (■,□), and homogeneous polymerization with CuBr/dMBpy (◆,◇). Theoretical M_n curve (-). [MMA]/[Cu]/[BPN] = 100/1/1 in 25% by v/v MMA in toluene at 90 °C.

Both catalysts produced a final polymer composition comparable to those produced by homogeneous catalysts CuBr/dMBpy and CuBr/pSdMBpy (entry 1 and 2, **Table 6.3**). The first order kinetic plot shows evidence of some chain termination (**Figure 6.7a**), especially at higher conversions. The plots of M_n with conversion were linear (**Figure 6.7b**) and relatively parallel with the theoretical line, although molecular weights were always higher than predicted. This observation is common to supported ATRP catalysts, and may result from poor deactivation of the growing chain at the outset of the polymerization [13-15]. The residual copper content, R_{Cu}, were less than 10 ppm in all the polymers analyzed (10 ppm was the detection limit of the analyses).

Table 6.4 Polymerization results for silica-CuBr/SdMBpy catalysts: [MMA]/[BPN] = 100.

Entry	Catalyst	$Rate_0$ (mol/L hr)	t (hr)	% Conv	$M_{n,Th}$	$M_{n,Exp}$	PDI	R_{Cu} (ppm)
1	CuBr/dMBpy	0.86	10	74	7400	8600	1.22	6840
2	SBA15(50)-CuBr/SdMBpy	0.76	24	44	4400	11600	4.74	<10
3	SBA15(100)-CuBr/SdMBpy	1.08	24	77	7700	10600	2.11	<10
4	CPG(240)-CuBr/SdMBpy	0.98	24	72	7200	8400	1.35	<10
5	Cab-O-Sil-CuBr/SdMBpy	1.43	17	78	7800	13000	1.29	<10

Polymerization conditions: [MMA]/[Cu]/[BPN] = 100/1/1 in 25% by v/v MMA in toluene at 90 ºC.

Figure 6.8 shows the first order kinetic plots and the evolution of M_n and PDI with conversion for polymerizations with [MMA]/[BPN] = 300. **Table 6.5** summarizes the polymerization results. Polymerization with SBA15(50)-CuBr/SdMBpy catalyst was not performed because of the poor performance for polymerization where [MMA]/[BPN] = 100. Polymerization with SBA15(100)-CuBr/SdMBpy was still ineffective as evidenced by the broad molecular weight distribution (PDI = 1.81). Again polymerizations with CuBr/SdMBpy immobilized on CPG(240) and Cab-O-Sil supports (entry 3 and 4, **Table 6.5**) were well controlled (CPG(240) with better control). The conversion and molecular weight distributions were comparable to homogeneous polymerization with CuBr/dMBpy and CuBr/pSdMBpy. The first order kinetic plots show evidence of some chain termination at high conversions (**Figure 6.8a**). The plots of M_n with conversion were linear (**Figure 6.8b**) and parallel with the theoretical line, although molecular weights were higher than predicted. The molecular weight distributions for both cases were slightly higher for polymerizations at the lower [MMA]/[BPN] ratio. This was attributed to the increased viscosity of the solutions causing less efficient transport in solution.

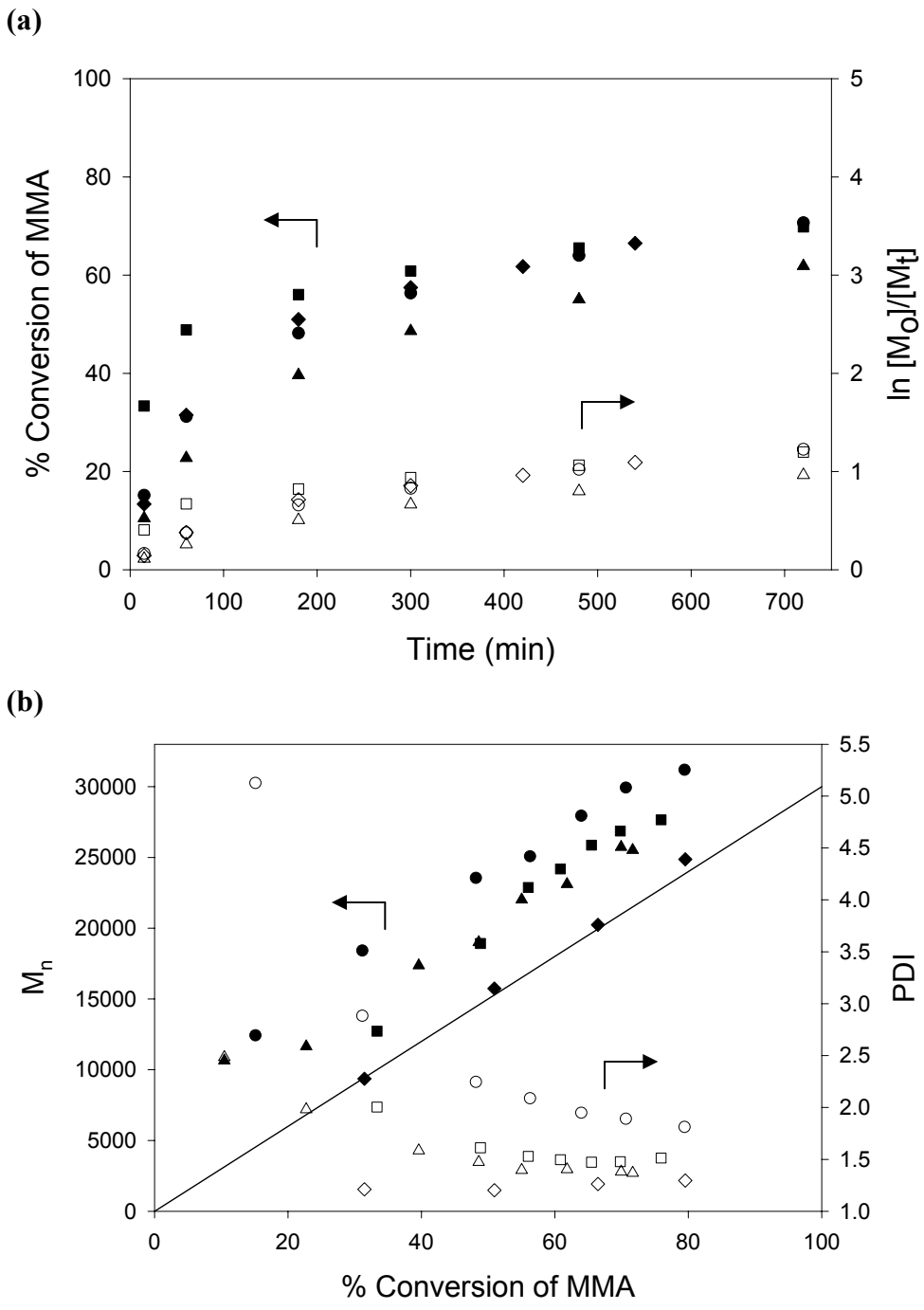

Figure 6.8 Kinetic plots for control experiments for silica-CuBr/SdMBpy polymerization catalysts, [MMA]/[BPN] = 300. Evolution of conversion and $\ln[M_o]/[M_t]$ with time (a) and evolution of M_n and PDI with monomer conversion (b). SBA15(100)-CuBr/SdMBpy (●,○), CPG(240)-CuBr/SdMBpy (▲,△), Cab-O-Sil-CuBr/SdMBpy (■,□), and homogeneous polymerization with CuBr/dMBpy (◆,◇). Theoretical M_n curve (-). [MMA]/[Cu]/[BPN] = 300/1/1 in 50% by v/v MMA in toluene at 90 °C.

Table 6.5 Polymerization results for silica-CuBr/SdMBpy catalysts: [MMA]/[BPN] = 300.

Entry	Catalyst	$Rate_0$ (mol/L hr)	t (hr)	% Conv	$M_{n,Th}$	$M_{n,Exp}$	PDI	R_{Cu} (ppm)
1	CuBr/dMBpy	2.25	16	79	23700	24900	1.30	1324
2	SBA15(100)-CuBr/SdMBpy	2.54	24	79	23800	31200	1.81	48
3	CPG(240)-CuBr/SdMBpy	1.76	24	70	21000	25700	1.38	168
4	Cab-O-Sil-CuBr/SdMBpy	5.62	24	76	22800	27700	1.52	<10

Polymerization conditions: [MMA]/[Cu]/[BPN] = 300/1/1 in 50% by v/v MMA in toluene at 90 ºC.

The R_{Cu} were no greater than 168 ppm in the polymers when catalyst recovery was done by sedimentation. However, when centrifugation was used to recover Cab-O-Sil-CuBr/SdMBpy, the R_{Cu} was less than 10 ppm. This observation may indicate that the higher Cu content in the final polymer (**Table 6.5**, entries 2 and 3) is due to entrapped silica catalyst. **Figure 6.9** shows an image of polymers prepared homogeneously with CuBr/dMBpy and heterogeneously with silica-CuBr/SdMBpy catalysts. The polymerization with all the immobilized silica-CuBr/SdMBpy catalysts afforded white polymers with no green color to them, giving visual confirmation of the supported catalysts ability to sequester the copper species with limited leaching.

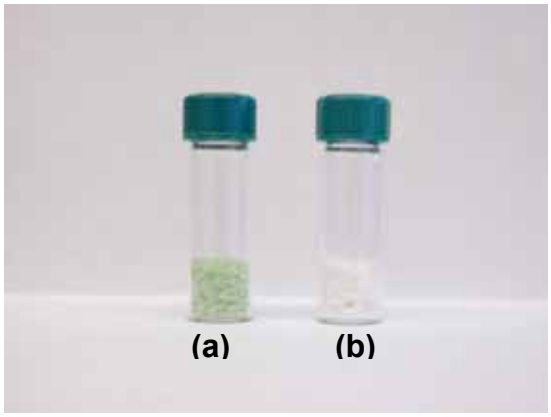

Figure 6.9 Polymers produced with CuBr/Bpy catalysts (a) homogeneous polymerization with CuBr/dMBpy and (b) heterogeneous polymerization with silica-supported CuBr/SdMBpy catalysts.

Although the undetectable Cu content in the final polymers and narrow PDI ([MMA]/[BPN] =100) give hope to the notion that a completely recoverable silica-supported ATRP catalyst may be in hand, there is not sufficient evidence to draw this conclusion. In fact, when three of the catalysts used in this work were analyzed for Cu content after the polymerization, it was apparent that some Cu leaching had occurred from the porous catalysts [SBA-15(100): Cu/Si = 0.135 before and Cu/Si = 0.105 after; CPG(240): Cu/Si = 0.076 before and Cu/Si = 0.065 after; Cab-O-Sil: Cu/Si = 0.069 before and Cu/Si = 0.064 after]. Furthermore, it is noted that when Matyjaszewski utilizes the homogeneous deactivator in conjunction with polymer supported CuBr/Bpy catalysts, excellent control can be obtained with soluble Cu concentrations as low as 15 ppm [8]. Indeed, there is no evidence in the open literature that good polymerization control can be achieved with no complex leaching. A small concentration of leached or homogeneous complex may in fact be a prerequisite for good polymerization control with

supported systems. This hypothesis fits with many prominent literature reports to date, for example references [8] and [2].

Effect of silica support structure

Of the three silica supports evaluated, CPG(240) and Cab-O-Sil EH5 were the most effective, with CPG(240) being more effective at higher [MMA]/[BPN] ratio. Cab-O-Sil EH5 is a commercially available fumed silica with a very small primary particle size, making it moderately soluble in hot toluene. Furthermore, it has no measurable porosity, meaning that all of its surface area is external. CPG(240) is also a commercially available porous silica with large polydisperse pore size and interconnecting pore network. In contrast, SBA-15 is a mesoporous silica material with straight mesopores in a hexagonal array [33, 34]. Although the mesopores are connected by small micropores [46], these micropores can be considered unimportant for the diffusion of relatively large species like polymer chains. Hence, in these polymerizations, each pore in the SBA-15 is essentially an isolated reaction environment with only a single entrance point and exit point at each end. These very different porosities of the supports would be expected to play a role in the effectiveness of the polymerizations. Indeed porosity does play a key role because the accessibility of the catalyst complex can be limited by the size of the pore and growing polymer.

The fact that CPG(240) and Cab-O-Sil supported catalysts give the best control over the polymerization points to the paramount importance of access of the growing polymer chain to the metal complexes, as previously reported in the literature [1, 2, 7, 8, 47]. It is important that the growing polymer chain can access the $CuBr_2$ complexes

relatively easily and return to their dormant state. The ease of this deactivation process is critical to having a controlled polymerization. When considering the porous SBA-15 catalysts, I observe that the polymerizations are generally less controlled, with the restricted mobility of the growing chains within the pores affecting the polymerization process. In the case of CPG(240), the larger interconnecting pore network facilitates transport and ultimately leads to better control because the pores are not isolated like SBA-15. The length of the flexible linker also contributes to improved control because it may allow the CuBr/SdMBpy complex to be solvated even when it is immobilized to a support. Indeed, Zhu showed that an optimized length for the support surface linkage leads to polymerizations with better control [11]. On the other hand, Cab-O-Sil is a nanosized and nonporous solid with less diffusion limitations compared to the other three supports. In addition, due to its small primary particle size, Cab-O-Sil is more miscible in toluene at the polymerization temperature. In this work, the best polymerization control over the polymerization was observed with Cab-O-Sil-CuBr/SdMBpy catalyst at [MMA]/[BPN] = 100. Slightly less control was observed at the higher ratio because the polymerization mixture started to gel (viscosity increased) as conversion increased. These are among the best controlled polymerizations reported on silica without using a deactivator, with PDIs akin to those reported by Zhu [11].

The initial rates for the polymerizations increased as follows for the supports: SBA-15(50) < CPG(240) ≈ SBA-15(100) < Cab-O-Sil. These results were inline with previous work on CuBr/PMI catalysts immobilized on different supports [2]. Higher initial rates were observed as pore size increases, with the highest over the nonporous catalyst. These observations were consistent with entrapment of some growing polymer

chains within the mesopores of the SBA-15 supports, resulting in slower polymerization rates.

Application of a soluble deactivator in silica-supported systems

Polymerizations with bpy catalysts immobilized by a multi-step grafting method on traditional polymeric supports have been shown to be ineffective for mediating well-controlled ATRP, for example reaching only moderate conversions (59%), with $M_{n,Exp}$ greatly disagreeing with $M_{n,Th}$ (71200 vs. 17100), and with a broad molecular weight distribution (PDI = 2.26) [7, 8]. This limited performance in controlling the polymerization has been attributed the poor polymerization results to an inefficient deactivation of the growing polymer chain resulting in uncontrolled propagation. To improve the deactivation process, a soluble deactivator complex, $CuBr_2/Me_6TREN$, was introduced with positive results. With the deactivator, the polymerization reached 96% conversion, $M_{n,Exp}$ agreed well with $M_{n,Th}$, and the molecular weight distribution was narrow (PDI = 1.29). This result clearly suggests the deactivation process was the cause of the poor catalysts performance. Use of a soluble deactivator is also reported with silica-supported catalysts, although the available data is more limited [8].

The soluble deactivator method may not be as efficient when silica supports are used due to strong interactions between the silica surface and the homogeneous complex as discussed below. Matyjaszewski's $CuBr_2/Me_6TREN$ deactivator complex was tested with the silica-CuBr/SdMBpy catalysts to determine if the conversion and polydispersity can be improved upon. When 5 mol % $CuBr_2/Me_6TREN$ (relative to immobilized copper) was added to the polymerization mixture with CPG(240)-CuBr/SdMBpy

([MMA]/[BPN] = 300), no improvement in the PDI was observed (conversion 73% and PDI = 1.51), although the $M_{n,Exp}$ = 22900 agreed better with $M_{n,Th}$ = 21900. It was speculated that the deactivator complex strongly adsorbed to the support surface similarly to Zhu's physisorbed CuBr/HMTETA ATRP system (aliphatic amines are known to adsorb strongly to silica) [48, 49]. The deactivator complex would now act as an immobilized complex and not its intended function, as a "shuttling agent" for the halogen. Two control experiments were undertaken to verify my assumption. First, the $CuBr_2$/Me_6TREN complex (20 wt %) was contacted with pristine CPG(240) silica (80 wt %) in dry toluene (polymerization solvent) and stirred for 1 hour. The solid was then recovered and washed in the glovebox with copious amount of toluene and vacuum dried. The same solid was then washed with copious amount of dry dichloromethane and THF and vacuum dried. **Figure 6.10** shows both thermogravimetric weight loss curves for $CuBr_2$/Me_6TREN/CPG(240) washed with toluene (a) and $CuBr_2$/Me_6TREN/CPG(240) washed with dichloromethane and THF (b) samples. The toluene wash was not able to remove any of the $CuBr_2$/Me_6TREN and the dichloromethane and THF wash was only able to remove a small amount. To see if the deactivator complex was interacting with the surface silanols, the same control experiment described above was performed with CPG(240) that was previously contacted with HMDS to remove the accessible surface silanols ("capped" CPG(240)). **Figure 6.11** shows the thermogravimetric weight loss curves for bare capped CPG(240) (a), $CuBr_2$/Me_6TREN/capped CPG(240) washed with toluene (b), and $CuBr_2$/Me_6TREN/capped CPG(240) washed with dichloromethane and THF (c). The toluene was unable remove the complex; although the dichloromethane and THF wash was able to remove much of the adsorbed species. Nonetheless, some

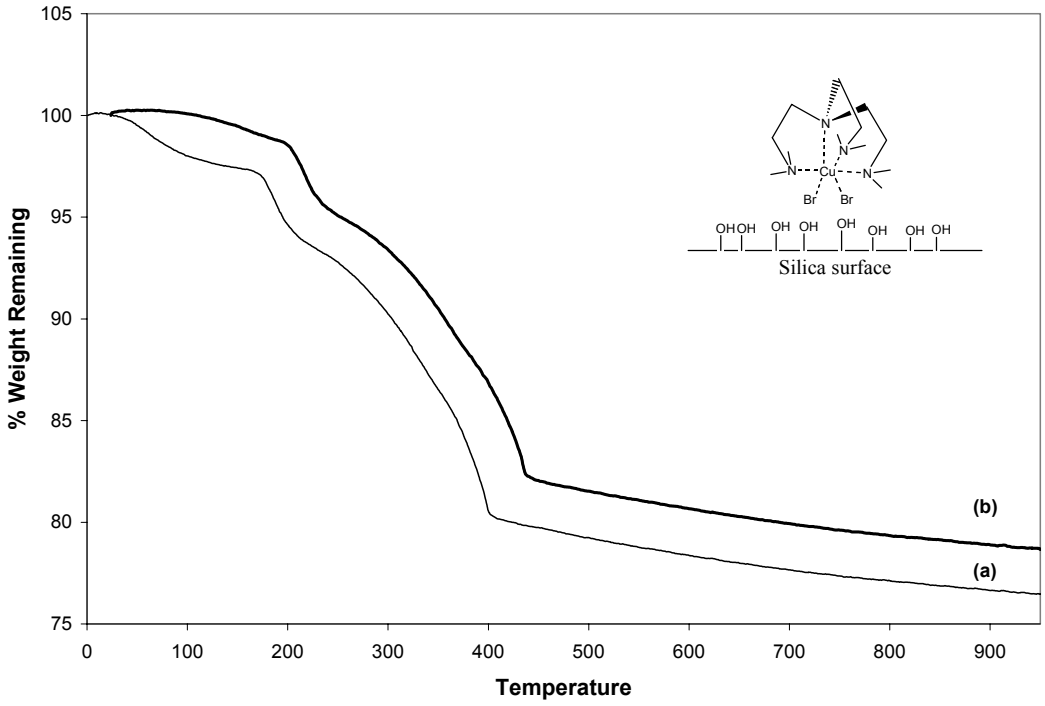

Figure 6.10 Thermogravimetric analysis curves for control experiment with $CuBr_2/Me_6TREN$ on uncapped CPG(240); (a) $CuBr_2/Me_6TREN$/CPG(240) washed with toluene and (b) $CuBr_2/Me_6TREN$/CPG(240) washed with dichloromethane and THF.

chemisorbed complex remained on the surface. These results indicate that the deactivator complex interacts with the silica surface and the nonpolar toluene solvent likely partitions the highly polar complex to the polar silica even when the surface silanols were removed. As a consequence, when using silica as the support, the deactivator complex is found to be ineffective for improving the deactivation process under the conditions reported here. Fortunately, with the current catalyst design, the deactivator was not needed because the CPG(240)- and Cab-O-Sil-CuBr/SdMBpy catalysts polymerize with excellent control and reasonable conversions in the absence of any added homogeneous agent (although some homogeneous species may exist due to leaching).

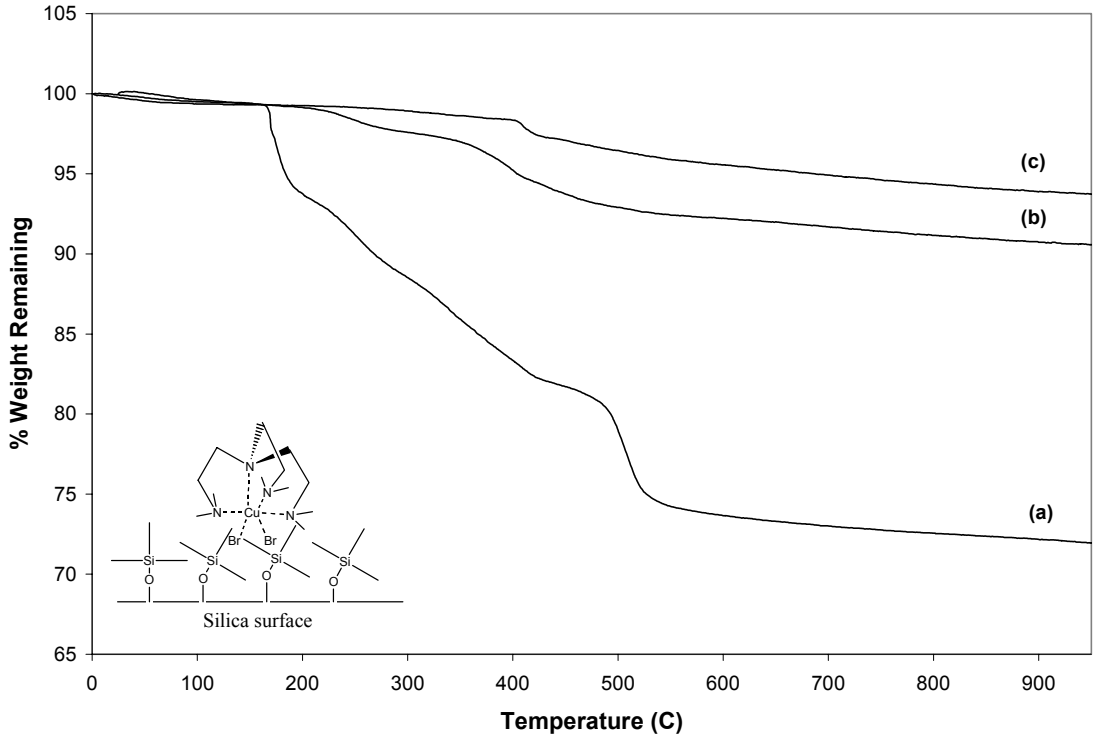

Figure 6.11 Thermogravimetric analysis curves for control experiment with $CuBr_2/Me_6TREN$ on capped CPG(240); (a) bare capped CPG(240), (b) $CuBr_2/Me_6TREN$/capped CPG(240) washed with toluene, and (c) $CuBr_2/Me_6TREN$/capped CPG(240) washed with dichloromethane and THF.

Regeneration of the immobilized silica-CuBr/SdMBpy catalysts

In previous studies done by Matyjaszewski [8] and Zhu [10], the immobilized CuBr/ligand has been regenerated back to the initial Cu(I) oxidation state for catalyst reuse. Without the regeneration process, the catalyst exhibited low activity and poor control because of the build up a high concentration of Cu(II) due to termination reactions. In addition, there have also been reports of ligand loss after each reuse (2^{nd} reuse, decrease = 39%; 3^{rd} reuse, decrease = 58%) [8]. In my work with immobilized silica-CuBr/PMI catalysts, the catalysts did not require regeneration and possessed

reasonable activity and improved control up to the sixth reuse at the same [Cu]/[Initiator] of the first use. This has been attributed to the presence of substantial leached copper species in the CuBr/PMI/SiO_2 system [2]. Unfortunately, polymerizations with recycled Cab-O-Sil-CuBr/SdMBpy catalyst without regeneration proceeded only very slowly ([MMA]/[BPN] = 100; 1st use, conversion = 78% and PDI = 1.29 in 17 hrs; 2nd use, conversion = 45% and PDI = 1.24 in 89 hrs), perhaps due to the fact that there is very limited or no leaching in this system. A slight improvement in molecular weight distribution when using recycled catalyst was observed, similar to immobilized CuBr/PMI systems [2]. The improvement was speculated to be due to the presence of Cu(II) at the beginning of the polymerization which slowed down the initial uncontrolled propagation commonly observed with immobilized ATRP catalysts. The recovered silica-CuBr/SdMBpy catalysts possessed a green color due to the high concentration of Cu(II) complexes immobilized. Therefore, it is seemed essential to reduce the immobilized Cu(II) complex back to the Cu(I) oxidation state to have catalysts with reasonable activity, as others have previously reported [8, 10].

Typical regeneration procedures involve stirring the used catalyst with zero valent copper powder or wire [8, 10], allowing the Cu(0) to reduce the Cu(II) back to Cu(I). Application of the $CuBr_2$/Me_6TREN complex as a "halogen-delivery messenger" in conjunction with copper wire was found to be a useful method of catalyst regeneration [8]. The Cu(0) wire reduces the $CuBr_2$/Me_6TREN to CuBr/Me_6TREN. Since the CuBr/Me_6TREN complex prefers to be in the Cu(II) oxidation state, it then reduces the immobilized $CuBr_2$/dMBpy catalysts to Cu(I) state and is itself reconverted to $CuBr_2$/Me_6TREN complex. Unfortunately, as demonstrated above, $CuBr_2$/Me_6TREN

adsorbs strongly to silica and can be ineffective for the halogen exchange process using the system reported here. Therefore, another regeneration technique needed to be developed so that the catalyst could be recycled.

To this end, I have developed a simple regeneration process involving a process akin to reverse ATRP [50, 51]. In reverse ATRP, the oxidation state of the copper complex is initially Cu(II) and the initiating group does not possess a halogen. A polymerization is initiated by conventional means and the high oxidation state metal complex serves to deactivate the growing chains. Promoting reverse ATRP with the used catalyst was probed as a methodology of regenerating/recycling the catalyst, however, it produced poor polymerization results ([MMA]/[BPN] = 300; conversion = 93%, $M_{n, Exp}$ = 19000, and PDI = 1.91) with the used CPG(240)-CuBr/$CuBr_2$/SdMBpy catalyst. Therefore, a regeneration process was developed that utilized AIBN as a catalyst treatment but without addition of monomer. When one equivalent of AIBN (to immobilized Cu) was added to the used catalyst in toluene and stirred at 90 ºC for 15 minutes, the solid turned from a dark green to dark red color. The color change of the solid indicated that a higher concentration of the immobilized copper exists in the Cu(I) oxidation state. The solid catalysts were recovered by filtration in the nitrogen glovebox, washed with copious amount of toluene and dichloromethane (to remove AIBN-derived species), vacuum dried overnight, and stored in a nitrogen glovebox until further use. Note that when the regeneration process was carried out for a longer time, the solid turned dark red initially, but eventually became dark green color. Therefore the regeneration time should remain short, but the exact time has not yet been optimized to

achieve the highest concentration of immobilized Cu(I) complexes (15 minutes was the time used in this work).

Catalyst recycling with AIBN regenerated catalysts

Catalysts regenerated with AIBN were recycled and the results were summarized in **Table 6.6**. The polymerization conditions used the same initial copper loading to determine the appropriate amount of monomer, initiator, and solvent to be added. Polymerizations with non-regenerated Cab-O-Sil-CuBr/SdMBpy proceed slower than the initial use ([MMA]/[BPN] =100: 1^{st} use, conversion = 78% in 17 hrs; 2^{nd} use, conversion = 45% in 89 hrs). However, when the catalyst was regenerated, the polymerization proceed faster than without the regeneration, but still slower than the first use (3^{rd} use, conversion = 54% in 24 hrs). In both cases, the molecular weight distributions were comparable to the first use (PDI = 1.29, 1.24, and 1.31 for 1^{st}, 2^{nd}, and 3^{rd} use, respectively). $M_{n,Exp}$ was always determined to be higher than the $M_{n,Th}$. The catalyst was then regenerated a second time and the catalysts was reused for a fourth time. This time the polymerization was allowed to run for 48 hours, achieving 65% conversion, and PDI = 1.23. The lower conversion was attributed to the presence of immobilized Cu(II) that was not regenerated. Results for polymerizations with AIBN-regenerated CPG(240)-CuBr/SdMBpy catalyst at the higher [MMA]/[BPN] ratio were similar to that of Cab-O-Sil-CuBr/SdMBpy described above. The activities were lower and the molecular weight distributions were comparable to the first use, but the $M_{n,Exp}$ agreed better with the $M_{n,Th}$. The lower conversions exhibited here could potentially be due to pore clogging, in addition to the presence of immobilized Cu(II). As noted above, the

immobilized catalysts reported here can be recycled by regeneration with AIBN. This regeneration technique is a useful addition to those previously described in the literature because no additional metal is added to the system.

Table 6.6 Polymerization with silica-CuBr/SdMBpy recycled catalysts.

Entry	Catalyst	[M]/[I]	t (hr)	% Conv	$M_{n,Th}$	$M_{n,Exp}$	PDI
1	Cab-O-Sil-CuB/SdMBpy-1	100	17	78	7800	13000	1.29
2	Cab-O-Sil-CuB/SdMBpy-2[1]	100	89	45	4500	5700	1.24
3	Cab-O-Sil-CuB/SdMBpy-3[2]	100	24	54	5400	7500	1.32
4	Cab-O-Sil-CuB/SdMBpy-4[2]	100	48	65	6500	7600	1.23
5	CPG(240)-CuBr/SdMBpy-1	300	24	70	21000	25700	1.38
6	CPG(240)-CuBr/SdMBpy-2[1]	300	48	60	18100	17100	1.41
7	CPG(240)-CuBr/SdMBpy-3[2]	300	72	50	15000	15600	1.34

Polymerization conditions: [MMA]/[BPN]/[Cu] = X/1 in Y% by v/v MMA in toluene at 90 ºC (X = 100, Y = 25; X = 300, Y = 50). 1. Polymerization without catalyst regeneration. 2. Polymerization with catalyst regenerated with AIBN.

Summary

A well-defined, immobilizable SdMBpyTMS ligand was synthesized and coordinated with CuBr and the CuBr/SdMBpyTMS ATRP complex was covalently immobilized on four different silica supports in one step. Characterization by a battery of techniques (^{13}C CP-MAS NMR, ^{29}Si CP-MAS NMR, FT-Raman spectroscopy, and elemental and thermogravimetric analyses) demonstrated that direct immobilization of the CuBr/SdMBpy complex was successful and the surface species consisted of immobilized mono- and bis-copper coordinated bpys, immobilized uncoordinated bpys, and possibly, small amounts of physisorbed copper. These catalysts were tested for the controlled polymerization of methyl methacrylate. SBA-15 type supports were ineffective catalysts because effective mass transport (and hence efficient deactivation) was inhibited by the pore size and isolated structure of the pore network. However, when using a support with a random network of larger pores (CPG(240)) and a nonporous and nanosized support (Cab-O-Sil EH5), controlled polymerizations were readily obtained. These catalysts allowed polymerizations to achieve reasonably high conversions with narrow molecular weight distributions. The polymers recovered possessed very low copper content in all cases, with most catalysts giving undetectable amount of Cu, implying that the catalysts did not leach to a significant extent. For the system described here, the conversion could not be improved by using Matyjaszewski's $CuBr_2/Me_6TREN$ complex (immobilized/soluble hybrid catalyst) because the soluble deactivator species adsorbed to the silica support strongly, therefore restricting its ability to act as a "shuttling agent". In addition, the $CuBr_2/Me_6TREN$ complex could not be used as a

"halogen-delivery messenger" as described in published regeneration procedure using Cu(0) as a reductant. A new regeneration procedure was developed using AIBN to reduce the immobilized Cu(II) complex. Regeneration by this new procedure eliminates addition of new copper metal into the system and the performance of the regenerated catalysts is on par with the first use. Thus, a new, recyclable silica-supported catalyst system that results in well-controlled polymerizations has been described along with a unique methodology for catalyst regeneration.

Experimental Section

Characterization

Thermogravimetric analysis (TGA) was carried out using a Netzsch simultaneous thermal analyzer STA 409 PC *Luxx* (TGA/DSC) by heating to 1000 °C at 20 K/min in air. Silica pore diameters and surface areas were determined using nitrogen physisorption data obtained with a Micromeritics ASAP 2000 system. The samples were pretreated at 90 °C for 1 h and 150 °C overnight under vacuum. The surface areas were analyzed by the BET method and the pore size distribution was determined using the BJH method applied to the adsorption branch of the isotherm [35]. X-ray powder diffraction patterns were recorded using CuK_α radiation on a Scintag X1 powder diffractometer. FT-Raman spectroscopy was performed using a Bruker IFS 66v/S equipped with dual FT-IR and FT-Raman benches and a CaF_2 beamsplitter. ^{1}H and ^{13}C solution NMR measurements were performed using a Mercury Vx 300 MHz with $CDCl_3$ used as solvent. Solid state ^{13}C and ^{29}Si cross-polarization magic angle spinning (CP-MAS) NMR spectra were collected on a Bruker DSX 300 and 400 MHz instruments, respectively. Typical ^{13}C CP-MAS parameters were 10000 scans, a 90º pulse length of 4 μs, and a delay of 4 s between scans. Typical ^{29}Si CP-MAS parameters were 2000 scans, a 90º pulse length of 5 μs, and a delay of 10 s between scans. Copper and silicon elemental analyses were performed by Galbraith Laboratories, Inc, Knoxville, TN or Chemisar Laboratories, Guelph, Canada, using ICP-AES. Carbon, hydrogen, and nitrogen contents were determined via CHN analysis by Galbraith Laboratories, Inc, Knoxville, TN or Chemisar Laboratories, Guelph, Canada. Conversion of the monomer

was determined using a Shimadzu GC 14-A gas chromatograph equipped with a FID detector using a HP-5 column (30 M length, 0.25 mm inner diameter, and 0.25 μm film thickness). The temperature program was: heating from 50 °C to 140 °C at 30 K/min and from 140 to 300 °C at 40 K/min under constant pressure with inlet and detector temperatures set constant at 330 °C. The molecular weight and molecular weight distributions were determined by gel permeation chromatography (GPC) using American Polymer Standards columns (10^5, 10^3, 10^2 Å) equipped with Waters 510 pump and a Waters 410 differential refractometer. THF was used as an eluent at the flow rate of 1 mL/min. Nine linear PMMA standards (700 – 2100K) were used for calibration of methyl methacrylate polymers.

Chemicals

Chloroform-d ($CDCl_3$; Cambridge Isotope Laboratories, Inc.; 99.8%), allyl bromide (Aldrich; 99%), diisopropyl amine (DiPA; Acros; 99+%), 1-propanethiol (Acros; 98%), dipropylsulfide (DPS; Acros; 98+%), and 2-bromoproprionitrile (BPN; Aldrich; 97%) were dried over 4 Å molecular sieves and stored under dry nitrogen. (3-Mercaptopropyl) trimethoxysilane (MPTMS; Aldrich; 95%) and copper (II) bromide ($CuBr_2$; Aldrich; 99%) were used as received and stored under dry nitrogen. n-Butyl lithium (n-BuLi; Aldrich; 0.6 M in hexanes), poly(ethylene glycol)-block-poly(propylene glycol)-block-poly(ethylene glycol) (EO-PO-EO; Aldrich), hydrochloric acid (HCl; JT-Baker; A.C.S. Reagent), tetraethyl orthosilicate (TEOS; Acros; 98%), hexamethyldisilazane (HMDS; Aldrich; 99%), and 1,3,5 trimethylbenzene (TMB; Aldrich; 97%) were used as received. Copper (I) bromide (CuBr; Acros; 98%) was

purified by stirring in glacial acetic acid for 5 hrs, washed with absolute ethanol and anhydrous diethyl ether, dried under vacuum for 12 hrs at room temperature, and stored under dry nitrogen. 4,4'-Dimethyl-2,2'-dipyridyl (dMBpy; Aldrich; 99%) and 2,2'-Azobis(2-methylpropionitrile) (AIBN; Aldrich; 99%) were recrystallized in methanol, recovered, dried under vacuum at room temperature for 12 hours, and stored under dry nitrogen. Methyl methacrylate (MMA; Aldrich; 99%) was passed three times through an inhibitor removal column (Aldrich-311332), distilled once under reduced pressure, degassed by three freeze/thaw cycles and stored under nitrogen at -22 °C. Toluene for polymerization (Acros; 99.8%) was distilled under reduced pressure over sodium/benzophenone, degassed by three freeze/thaw cycles and stored under nitrogen. 2-Bromopropionitrile was stored in a 0.47 M stock solution in dry toluene under nitrogen. THF (Aldrich, HPLC grade inhibitor-free, >99%) was used as received for the eluent in GPC analysis. Cab-O-Sil EH5 (Cabot) and CPG (CPG(240); CPG, Inc.; CPG00240B) were dried under vacuum for 12 hrs at room temperature and stored under nitrogen. Hexanes (Aldrich; >99%), methylene chloride (CH_2Cl_2; Aldrich; >99%), tetrahydrofuran (THF; Aldrich; >99%), and diethylether (Aldrich; >99%) were dried and deoxygenated using a purification system and stored under nitrogen in a glovebox [52]. Tris(2-(dimethylamino)ethyl)amine (Me_6TREN) was synthesized according to literature procedures [53], dried with $MgSO_4$, and stored under nitrogen in a glovebox.

Syntheses

All syntheses described below were carried out under dry nitrogen in a glovebox unless otherwise noted. Schlenk techniques were used for manipulating reaction mixtures outside the nitrogen glovebox. All solvents used in the synthesis of these materials were anhydrous and deoxygenated.

Preparation of SBA-15 (50 and 100 Å pores)

Mesoporous silica SBA-15 was synthesized utilizing the triblock poly(ethylene oxide)-poly(propylene oxide)-poly(ethylene oxide) (EO-PO-EO) nonionic surfactant as the structure-directing agent [33, 34]. In a typical preparation, 12.43 g of EO-PO-EO, 273.92 g of DI H_2O, and 86.60 g 38% aqueous HCl were stirred at room temperature until the triblock copolymer completely dissolved. Then 27.05 g of TEOS was added to the solution and stirred for 5 minutes. The mixture was distributed into ten Parr Teflon-line autoclaves and agitated at 50 °C for 20 hrs. The solid product was recovered by filtration, washed with DI H_2O extensively, and air-dried at 50 °C overnight. Calcination was carried out by slowly increasing temperature from room temperature to 200 °C at 1.2 K/min under nitrogen enriched atmosphere. The temperature was held at 200 °C for 1 hr and then slowly increased to 500 °C at 2 K/min under oxygen enriched atmosphere. The temperature was held at 500 °C for 6 hrs. The solid product was dried under vacuum for 12 hrs and stored under dry nitrogen in a glovebox, yielding approximately 8 g of solid.

Large pore SBA-15(100) was synthesized similar to the 50 Å material except 1,3,5-trimethylbenzene (TMB) was used as a swelling co-solvent. In a typical preparation, 12.00 g of EO-PO-EO, 317.77 g of DI H_2O, 1.50 g of TMB, and 86.60 g

38% aqueous HCl were stirred at room temperature until the triblock copolymer completely dissolved. Then 25.63 g of TEOS was added to the solution and stirred for 5 min. The mixture was distributed into ten Parr Teflon-line autoclaves and agitated at 35 °C for 20 hrs and then aged at 100 °C without stirring for 24 hrs. The solid product was recovered by filtration, washed with DI H_2O extensively, and air-dried at 50 °C overnight. Calcination was carried out under the same conditions described for the 50 Å pore material. The solid product was dried under vacuum for 12 hrs and stored under dry nitrogen in a glovebox, yielding approximately 7 g of solid.

Preparation of 4'-But-3-enyl-4-methyl-[2,2']bipyridinyl, (allyl dMBpy)

Preparation was performed as previously described [31]. Dry THF (50 mL) and 1.449 g of DiPA (0.0142 mol) were added to a 250 mL flask in a nitrogen glovebox. The reaction mixture was cooled to 0 ºC and 8.4 mL of n-BuLi (0.0132 mol) was slowly added dropwise under positive argon pressure. After the addition was complete, the reaction mixture was stirred at 0 ºC for 30 minutes followed by addition of a solution of 2.422 g of dMBpy (0.0132 mol) in dry THF (100 mL) by cannula. The reaction mixture immediately turned a dark purplish color and was allowed to stir at 0 ºC for an additional 1 hour under argon on a Schlenk line. Subsequently, a mixture of dry THF (10 mL) and 1.620 g of allyl bromide (0.0132 mol) were added dropwise by syringe under positive argon pressure. The reaction mixture was stirred at 0 ºC for an additional 2 hours and then it was allowed to warm to room temperature overnight. The reaction mixture was subsequently quenched with 10 mL DI H_2O and the THF was removed by rotovap. The resulting product was extracted with diethyl ether and dried over $MgSO_4$. The final

product was recovered by rotovap to yield 2.4 g of viscous orange oil. The product was purified by vacuum sublimation at 100 ºC to remove unsubstituted dMBpy. The product was degassed and stored under dry nitrogen in a glovebox. $C_{15}H_{16}N_2$ (2.81 g, yield 95%) ^{1}H-NMR ($CDCl_3$): δ = 2.43 (s, 3H, -C<u>H</u>$_3$), δ = 2.46 (m, 2H, -CH_2C<u>H</u>$_2$CH=CH_2), δ = 2.80 (t, 2H, -C<u>H</u>$_2$$CH_2$CH=$CH_2$), δ = 5.02 (t, 2H, -$CH_2CH_2$CH=C<u>H</u>$_2$), δ = 5.84 (m, 1H, -$CH_2CH_2$C<u>H</u>=$CH_2$), δ = 7.13 (d, 2H, -($CH_3$ or CH_2)-CC<u>H</u>CHNCCH-), δ = 8.24 (s, 2H, -(CH_3 or CH_2)-CCHCHNCC<u>H</u>-), δ = 8.54 (d, 2H, -(CH_3 or CH_2)-CCHC<u>H</u>NCCH-).

Preparation of 4'-{4-[3-(Trimethoxy-silanyl)-propylsulfanyl]-butyl}-4-methyl-[2,2']bipyridinyl, (SdMBpyTMS)

A mixture of 2.0 g of Allyl dMBpy (8.90 mmol), 8.75 g of MPTMS (44.5 mmol), 20 mg of AIBN, and dry $CHCl_3$ (50 mL) were added to a 100 mL flask. The reaction mixture was refluxed for 12 hours under argon. The $CHCl_3$ was removed by vacuum and the product was isolated by a careful vacuum distillation of the light volatiles and excess MPTMS at 80 ºC for 1 hour at 10 mTorr to yield 3.75 g of a viscous orange oil. The product was degassed and stored under dry nitrogen in a glovebox. $C_{21}H_{32}N_2O_3SSi$ (3.70 g, yield 99%). ^{1}H-NMR ($CDCl_3$): δ = 0.77 (d, 2H, -CH_2C<u>H</u>$_2$Si-), δ = 1.66 (m, 4H, -C<u>H</u>$_2$$CH_2SCH_2$C<u>H</u>$_2$-), δ = 1.80 (m, 2H, -C<u>H</u>$_2$$CH_2CH_2SCH_2CH_2CH_2$Si-), δ = 2.43 (s, 3H, -C<u>H</u>$_3$), δ = 2.50 (m, 4H, -C<u>H</u>$_2$SC<u>H</u>$_2$-), δ = 2.71 (t, 2H, -C<u>H</u>$_2$$CH_2CH_2CH_2SCH_2CH_2CH_2$Si-), δ = 3.55 (s, 9H, -Si(OC<u>H</u>$_3$)$_3$), δ = 7.12 (d, 2H, -(CH_3 or CH_2)-CC<u>H</u>CHNCCH-), δ = 8.22 (s, 2H, -(CH_3 or CH_2)-CCHCHNCC<u>H</u>-), δ = 8.54 (d, 2H, -(CH_3 or CH_2)-CCHC<u>H</u>NCCH-).

Preparation of 4-Methyl-4'-(4-propylsulfanyl-butyl)-[2,2']bipyridinyl, (pSdMBpy)

A mixture of 2.0 g of Allyl dMBpy (8.90 mmol), 3.40 g of propanethiol (44.5 mmol), 20 mg of AIBN, and dry $CHCl_3$ (50 mL) were added to a 100 mL flask. The reaction mixture was refluxed for 12 hours under argon. The $CHCl_3$ was removed by vacuum and the product was isolated by a careful vacuum distillation of the light volatiles and excess propanethiol at 80 ºC for 1 hour at 10 mTorr to yield 3.75 g of a viscous orange oil. $C_{18}H_{24}N_2S$ (2.67 g, yield >99%). ^{1}H-NMR ($CDCl_3$): δ = 0.95 (t, 3H, -$SCH_2CH_2C\underline{H}_3$), δ = 1.58 (m, 4H, -$C\underline{H}_2CH_2SCH_2C\underline{H}_2$-), δ = 1.79 (m, 2H, -$C\underline{H}_2CH_2CH_2SCH_2CH_2CH_3$), δ = 2.42 (s, 3H, -$C\underline{H}_3$), δ = 2.49 (m, 4H, -$C\underline{H}_2SC\underline{H}_2$-), δ = 2.70 (t, 2H, -$C\underline{H}_2CH_2CH_2CH_2SCH_2CH_2CH_3$), δ = 7.13 (d, 2H, -($CH_3$ or CH_2)-$CC\underline{H}CHNCCH$-), δ = 8.21 (s, 2H, -(CH_3 or CH_2)-$CCHCHNCC\underline{H}$-), δ = 8.55 (d, 2H, -(CH_3 or CH_2)-$CCHC\underline{H}NCCH$-).

Preparation of SBA-15(50Å)-CuBr/SdMBpy immobilized catalyst

To a 100 mL bottom flask, a solution 1.00 g of SdMBpyTMS (2.37 mmol) and 5 mL of dry toluene was slowly added to a stirring mixture of 0.17 g of CuBr (1.86 mmol) in 50 mL of dry toluene at 70 ºC in a nitrogen glovebox. The resulting light brown mixture was then stirred at 70 °C for 30 minutes under nitrogen or until the reaction mixture appears to be a dark reddish homogeneous solution. Then 2.00 g of SBA-15 (50 Å pores) was added to the reaction mixture, sealed with a valve, and removed from the nitrogen glovebox. Then the reaction mixture was stirred at 110 °C for 48 hrs under argon. The reaction flask was transferred into the nitrogen glovebox and the solid product was recovered and washed, once with 100 mL of dry toluene, once with 100 mL

of dry hexanes, and once with copious amount of dry dichloromethane until the solvent filtered out was clear. The dark reddish powder was dried under vacuum at room temperature for 12 hrs and stored under dry nitrogen in a glovebox. CHN, Si, and Cu analyses are summarized in **Table 6.7**.

Preparation of SBA-15(100Å), CPG(240Å), and Cab-O-Sil EH5 – CuBr/SdMBpy immobilized catalysts

In a similar manner to the procedure described above for SBA-15 (50 Å pores), a supported CuBr/SdMBpy complex was immobilized on a larger pore SBA-15 (100 Å pores), CPG(240 Å pores), and nonporous Cab-O-Sil EH5 silica supports. All the immobilized catalysts were recovered, washed, and stored under the same conditions. CHN, Si, and Cu analyses are summarized in **Table 6.7**

Table 6.7 Elemental analysis results for immobilized silica CuBr/SdMBpy catalysts.

Entry	Catalysts	% C	% H	% N	% Si	% Cu
1	SBA15(50)-CuBr/SdMBpy	16.28	1.99	1.64	28.70	2.55
2	SBA15(100)-CuBr/SdMBpy	15.67	2.55	2.54	29.32	3.97
3	CPG(240)-CuBr/SdMBpy	7.13	1.51	1.80	32.25	2.44
4	Cab-O-Sil-CuBr/SdMBpy	13.93	1.34	1.64	34.49	2.39

Experimental methods

Polymerization

For polymerization with the homogeneous CuBr/dMBpy or CuBr/pSdMBpy catalyst, the following recipe was typical: [MMA]/[dMBpy]/[Cu]/[BPN] = X/2/1/1 in Y% by v/v MMA in toluene or diphenylether (X = 300, Y = 50 or X = 100, Y = 25). For example, (X = 300, Y = 50 in toluene) to a 50 mL round-bottom flask with a sidearm valve, 4.00 g of MMA (0.040 mol, 4.24 mL), 0.049 g of dMBpy (0.266 mmol), 0.019 g of CuBr (0.133 mmol), and 0.06 g of BPN (0.133 mmol, 283 μL of initiator stock solution) were added in 3.68 g of toluene (4.24 mL) under nitrogen. The polymerization vessel was immersed in an oil bath preset to 90 °C. At set time intervals, 0.1 mL aliquots of polymerization solution were removed via syringe and placed in a vial. The vials were immediately quenched in a dry ice/acetone bath. Subsequently, 25 μl of sample was added to 1.5 mL THF for GC conversion analysis. The remaining sample was dried, re-dissolved in HPLC grade THF to 8.0 mg/mL, and filtered through a Gelman Acrodisc PTFE filter (0.2 μm) for GPC analysis. The conversion of MMA was followed by GC and molecular weights and molecular weight distributions were determined by GPC.

For polymerization using immobilized silica-CuBr/SdMBpy catalysts, the following recipe was typical: [MMA]/[Cu]/[BPN] = X/1/1 in Y% by v/v MMA in toluene at 90 ºC (X = 300, Y = 50 or X = 100, Y = 25). For instance, (X = 100, Y = 25) to a 10 mL Schlenk tube with a sidearm valve, 0.20 g of CPG(240)-CuBr/SdMBpy (8.82×10^{-2} mmol of Cu, 0.44 mmol Cu/g-catalyst), 0.80 g of MMA (8.82 mmol), and 170 μL of initiator stock solution BPN (8.82×10^{-2} mmol) were added to 2.19 g of toluene under nitrogen. The polymerization vessel was immersed in an oil bath preset to 90 °C.

Samples were taken at preset times and quenched using the procedure described above. Kinetic analysis and polymer characterization were carried out in a similar manner described for the homogeneous polymerization. After the polymerization, the catalysts were recovered from the remaining polymerization solution by sedimentation (SBA15(50 and 100)) or centrifugation (Cab-O-Sil EH5). The polymers were then precipitated in 50 mL of hexane and the polymers were recovered and dried as a white powder. The dried polymers were analyzed for trace amounts of copper.

Catalyst regeneration

The immobilized silica-CuBr/SdMBpy catalysts were regenerated with AIBN after each use when catalyst recycling was planned. The used catalysts were recovered from the polymerization solution by filtration or centrifugation and washed with copious amounts of toluene. The catalyst was transferred into a pressure tube reactor (i.e. 0.20 g of CPG(240)-CuBr/SdMBpy, 0.088 mmol of Cu). Then 3.00 g of toluene and an equivalent of AIBN to Cu (8.82×10^{-2} mmol or 14.45 mg of AIBN) were added to the reaction tube. The pressure tube reactor was sealed and placed in preheated oil bath at 90 ºC. The mixture was stirred for 15 minutes. The pressure tube reactor was transferred into the glovebox where the catalyst was recovered by filtration or centrifugation and washed with copious amounts of toluene and dichloromethane. The catalyst was dried under high vacuum for 12 hrs and stored under dry nitrogen in a glovebox for further use. Subsequent catalyst regenerations (i.e. 2^{nd} and 3^{rd} regeneration of the same catalyst) were performed in a similar manner described above.

Catalyst recycling

For polymerization with the immobilized silica-CuBr/SdMBpy catalyst when catalyst recycling was planned, the following recipe was typical: [MMA]/[Cu]/[BPN] = X/1/1 in Y% by v/v MMA in toluene (X = 300, Y = 50 or X = 100, Y = 25). For instance, (X = 100, Y = 25) to a 10 mL Schlenk tube with a sidearm valve, 0.20 g of regenerated CPG(240)-CuBr/SdMBpy (8.82×10^{-2} mmol of Cu, 0.44 mmol Cu/g-catalyst), 0.80 g of MMA (8.82 mmol), and 170 μL of initiator stock solution BPN (8.82×10^{-2} mmol) were added to 2.19 g of toluene under nitrogen. A 25 μL sample was taken immediately after mixing and prior to start of the polymerization to establish the reference conversion point at time zero. The polymerization vessel was immersed in an oil bath preset to 90 °C for a set time. The polymerization vessel was cooled by immersing in a dry ice/acetone bath and retransferred into a glovebox. A 25 μL sample was taken after the polymerization to determine the final conversion by GC. The polymerization solution was transferred into a 20 mL scintillation vial and filled with toluene (under nitrogen) for catalyst recovery. The vial was then centrifuged for 10 minutes at 3000 rpm. After centrifugation, the vial containing a lower solid catalysts layer and an upper liquid polymerization solution layer was transferred back into the glovebox and the supernatent toluene/polymerization solution was decanted. The polymers (1^{st} use, 2^{nd} use, etc.) were precipitated from the supernatant toluene/polymer solution described above by addition to 50 mL of hexane. The polymer was recovered and dried. The polymer molecular weight and polydispersity were determined by GPC. If catalyst recycling was planned for subsequent reuse, the procedure described above for catalysts regeneration was performed.

References

[1] J. V. Nguyen and C. W. Jones, Journal of Polymer Science, Part A: Polymer Chemistry 42 (2004) 1367.

[2] J. V. Nguyen and C. W. Jones, Journal of Polymer Science, Part A: Polymer Chemistry 42 (2004) 1384.

[3] J.-S. Wang and K. Matyjaszewski, Macromolecules 28 (1995) 7572.

[4] J.-S. Wang and K. Matyjaszewski, Macromolecules 28 (1995) 7901.

[5] D. M. Haddleton, D. J. Duncalf, D. Kukulj, M. C. Crossman, S. G. Jackson, S. A. F. Bon, A. J. Clark, and A. J. Shooter, European Journal of Inorganic Chemistry (1998) 1799.

[6] D. M. Haddleton, M. C. Crossman, B. H. Dana, D. J. Duncalf, A. M. Heming, D. Kukulj, and A. J. Shooter, Macromolecules 32 (1999) 2110.

[7] S. C. Hong, H.-J. Paik, and K. Matyjaszewski, Macromolecules 34 (2001) 5099.

[8] S. C. Hong and K. Matyjaszewski, Macromolecules 35 (2002) 7592.

[9] Y. Shen, S. Zhu, and R. Pelton, Macromolecules 34 (2001) 3182.

[10] Y. Shen, S. Zhu, F. Zeng, and R. Pelton, Journal of Polymer Science, Part A: Polymer Chemistry 39 (2001) 1051.

[11] Y. Shen, S. Zhu, and R. Pelton, Macromolecules 34 (2001) 5812.

[12] Y. Shen and S. Zhu, Macromolecules 34 (2001) 8603.

[13] M. E. Honigfort and W. J. Brittain, Macromolecules 36 (2003) 3111.

[14] S. Liou, J. T. Rademacher, D. Malaba, M. E. Pallack, and W. J. Brittain, Macromolecules 33 (2000) 4295.

[15] D. M. Haddleton, D. Kukulj, and A. P. Radigue, Chemical Communications (1999) 99.

[16] C. D. Nunes, M. Pillinger, A. A. Valente, I. S. Goncalves, J. Rocha, P. Ferreira, and F. E. Kuhn, European Journal of Inorganic Chemistry (2002) 1100.

[17] C. D. Nunes, A. A. Valente, M. Pillinger, A. C. Fernandes, C. C. Romao, J. Rocha, and I. S. Goncalves, Journal of Materials Chemistry 12 (2002) 1735.

[18] N. W. Barnett, R. Bos, H. Brand, P. Jones, K. F. Lim, S. D. Purcell, and R. A. Russell, Analyst (Cambridge, United Kingdom) 127 (2002) 455.

[19] F. Geneste, C. Moinet, and G. Jezequel, New Journal of Chemistry 26 (2002) 1539.

[20] C. Maillet, P. Janvier, M.-J. Bertrand, T. Praveen, and B. Bujoli, European Journal of Organic Chemistry (2002) 1685.

[21] C. Maillet, P. Janvier, M. Pipelier, T. Praveen, Y. Andres, and B. Bujoli, Chemistry of Materials 13 (2001) 2879.

[22] K. F. Mongey, J. G. Vos, B. D. Maccraith, C. M. McDonagh, C. Coates, and J. J. McGarvey, Journal of Materials Chemistry 7 (1997) 1473.

[23] M. Ogawa, T. Nakamura, J.-I. Mori, and K. Kuroda, Microporous and Mesoporous Materials 48 (2001) 159.

[24] M. M. Collinson, B. Novak, S. A. Martin, and J. S. Taussig, Analytical Chemistry 72 (2000) 2914.

[25] P. Ghosh and T. G. Spiro, Journal of the American Chemical Society 102 (1980) 5543.

[26] A. Kar-Wai Cheng, W.-Y. Lin, S.-G. Li, C.-M. Che, and W.-Q. Pang, New Journal of Chemistry 23 (1999) 733.

[27] H. R. Li, J. Lin, H. J. Zhang, H. C. Li, L. S. Fu, and Q. G. Meng, Chemical Communications (Cambridge, United Kingdom) (2001) 1212.

[28] F. Odobel, B. Bujoli, and D. Massiot, Chemistry of Materials 13 (2001) 163.

[29] F. Odobel, D. Massiot, B. S. Harrison, and K. S. Schanze, Langmuir 19 (2003) 30.

[30] Y. Sato, M. Kagotani, and Y. Souma, Journal of Molecular Catalysis A: Chemical 151 (2000) 79.

[31] C. G. Griggs and D. J. H. Smith, Journal of the Chemical Society, Perkin Transactions 1: Organic and Bio-Organic Chemistry (1972-1999) (1982) 3041.

[32] M. B. Smith and J. March, March's Advanced Organic Synthesis: Reactions, Mechanism, and Structure, John Wiley, New York, 2001.

[33] D. Zhao, J. Feng, Q. Huo, N. Melosh, G. H. Frederickson, B. F. Chmelka, and G. D. Stucky, Science (Washington, D. C.) 279 (1998) 548.

[34] D. Zhao, Q. Huo, J. Feng, B. F. Chmelka, and G. D. Stucky, Journal of the American Chemical Society 120 (1998) 6024.

[35] M. Kruk, M. Jaroniec, C. H. Ko, and R. Ryoo, Chemistry of Materials 12 (2000) 1961.

[36] H. Baranska, A. Labudzinska, and J. Terpinski, Laser Raman Spectrometry, Wiley, New York, 1987.

[37] C. Kaes, A. Katz, and M. W. Hosseini, Chemical Reviews (Washington, D. C.) 100 (2000) 3553.

[38] Y. Shen, S. Zhu, and R. Pelton, Macromolecular Rapid Communications 21 (2000) 956.

[39] G. Zheng and H. D. H. Stoever, Macromolecules 35 (2002) 6828.

[40] Y. Tsujii, M. Ejaz, S. Yamamoto, T. Fukuda, K. Shigeto, K. Mibu, and T. Shinjo, Polymer 43 (2002) 3837.

[41] J. D. Jeyaprakash, S. Samuel, R. Dhamodharan, and J. Ruhe, Macromolecular Rapid Communications 23 (2002) 277.

[42] T. Tao and G. E. Maciel, Journal of the American Chemical Society 122 (2000) 3118.

[43] K. Matyjaszewski and J. Xia, Chemical Reviews 101 (2001) 2921.

[44] J.-L. Wang, T. Grimaud, and K. Matyjaszewski, Macromolecules 30 (1997) 6507.

[45] J. L. De la Fuente, M. Fernandez-Sanz, M. Fernandez-Garcia, and E. L. Madruga, Macromolecular Chemistry and Physics 202 (2001) 2565.

[46] M. Imperor-Clerc, P. Davidson, and A. Davidson, Journal of the American Chemical Society 48 (2000) 11925.

[47] G. Kickelbick, H.-j. Paik, and K. Matyjaszewski, Macromolecules 32 (1999) 2941.

[48] Y. Shen, S. Zhu, F. Zeng, and R. H. Pelton, Macromolecules 33 (2000) 5427.

[49] Y. Shen, S. Zhu, F. Zeng, and R. Pelton, Macromolecular Chemistry and Physics 201 (2000) 1387.

[50] K. Matyjaszewski and B. E. Woodworth, Macromolecules 31 (1998) 4718.

[51] J. Xia and K. Matyjaszewski, Macromolecules 32 (1999) 5199.

[52] A. B. Pangborn, M. A. Giardello, R. H. Grubbs, R. K. Rosen, and F. J. Timmers, Organometallics 15 (1996) 1518.

[53] M. Ciampolini and N. Nardi, Inorg. Chem. 5 (1966) 41.

CHAPTER 7

RECYCLABLE POLYMERIZATION CATALYSTS: METHYL METHACRYLATE POLYMERIZATION WITH SILICA-SUPPORTED CUBR-BIPYRIDINE ATOM TRANSFER RADICAL POLYMERIZATION CATALYSTS

Abstract

Physisorbed and covalently immobilized CuBr/Bipyridine (Bpy) atom transfer radical polymerization (ATRP) catalysts are supported on non-porous fumed silica Cabosil EH5 by a preassembled complex approach. The catalysts are characterized by elemental analysis, thermogravimetric analysis, and UV/vis spectroscopy. The UV/vis spectra confirmed the immobilization of Cu(I)/Bpy complexes based on the observed ligand $\pi - \pi^*$ and charge-transfer $t_{2g} - \pi^*$ transitions. The supported catalysts are used for the polymerization of methyl methacrylate, promoting the polymerization to moderate conversions with good control, giving molecular weights similar to theoretical values and low PDIs. The used, Cu(II)-containing catalysts were subjected to a regeneration process using AIBN, producing increased concentrations of Cu(I) species on the surface for the tethered system. No regeneration was possible under the conditions utilized here for the physisorbed catalyst, likely due to strong complex-surface interactions. The regeneration was followed by UV/vis spectroscopy and the conditions were optimized to give high polymerization rates upon catalyst recycle. Leaching experiments indicate that the tethered systems results in no detectable soluble copper species in this work and that the majority of the catalytic transformations occur on the catalyst surface. In contrast, the physisorbed catalyst resulted in a substantial amount of leached copper species in solution and the soluble species were capable of controlling the polymerization in the

absence of the solid, although with extremely low rates. The covalently tethered system performed better than the physisorbed system in all aspects, with better polymerization control, undetectable leaching, and an effective catalyst regeneration method.

Introduction

Until now, my focus was mainly on developing and improving immobilized ATRP polymerization catalysts that produce well-defined polymers with efficient catalyst recovery [1-3]. However, less attention has been focused on optimizing polymerization conditions, catalyst regeneration, and recycle. In addition, there has been some debate in the literature concerning the reason for loss in catalyst activity during recycle, as well as the location of the active catalytic sites.

Indeed, in all cases, the polymerization rate decreases after the first use. Essentially two potential reasons have been proposed [4]. First, for copper-containing catalysts, Cu(I)/ligand species are immobilized for the first catalyst use, but due to chain termination and/or the stability of the copper-ligand complex in the Cu(II) oxidation state, Cu(II) species accumulate on the support surface after the polymerization [5]. As a result, when these catalysts are recycled, they display decreased polymerization rates, as chains are only initiated by Cu(I) species. To recover the catalyst activity, the catalyst needs to be "regenerated". Various regeneration methods have been utilized but the extent of Cu(I) regeneration has not been directly probed [3, 6, 7]. The second proposed reason for decreased rates upon recycle is the loss of immobilized catalyst due to leaching – fewer polymerization-initiation sites remain on the solid support.

The second reason leads to the debate on the location of the catalytic active site. Are all the important polymerization processes (i.e., initiation, activation, and deactivation) occurring in the solution phase and away from the immobilized catalyst complexes? To be more specific, are the active copper species leaching from the solid

support and effectively controlling the entire polymerization process in the solution phase? These questions can only be answered with stable covalently tethered catalysts.

In Chapter 6 silica-tethered CuBr/bipyridine (Bpy) ATRP catalysts are described [3]. Catalysts immobilized on controlled pore glass with a 240Å pore diameter (CPG-240) and nonporous Cabosil EH5 exhibited the best polymerization results, with moderate conversions, PDIs as low as 1.25, and low residual copper content in the final polymer [3]. These silica-tethered CuBr/Bpy catalysts performed better than CuBr/PMI catalysts in terms of polymerization control and catalyst stability, however CuBr/PMI catalysts allowed the polymerizations to achieve higher conversions and did not require catalyst regeneration [2]. In both cases, leached copper could not be ruled out as soluble species that potentially help mediate the deactivation process similar to Matyjaszewski's dual immobilized catalyst/soluble deactivator system [7, 8].

In this chapter, I probe the CuBr/Bpy system with three key issues as foci. First, I evaluate both silica-tethered and physisorbed CuBr/Bpy systems (**Figure 7.1**) in the controlled polymerization of methyl methacrylate, with a focus on the role of the immobilization method on catalytic performance. Second, I evaluate the effectiveness of a unique catalyst regeneration procedure that I developed, with spectroscopic characterization of the state of the copper species before and after reaction and regeneration. Third, I elucidate the role of leached copper species on the course of the polymerization in both the tethered and physisorbed systems.

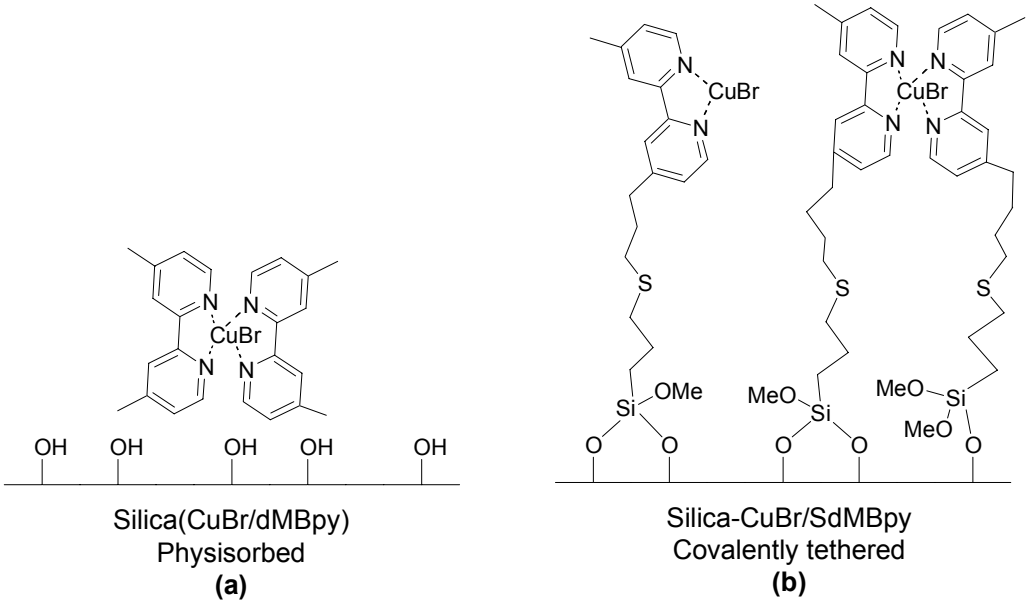

Figure 7.1 Theoretical illustrations of physisorbed CuBr/dMBpy (a) and covalently tethered silica-CuBr/SdMBpy (b).

Results and Discussion

Catalyst synthesis and characterization

Two types of catalysts are reported in this work, using the following notation. Silica-tethered CuBr/Bpy complexes are denoted Cabosil-CuBr/SdMBpyTMS [3], with the dash indicating a covalent tether. Catalysts with CuBr/Bpy complexes physically adsorbed onto silica supports are labeled Cabosil(CuBr/SdMBpyTMS).

The covalent immobilization of CuBr/SdMBpyTMS complex on to Cabosil was previously reported [3]. A battery of characterization techniques showed a mixture of mono and bis copper coordinated Bpy complexes and uncoordinated Bpys were covalently attached to the silica surface. ^{13}C CPMAS NMR showed the successful covalent immobilization of Bpy ligands on the silica support (**Figure 6.3 page**) [3]. The combination of FT-Raman spectroscopy and elemental analysis revealed a potential for several different immobilized Bpy species (i.e. immobilized CuBr(Bpy), $CuBr(Bpy)_2$, and Bpy). However, the oxidation state of the immobilized complex was not directly probed. For this work, diffuse-reflectance ultraviolet-visible spectroscopy (UV/vis) was used to determine the oxidation state of the immobilized complexes. For reference, the UV/vis spectra of homogeneous reference compounds and complexes in the solid state were obtained to determine the transitions for the ligand and copper complexes. **Figure 7.2** shows the UV/vis spectra for CuBr, dimethylbipyridine (dMBpy), CuBr/dMBpy, and $CuBr_2$/dMBpy. The $\pi - \pi^*$ transition of the uncomplexed dMBpy (**Figure 7.2a**) appears between 250 – 350 nm. After complexation of both Cu(I) and Cu(II) bromide species, the breadth of the transition shifts to 400 and 450 nm, respectively (**Figure 7.2c and d**,

respectively). The metal to ligand charge-transfer band (MLCT) (t_{2g} – π^*) for CuBr/dMBpy complex appears between 400 – 600 nm, consistent with a Cu(I) oxidation state. The d-d transition for $CuBr_2$/dMBpy complex has a broad band between 600 – 800 nm, indicative of a Cu(II) oxidation state. The π – π^*, MLCT, and d-d transitions were similar to those reported for solution phase UV/vis spectra of similar CuX_n/Bpy species [9-12].

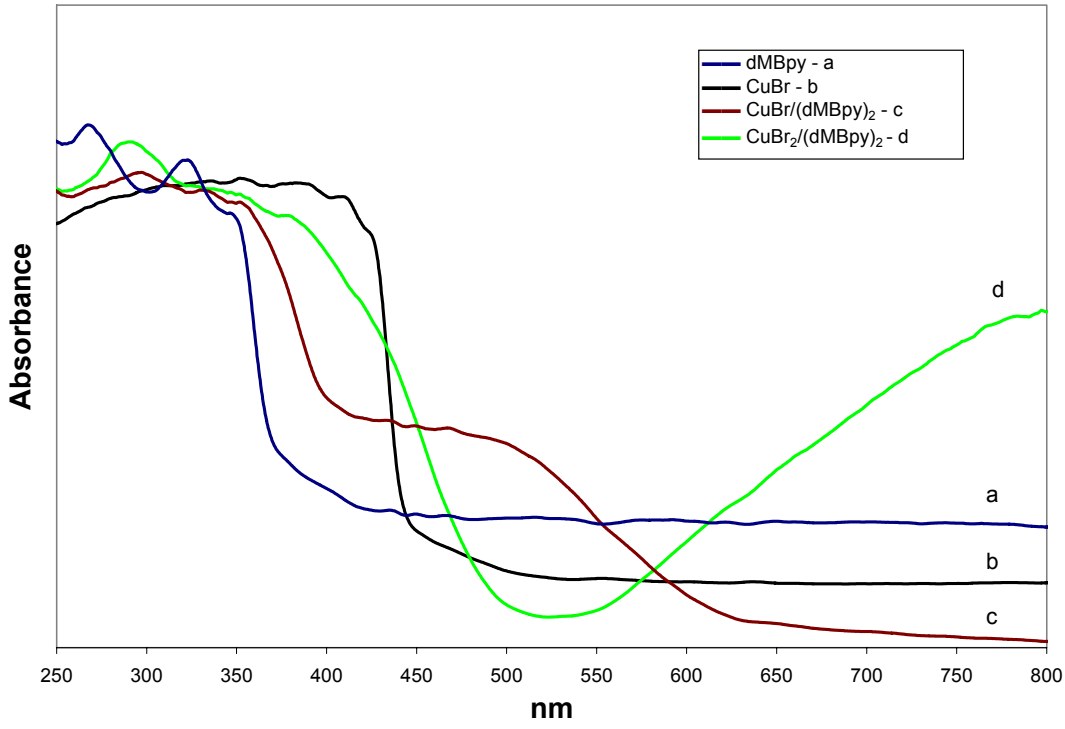

Figure 7.2 UV/vis spectra (vs. PTFE) of reference compounds (a) dMBpy, (b) CuBr, (c) $CuBr/(dMBpy)_2$, and (d) $CuBr_2/(dMBpy)_2$.

Figure 7.3 shows the UV/vis spectra of various components of CuBr/SdMBpyTMS on to Cabosil. The π – π* transition of the immobilized uncomplexed dMBpy ligand appears between 260 – 310 nm. The immobilized CuBr/SdMBpy complex has π – π* transition at 270 - 340 nm and MLCT band between 350 – 650 nm. The broadness of the MLCT transition may be indicative of the immobilized CuBr/SdMBpy complex possessing several different symmetries on the surface (i.e. distorted tetrahedral geometry, CuBr(Bpy), $CuBr(Bpy)_2$, and free CuBr) [13],

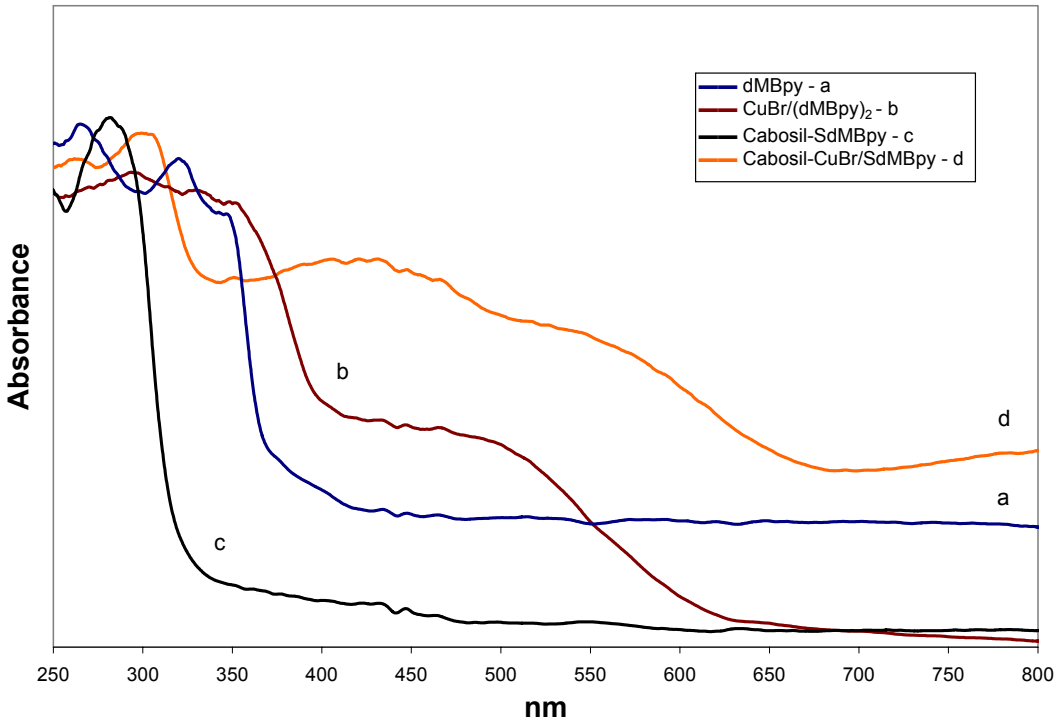

Figure 7.3 Immobilization of Cabosil-CuBr/SdMBpy followed by UV/vis spectroscopy. UV/vis spectra (vs. PTFE) of (a) dMBpy, (b) $CuBr/(dMBpy)_2$, (c) Cabosil-SdMBpy, and (d) Cabosil-CuBr/SdMBpy.

which is consistent with my previous results [3]. There also appears to be a transition beyond 600 nm that was attributed to low concentration of Cu(II) species on the surface. Nevertheless, it appears by UV/vis spectroscopy that the Cabosil-CuBr/SdMBpy catalyst surface is dominated by a much higher concentration of Cu(I)/SdMBpy complexes, as was intended. The catalyst loading determined by CHN, Cu, and Si microanalysis was 0.46 mmol SdMBpy g-catalyst^{-1} and 0.34 mmol Cu g-catalyst^{-1}. The ligand/metal ratio was 1.35 (L/M ratio of 2 was targeted for the catalyst synthesis). The presence of excess metal relative to ligand indicates that some free CuBr or some mono-coordinated Bpy ligands exist on the surface. Although the difference between mono and bis coordinated Bpy ligands can not be discerned by FT-Raman or UV/vis spectroscopy, previous FT-Raman studies do provide evidence for a small population of unligated Bpy ligands [3].

CuBr/dMBpy complex was physisorbed on Cabosil support in a similar manner to the covalent immobilization to give Cabosil(CuBr/dMBpy). However, polar solvents were not used to wash the catalyst because the solvent will strip the physisorbed complex from the silica surface [1]. UV/vis spectroscopy was again used to determine the nature of the immobilized species. **Figure 7.4** shows a comparison of the UV/vis spectrum for CuBr/dMBpy complex, and immobilized Cabosil-CuBr/SdMBpy and Cabosil(CuBr/dMBpy) catalyst. Both immobilized catalysts have similar UV/vis spectra, however the Cabosil(CuBr/dMBpy) catalyst does not appear to have the Cu(II) transition beyond 600 nm. The Cabosil(CuBr/dMBpy) catalyst loading was 0.92 mmol dMBpy g-catalyst^{-1} and 0.53 mmol Cu g-catalyst^{-1}. The 1.73 ligand/metal ratio was much closer to the target value than in the tethered case.

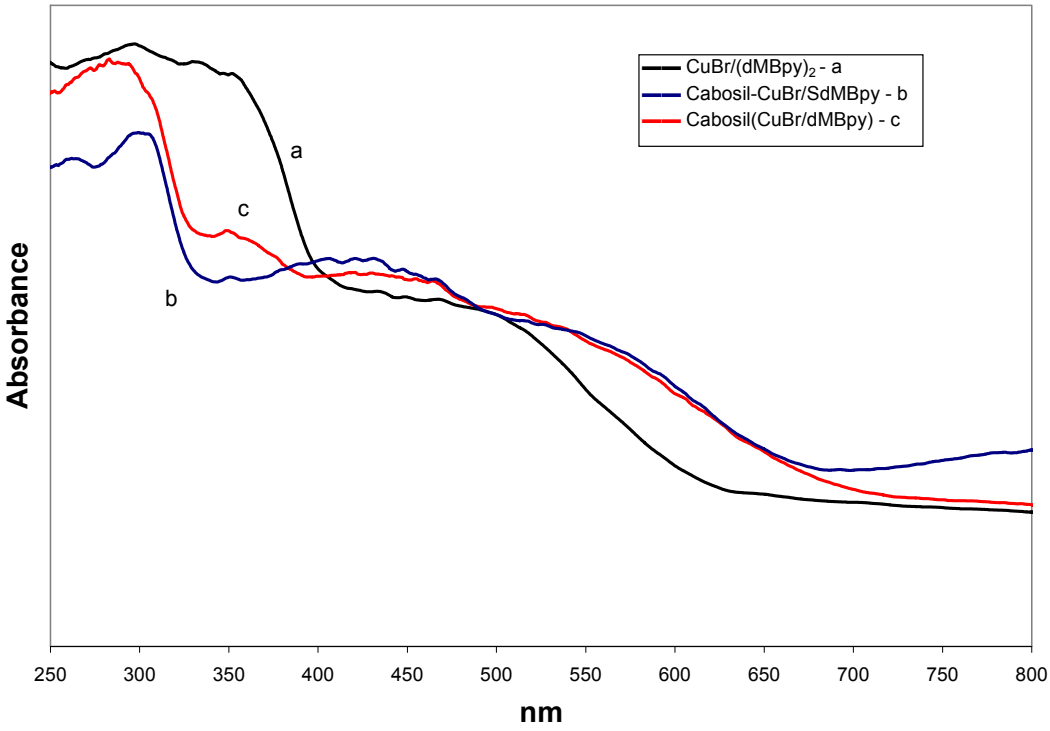

Figure 7.4 UV/vis comparison of non-immobilized and immobilized CuBr/dMBpy complexes. UV/vis spectra (vs. PTFE) of (a) CuBr/$(dMBpy)_2$, (b) covalent Cabosil-CuBr/SdMBpy, and (c) physisorbed Cabosil(CuBr/dMBpy).

Polymerization of MMA

The solid catalysts were used for the heterogeneous polymerization of methyl methacrylate (MMA). In addition to using both the covalent and physisorbed catalysts, a heterogeneous one-pot polymerization technique and homogeneous polymerization were used to compare the effect of immobilizing the CuBr/Bpy complex onto silica. The one-pot polymerization was similar to a homogeneous polymerization; however bare Cabosil silica was added to the homogeneous complex in solution at the start of the polymerization. This represents a system to test whether bare silica can effectively adsorb the free complex *in-situ* and whether this will have any affect on the

polymerization. Two different monomer to initiator ratios ([MMA]/[BPN] = 100 and 300) were investigated to determine the effect of polymer molecular weight and the silica support structure have on the MMA conversion and final polydispersity of the polymer. Lastly, the catalysts were removed by centrifugation and the polymerization solutions were analyzed for residual or leached copper. It was speculated in my previous report [2, 3], that ppm levels of leached copper species can help mediate the controlled polymerization similar to Matyjaszewski's immobilized/soluble hybrid catalyst system (PS8-dMBpy/CuBr:$CuBr_2$/Tris(2-(dimethylamino)ethyl)amine (or Me_6TREN) [7] and Zhu's physisorbed hexamethyltriethylenetetramine (or HMTETA)/CuBr/Silica system [4]. Discussion on the nature and location of the catalyst active site for covalent and physisorbed CuBr/dMBpy immobilized catalysts on Cabosil will be given in a later section.

Table 7.1 summarizes the results of the polymerizations. **Figure 7.5** shows the kinetic plots, the evolution of M_n, and polydispersity index (PDI) vs. conversion plots for [MMA]/[BPN] = 100. The homogeneous polymerization reached 73% conversion, M_n = 10000, and PDI = 1.22. The covalent Cabosil-CuBr/SdMBpy catalyst was the only catalyst to perform similarly to the homogeneous catalyst, however the molecular weight distribution was slightly broader (PDI = 1.31). Both the physisorbed Cabosil(CuBr/dMBpy) and one-pot polymerizations performed poorly compared to the homogeneous polymerization, with conversions reaching only 56% and PDI > 1.30. The severity of chain termination in these two polymerizations was much greater as seen in the significant curvature in the pseudo first order plots (ln[Mo]/[Mt] versus time plots)

Table 7.1 Polymerization results for Cabosil-immobilized CuBr/Bpy catalysts.

X	Catalyst Condition	Conversion (final)	$M_{n,Th}$	$M_{n,Exp}$	PDI	R_{Cu}
100	Homogeneous	73	7300	10000	1.22	2193
	Covalent	73	7300	10000	1.31	<1
	Physisorbed	56	5600	9300	1.39	37
	One-pot	56	5600	8600	1.31	68
300	Homogeneous	80	24000	24900	1.30	2031
	Covalent	76	22800	27700	1.51	<1
	Physisorbed	89	26700	33100	1.57	115
	One-pot	61	18300	27500	1.56	219

Polymerization conditions: [MMA]/[Cu]/[BPN] = X/1/1 in Y% MMA in toluene at 90º for 24 hours (X = 100, Y = 25; X = 300, Y = 50). Only the final conversion was determined in these polymerizations.

and low reactivity after 2 hours. The poor results could be the result of the short catalyst distance away from the solid support, if most of the sites remain adsorbed under reaction conditions. Since the CuBr/dMBpy catalysts are physisorbed to the support, unlike the covalently tethered, potentially more accessible CuBr/SdMBpy catalysts, it could be difficult for the growing polymer chain to interact with immobilized catalyst because of steric constraints. As the polymer molecular weight increases this case could be exacerbated even more. In the case of the tethered CuBr/SdMBpy catalysts, the active site is likely better solvated in the polymerization solution because of the linker. Zhu and coworkers showed that there was an optimal linker length for their immobilized ATRP catalysts to achieve well behaved polymerizations in a related system [14]. Upon completion of the polymerizations, the solid catalysts particles were removed by centrifugation and the recovered polymerization solutions were analyzed by copper microanalysis for residual copper content, R_{Cu}. Both homogeneous polymerizations ([MMA]/[I] = 100 and 300) had approximately R_{Cu} ~ 2000 ppm. Polymerizations

performed with covalently immobilized catalyst had undetectable amounts of copper in the solution, while those performed with physisorbed and one-pot methodologies leached copper, but less than the homogeneous polymerizations. For the physisorbed and one-pot polymerization with [MMA]/[I] = 100, the residual copper found were less than at [MMA]/[I] = 300. The higher copper contents were attributed to poorer recovery of the catalyst particles from the more viscous higher molecular weight polymerization solution.

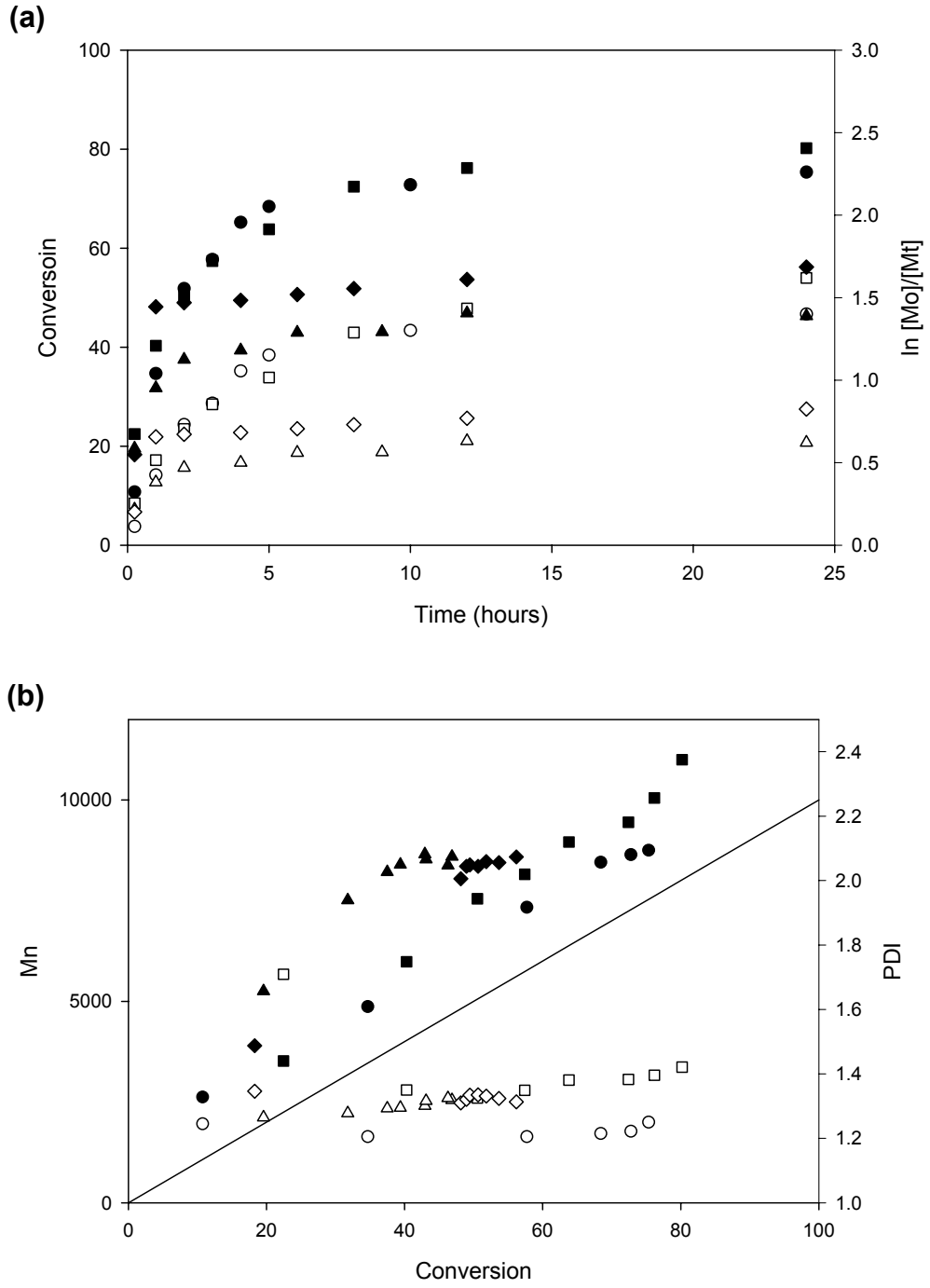

Figure 7.5 Kinetic plots for various immobilized Cabosil CuBr/Bpy polymerization catalysts, [MMA]/[BPN] = 100. Evolution of conversion and $\ln[M_o]/[M_t]$ with time (a) and evolution of M_n and PDI with monomer conversion (b). (●,○) homogeneous CuBr/dMBpy, (■,□) covalent Cabosil-CuBr/SdMBpy, (◆,◇) physisorbed Cabosil(CuBr/dMBpy), and (▲,△) one-pot with Cabosil and CuBr/dMBpy. Theoretical M_n curve (-). Shaded symbol = left axis; open symbol = right axis. Polymerization conditions: [MMA]/[Cu]/[BPN] = 100/1/1 in 25% by v/v MMA in toluene at 90 °C.

Figure 7.6 shows the kinetic plots, the evolution of M_n with conversion, and PDI vs. conversion plots for [MMA]/[BPN] = 300. The homogeneous polymerization reached 82% conversion, with $M_{n,Exp}$ = 26800 and PDI = 1.31. All heterogeneous polymerizations had polydispersities greater than 1.50 and there is evidence of chain termination as indicated by the curvature in the ln[Mo]/[Mt] versus time plots. In general the conversions were higher than those for [MMA]/[BPN] = 100. The higher monomer concentration in these polymerizations may be a reason why higher conversions were achieved. The increase in PDI relative to the homogeneous polymerization was caused by Cabosil support [3]. Addition of the supported catalyst increases the viscosity of the polymerization solution even before the reaction begins. As the conversion increases, the gelation of the polymerization solution was observed and this can cause significant mass transport problems, thereby decreasing the frequency of the activation/deactivation steps and increasing the PDI. Current research is underway seeking alternative supports and methods to increase the active site density on the support to alleviate this problem.

Catalyst regeneration and recycling

Three different methodologies of regenerating immobilized ATRP catalysts have been reported. The first two involve addition of zero valent copper in the form of copper powder or wire, Cu(0). The Cu(0) is stirred with the spent catalyst to reduce the Cu(II) to Cu(I) – [Cu(II) + Cu(0) → 2 Cu(I)] [6]. In the last method, Matyjaszewski and coworkers use the soluble Me_6TREN ligand with Cu(0) wire to regenerate the spent PS8-dMBpy/$CuBr_2$ catalyst [7]. Similar to its proposed behavior as a deactivator species in

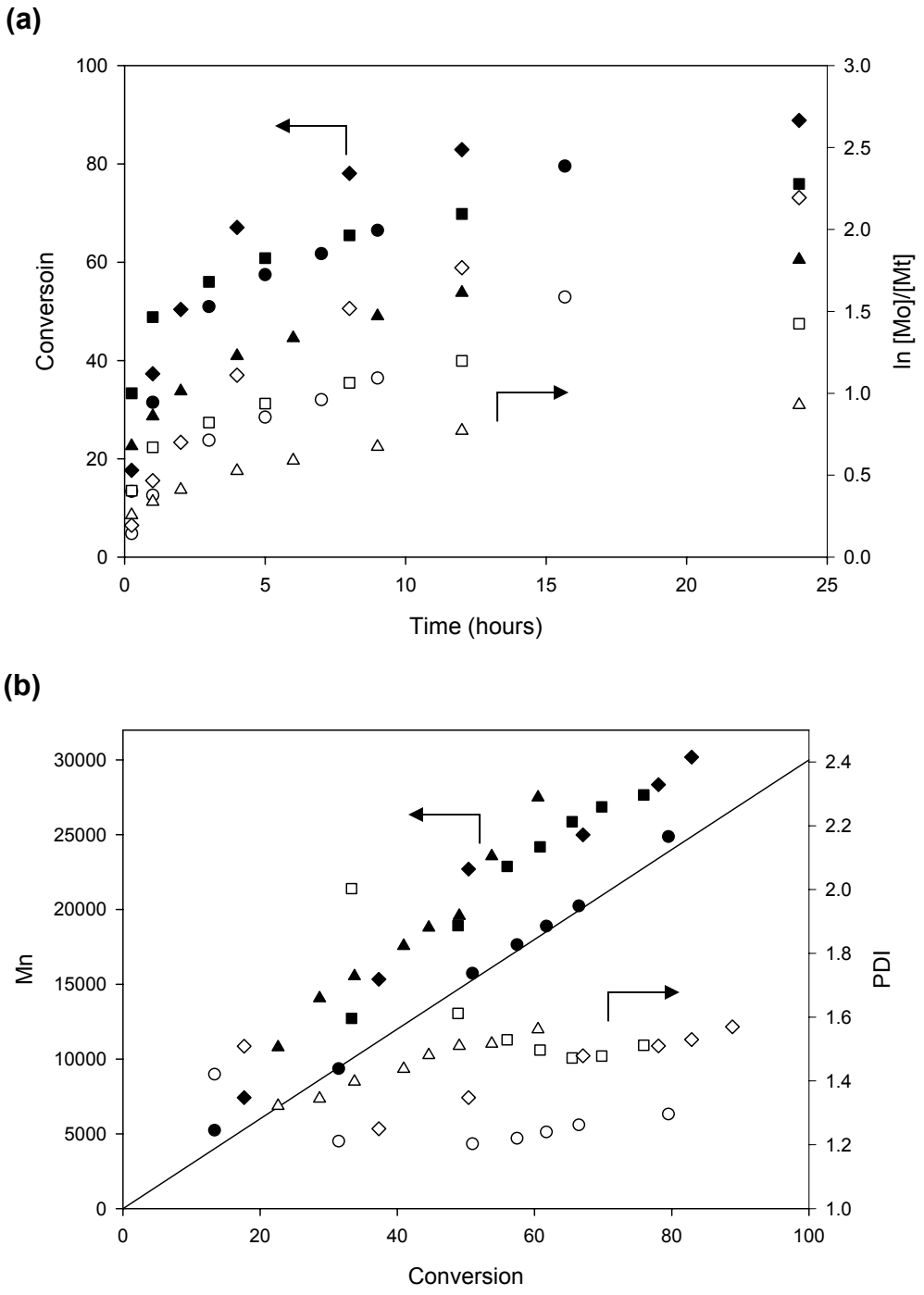

Figure 7.6 Kinetic plots for various immobilized Cabosil CuBr/Bpy polymerization catalysts, [MMA]/[BPN] = 300. Evolution of conversion and $\ln[M_o]/[M_t]$ with time (a) and evolution of M_n and PDI with monomer conversion (b). (●,○) homogeneous CuBr/dMBpy, (■,□) covalent Cabosil-CuBr/SdMBpy, (◆,◇) physisorbed Cabosil(CuBr/dMBpy), and (▲,△) one-pot with Cabosil and CuBr/dMBpy. Theoretical M_n curve (-). Shaded symbol = left axis; open symbol = right axis. Polymerization conditions: [MMA]/[Cu]/[BPN] = 300/1/1 in 50% by v/v MMA in toluene at 90 °C.

the polymerization, the soluble Me_6TREN transports Cu(0) to the immobilized catalyst to be reduced to Cu(I). However, these regeneration methods add additional copper to immobilized catalysts.[5] In most cases, the reuse of these regenerated catalysts leads to poorer polymerization results compared to the first use (i.e. lower conversions and higher PDIs) [6, 7].

In my previous work, I have shown that the covalently tethered Cabosil-CuBr/SdMBpy catalysts can be recycled up to three times by regenerating the catalysts without addition of additional copper using a simple treatment with AIBN [3]. Without the catalyst regeneration, the recycle reactions proceeded slowly, with the polymerization reaching 25% conversion after 24 hours and 45% after 89 hours (compared to 1st use: conversion = 73% and PDI = 1.31 after 24 hours). Upon completion of the polymerization, a higher concentration of Cu(II) immobilized species was hypothesized to exist on the catalyst support because of chain termination and the tendency of the Bpy ligand to stabilize Cu(II) relative to Cu(I) [5]. The existence of Cu(II) species on the catalysts was supported by the bright green color of the catalyst during and after the polymerization caused by chain termination events. Further evidence for the presence of immobilized Cu(II) species comes from the UV-vis spectra of the used Cabosil-CuBr/SdMBpy shown in **Figure 7.7b**. The MLCT band for Cu(I) has a much lower absorbance intensity compared to the fresh catalyst (**Figure 7.7a**) and a distinct Cu(II) band between 600 – 750 nm appears. After catalyst regeneration the recycled catalysts achieved higher conversions and activity than polymerizations performed with the used non-regenerated catalyst (1st use, fresh catalyst: conversion = 78%, $M_{n,Exp}$ = 13000, and

[5] Although copper microanalyses were not performed on these catalysts after the regeneration, it can be assumed by using these regeneration techniques involving copper wire or powder; additional copper must be added to the system.

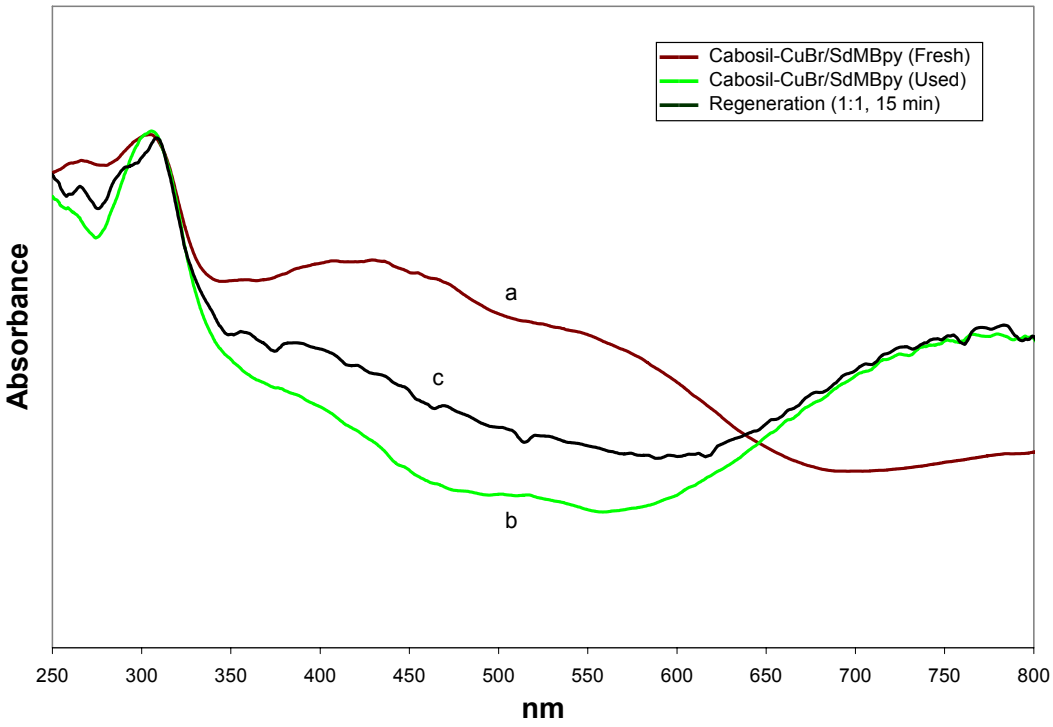

Figure 7.7 UV/vis comparison (vs. PTFE) of covalent Cabosil-CuBr/SdMBpy (a) fresh, (b) used, and (c) regenerated catalysts. Polymerization conditions: [MMA]/[Cu]/[BPN] = 100/1/1 in 25% by v/v MMA in toluene at 90 °C. Regeneration conditions: [AIBN]/[Cu] = 1 in 4 mL of toluene at 90 °C for 15 minutes.

PDI = 1.29 after 17 hours; 2nd use, non-regenerated catalyst: conversion = 45%, $M_{n,Exp}$ = 5700, and PDI = 1.24; 3rd use, regenerated catalyst: conversion = 65%, $M_{n,Exp}$ = 7600, and PDI = 1.23 after 48 hours, [MMA]/[BPN] = 100) [3]. **Figure 7.8** shows the Cabosil-CuBr/SdMBpy catalyst before (7.8a) and after (7.8b) regeneration. Over a period of 15 minutes the catalyst mixture turned from a green to dark reddish brown color. The UV/vis spectra of the regenerated catalyst (**Figure 7.7c**) shows the intensity increase of the Cu(I) band, however a Cu(II) band still remains. Optimization of the catalyst regeneration will be discussed in a subsequent section.

An attempt to regenerate the physisorbed Cabosil(CuBr/dMBpy) catalyst was also undertaken. The regeneration procedure was modified because the recovered catalyst could not be washed with DCM, therefore the catalyst was washed extensively with toluene. During regeneration, the color of the regenerated catalyst did not change significantly compared to the Cabosil-CuBr/SdMBpy catalyst (**Figure 7.8c** and **d**). The UV/vis spectra of the catalyst before and after regeneration only shows a slight increase in absorbance intensity of the Cu(I) transition (**Figure 7.9b and c**, respectively).

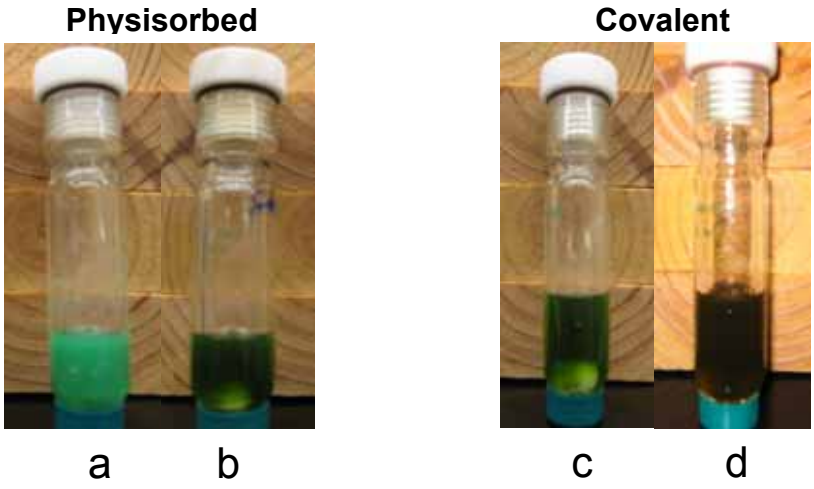

Figure 7.8 Digital images of used and regenerated Cabosil CuBr/Bpy catalysts: (a) used and (b) "regenerated" physisorbed Cabosil(CuBr/dMBpy) and (c) used and (d) regenerated covalent Cabosil-CuBr/SdMBpy.

Recycling of the catalyst resulted in a polymerization that reached 12% conversion, $M_{n,Exp}$ = 2400, and PDI = 1.54 after 24 hours (compared to 1st use: conversion = 56 and PDI = 1.39 after 24 hours). Thus, reaction rates are depressed and control over the polymerization is poor. Although not shown here, the GPC trace shows a small higher molecular weight signal likely due to desorbed polymer from the first polymerization. This is an important observation, as residual polymer may play a key role in preventing effective catalyst recycle as well as in determining the amount of leaching of copper species during the reaction The physisorbed Cabosil(CuBr/dMBpy) catalyst cannot be regenerated or recycled using the conditions described here.

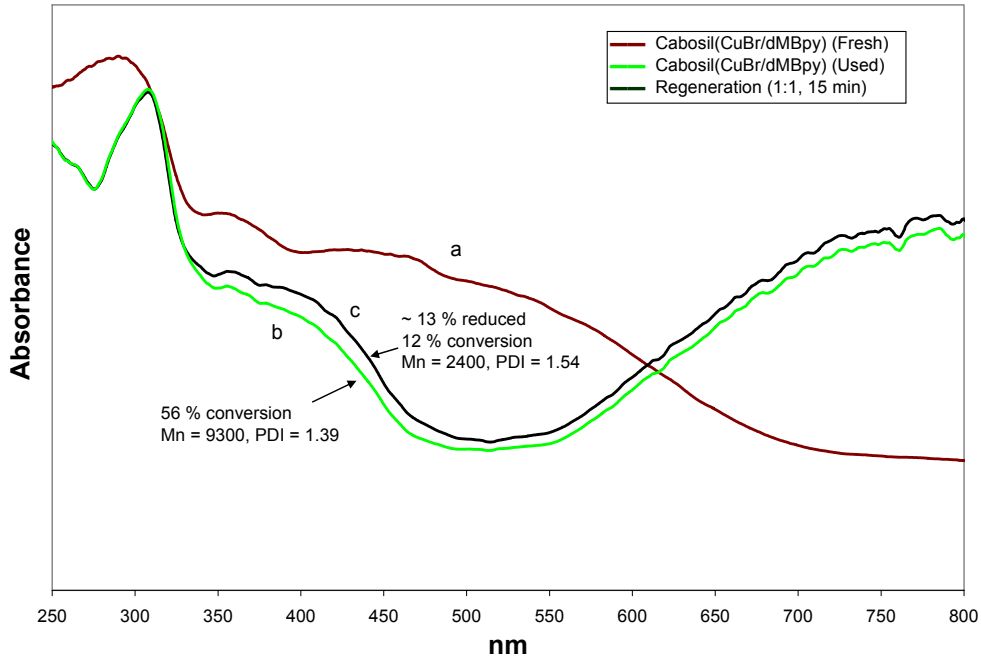

Figure 7.9 UV/vis comparison (vs. PTFE) of physisorbed Cabosil(CuBr/dMBpy): (a) fresh, (b) used, and (c) regenerated catalysts. Polymerization conditions: [MMA]/[Cu]/[BPN] = 100/1/1 in 25% by v/v MMA in toluene at 90 °C. Regeneration conditions: [AIBN]/[Cu] = 1 in 4 mL of toluene at 90 °C for 15 minutes.

The ability to remove the reacted polymer after the catalyst recovery is an important process during the regeneration procedure. The entangled polymer may coat the catalyst particle, thus preventing the AIBN radical's ability to reduce the immobilized Cu(II) species. The amount of polymer entangled on the catalyst particle after recovery was quantified by thermogravimetric analyses and the results are summarized in **Table 2**. The organic content of the physisorbed catalyst increased up to 76% and as high as 91%, for [MMA]/[BPN] = 100 and 300, respectively. In the case of the covalently tethered catalyst washed with DCM, the increased organic content was as low as 4% and as high as 30%, for [MMA]/[BPN] = 100 and 300, respectively. Clearly, the effective washing of the used catalyst with DCM was important for polymer recovery and catalyst regeneration.

Table 7.2 Thermogravimetric analysis of Cabosil-immobilized CuBr/Bpy catalysts.

Catalyst	X	g organics/g SiO_2[a]	% Increased organics
Cabosil-CuBr/SdMBpy	0	0.26	---
Cabosil-CuBr/SdMBpy	100	0.28	4.8
Cabosil-CuBr/SdMBpy	300	0.34	30.4
Cabosil(CuBr/SdMBpy)	0	0.25	---
Cabosil(CuBr/SdMBpy)	100	0.44	76.4
Cabosil(CuBr/SdMBpy)	300	0.48	91.9

a. Calculated based on organics loss from 200 – 500 ºC by TGA
Polymerization conditions: [MMA]/[Cu]/[BPN] = X/1/1 in Y% MMA in toluene at 90º for 24 hours (X = 100, Y = 25; X = 300, Y = 50).

Another potential reason why catalyst regeneration was ineffective for the physisorbed case could be that the immobilized CuBr/dMBpy is too tightly bound to the silica surface, as speculated above. If this is true, a covalent tether may be important for regeneration because it may allow for the necessary distance away from the support through solvation promoted by the long surface tether. To test this hypothesis, a *Cu(II)* Cabosil($CuBr_2$/dMBpy) catalyst was prepared and the reduction of Cu(II) to Cu(I) species was performed with AIBN. In this case, there is no polymer associated with the solid that might block access to the surface sites. Regeneration with AIBN did not occur to any significant extent over 60 minutes because the catalyst mixture only turned to a darker shade of green, not the distinct reddish brown color observed with the covalently immobilized catalyst after 10 minutes. This result indicates that the CuBr/dMBpy complex may be interacting with the surface in way that prevents effective regeneration of the catalyst and that a tethered complex and good solvation of the immobilized $CuBr_2$/dSMBpy complexes are the key items that are necessary for catalyst regeneration.

Optimization of catalyst regeneration

The standard conditions previously reported for AIBN regeneration were an equivalent amount of AIBN reducing agent to immobilized copper (1:1 AIBN:Cu) in toluene at 90 ºC for 15 minutes [3]. Here, a series of regeneration conditions were investigated to determine the optimal reducing agent concentration and time for regeneration. The AIBN concentration was varied from 0.5 – 2.0 equivalents to probe the effect of radical concentration (one AIBN molecule creates two radicals). Ultimately, the regeneration appears to be a dynamic process, as it was observed that as the

regeneration time increases, the reaction solution changes from green to a dark reddish brown color and then back to bright green again. Therefore, the regeneration time was varied and the increase/decrease of the Cu(I) transition intensity relative to the fresh and used Cabosil-CuBr/SdMBpy catalyst was monitored by UV/vis measurements of the recovered, washed, and dried regenerated solid catalyst samples. **Table 7.3** summarizes the results for catalyst regeneration experiments. The fraction of Cu(II) reduced was *roughly estimated* by analyses of the UV/vis plots relative to the area in the spectra associated with Cu(I) and Cu(II) species[6]. When comparing the conditions where the AIBN concentration was varied and regeneration time was kept constant at 15 minutes,

Table 7.3 Results of catalyst regeneration optimization of Cabosil-CuBr/SdMBpy catalysts.

Condition[1]	% Reduced[2]	Conversion[3] (1 hr)	Conv. (final)	$M_{n,Th}$	$M_{n,Ex}$	PDI
First Use	---	40	73	7300	10000	1.31
0.5:1 15 mins	13	10	33	3300	4800	1.28
1:1 15 mins	33	18	44	4400	6200	1.24
1:1 30 mins	52	19	48	4800	7300	1.27
1:1 60 mins	61	20	52	5200	7700	1.36
1:1 90 mins	42	17	46	4600	6900	1.32
2:1 15 mins	54	21	56	5600	7500	1.40
2:1 30 mins	38	18	44	4400	6800	1.35

1. Regeneration conditions were AIBN:Cu molar ratio for X minutes
2. % Cu(II) reduced to Cu(I) estimated by gravimetric analysis of UV/vis plots
3. Conversion determined by GC

[MMA]/[Cu]/[BPN] = 100/1/1 in 25% MMA in toluene at 90º for 24 hours.

[6] Although our UV/vis spectra are not strictly quantitative, it was possible to estimate the amount of Cu(II) that was reduced back to Cu(I) via analysis of the spectra after normalization of the heights of the high energy peaks associated with the Bpy ligand. Note – this analysis is semi-quantitative and is primarily carried out to establish a trend, not the exact amounts of Cu(I) and Cu(II) on the surface. Quantitative analysis of paramagnetic Cu(II) species on the catalyst via SQUID magnetometry proved troublesome with our low copper loadings. X-ray photoelectron spectroscopy was ruled out as a quantification method as Cu(II) species on the catalyst surface are reduced *in situ* to Cu(I) during the measurement [24, 25].

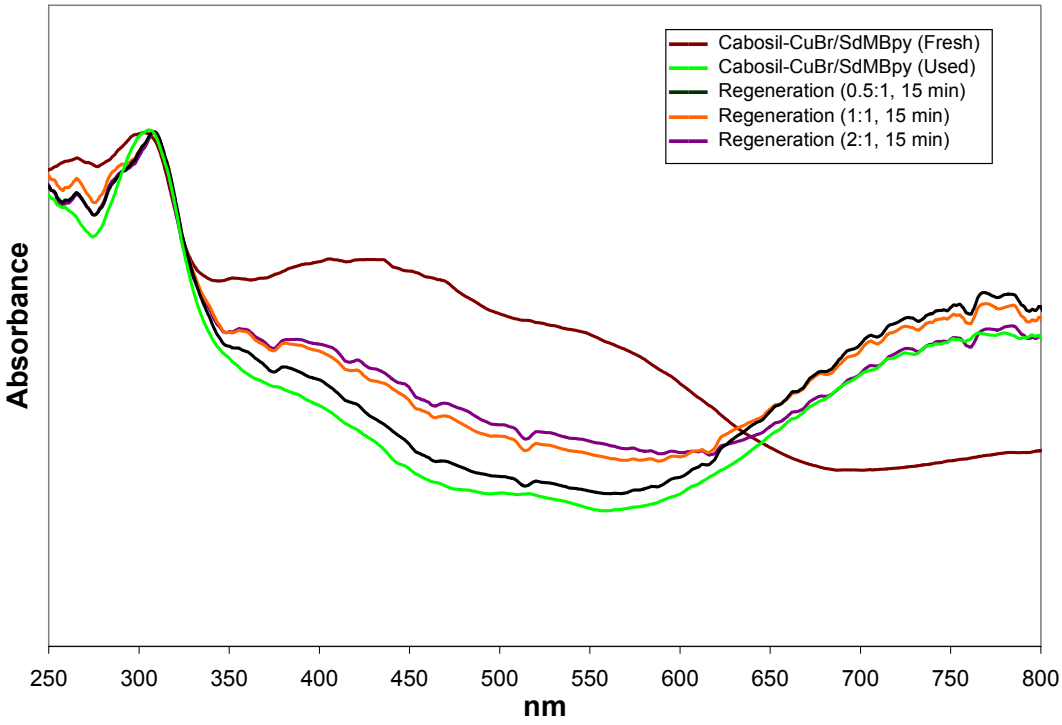

Figure 7.10 UV/vis comparison (vs. PTFE) of regenerated catalyst of varying treatments of AIBN concentrations. Regeneration conditions: [AIBN]/[Cu] = 0.5, 1, or 2 in 4 mL of toluene at 90 °C for 15 minutes. Polymerization conditions: [MMA]/[Cu]/[BPN] = 100/1/1 in 25% by v/v MMA in toluene at 90 °C.

the highest increase in Cu(I) concentration was when 2 equivalents of AIBN was used (~54% reduced). **Figure 7.10** shows the UV/vis spectra for each regenerated catalyst when the AIBN concentration was varied. The polymerization rates correlated with the estimated % reduced values determined by UV/vis, as the highest conversion observed in polymerizations with the regenerated catalysts after 1 and 24 hours was also for 2 equivalents of AIBN. Next the AIBN concentration was held constant and the regeneration time was varied from 15 – 90 minutes (1:1 AIBN:Cu). **Figure 7.11** shows the UV/vis spectra for each regenerated catalyst when the regeneration time was varied. The absorbance intensity of the Cu(I) transition was highest at 60 minutes and decreased

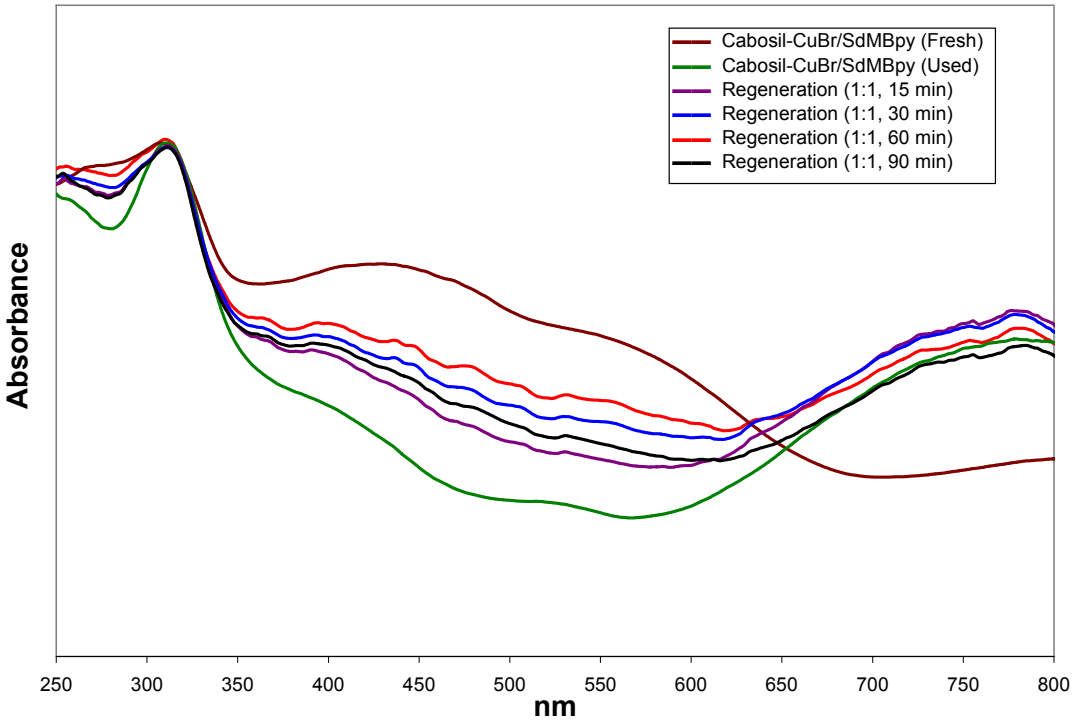

Figure 7.11 UV/vis comparison (vs. PTFE) of regenerated catalyst of varying treatment times. Regeneration conditions: [AIBN]/[Cu] = 1 in 4 mL of toluene at 90 °C for 15, 30, 60, and 90 minutes. Polymerization conditions: [MMA]/[Cu]/[BPN] = 100/1/1 in 25% by v/v MMA in toluene at 90 °C.

to a lower intensity after 90 minutes (~61% and ~42% reduced, respectively). The highest conversion in polymerizations with regenerated catalysts was achieved after 24 hours with the catalyst regenerated under the following conditions: [AIBN]/[Cu] = 2 for 15 minutes. Complete reduction of the immobilized Cu(II) back to Cu(I) was never achieved, as there always was a remaining Cu(II) transition above 600 nm. This is not altogether a problem, however, as the initial presence of Cu(II) has been shown to help better control the polymerization at earlier reaction times [3]. Although this UV/vis study is only semi-quantitative, its utility is clear based on an analysis of **Figure 7.12**. The data

in **Figure 7.12** indicate that the fraction of Cu(I) that was reduced to Cu(II) as estimated from the spectra correlates well with the conversion of monomer after 1 hour. Thus, this analysis can suggest conditions that would be best for catalyst regeneration if high rates are desired, with the suggested conditions being a 1:1 AIBN:Cu ratio for 60 minutes.

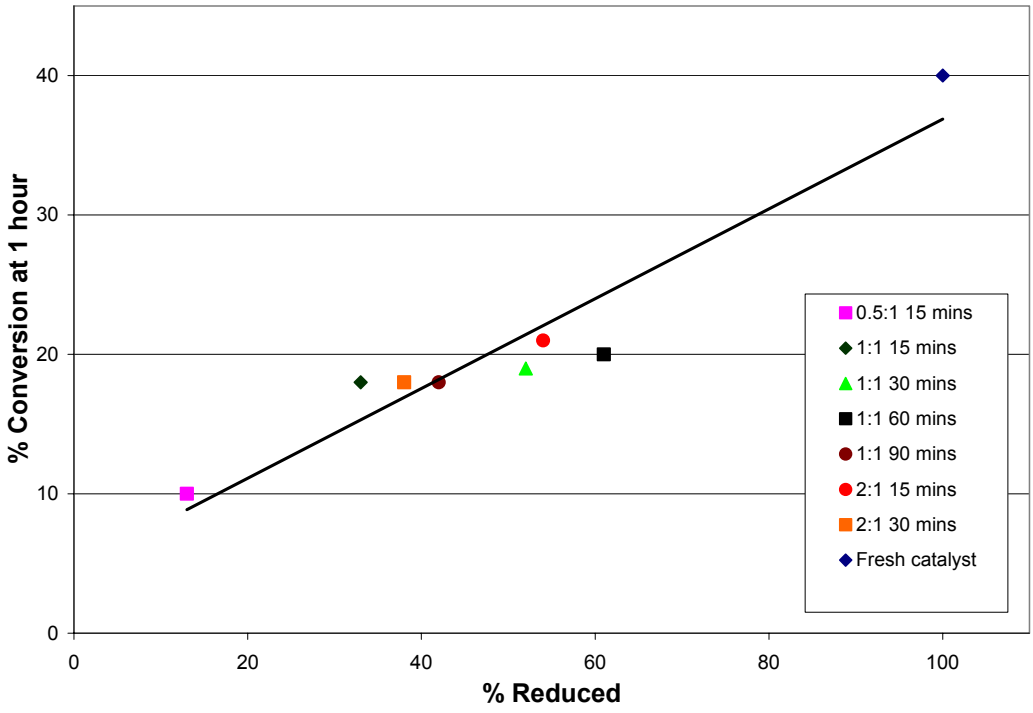

Figure 7.12 Plot of % Conversion at 1 hour vs. % Reduced plot for regenerated catalysts. Polymerization conditions: [MMA]/[Cu]/[BPN] = 100/1/1 in 25% by v/v MMA in toluene at 90 °C for 24 hours.

Nature of the catalyst active site

There has been some speculation on the nature and location of catalyst active site in the literature because the supported catalyst loses significant activity after recycling and in some cases the ability to mediate a controlled polymerization [2-4, 7, 15-17]. As noted earlier, essentially two potential reasons have been discussed in the literature to explain this loss of activity: 1) accumulation of Cu(II) on the catalyst surface after the polymerization and 2) a loss of immobilized catalyst due to leaching. In Matyjaszewski's polymer-immobilized CuBr/dMBpy system (PS8-dMBpy/CuBr), the catalyst could not effectively mediate a controlled polymerization as an all heterogeneous system [7, 8]. However, when the soluble $CuBr_2$/Me_6TREN deactivator complex was introduced, even in very small amounts (0.3 mol% deactivator to immobilized copper), the polymerization became controlled. Matyjaszewski surmised that the single component, all CuBr/dMBpy immobilized catalyst could not mediate a controlled polymerization because of poor mass transport processes around the support that led to a slow deactivation rate for the growing polymer chains. In support of this hypothesis, Brittain showed that a less cross-linked polymer support was better for the solubility of catalyst particle [18]. When Matyjaszewski's immobilized/soluble hybrid catalyst system was used, the effective shuttling of the halogen from the polymer immobilized **Br**-CuBr/dMBpy (Cu(II)) complex to the growing polymer chain radical ($\mathbf{P_n^{\bullet}}$) was accomplished (deactivating the polymer chain, $\mathbf{P_n}$-**Br**).[7] The importance of the soluble deactivator suggests that polymerization control occurs both in the liquid phase and on the catalyst surface (polymerization is not entirely heterogeneous). After catalyst regeneration with Cu(0),

[7] For a complete discussion on mass transport and deactivation processes in ATRP please refer to work reported by Matyjaszewski and coworkers [7, 8] and a review written by Shen [17].

the catalyst activity and ability to control the polymerization decreased (conversion decreased, PDI increased: 1^{st} = 95%, 1.34; 2^{nd} = 90%, 1.41; 3^{rd} = 70%, 1.58) [7]. A reduction of copper and ligand content per gram of catalyst was also reported, but the "loss" was likely due to growth of grafted polymer on the support and entangled polymer around the support adding to overall weight of the catalyst. Accumulation of Cu(II) is a more likely cause for the loss in activity. From my results on catalyst regeneration and UV/vis characterization, it is possible that with most regeneration procedures, only some of the Cu(II) species are reduced back to Cu(I). Therefore, the presence of Cu(II) will decrease the polymerization rate. Thus, with covalently *tethered* catalysts systems, it appears that residual Cu(II), even after regeneration, is at least partly responsible for reduced polymerization rates of the catalysts upon recycle. Copper loss appears to be less of an issue.

Zhu and coworkers recently reported ongoing work discussing the potential location of the catalytic sites for immobilized ATRP catalyst (in solution as soluble species or on the support), in particular the location of the catalytic site for *physisorbed* hexamethyltriethyltetraamine (HMTETA) /CuBr on silica [4]. Zhu found after removal of the solid catalyst by a hot filtration, reaction in the solid-free polymerization solution continued from 20 – 90 % conversion and effective control was maintained without the solid catalyst. This indicates that the location of the important catalytic sites (and therefore the location of the polymerization activation and deactivation process) was in the homogeneous liquid phase. Zhu indicates that the physisorbed HMTETA/CuBr on silica acts as a catalyst reservoir, partitioning significant quantities of complex into solution and the homogeneous complex mediates the polymerization. Unfortunately,

analysis for copper in the final polymerization solution was not performed to quantify extent of leaching. Even if a relatively small amount of catalyst leached from the surface in this case, it still may be possible to continue to polymerize effectively. This is due to the nature of the catalyst ligand. Copper complexes based on multidentate amine ligands, like HMTETA, are known to possess high transfer rates and good control even at lower catalyst concentrations [19-21]. The fact that the polymerization continued in Zhu's case is therefore not surprising. Hence, generalizations about the location of the catalyst active site in other systems cannot be made based on results with HMTETA/CuBr/Silica physisorbed catalysts.

I recently reported two silica-immobilized ATRP catalyst systems [1-3]. The first a CuBr/2-Pyridylmethanimine (CuBr/PMI) complex immobilized on various silica supports. I found the catalyst allowed for high conversions and moderate control (PDI ~ 1.50) for the first use and it still maintained very good conversions and even better control (PDI ~ 1.25) *without* catalyst regeneration after recycling. Since the catalyst did not need to be regenerated for further recycle, this suggests that a higher concentration of immobilized Cu(I) was maintained after the polymerization. Klumperman et al. showed that PMI ligands have a tendency to stabilize the Cu(I) oxidation state and Bpy derivatives stabilize Cu(II) oxidation states [5]. This explains the observation that CuBr/Bpy immobilized catalysts need to be regenerated and CuBr/PMI catalysts do not for effective recycling. In the CuBr/PMI case, even though I found that ligand and copper leached away from the catalyst support during each catalyst use (in each of the 6 recycles), sufficient activity was maintained to reach high conversions as well as produce polymers with narrow polydispersities. Since substantial leaching was evident for the

CuBr/PMI system, in this work, I performed a leaching test to determine if soluble species could be responsible for all the activation and deactivation steps in the ATRP cycle. An air-free swivel frit was used to filter the catalyst particle from the hot polymerization solution under a rigorously dioxygen-free argon atmosphere [22]. After the catalyst was removed, the monomer conversion only slightly increased from 8 to 16%, indicating the solid represents an important component of the catalyst system. The resulting final polymer had very broad molecular weight distribution (>2), considerably higher than when the solid catalyst is left in the polymerization solution (as low as 1.20) [2]. The low conversions and increased PDI suggests the immobilized PMI catalyst is necessary to maintain activity and control of the polymerization.

Unlike Matyjaszewski's immobilized/soluble hybrid catalyst system, my silica-immobilized CuBr/SdMBpy catalyst could effectively control the polymerization of MMA without addition of a soluble deactivator, although with lower conversions reported. This catalyst system was better than my reported CuBr/PMI system because the Bpy ligand on the surface was found to be stable, as indicated by the colorless solution of the recovered polymerization liquid, the low PDIs achieved without a catalyst pretreatment, and trace or zero copper leaching. However, since trace amounts of leached copper were found in the polymer [3], one could not rule out the possibility that the leached copper species were critically important in facilitating the deactivation processes in the liquid phase. Matyjaszewski showed the addition of soluble $CuBr_2$/dMBpy as a deactivator was ineffective compared to $CuBr_2$/Me_6TREN, therefore

it is unlikely leached $CuBr_2$/Bpy species are critical in the deactivation process for my immobilized catalyst system [7]. Nonetheless, to test if leached species are important, a leaching test was performed for Cabosil-CuBr/SdMBpy. The results of the leaching test are summarized in **Table 7.4**. The polymerization mixture was charged in the air-free swivel frit [22] and after the catalyst particles were removed the polymerization only continued from 16 to 26% and the PDI increased from 1.60 to 1.91. The reaction rate dramatically decreased and the molecular weight distribution broadened indicating that the immobilized catalytic species are critical for maintaining activity and achieving good polymerization control. Indeed, copper microanalyses of the recovered polymerization solution showed that no detectable leaching had occurred (< 1 ppm copper).

Table 7.4 Results of leaching experiments Cabosil immobilized CuBr/Bpy catalysts.

Catalyst	Time (min)	% Conversion	$M_{n, Ex}$	PDI	R_{Cu}
Cabosil-CuBr/SdMBpy	15	16	3100	1.60	---
Cabosil-CuBr/SdMBpy	1440	26	4200	1.91	<1
Cabosil(CuBr/dMBpy)	15	17	4900	1.38	---
Cabosil(CuBr/dMBpy)	1440	23	5200	1.31	12

Polymerization conditions: [MMA]/[Cu]/[BPN] = 100/1/1 in 25% MMA in toluene at 90º.

Finally, the leaching test was also performed on the physisorbed Cabosil(CuBr/dMBpy) catalyst. In this case, the conversion increase was low (17 to 23%), but the PDI decreased from 1.38 to 1.31. Observations after the polymerization showed leached CuBr/dMBpy accumulated on the flask wall, indicating that substantial leaching occurred. Thus, in this physisorbed system, leached metal species are present in high enough concentration to control the polymerization, although polymerization rates in the presence of only soluble copper were very low.

Thus, control in the tethered Cabosil-CuBr/dMBpy system is derived from reactions associated with immobilized metal complexes. In the tethered CuBr-PMI systems previously reported [2], leached species exist in solution but these are not present in high enough concentration to mediate a controlled polymerization; thus, tethered active species are also important in this system. In the physisorbed Cabosil(CuBr/dMBpy) system, substantial leached species are observed and these are capable of mediating a controlled polymerization, although with extremely low rates. These results imply that the physisorbed $CuBr_n$/Bpy species may not play a key role in controlling the reaction due to poor local solvation.

Summary

Immobilized Cu(I) complexes represent a rare example of a recoverable and recyclable polymerization catalyst. Here, CuBr/dMBpy complexes were immobilized via a covalent tether and via physisorption on nonporous Cab-O-Sil silica supports. The catalysts mediated the controlled polymerization of MMA for low target molecular weights, with PDIs nearly approaching that of the homogeneous catalyst. Both catalysts allowed for recovery of most of the CuBr species, although the physisorbed catalyst leached significant amounts of soluble copper species into solution. In contrast, the tethered system resulted in no detectable leached copper species.

A unique catalyst regeneration method I previously reported was applied to both types of catalyst. Treatment with AIBN effectively reduced some of the copper species from Cu(II) to Cu(I) in the tethered system, with the regeneration process easily monitored by UV/vis spectroscopic analysis of the catalysts. In contrast, the physisorbed catalyst could not be regenerated under the conditions of this study. The fraction of Cu(II) reduced back to Cu(I) as estimated by UV/vis spectroscopy correlated well with the initial polymerization performance of the regenerated systems.

Leaching studies indicate that the soluble copper released from the physisorbed system is capable of mediating a controlled polymerization, even in the absence of the solid catalyst, although reaction rates were low. In contrast, the tethered system did not leach measurable amounts of copper and the silica-supported CuBr species were responsible for mediating a controlled polymerization.

Finally, a one-pot polymerization technique, where bare silica was added to a homogeneous polymerization, could be used to trap most of the homogeneous CuBr/dMBpy catalyst, allowing recovery of most of the copper species from solution. The one-pot system behaved similarly to the physisorbed catalyst, and was overall inferior to the tethered system.

Experimental Section

Characterization

Silica pore diameters and surface areas were determined using dinitrogen physisorption data obtained with a Micromeritics ASAP 2000 system. The surface areas were analyzed by the BET method and the pore size distribution was determined using the BJH method applied to the adsorption branch of the isotherm. ^{1}H NMR (300 MHz) spectra were determined on a Mercury VX instrument. A Netzsch Thermoanalyzer STA409 was used for simultaneous thermal analysis combining thermogravimetric analysis (TGA) and differential scanning calorimetry (DSC) with a heating rate of 20 ºC/min in 30 mL/min air flow. Diffuse-reflectance ultraviolet-visible (UV/vis) spectroscopy was performed on solid materials in a dry glovebox with an Ocean Optics USB2000 fiber optic spectrometer using a PTFE diffuse reflectance standard. Copper and silicon elemental analyses were performed by Galbraith Laboratories, Inc, Knoxville, TN or Chemisar Laboratories, Guelph, Canada, using ICP-AES. Carbon, hydrogen, and nitrogen contents were determined via CHN analysis by Galbraith Laboratories, Inc, Knoxville, TN. Gas chromatographic analyses were performed on a Shimadzu GC 14-A gas chromatograph equipped with a flame ionization detector and an HP-5 column (length = 30 m, inner diameter = 0.25 mm, and film thickness = 0.25 μm). The temperature program for GC analysis was: heating from 50 °C to 140 °C at 30 K/min and from 140 to 300 °C at 40 K/min under constant pressure with inlet and detector temperatures set constant at 330 °C. The molecular weight and molecular weight distributions were determined by gel permeation chromatography (GPC) using American

Polymer Standards columns (10^5, 10^3, 10^2 Å) equipped with Waters 510 pump and a Waters 410 differential refractometer. THF was used as an eluent at the flow rate of 1 mL/min. Nine linear PMMA standards (700 – 2100K) were used for calibration of methyl methacrylate polymers.

Chemicals

2-Bromoproprionitrile (BPN; Aldrich; 97%) was dried over 4 Å molecular sieves and stored under dry nitrogen. Copper (II) bromide ($CuBr_2$; Aldrich; 99%), 4,4'-dimethyl-2,2'-dipyridyl (dMBpy; Aldrich; 99%), and 2,2'-Azobis(2-methylpropionitrile) (AIBN; Aldrich; 99%) were used as received and stored under dry nitrogen. Copper (I) bromide (CuBr; Acros; 98%) was purified by stirring in glacial acetic acid for 5 hrs, washed with absolute ethanol and anhydrous diethyl ether, dried under vacuum for 12 hrs at room temperature, and stored under dry nitrogen. Methyl methacrylate (MMA; Aldrich; 99%) was passed three times through an inhibitor removal column (Aldrich-311332), distilled once under reduced pressure, degassed by three freeze/pump/thaw cycles and stored under dry nitrogen at -22 °C. Toluene for polymerization (Acros; 99.8%) was distilled under reduced pressure over sodium/benzophenone, degassed by three freeze/thaw cycles and stored under dry nitrogen. 2-Bromopropionitrile was stored in a 0.46 M stock solution in dry toluene under dry nitrogen. Tetrahydrofuran (Aldrich, HPLC grade inhibitor-free, >99%) was used as received for the eluent in GPC analysis. Cabosil EH5 (Cabot) was dried under vacuum for 12 hrs at 200 ºC and stored under dry nitrogen. Cabosil is a fumed, nonporous silica with multiparticle aggregates having a length of 0.2-0.3 micron (individual particles have nanosized features), a surface area of

335 m^2/g, and 2.7 mmol-OH g-solid^{-1} determined by dinitrogen physisorption and TGA analyses, respectively. Hexanes (Aldrich; >99%), methylene chloride (CH_2Cl_2; Aldrich; >99%), and tetrahydrofuran (THF; Aldrich; >99%) were dried and deoxygenated using a purification system and stored under dry nitrogen [23]. 4'-{4-[3-(Trimethoxy-silanyl)-propylsulfanyl]-butyl}-4-methyl-[2,2']bipyridinyl, (SdMBpyTMS) was synthesized following literature methods [3]. Powders of CuBr/dMBpy and $CuBr_2$/dMBpy complexes used for UV/vis spectroscopy were formed by mixing the ligand to metal (2:1 ratio) in THF. The complexes were recovered by filtration and dried under vacuum for analysis. All reactions and polymerizations were carried out under a dry nitrogen/argon atmosphere in a MBraun UniLab 2000 drybox and/or using standard Schlenk line techniques.

Syntheses

Preparation of (Cabosil(CuBr/dMBpy) physisorbed catalyst

To a 100 mL bottom flask, a solution 1.00 g of dMBpy (5.45 mmol) and 5 mL of dry toluene was slowly added to a stirring mixture of 0.391 g of CuBr (2.73 mmol) in 50 mL of dry toluene at 70 ºC in a nitrogen glovebox. The resulting light brown mixture was then stirred at 70 °C for 30 minutes under nitrogen or until the reaction mixture appears to be a dark reddish brown homogeneous solution. Then the mixture was added to a 250 mL flask containing 3.00 g of Cab-O-Sil EH5 and 100 mL of dry toluene, sealed with a valve, and removed from the nitrogen glovebox. Then the reaction mixture was stirred at 110 °C for 48 hrs under argon. The reaction flask was transferred into the nitrogen glovebox after three freeze/pump/thaw cycles and the solid product was

recovered and washed, once with 100 mL of dry toluene and once with copious amounts of dry hexanes until the solvent filtered out was clear. The dark reddish brown powder was dried under vacuum at room temperature for 12 hrs and stored under dry nitrogen in a glovebox. CHN, Si, and Cu analyses showed 0.92 mmol dMBpy g-catalyst^{-1} and 0.53 mmol Cu g-catalyst^{-1}.

Preparation of Cabosil-CuBr/dMBpy covalently immobilized catalyst

Catalyst preparation was followed from literature procedures [3]. To a 100 mL flask, 1.00 g of SdMBpyTMS (2.37 mmol) and 5 mL of dry toluene was slowly added to a stirring mixture of 0.17 g of CuBr (1.19 mmol) in 50 mL of dry toluene at 70 ºC in a nitrogen glovebox. The resulting light brown mixture was then stirred at 70 °C for 30 minutes under nitrogen or until the reaction mixture appears to be a dark reddish brown homogeneous solution. Then the mixture was added to a 250 mL flask containing 2.00 g of Cab-O-Sil EH5 and 100 mL of dry toluene, sealed with a valve, and removed from the nitrogen glovebox. Then the reaction mixture was stirred at 110 °C for 48 hrs under argon. The reaction flask was transferred into the nitrogen glovebox after three freeze/pump/thaw cycles and the solid product was recovered and washed, once with 100 mL of dry toluene, once with 100 mL of dry hexanes, and once with copious amount of dry dichloromethane until the solvent filtered out was clear. The dark reddish brown powder was dried under vacuum at room temperature for 12 hrs and stored under dry nitrogen in a glovebox. CHN, Si, and Cu analyses showed 0.46 mmol SdMBpy g-catalyst^{-1} and 0.34 mmol Cu g-catalyst^{-1}.

Experimental methods

Homogeneous Polymerization

For homogeneous polymerization of MMA with CuBr/dMBpy, the following conditions were typical: [MMA]/[dMBpy]/[Cu]/[BPN] = X/2/1/1 in Y% by v/v MMA in toluene (X = 300, Y = 50 or X = 100, Y = 25). For example, (X = 100, Y = 25 in toluene) to a 10 mL flask with a sidearm valve, 0.94 g of MMA (9.42 mmol, 1 mL), 34.7 mg of dMBpy (0.188 mmol), 13.5 g of CuBr (0.094 mmol), and 204 μL of BPN initiator stock solution (0.094 mmol) were added in 2.60 g of toluene (3 mL) under nitrogen. The polymerization vessel was immersed in an oil bath preset to 90 °C. At set time intervals, 0.1 mL aliquots of polymerization solution were removed via syringe and placed in a vial. The vials were immediately quenched in a dry ice/acetone bath. Subsequently, 25 μl of sample was added to 1.5 mL acetone for GC analysis to monitor MMA conversion. The remaining sample was dried, re-dissolved in HPLC grade THF to 8.0 mg/mL, and filtered through a Gelman Acrodisc PTFE filter (0.2 μm) for GPC analysis to determine polymer molecular weight and molecular weight distribution. After the polymerization, the catalyst was recovered from the remaining polymerization solution by centrifugation. The polymerization solutions were analyzed for trace amounts of copper.

Polymerization with physisorbed CuBr/Bpy catalyst on Cabosil

For heterogeneous polymerization of MMA using CuBr/Bpy physisorbed on silica, the following conditions were typical: [MMA]/[Cu]/[BPN] = X/1/1 in Y% by v/v MMA in toluene at 90 ºC (X = 300, Y = 50 or X = 100, Y = 25). For instance, (X = 100, Y = 25) to a 10 mL Schlenk tube with a sidearm valve, 0.15 g of Cabosil-CuBr/SdMBpy

(5.00×10^{-2} mmol of Cu, 0.34 mmol Cu/g-catalyst), 0.48 g of MMA (5.00 mmol), and 97 μL of initiator stock solution BPN (5.00×10^{-2} mmol) were added to 1.25 g of toluene under nitrogen. The polymerization vessel was immersed in an oil bath preset to 90 °C. Samples were taken at preset times and quenched using the procedure described above. Kinetic analysis and polymer characterization were carried out in a similar manner described for the homogeneous polymerization. After the polymerization, the catalyst was recovered from the remaining polymerization solution by centrifugation. The polymerization solutions were analyzed for trace amounts of copper. Cabosil-CuBr/SdMBpy catalyst was washed with copious amounts of dry DCM and Cabosil(CuBr/dMBpy) was washed with copious amounts of dry toluene. The catalysts were vacuum dried and stored under nitrogen for further characterization and reuse.

One-pot polymerization with CuBr/dMBpy and Cabosil

For one-pot polymerization of MMA with CuBr/dMBpy and Cabosil, the following condition was typical: [MMA]/[dMBpy]/[Cu]/[BPN] = X/2/1/1 in Y% by v/v MMA in toluene and 0.10 g of Cabosil (X = 300, Y = 50 or X = 100, Y = 25). For example, (X = 100, Y = 25 in toluene) to a 10 mL flask with a sidearm valve, 0.94 g of MMA (9.42 mmol, 1 mL), 34.7 mg of dMBpy (0.188 mmol), 13.5 g of CuBr (0.094 mmol), 0.10 g of Cabosil, and 204 μL of BPN initiator stock solution (0.094 mmol) were added in 2.60 g of toluene (3 mL) under nitrogen. The polymerization vessel was immersed in an oil bath preset to 90 °C. Samples were taken at preset times and quenched using the procedure described above. Kinetic analysis and polymer characterization were carried out in a similar manner described for the homogeneous

polymerization. After the polymerization, the catalyst was recovered from the remaining polymerization solution by centrifugation. The polymerization solutions were analyzed for trace amounts of copper.

Catalyst regeneration

The spent immobilized Cabosil-CuBr/SdMBpy or Cabosil(CuBr/dMBpy) catalyst was regenerated with AIBN using my literature procedure [3]. The used catalysts were recovered from the polymerization solution by centrifugation and washed with copious amounts of DCM and then toluene. The catalyst was transferred into a vial (i.e. 0.15 g of Cabosil-CuBr/SdMBpy, 0.050 mmol of Cu). Then 3.00 g of toluene and an equivalent of AIBN to Cu (0.050 mmol or 9 mg of AIBN) were added to the vial. The sealed vial was placed into a preheated oil bath at 90 ºC. The mixture was stirred for a predetermined time. The catalyst was the recovered by filtration and washed with copious amounts of toluene and dichloromethane. The catalyst was dried under vacuum for 12 hrs and stored under dry nitrogen in a glovebox for further characterization and reuse. (Note – physisorbed catalysts were only washed with toluene.)

Catalyst recycling

Regenerated catalyst was recycled by adding a fresh charge of monomer, solvent, and initiator. For example, the following condition was typical: [MMA]/[Cu]/[BPN] = 100/1/1 in 25 % by v/v MMA in toluene at 90 ºC. To a 10 mL Schlenk tube with a sidearm valve, 0.15 g of Cabosil-CuBr/SdMBpy (5.00×10^{-2} mmol of Cu, 0.335 mmol Cu/g-catalyst), 0.48 g of MMA (5.00 mmol), and 97 μL of initiator stock solution BPN

(5.00×10^{-2} mmol) were added to 1.25 g of toluene under nitrogen. The polymerization vessel was immersed in an oil bath preset to 90 °C. MMA conversion and polymer characterization were carried out in a similar manner described for homogeneous polymerizations.

Evaluation of catalyst leaching

An air-free swivel medium frit filter was used to hot filter the catalyst to test for catalyst leaching [22]. For example, the following condition was typical: [MMA]/[Cu]/[BPN] = 100/1/1 in 25 % by v/v MMA in toluene at 90 ºC. To a 10 mL Schlenk tube with a sidearm valve, 0.30 g of Cabosil-CuBr/SdMBpy (10.00×10^{-2} mmol of Cu, 0.335 mmol Cu/g-catalyst), 0.96 g of MMA (10.00 mmol), and 195 μL of initiator stock solution BPN (10.00×10^{-2} mmol) were added to 2.50 g of toluene under nitrogen and then the 10 mL flask was attached to one end of the swivel frit. An empty 15 mL receiving flask with stir bar was attached to the other end. The complete apparatus was sealed and attached to the Schlenk line. The flask with polymerization mixture in was then immersed in a 90 ºC oil bath. At 15 minutes the oil bath was removed and a 0.2 mL sample was taken through the side arm under positive argon pressure. The swivel frit apparatus was then rotated 180º and the polymerization solution was filtered through the frit with a partial static vacuum to remove the Cabosil-CuBr/SdMBpy catalyst and collected into the 15 mL receiving flask. The oil bath was returned and the polymerization solution continued to react for 24 hours. The final polymerization solution was then analyzed for conversion, molecular weight, polydispersity, and residual copper content.

References

[1] J. V. Nguyen and C. W. Jones, Journal of Polymer Science, Part A: Polymer Chemistry 42 (2004) 1367.

[2] J. V. Nguyen and C. W. Jones, Journal of Polymer Science, Part A: Polymer Chemistry 42 (2004) 1384.

[3] J. V. Nguyen and C. W. Jones, Macromolecules 37 (2004) 1190.

[4] S. Faucher and S. Zhu, Macromolecular Rapid Communications 25 (2004) 991.

[5] B. Klumperman and G. Chambard, Polymer Preprints 40 (1999) 329.

[6] Y. Shen, S. Zhu, F. Zeng, and R. Pelton, Journal of Polymer Science, Part A: Polymer Chemistry 39 (2001) 1051.

[7] S. C. Hong and K. Matyjaszewski, Macromolecules 35 (2002) 7592.

[8] S. C. Hong, H.-J. Paik, and K. Matyjaszewski, Macromolecules 34 (2001) 5099.

[9] J. M. Lehn, A. Rigault, J. Siegel, J. Harrowfield, B. Chevrier, and D. Moras, Proceedings of the National Academy of Sciences 84 (1987) 2565.

[10] C. D. Eisenbach and U. S. Schubert, Macromolecules 26 (1993) 7372.

[11] U. S. Schubert and C. D. Eisenbach, Polymer Preprints 40 (1999) 222.

[12] U. S. Schubert and G. Hochwimmer, Macromolecular Rapid Communications 22 (2001) 274.

[13] M. T. Miller, P. K. Gantzel, and T. B. Karpishin, Inorganic Chemistry (1998) 2285.

[14] Y. Shen, S. Zhu, and R. Pelton, Macromolecules 34 (2001) 5812.

[15] S. Ding, J. Yang, M. Radosz, and Y. Shen, Journal of Polymer Science, Part A: Polymer Chemistry 42 (2003) 22.

[16] J. Yang, S. Ding, M. Radosz, and Y. Shen, Macromolecules 37 (2004) 1728.

[17] Y. Shen, H. Tang, and S. Ding, Progress in Polymer Science 29 (2004) 1053.

[18] M. E. Honigfort and W. J. Brittain, Macromolecules 36 (2003) 3111.

[19] J. Queffelec, S. G. Gaynor, and K. Matyjaszewski, Macromolecules 33 (2000) 8629.

[20] Y. Inoue and K. Matyjaszewski, Macromolecules 37 (2004) 4014.

[21] J. Gromada, J. Spanswick, and K. Matyjaszewski, Macromolecular Chemistry and Physics 205 (2004) 551.

[22] B. J. Burger and J. E. Bercaw, ACS Symposium Series 357 (1987) 79.

[23] A. B. Pangborn, M. A. Giardello, R. H. Grubbs, R. K. Rosen, and F. J. Timmers, Organometallics 15 (1996) 1518.

CHAPTER 8

CONCLUSIONS AND IMPACT

Conclusions

The objective of this work was to develop the science and engineering of immobilized Atom Transfer Radical Polymerization catalysts. The development and knowledge gained from this work will hopefully lead to the eventual technological development of ATRP in commercial practices. In developing ATRP, I have chosen to study two catalyst systems and take them through the catalyst design process by applying the ideas of an "ideal" catalyst. I chose to immobilize Haddleton's CuBr/pyridylmethanimine complex [1-3] and Matyjaszewski's benchmark CuBr/bipyridine complex [4-6]. The process began with identifying and designing different immobilization strategies that would potentially lead to heterogenized homogeneous ATRP catalysts. Next, the synthesis and characterization of the catalyst materials were performed and then tested for the polymerization of methyl methacrylate. Then I identified which system performed the best in terms of polymerization performance (conversion and control), stability, and recyclability and optimized the polymerization and catalyst regeneration conditions for the chosen systems.

The accomplishments shown in this thesis included the first comprehensive study attempting to elucidate the role of synthetic methods and support structures on the immobilization of CuBr/PMI complexes for the controlled ATRP of MMA [7, 8]. Four synthetic routes were identified for immobilizing CuBr/PMI complexes and through extensive analytical and spectroscopic characterization I found that the pre-assembled

complex approach (M4) resulted in the most homogeneous material; however not all unwanted surface species were eliminated [7]. The pre-assembled complex approach was a significant advancement for immobilized CuBr/PMI complexes because the prior art involved multiple grafting steps, instead of a single step to achieve the immobilized complex. From my findings, multi-step grafting approaches yielded materials having a higher degree of surface heterogeneity compared to those that required less synthetic steps. It should be mentioned that less efficient grafting reactions (high conversion and selectivity towards desired reaction), compared to aminoimine forming reactions, would likely lead to a more heterogeneous surfaces for silica-supported catalysts. When I tested these catalysts for the polymerization of MMA, I found that synthetic methodology did not have any affect on polymerization performance on catalysts supported non-porous Cabosil EH5, but did impact the performance of mesoporous SBA15 immobilized catalysts [8]. The smaller pore size and isolated pores of the chosen SBA15 supports ultimately contributed to the poor polymerization performance. I later tested a silica support that possessed a higher pore diameter and interconnecting pore channels for silica-immobilized CuBr/Bpy complexes [9]. Although I was able to recycle PMI-based catalysts up to six cycles with each cycle giving a better performance than the first catalyst use (improved PDI), catalyst leaching was observed. Even though catalyst leaching was not significant enough to cause complete catalyst deactivation and decomposition, parallel investigations found that silica-immobilized CuBr/Bpy catalysts performed better in all aspects of polymerization control and catalyst stability [9].

Even though Matyjaszewski had already developed a well-behaved dual catalyst system utilizing polymer-supported CuBr/Bpy complexes and soluble $Me_6TREN/CuBr_2$

deactivator complexes [10, 11], significant improvements and variations could be made involving less expensive silica supported systems. In my opinion, improvements in synthetic immobilization methodology for CuBr/Bpy complexes and support selection should eliminate the need for addition of soluble metal deactivators. My attempts to avoid the previously reported inefficient multi-step grafting method for silica-immobilized metal/Bpy complexes lead to the first silica immobilizable asymmetric bipyridine ligand containing an alkoxysilane functionality, [3-(trimethyoxy-silanyl)-propylsulfanyl]-butyl}-4'-methyl-[2,2']bipyridyl or SdMBpyTMS [9]. Applying the knowledge gained from my investigation of silica-immobilized CuBr/PMI complexes [7, 8], I utilized SdMBpyTMS for the pre-assembled complex approach resulting in the first one-step procedure to immobilizing covalently tethered CuBr/Bpy complexes on silica supports. A battery of characterization techniques revealed an immobilized surface consisting of covalently immobilized mono and bis-coordinated CuBr/Bpys and uncoordinated Bpys, and in some cases, excess CuBr likely ligated to surface silanols. Even though a completely uniform surface was not achieved, it was still a significant improvement compared to previously reported works [12-15]. When I tested the catalyst for the polymerization of MMA, I found that tethered CuBr/Bpy complexes immobilized on CPG(240) and Cabosil EH5 silica supports performed similarly to homogeneous catalyst complex, CuBr/dMBpy, with the advantage of complete solid catalyst recovery from the polymerization solution and without the use of Matyjaszewski's soluble metal deactivator complex [9].

Although the silica-immobilized CuBr/Bpy catalyst could not be directly recycled like the CuBr/PMI system because the stabilization of Cu(II) deactivated catalyst species

in the Bpy system was higher, I developed a new regeneration procedure that did not involve the addition of new copper atoms to the catalyst [9]. A simple AIBN treatment of the used catalyst effectively reduced Cu(II) to Cu(I) resoling in a regenerated catalyst. When the catalyst was recycled, it possessed higher polymerization rates and better polymerization control than non-regenerated catalyst. Residual copper analyses suggest the CuBr/Bpy catalyst is more stable than the CuBr/PMI catalyst.

Our final studies investigated the importance of covalent tethering versus physisorption of CuBr/Bpy complexes [16]. In addition, the catalyst regeneration process was optimized to achieve the highest regenerated concentration of immobilized Cu(I) species. I found that surface tethering was important for removal of the entangled polymer from the recovered catalyst particle and was also necessary for catalyst regeneration. The covalent tether allowed the immobilized CuBr/Bpy complexes to be solvated in the polymerization and regeneration solution. On the other hand, physisorbed CuBr/Bpy catalyst were too tightly bound to the silica surface giving polymerizations with less control and preventing the catalyst from being effectively regenerated and recycled. Further spectroscopic characterization by diffuse reflectance UV/vis confirmed the immobilization of Cu(I)/Bpy species, but no structural knowledge of the catalyst geometry could be interpreted from the data. I also used UV/vis spectroscopy to monitor the regeneration process and found it to be an effective tool to correlate the fraction of Cu(II) sites reduced with the initial catalyst reactivity. To date, there have been no other reports characterizing the ATRP catalyst regeneration process [16].

To conclude, after identifying two catalyst systems for potential industrial utility, I completely redesigned the synthetic and immobilization strategy for these silica-

supported catalysts [7-9, 16]. In my opinion, the more promising system is the silica-immobilized CuBr/Bpy catalyst based on its ability to control the polymerization control, its catalyst stability, and its recyclability. While much work is still needed to improve the catalyst (i.e. increase catalyst loading and further improve regeneration process), a solid foundation has been established for other researchers to continue work in the area of silica-immobilized ATRP catalysts.

Impact

The impact of this work will contribute to the fundamental science and engineering of how Atom Transfer Radical Polymerization can be applied to commercial practices. Currently most large commodity high molecular weight polymers are produced by single use immobilized metallocene and Ziegler Natta catalysts [17]. Since ATRP catalysts are less efficient catalysts in terms of reactivity and turn over frequency and ATRP is commonly performed in solution, high molecular weight polymers on order of the metallocene and Ziegler Natta catalysts are not realistically achievable. Therefore the market niche for ATRP is markets that target low molecular polymers (< 30K MW). These markets include adhesives, lubricants, dispersants, coatings, surfactants, thermoplastic elastomers, gel additives as well as many electronic and biomedical applications [18-20]. For ATRP to be practiced in industry, the supported catalysts not only need to possess the characteristics of homogeneous ATRP catalysts (precise macromolecular control and ability to synthesize copolymers), but also need to be fully recoverable and recyclable. The catalysts that were developed in this thesis indeed meet the mentioned criteria [7-9, 16].

In addition, this work impacts the broader field of catalysis. Prior to the first report of immobilized ATRP catalysts, few examples of recyclable transition metal polymerization catalysts existed. I developed two solid supported recyclable polymerization catalysts and established (i) synthetic protocols, (ii) polymerization condition and procedures, and (iii) recovery, regeneration, and recycling techniques for

both systems [7-9, 16]. In addition, these copper based ligand complexes can potentially be used as catalyst for other reactions.

2,2'-Bipyridine is the most widely studied ligand over the past century [21]. A SciFinder Scholar search in February 2005 resulted in >24000 hits on the keyword bipyridine alone (**Figure 8.1**). The potential use of SdMBpyTMS as a scaffold for immobilized bipyridines or metal/bipyridine complexes on surfaces can be extended to these studies and applications. These SdMBpy-based materials can be used in fundamental studies (e.g., photoluminescent, catalysis, and coordination chemistry) and a variety of applications (e.g., catalysis, sensors, and adsorbents).

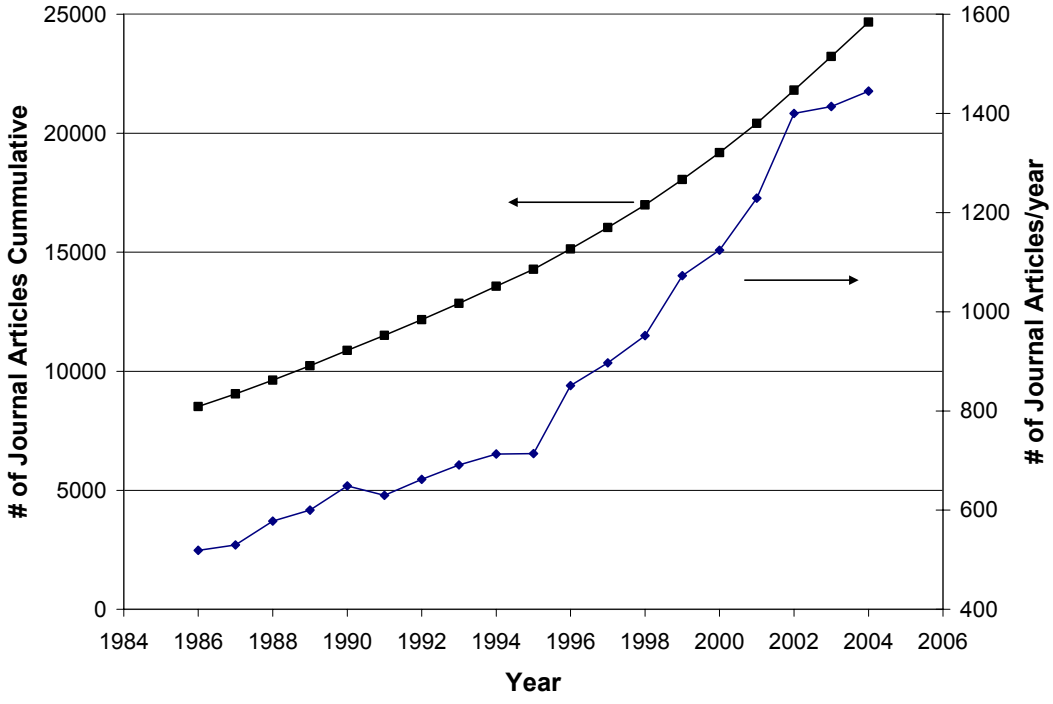

Figure 8.1 Plot for SciFinder Scholarsearch on bipyridine from 1986 – 2004 (February 2005).

The last chapter will first discuss suggested future work including potential improvements of the current silica-immobilized Cu/Bpy ATRP catalysts. Then some examples of metal/Bpy complexes that catalyze other reactions are noted. Finally, it is suggested how the SdMBpyTMS ligand can be used for other material applications.

Acknowledgements

The National Science Foundation is gratefully acknowledged for the partial support of this work (CTS-0210460). CWJ thanks the Shell Oil Company Foundation and Oak Ridge Associated Universities for partial support of this work through a Faculty Career Initiation Award and a Ralph Powe Junior Faculty Award, respectively. JVN thanks the Nanoscience and Technology Fellowship program for partial support of this work. I thank Dr. Angus Wilkinson for the use of the X-ray diffractometer and Dr. Johannes Liesen for advice with solid state NMR experiments.

JVN thanks the Jones research group for their help with my research and their entertainment when my research was not going well. In addition, I greatly thank Dr. Kunquan "Quin" Yu for his chemistry expertise, without his contribution, I probably would be still developing these immobilized catalysts. Lastly, I would like to thank Dr. Marcus Weck and his research group for excellent suggestions towards my research during the Jones-Weck joint research meetings.

References

[1] D. M. Haddleton, M. C. Crossman, B. H. Dana, D. J. Duncalf, A. M. Heming, D. Kukulj, and A. J. Shooter, Macromolecules 32 (1999) 2110.

[2] D. M. Haddleton, D. J. Duncalf, D. Kukulj, M. C. Crossman, S. G. Jackson, S. A. F. Bon, A. J. Clark, and A. J. Shooter, European Journal of Inorganic Chemistry (1998) 1799.

[3] D. M. Haddleton, C. B. Jasieczek, M. J. Hannon, and A. J. Shooter, Macromolecules 30 (1997) 2190.

[4] J.-S. Wang and K. Matyjaszewski, Journal of the American Chemical Society 117 (1995) 5614.

[5] J.-S. Wang and K. Matyjaszewski, Macromolecules 28 (1995) 7572.

[6] J.-S. Wang and K. Matyjaszewski, Macromolecules 28 (1995) 7901.

[7] J. V. Nguyen and C. W. Jones, Journal of Polymer Science, Part A: Polymer Chemistry 42 (2004) 1367.

[8] J. V. Nguyen and C. W. Jones, Journal of Polymer Science, Part A: Polymer Chemistry 42 (2004) 1384.

[9] J. V. Nguyen and C. W. Jones, Macromolecules 37 (2004) 1190.

[10] S. C. Hong and K. Matyjaszewski, Macromolecules 35 (2002) 7592.

[11] S. C. Hong, H.-J. Paik, and K. Matyjaszewski, Macromolecules 34 (2001) 5099.

[12] N. W. Barnett, R. Bos, H. Brand, P. Jones, K. F. Lim, S. D. Purcell, and R. A. Russell, Analyst (Cambridge, United Kingdom) 127 (2002) 455.

[13] P. Ghosh and T. G. Spiro, Journal of the American Chemical Society 102 (1980) 5543.

[14] C. D. Nunes, M. Pillinger, A. A. Valente, I. S. Goncalves, J. Rocha, P. Ferreira, and F. E. Kuhn, European Journal of Inorganic Chemistry (2002) 1100.

[15] C. D. Nunes, A. A. Valente, M. Pillinger, A. C. Fernandes, C. C. Romao, J. Rocha, and I. S. Goncalves, Journal of Materials Chemistry 12 (2002) 1735.

[16] J. V. Nguyen and C. W. Jones, in Journal of Catalysis, 2005.

[17] G. G. Hlatky, Chemical Reviews (Washington, D. C.) 100 (2000) 1347.

[18] K. Matyjaszewski, Controlled Radical Polymerization, American Chemical Society, Washington, DC, 1998.

[19] K. Matyjaszewski, Advances in Controlled/Living Radical Polymerization, Oxford University Press, Washington, DC, 2003.

[20] K. Matyjaszewski and J. Xia, Chemical Reviews 101 (2001) 2921.

[21] C. Kaes, A. Katz, and M. W. Hosseini, Chemical Reviews (Washington, D. C.) 100 (2000) 3553.

CHAPTER 9

FUTURE WORK AND DIRECTIONS

Improvements on Silica-CuBr/SdMBpy ATRP Catalyst

Increase catalyst loading

One of the key improvements yet to be made for the immobilized silica-CuBr/SdMBpy catalyst is to improve the loading of the ligand on the surface, in an effort to increase the copper loading. Currently, the highest bipyridine loading on Cabosil by elemental analysis is 0.58 mmol Bpy/g Cat [1]. The loading is nearly half the value observed on the same support for PMI [2]. Two methods to increase the CuBr/Bpy loading are suggested. The first is to find higher surface area supports and secondly an organic catalyst could be added during the immobilization step to catalyze the alkoxy-silanol reaction to the surface. Silica materials MS3030 and MS3050 are two potential new supports. These microspheres have V-shaped pores or cavities on the surface that do not interconnect. The surface area and pore size are summarized in the **Table 9.1** below. Surface loading can be increased due to the higher surface area and higher concentration of surface silanols available.

Table 9.1 Summary of silica support properties.

Support	Surface Area (m2/g)	Pore size (Å)
Cabosil EH5	300	---
MS3030	300	400
MS3050	500	240

1. Surface area and pore size determined by dinitrogen physisorption.

Secondly, another potential method to increase surface loading is to add an organic base to the immobilization reaction. For example, the high loadings observed when immobilizing 3-aminopropyltrimethoxysilane on silica was contributed to its ability to self catalyze the surface reaction with its basic amine functionality [3]. The addition of ethanol or triethylamine as mild base to catalyze the surface reaction as well as open bridged siloxanes could potentially increase the surface loading. Ethanol is known to open up surface siloxane bridges, however it can compete for reactions with silanols. Triethylamine could also potentially act similar to amine functionality on the aminopropylsilane, but can also compete for binding with CuBr.

Catalyst regeneration

As a coincidental result from trying to find analytical techniques to determine Cu(II) concentrations on the Cabosil-CuBr/SdMBpy catalysts, Cu(II) reduction can occur *in situ* during XPS measurements [4, 5]. The Cu(II) ions are photoelectron reduced by contact with the Al-Kα electron source from the XPS instrument. Visually, the location of the beam changed from a bright green to a dark brown spot on the catalyst sample. During the measurement, no signal corresponding to Cu(II) oxidation state was observed, only Cu(I) was detected. Complete catalyst regeneration can potentially occur by exposing the used catalyst to Al-Kα electron beam, however regeneration effectiveness may be limited to penetration depth and size of the beam.

New Immobilizable Bipyridine Synthesis

One of the drawbacks of synthesizing an immobilizable asymmetric mono bipyridine ligand was the uncertainty when characterizing the catalyst material. A key question that could not be answered was the composition of the immobilized complex -- where the majority of the immobilized CuBr/Bpy complexes mono- or bis-coordinated bipyridines [1, 6]? Analytical and spectroscopic techniques could not distinguish between the two species. If one was able to synthesize two bipyridines attached to the same silane, it would increase the chances of bis-coordination. **Figure 9.1** shows a potential reaction sequence using 5,5'-dimethyl-2,2'-bipyridine precursor. The length of the linker between the two bipyridine ligands may need to be extended to ensure enough flexibility for bis-coordination. The new bipyridine silane can then be complexed with CuBr and immobilized on silica via the pre-assembled complex approach.

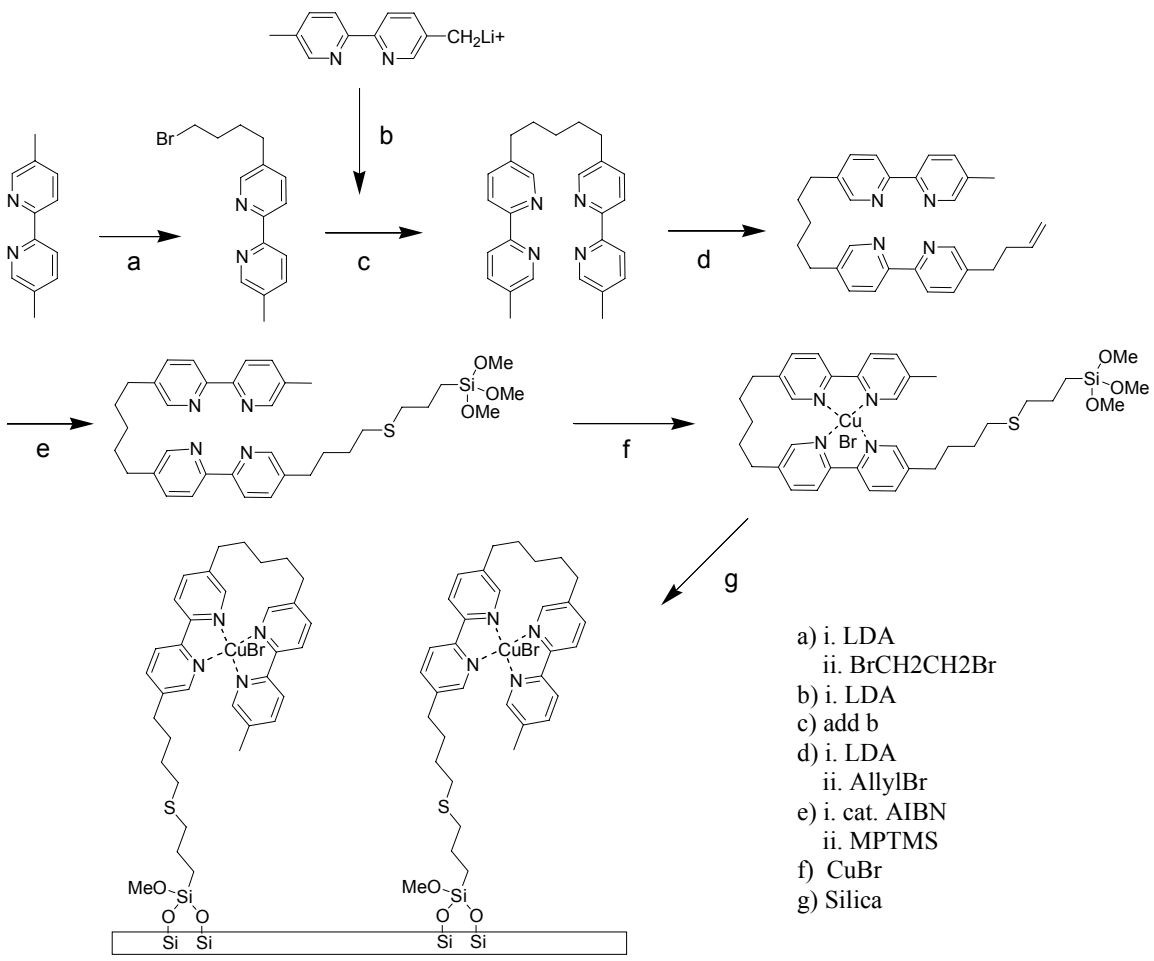

Figure 9.1 Synthetic route to silica-immobilized bis-coordinated CuBr/Bpy complexes.

New Catalysts

Catalytic reactions involving silica immobilized metal/bipyridine catalyst

Although there are hundreds of reactions using metal/bipyridine complexes as catalyst, only a few examples will be given based on interest of the Jones research group. Two areas have been actively under investigation in the Jones research group are reactions performed in the gas phase and polymerization catalysis.

Gas phase production of dimethylcarbonate

There has been a growing push in green chemistry and environmental sustainability to convert carbon dioxide (CO_2) gas to industrially useful compounds [7-9]. One the most attractive synthetic goal is to convert CO_2 in the presence of methanol to dimethylcarbonate (DMC) [7-9]. DMC is an environmentally benign chemical and a unique chemical intermediate with versatile chemical reactivity. For instance, methylation reactions are usually carried out using methyl halides or dimethyl sulfates. Both reagents are toxic and corrosive chemicals and require a stoichiometric amount of base to methylate and produce a stoichiometric amount of inorganic salts as waste [8]. DMC is a substitute for both reagents, thus eliminating the use of these corrosive and high waste producing reagents.

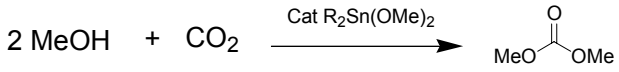

Figure 9.2 Catalytic carbonate synthesis of dimethylcarbonate [10].

The reaction shown in **Figure 9.2** has been studied extensively, however using tin as a catalyst poses additional toxicity problems [10]. Recently several investigations have been reported using immobilized diamine copper salt complexes for the gas phase conversion of CO_2 and methanol to DMC [7, 9, 11]. Future work in the Jones lab could involve immobilizing $CuCl_2$/SdMBpy complexes on SBA15 support for the potential gas phase conversion CO_2 to DMC (**Figure 9.3**). $CuCl_2$/Bpy complexes can be immobilized via the pre-assembled complex approach using SdMBpyTMS [7, 11].

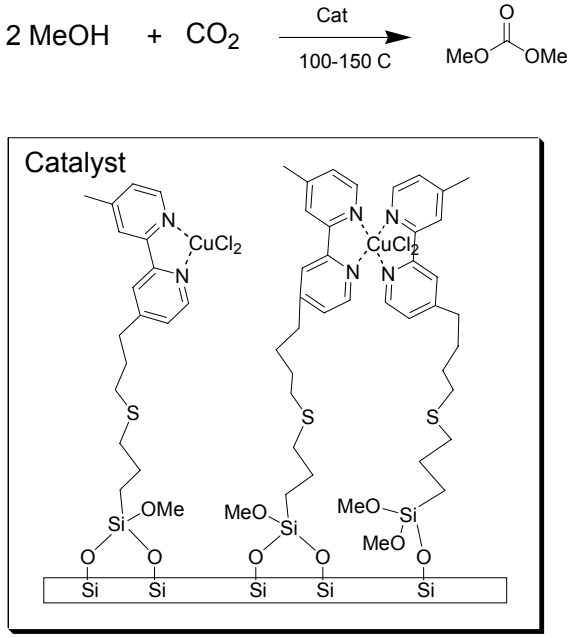

Figure 9.3 Potentially new $CuCl_2$/Bpy catalyst for carbonate synthesis of DMC [7, 11].

Copolymerization of CO with alkenes catalyzed by immobilized Pd catalysts

The copolymerization of carbon monoxide and alkenes to produce polyketones has attracted interest in both industry and academia [12]. The starting materials are readily available and the polyketone can be easily derivatized through the carbonyl group on the polymer backbone to make interesting new materials (**Figure 9.4**). The state of the art catalyst systems are dppp-Pd catalysts. Typical reaction rates are around ~10^4 mol of converted ethene (mol Pd)$^{-1}$ h^{-1} with average molecular weight of ~20000 (dppp/HOTs/MeOH, 65 ºC) and 100% selectivity towards alternating copolymer [12].

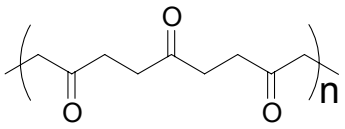

Figure 9.4 Polyketone

The polymers are highly stable (T_m = 260 ºC) and insoluble in most organic solvents [12]. Recently Bianchini et al. reported a bis-chelated palladium (II) complex containing dinitrogen ligands for the copolymerization of carbon monoxide and ethane [13]. They found by adding both 1,4-benzoquinone (BQ) and p-toluenesulfonic acid (TsOH) with the catalyst gives higher productivities than the state of the art dppp-based catalysts. The highest productivity was observed for 2,2,'-bipyridine-based catalysts ([Pd(meso-bdpp)(N,N'-bpy)]$(PF_6)_2$, 8.6 kg copolymer (g Pd)$^{-1}$ h^{-1}) and maintaining chemo and regioselectivity.

These homogeneous polymerizations are normally performed in batch reactors on a small scale, however for large-scale industrial polymerizations, homogeneous catalysts

are not suitable due to reactor fouling [14-16]. Hence, supported catalysts are more suitable for industrial implementation of these new catalysts. **Figure 9.5** shows how I can utilize SdMBpyTMS ligands to immobilize [Pd(meso-bdpp)(N,N'-bpy)]$(PF_6)_2$ complexes for the CO and alkene copolymerization.

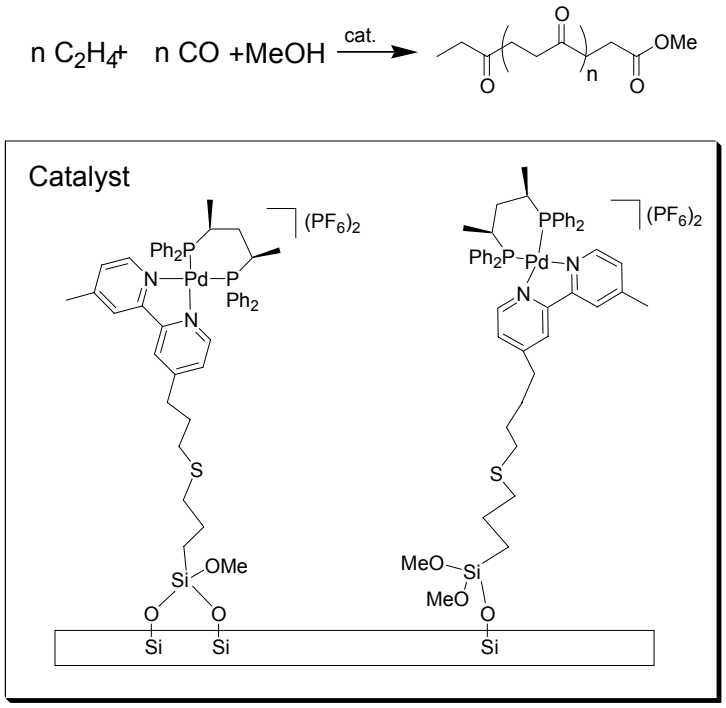

Figure 9.5 Immobilized [Pd(meso-bdpp)(N,N'-bpy)]$(PF_6)_2$ complexes.

New Material Applications

Materials for separation and sensor applications

As mentioned in the previous chapter, bipyridine ligands are the most widely investigated systems in the literature. The main reason why bipyridine is so popular is because of its ability to bind/coordinate to most transition metals. Bipyridine functionalized materials can be used for a variety of applications. Two applications will be proposed below.

Metal ion absorbents

Metal ion absorbents or metal sponges are particularly useful to separate out heavy metals from waste streams and to purify water [17, 18]. Since bipyridines have a high affinity to bind most metals in the periodic table of elements, filters packed with silica functionalized bipyridines would be advantageous for applications that require low levels of metal impurities (i.e., drinking water purification and pharmaceutical). **Figure 9.6** shows the separation process using bipyridine functionalized materials.

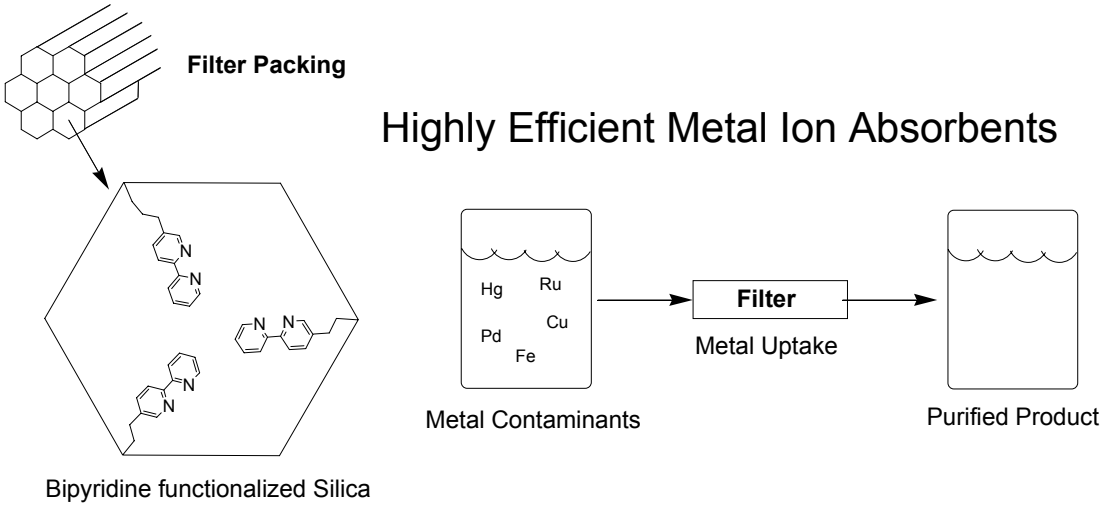

Figure 9.6 Metal ion absorbents for purification process.

Functionalized bipyridine materials for sensor applications

Since most metal/bipyridine complexes absorb in the ultraviolet or visible region of the electromagnetic spectrum, for this reason these species are excellent candidates for sensing applications. The transition metal/bipyridine complexes can be reduced or oxidized to a different oxidation state. The different oxidation states tend to absorb differently, therefore the complexes can be used for photoluminescence visual sensors. A color change indicates a change in the complex (e.g., presence of a new species). The concentration of a complex or complexes can be detected by the absorbance intensity of UV/vis measurements. The absorbance, A, can be expressed through Beer's Law (1).

$$A = \mathbf{a} \times \mathbf{b} \times \mathbf{c} \qquad (1)$$

Where, **a** is a proportionality constant called absorptivity, **b** is the path length through the solution, and **c** is the concentration of the absorbing species. Absorbance is directly proportional to concentration, consequently monitoring of a chemical species that reduces or oxidizes the complex can be detected. Below are some examples of how the immobilizable SdMBpyTMS ligand can be used in a variety of sensor applications.

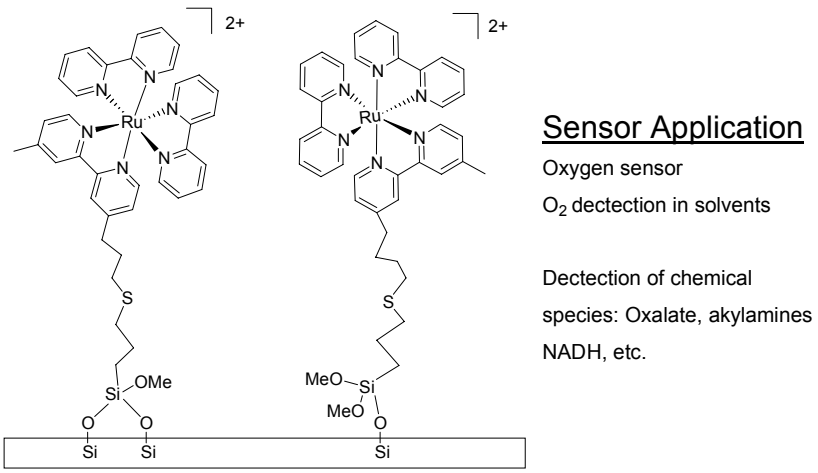

Figure 9.7 Immobilized tris(bipyridine)Ru(II) complex for sensor applications [19].

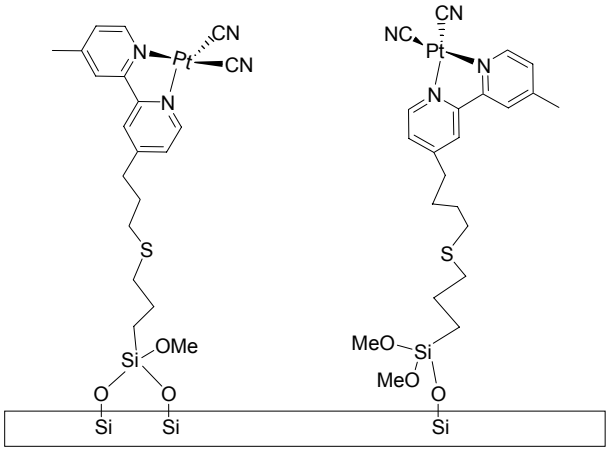

Figure 9.8 Immobilized [Pt(bipyridine)$(CN)_2$] complex for oxygen sensing [20].

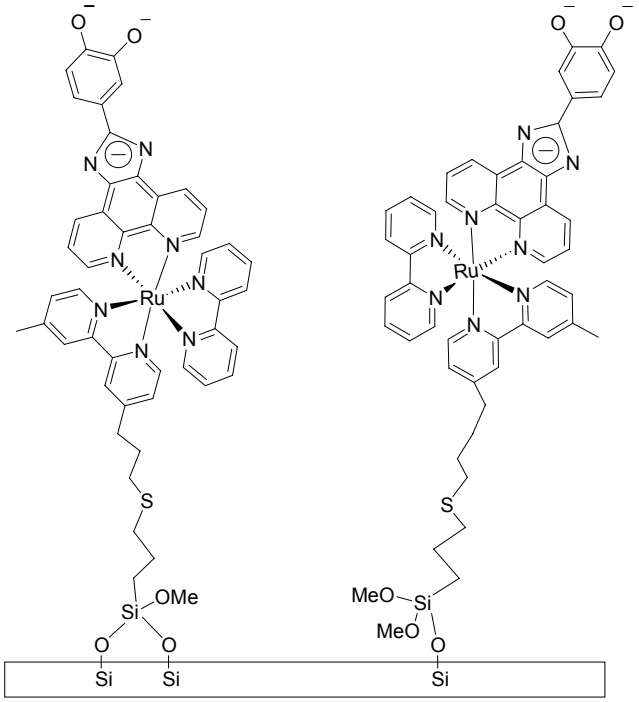

Figure 9.9 Immobilized $[Ru(bpy)_2(dhip)]^-$ for pH sensing and DNA binding [21].

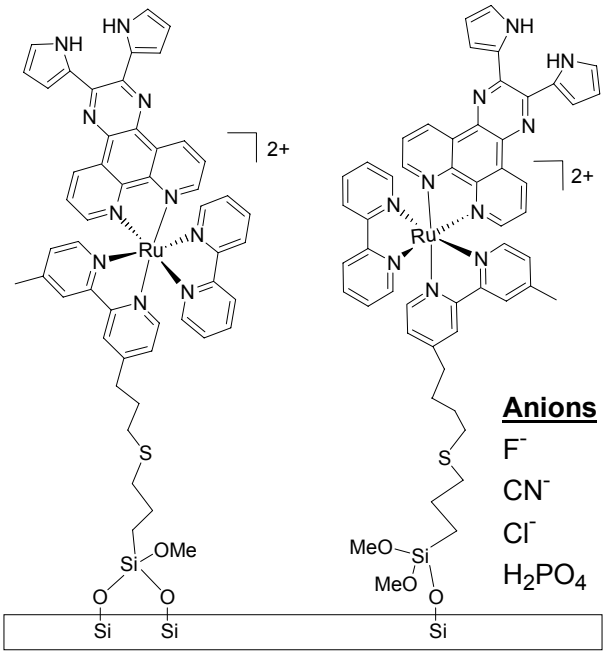

Figure 9.10 Immobilized [Ru(bpy)2DPQ]2+ complex for lifetime-based sensor for cyanide and related anions [22].

References

[1] J. V. Nguyen and C. W. Jones, Macromolecules 37 (2004) 1190.

[2] J. V. Nguyen and C. W. Jones, Journal of Polymer Science, Part A: Polymer Chemistry 42 (2004) 1367.

[3] S. A. Kanan, W. T. Y. Tze, and C. P. Tripp, Langmuir 18 (2002) 6623.

[4] F. Parmigiani and L. E. Depero, Strutural Chemistry 5 (1994) 117.

[5] W. R. Tikkanen, C. Krueger, K. D. Bomben, W. L. Jolly, W. C. Kaska, and P. C. Ford, Inorganic Chemistry 23 (1984)

[6] J. V. Nguyen and C. W. Jones, in Journal of Catalysis, 2005.

[7] Y. Z. Yuan, W. Cao, and W. Z. Weng, Journal of Catalysis 228 (2004) 311.

[8] P. Tundo, S. Memoli, D. Herault, and K. Hill, Green Chemistry 6 (2004) 609.

[9] Y. Cao, J. C. Hu, P. Yang, W. L. Dai, and K. N. Fan, Chemical Communications (2003) 908.

[10] J. C. Choi, T. Sakakura, and T. Sako, Journal of the American Chemical Society 121 (1999) 3793.

[11] W. Cao, H. B. Zhang, and Y. Z. Yuan, Catalysis Letters 91 (2003) 243.

[12] E. Drent and P. H. M. Budzelaar, Chemical Reviews 96 (1996) 663.

[13] C. Bianchini, H. M. Lee, P. Barbaro, A. Meli, S. Moneti, and F. Vizza, New Journal of Chemistry 23 (1999) 929.

[14] J. Queisser, M. Slany, and A. Ludwig, (BASF A.-G., Germany). Application: DE 97-19746279, 1999, p. 16 pp.

[15] A. Sommazzi, G. Lugli, F. Calderazzo, D. Belli dell'Amico, and F. Garbassi, (ENICHEM S.p.A., Italy). Application: EP 93-200617, 1993, p. 9 pp.

[16] A. Sommazzi, G. Lugli, F. Garbassi, F. Calderazzo, and D. Belli dell'Amico, (ENICHEM S.p.A., Italy). Application: EP 93-200618, 1993, p. 9 pp.

[17] S. Dai, M. C. Burleigh, Y. H. Ju, H. J. Gao, J. S. Lin, S. J. Pennycook, C. E. Barnes, and Z. L. Xue, Journal of the American Chemical Society 122 (2000) 992.

[18] S. Dai, M. C. Burleigh, Y. Shin, C. C. Morrow, C. E. Barnes, and Z. Xue, Angewandte Chemie, International Edition 38 (1999) 1235.

[19] T. M. Downey and T. A. Nieman, Analytical Chemistry 64 (1992) 261.

[20] W. W. S. Lee, K. Y. Wong, and X. M. Li, Analytical Chemistry 65 (1993) 255.

[21] G. Y. Bai, K. Z. Wang, Z. M. Duan, and L. H. Gao, Journal of Inorganic Biochemistry 98 (2004) 1017.

[22] P. Anzenbacher, D. S. Tyson, K. Jursikova, and F. N. Castellano, Journal of the American Chemical Society 124 (2002) 6232.